Teleconnections and dynamical influences on intraseasonal rainfall variability over Vietnam

Hong Hanh Le

THÈSE

En vue de l'obtention du

DOCTORAT DE L'UNIVERSITÉ DE TOULOUSE

Délivré par l'Université Toulouse 3 - Paul Sabatier

Présentée et soutenue par

Hong Hanh LE

Le 12 mai 2023

TÉLÉCONNEXIONS ET INFLUENCES DYNAMIQUES SUR LA VARIABILITÉ INTRASAISONNIÈRE DES PRÉCIPITATIONS AU VIETNAM

Ecole doctorale : **SDU2E - Sciences de l'Univers, de l'Environnement et de l'Espace**

Spécialité : **Océan, Atmosphère, Climat**

Unité de recherche :
LEGOS - Laboratoire d'Etudes en Géophysique et Océanographie Spatiale

Thèse dirigée par
Nicholas HALL et Thanh NGO DUC

Jury

M. Andreas FINK, Rapporteur
M. Satoru YOKOI, Rapporteur
M. Francis CODRON, Rapporteur
M. Jean-Philippe DUVEL, Examinateur
M. Pascal ROUCOU, Examinateur
M. Nicholas HALL, Directeur de thèse
M. Thanh NGO-DUC, Co-directeur de thèse
Mme Isabelle DADOU, Présidente

Acknowledgments

My PhD journey has come to an end, and it's been a mix of tough times and joyful moments. Even though there were challenges, I had my mentors, friends and family by my side, making the experience special and meaningful.

To my supervisor, Prof. Nick HALL, and my co-supervisor, Prof. Thanh NGO-DUC, I am deeply thankful for your mentorship and expertise that have shaped my research and academic growth. Your dedication and insights have been invaluable sources of inspiration.

I would like to especially express my gratitude to Mr. Nick whose exceptional patience and unwavering support helped shape the trajectory of my doctoral journey. Despite my initial trials and shortcomings, he stood by me with limitless patience. He readily repeats explanations until clarity is reached, gives me constant encouragement to improve my understanding of the subject and also instils in me a sense of determination to overcome obstacles. I am truly blessed to have you as my supervisor, guide and inspiration in this academic adventure.

I am also deeply appreciative of Mr. Thanh, my co-supervisor, who provided me with an opportunity to work with him and the REMOSAT team in Vietnam with support from LMI LOTUS/USTH. This experience has been transformative, providing me with insights and practical knowledge that extend beyond academia. The guidance of Thanh is both a mentor and a colleague. His willingness to share his expertise, projects and academic career is a rich experience that complements my academic pursuits. It has been an honor to join Thanh's team and his guidance has broadened my horizons, providing a combination of academic learning and practical insights that will shape my future career.

I'm extremely grateful to Dr. Pascal Roucou and Dr. Marine Herrmann - the follow-up committee members. They played a major role in shaping the final outcome of my PhD thesis. Their critical reviews, constructive feedback, and thoughtful suggestions have been instrumental in enhancing the overall quality and depth of my research. Their expertise and attention to detail have guided me to refine my work and ensure academic quality. I am grateful for their dedication and insightful input, which were integral in making my thesis a more comprehensive and impactful contribution to the field.

I also would like to express my gratitude to all members of the PhD jury who made significant contributions, especially Raporteurs. Their dedicated commitment of time, their wealth of expertise, and the valuable insights they provided during the evaluation process have been conductive in enhancing the scholarly significance of my thesis. Their thorough examination and thoughtful recommendations not only underscore the rigour of my work but also contribute to its credibility and academic value.

I am extremely grateful to Le ministère de l'Enseignement supérieur, de la Recherche et de l'Innovation (MESRI) funding for providing me with a PhD contract signing with Universite Paul Sabatier - UPS; so that I can focus on my research and academic goals. This support has

been very important in allowing me to dedicate my efforts to the advancement of knowledge in my field. In addition, I would like to express my gratitude to TESS funding - Doctoral School SDU2E, for the mobility grant that has facilitated opportunities to collaborate, learn, and network. Their support not only broadened my horizons but also enriched my learning journey by allowing me access to diverse perspectives and experiences. The contributions of these fundings have played an important role in my doctoral journey and I truly appreciate their belief in my potential and commitment to advancing my academic growth.

I extend my heartfelt gratitude to the dedicated administrative personnel at the LEGOS laboratory for their invaluable support to me, especially Mrs. Brigitte Cournou and Mr. Frederic Marin. Your support behind the scenes has been like an indispensable ingredient in PhD work that made everything run smoothly and kept me focused on my work.

A special acknowledgement goes to the esteemed president of SDU2E - Mrs. Genevieve Soucail for providing insightful advice on achieving a harmonious work-life balance, especially when I was pregnant with a lot of worries. I am grateful for your advice on the significance of holistic well-being during PhD.

And to all my fantastic friends (Hue, Tung, Bich, Adelaide, Julia, Gabriela, Margot, Manon, etc.) who've been there for me, you rock! Your help, encouragement, and those random coffee breaks have been the fuel that kept me going. You've turned the tough times into manageable ones and the good times into unforgettable ones. Your friendship has been crucial and kept me going, and I'm beyond lucky to have you in my corner. Cheers to us, and here's to many more adventures ahead!

Finally, I want to dedicate my deepest appreciation to my family in Vietnam. To my grandma, parents, and my two younger sisters, your love and belief in me have been my rock. Even from afar, you've been my cheerleader, and your support has meant the world to me.

And to my husband - Trung and our little baby - Minh Tri, thanks for your appearance in my life, you've been my daily dose of motivation. Your patience, understanding, love and even your smile have kept me going, even when things got tough. Words cannot express my gratitude for both of you.

Once again, thank you from the bottom of my heart to everyone who has been a part of this journey. Your impact has been immeasurable, and I am forever grateful. I will carry forward the lessons, memories, and connections for the next phase of my life.

Toulouse, 10th August, 2023

Le Hong Hanh

Résumé — La variabilité intrasaisonnière des précipitations au Vietnam a une grande amplitude et une complexité considérable, avec beaucoup de variations entre les sous-régions. L'objectif de cette étude est d'abord d'évaluer la contribution des termes du bilan d'humidité aux événements régionaux pour les anomalies positives et négatives des précipitations ; puis d'analyser ces événements régionaux opposés, Wet et Dry, pour identifier les précurseurs dynamiques à grande échelle et leurs voies d'influence. Une attention particulière est accordée à la non-linéarité ou à l'asymétrie de l'influence et à la sensibilité au choix de la région, du seuil et de la quantité de composite. Une combinaison d'approches d'observation et de modélisation est utilisée à grande échelle et à l'échelle régionale.

Une base de données de réanalyse (ERAi, 1979-2016) est utilisée pour construire des composites humides et secs sur le Vietnam en utilisant la convergence du flux d'humidité verticalement intégré (VIMC) comme indicateur des précipitations. À l'échelle régionale, la VIMC est en bonne corrélation avec les précipitations réanalysées. La dynamique à grande échelle associée aux événements Nord et Sud opposés montre des précurseurs à grande échelle asymétriques et des voies d'influence différentes. Deux voies extratropicales et une voie tropicale émergent et sont distinctes pour les événements humides et secs et les régions Nord et Sud.

L'étude de modélisation globale utilise le modèle global DREAM. Deux régions cibles, le Nord et le Sud du Vietnam, sont étudiées à partir d'un ensemble d'expériences de chauffage pour trouver l'emplacement de la perturbation initiale qui donne le plus d'influence. Une technique de "nudging" est ensuite appliquée dans cette région pour simuler des précurseurs réalistes. Pour le Nord du Vietnam, à une delai de 2 semaines, il n'y a qu'une influence extratropicale. Les sources tropicales influencent le Nord et le Sud dans une limite de 9 jours. La réponse du modèle montre deux voies distinctes cohérentes avec les observations. Pour différents états de base, la réponse du modèle dépend de la conjonction entre les précurseurs et les jets atlantique et asiatique. L'analyse du traçage de rayons d'ondes de Rossby sur différents états est utilisée pour révéler des trajectoires à haute latitude cohérentes avec les composites observés. Les trajectoires à haute latitude émanent de la région Europe-Asie de l'Est et arrivent sur le Vietnam en 1 à 2 semaines. Les positions des sources d'ondes de Rossby sur l'Europe et l'Asie de l'Est dépendent de l'état dre base.

Une étude de descent d'échelle est ensuite entreprise en utilisant le modèle régional RegCM4 sur le domaine de l'Asie du Sud-Est, forcé par le jeu de données ERAi. Le composite de la sortie de RegCM est assemblé par l'indice régional montré dans l'analyse observationnelle. Les composites de tous les termes du bilan d'humidité sont étudiés. Le forçage extratropical conduit à des modèles d'anomalies de précipitations à grande échelle sur l'ensemble du domaine pour tous les événements. En particulier, les événements NVN et les événements humides CVN ont été reproduits avec succès. Cependant, les précipitations locales sur le SVN et le CVN (sec) n'ont pas été reproduites. La reproduction des termes du bilan hydrique par le RegCM montre une simulation cohérente du TIMC pour tous les événements et

des formes de précipitations à grande échelle qui correspondent à l'anomalie VIMC, mais il y a une inversion de signe pour l'évaporation pour tous les événements. L'absence de signal reproduit sur la mer de Chine suggère que le modèle régional a du mal à propager certains signaux tropicaux, et que la dynamique à grande échelle, y compris les influences extratropicales et tropicales, doit être attribuée différemment aux événements humides et secs sur les sous-régions du Vietnam.

Mots clés : Téléconnexions, DREAM, RegCM, précipitations au Vietnam, Intrasaisonnière Variation, ondes de Kelvin de Rossy.

Abstract — The intraseasonal variability of Vietnam rainfall has a large amplitude and considerable complexity, with much variation between the subregions. The objective of this study is first to assess the contribution of moisture budget terms to regional events for positive and negative rainfall anomalies; then to analyse these opposite regional events, Wet and Dry, to identify large-scale dynamical precursors and their pathways of influence. Particular attention is paid to nonlinearity or asymmetry of the influence and to the sensitivity to the choice of region, threshold and composited quantity. A combination of observation and modeling approaches is used at large and regional scales.

A reanalysis dataset (ERAi, 1979-2016) is used to construct Wet and Dry composites over Vietnam subregions using the Vertically Integrated Moisture Flux Convergence (VIMC) as a proxy for rainfall. At regional scales VIMC correlates well with reanalysed rainfall. The large-scale dynamics associated with opposing North and South events show asymmetrical large-scale precursors and different pathways of influence. The exact nature of the precursors is sensitive to the definition of the composite index. Two extratropical pathways and one tropical pathway emerge that are distinct for Wet and Dry events; and North and South regions.

The global modeling study uses the global spectral model DREAM in stationary wave configuration. Basic state derived from summer ERAi reanalysis have been used to further investigate the pathways. Two target regions, North and South Vietnam, are investigated from a set of heating experiments to find the initial perturbation location that gives the most influence. A nudging technique is then applied in that region to simulate realistic precursors. We found that for North Vietnam at a range of 2 weeks, there is only extratropical influence. Tropical sources influence both North and South in a limit of 9 days. The model response to 15-day lag European precursors shows two distinct pathways consistent with observations, especially for Wet events. Although the jet pathway is more reproducible on the climatological basic state, for different basic states the model response is dependent on the conjunction between precursors and the basic state jet including both Atlantic and Asian jets.

Analysis of Rossby wave ray-tracing on different states is also used to reveal high-latitude pathways that are consistent with observed composites. High-latitude pathways emanate from the Europe-Eastern Asia region and arrive over Vietnam in 1-2 weeks. The positions of Rossby wave sources over Europe-Eastern Asia are dependent on the basic state. Another preferred location for Rossby wave propagation to Vietnam is Mongolia. Wave numbers K1 and K3 take only 1-2 days to arrive over Vietnam, and this is not sensitive to the basic state. This direct source study indicates the way anomalies might grow along the jet and then directly influence Vietnam via Rossby wave propagation.

A downscaling study - preliminary work, is then undertaken using the regional model RegCM4 over the Southeast Asia domain, forced by ERAi. The composite of RegCM output is assembled by the regional index from the observational analysis. Extratropical forcing

leads to large-scale rainfall anomaly patterns over the whole domain for all events. NVN events and CVN-Wet events were successfully reproduced, but local rainfall over SVN and CVN-Dry event was not. The reproduction of moisture budget terms by RegCM shows a consistent simulation of tendency of moisture column for all events and large-scale patterns of rainfall that correspond to the VIMC anomaly, but there is a reversed sign for Evaporation. A lack of signal over the South China Sea suggests that the regional model has difficulty propagating some tropical signals and that large-scale dynamics, including extratropical and tropical influences, should be attributed to the wet and dry events over Vietnam subregions differently.

Keywords: Teleconnections, DREAM, RegCM, Vietnam rainfall, Intraseasonal Variation, Rossby waves, Kelvin waves.

Contents

List of Figures

List of Tables

Acronyms

ENSO	*El Niño – Southern oscillation*
ISV	*Intraseasonal Variation/Variability*
ISO	*Intraseasonal Oscillation*
MJO	*Madden-Julian Oscillation*
VIMC	*Vertically Integrated Moisture flux Convergence*
TIMC	*Tendency of Integrated Moisture Column*
EVP	*Evaporation*
PPT	*Precipitation*
AMF	*Anomalous Moisture Flux*
DREAM	*Modified Normalized Difference Water Index*
RCM	*Root Mean Square Error*
RegCM4	*Rational Polynomial Coefficient*
FROGs	*Frequent Rainfall Observations on GridS*
APHRODITE	*Asian Precipitation-Highly Resolved Observational Data Integration Towards Evaluation of the Water Resources*
VnGP	*Vietnam high-resolution Gridded Precipitation*
CSC	*South China Sea*
NWP	*North Western Pacific*
AS	*Asia Monsoon*
OLR	*Outgoing Longwave Radiation*
PC	*Principal Component*
CCEWs	*Convectively Coupled Equatorial Waves*
ER	*Equatorial Rossby (wave)*
MRG	*Mixed Rossby-Gravity (wave)*
CAOs	*Cold Air Outbreaks*

Introduction

Introduction général

Le Vietnam est situé dans la péninsule indochinoise. Il est fortement impacté par le système de la mousson asiatique, un phénomène d'échelle planétaire. De plus, la bande continentale a la forme de la lettre S, s'étendant de la latitude 23 23' Nord à 8 27' Nord. Elle présente une topographie variée de collines, de plaines, de côtes et de plateaux continentaux, ce qui entraîne une diversité des caractéristiques climatiques et hydrologiques sous-régionales. Au nord du Vietnam, il y a quatre saisons : printemps, été, automne et hiver, mais au sud, il n'y a que deux saisons : humide et sèche.

L'économie vietnamienne dépend de l'agriculture et de l'énergie hydroélectrique dont l'approvisionnement dépend fortement du budget hydrologique. Comme l'indique le ministère de l'agriculture et du développement rural pour la période 2012-2019, les terres agricoles représentent 80,4% de la superficie totale du Vietnam et contribuent à 14% du GDP (GSO.GOV.VN). Selon Vietnam Electricity, l'hydroélectricité représente plus de 30% de la production totale d'électricité de l'ensemble du système national, et il existe un potentiel supplémentaire avec de nombreuses capacités inexploitées (GIZENERGY.ORG.VN).

Le concept d'hydrologie mentionné dans cette étude appartient à l'hydrométéorologie qui se concentre sur l'eau de la surface de la terre à l'ensemble de l'atmosphère. Si toute l'eau présente dans l'atmosphère était condensée, elle ne couvrirait la surface de la planète qu'à hauteur d'un pouce en moyenne. Cependant, c'est comme un TGV (Train à Grande Vitesse) comparé à la circulation océanique ou au transport par voie fluviale et peut déplacer l'eau autour du globe. Dans cette étude, nous nous concentrons sur l'apport, le transport et l'élimination de l'eau de l'atmosphère (USGS.GOV).

Dans le bilan hydrologique, l'évaporation et la transpiration sont des processus qui transforment l'eau liquide en vapeur. La vapeur est transportée vers le haut de l'atmosphère par des courants d'air ascendants. Elle se condense ensuite en nuages grâce à des températures plus froides en altitude, où des vents forts déplacent les nuages dans le monde entier jusqu'à ce que l'eau tombe sous forme de précipitations. Il convient de noter qu'environ 10% des précipitations proviennent de la transpiration et que 90% de l'eau présente dans l'atmosphère est fournie par l'évaporation.

Les précipitations sont considérées comme un élément clé du bilan hydrologique qui a le plus d'impact direct sur les secteurs économiques et sociaux du monde entier. Le rapport sur le risque climatique du Groupe de la Banque mondiale et de la Banque asiatique de développement montre que les pertes sociales et économiques du Vietnam sont principalement attribuées aux catastrophes naturelles, notamment les inondations, les tempêtes et les sécheresses, entre 1900 et 2020 (worldbank.org, a). Figure 1, ils indiquent en détail que le Vietnam est un pays extrêmement exposé aux inondations (1er rang), ainsi qu'aux cyclones tropicaux

et aux risques associés (8e rang). Suivie par la sécheresse, cette exposition est classée 82e mais reste importante comme le souligne la grave sécheresse de 2015-2017.

L'amélioration de nos connaissances sur les précurseurs des événements extrêmes ainsi que la qualité des prévisions par l'augmentation de leur portée est un domaine de recherche important pour améliorer la vie quotidienne des gens et contribuer à la défense et à la sécurité nationales. Comme l'a enregistré le Centre national d'hydrométéorologie, cette sécheresse - la pire depuis 90 ans - a été causée par le fort El Nino de 2015-2016 qui est l'un des plus longs de ces 60 dernières années. En 2015, les catastrophes naturelles ont été moins nombreuses mais l'intensité de l'impact de certains événements a atteint un niveau record. La région centrale du Vietnam a souffert d'une grave sécheresse pendant de nombreux mois et les pluies sont arrivées à la fin de l'automne avec moins de 30 à 50% de la période précédente. Cela a dévasté la récolte de riz et a donné lieu à des alertes sur la capacité des bassins des barrages hydroélectriques, qui a diminué de 25% par rapport à l'année précédente.

Dans l'atmosphère, le mouvement se produit à diverses échelles, et différents processus dynamiques atmosphériques peuvent être identifiés en termes d'échelles spatiales et temporelles Figure 2. Selon l'échelle spatiale, quatre catégories peuvent être définies. La micro-échelle est l'étude des phénomènes atmosphériques à une échelle d'environ 1 kilomètre ou moins. Par exemple, la turbulence locale causée par des bâtiments et d'autres obstacles (comme des collines individuelles) est présentée à cette échelle. La méso-échelle est l'étude des phénomènes atmosphériques dont l'échelle horizontale est comprise entre 1 km et 100 km. Les systèmes de méso-échelle durent de moins d'un jour à plusieurs jours. Les événements auxquels on s'intéresse généralement sont les tornades, les orages, les fronts, les bandes de précipitations dans les cyclones tropicaux et extratropicaux, et les systèmes météorologiques générés par la topographie, comme les ondes de montagne et les brises de mer et de terre. L'échelle synoptique est axée sur les changements à des échelles allant jusqu'à 1000 km et jusqu'à un mois dans le temps et l'espace. À cette échelle, l'accélération de Coriolis joue un rôle principal dans les prévisions des masses d'air en mouvement. Les phénomènes typiquement décrits par la météorologie synoptique comprennent des événements tels que les cyclones extratropicaux, les creux et les crêtes baroclines. A l'échelle globale, c'est l'étude des modèles météorologiques liés au transport de chaleur ou aux oscillations à très grande échelle avec une période de temps de l'ordre de mois comme l'oscillation Madden-Julian ou d'années comme El Niño-Southern Oscillation.

Sous l'échelle de temps saisonnière, les processus intrasaisonniers incluant l'oscillation Madden-Julienne, les ondes planétaires et les cyclones tropicaux sont considérés comme des modèles typiques de variabilité dans cette gamme. Ces processus ont une échelle spatiale de 10e5 à 10e8 km, et une échelle temporelle de quelques semaines à quelques mois. Cela montre que l'échelle temporelle et l'échelle spatiale sont bien distinctes des processus saisonniers. Nous notons que les extrêmes sont souvent liés à des processus physiques différents de ceux qui régissent les moyennes à long terme. Par conséquent, les facteurs conduisant à une variabilité intrasaisonnière anormale pourraient être différents des facteurs saisonniers, et doivent donc être étudiés plus avant.

Selon l'échelle spatiale, quatre catégories peuvent être définies. La micro-échelle est l'étude

des phénomènes atmosphériques à une échelle d'environ 1 kilomètre ou moins. Par exemple, la turbulence locale causée par des bâtiments et d'autres obstacles (comme des collines individuelles) est présentée à cette échelle. La méso-échelle est l'étude des phénomènes atmosphériques dont l'échelle horizontale est comprise entre 1 km et 100 km. Les systèmes de méso-échelle durent de moins d'un jour à plusieurs jours. Les événements auxquels on s'intéresse généralement sont les tornades, les orages, les fronts, les bandes de précipitations dans les cyclones tropicaux et extratropicaux, et les systèmes météorologiques générés par la topographie, comme les vagues de montagne et les brises de mer et de terre. L'échelle synoptique est axée sur les changements à des échelles allant jusqu'à 1000 km et jusqu'à un mois dans le temps et l'espace. À cette échelle, l'accélération de Coriolis joue un rôle principal dans les prévisions des masses d'air en mouvement. Les phénomènes typiquement décrits par la météorologie synoptique comprennent des événements tels que les cyclones extratropicaux, les creux et les crêtes baroclines. A l'échelle globale, c'est l'étude des modèles météorologiques liés au transport de chaleur ou aux oscillations à très grande échelle avec une période de temps de l'ordre de mois comme l'oscillation Madden-Julian ou d'années comme El Niño-Southern Oscillation.

La variabilité du climat est alors également considérée sur des échelles de temps et d'espace. Il s'agit d'une information statistique, d'une synthèse des variations météorologiques portant sur une zone spécifique pendant un intervalle déterminé avec un ensemble de données suffisamment long - généralement supérieur à 30 ans. Elle est différente de la variabilité météorologique qui décrit l'état de l'atmosphère au jour le jour et ses variations à court terme (de quelques heures à quelques jours). La variabilité totale d'une série chronologique peut être décomposée en différentes échelles de temps (comme indiqué ci-dessous). Ensuite, les processus atmosphériques associés à ces échelles de temps peuvent être étudiés plus en détail en fonction des objectifs de l'étude.

Variabilité totale = Variabilité climatique + Variabilité météorologique (perturbation synoptique)

avec : Variabilité climatique = Tendances + Cycle annuel + Variabilité intrasaisonnière.

Pour l'hydrologie sur l'ensemble du Vietnam, les tendances dominantes pour les précipitations annuelles sont à la baisse mais ne sont pas statistiquement significatives (Nguyen et al., 2014). Le cycle annuel des précipitations est conditionné par l'impact de la circulation de la mousson asiatique et son inversion de la direction du vent. La variabilité annuelle des précipitations est normalement attribuée à la variabilité du système de mousson, à la topographie et au phénomène ENSO (Nguyen et al., 2014). La présence de l'orographie conduit à un climat plus diversifié en raison de ses impacts non seulement locaux mais aussi à grande échelle avec la circulation de la mousson.

La variabilité intrasaisonnière des précipitations au Vietnam présente un grand intérêt et a été étudiée dans des études récentes. Certaines études montrent des caractéristiques de la VSI dans des intervalles de temps spécifiques associés à des processus intrasaisonniers. Ces processus atmosphériques peuvent être influencés soit par les tropiques, soit par les extratropiques. D'autres étudient un certain événement et indiquent ensuite l'interaction tropique-

extratropique. Tous montrent la multiplicité des régions et l'utilisation de différents critères pluviométriques et échelles de temps de considération. Il est nécessaire d'étudier la sensibilité des conclusions à ces considérations. En outre, jusqu'à présent, il y a encore un manque de recherche sur le budget hydrologique associé à la variabilité intrasaisonnière.

Dans ce contexte, l'objectif principal de ce travail est d'étudier le bilan hydrologique et les influences dynamiques tropicales et à distance sur la variabilité intrasaisonnière des précipitations au Vietnam à différentes échelles par différentes approches.

Le premier chapitre présente les caractéristiques du climat pluvial du Vietnam, y compris le cycle annuel et la variabilité intrasaisonnière. Le cycle annuel des précipitations au Vietnam est d'abord présenté avec les modèles annuels, la topographie et le budget hydrologique. Nous présentons ensuite la circulation à grande échelle qui contrôle directement le cycle annuel, ainsi que le concept des liens avec le forçage à grande échelle. Ensuite, la variabilité intrasaisonnière des précipitations, y compris une description statistique de l'échelle de temps et des caractéristiques physiques, sera présentée selon les études précédentes. Ceci est suivi par une revue de la littérature sur les facteurs d'influence possibles de la variabilité intrasaisonnière des précipitations au Vietnam. Enfin, les objectifs et les approches de cette thèse sont énumérés, suivis par le plan du manuscrit.

Ce document a été rédigé en anglais, mais un résumé, une introduction général et une conclusion en français ont été inclus.

General Introduction

Vietnam is located on the Indochinese Peninsula. It is strongly impacted by the Asian Monsoon system - a planetary-scale phenomenon. In addition, the mainland strip is shaped like the letter S, extending from latitude 23°23' North to 8°27' North. It has a diverse topography of hills, plains, coasts, and continental shelves which leads to diversity in subregional climate and hydrological characteristics. In North Vietnam, there are four seasons: spring, summer, autumn, and winter, but in the South, there are just two seasons: wet and dry.

Vietnam's economy is dependent on agriculture and hydroelectric power whose supply relies heavily on the hydrology budget. As reported by the Ministry of Agriculture and Rural Development from 2012 to 2019, agricultural land accounts for 80.4% of Vietnam's total area and contributes 14% of GDP (GSO.GOV.VN). According to Vietnam Electricity, hydroelectricity accounts for more than 30% of the total electricity output of the whole national system, and there is further potential with a lot of unexploited capacity (GIZENERGY.ORG.VN).

The concept of hydrology mentioned in this study belongs to hydrometeorology which focuses on the water from the earth's surface to the whole atmosphere. If all the water in the atmosphere were to be condensed out, it would cover the surface of the planet only to an average of about an inch. However, it is like a TGV (Train à Grande Vitesse - in French - high-speed train) compared to the ocean circulation or water-ground transport and can move water around the globe (USGS.GOV). In this study, we are interested in the input, transport, and removal of water from the atmosphere.

In the hydrology budget, evaporation and transpiration are processes that change liquid water into vapour. The vapour is carried upward into the atmosphere by rising air currents. It then condenses into clouds due to cooler temperatures aloft where strong winds move clouds travelling around the world until the water falls as precipitation. It is worth noting that just about 10% of the precipitation comes from transpiration, and 90% of water in the atmosphere is supplied by evaporation (USGS.GOV). Among that, precipitation or rainfall is considered a key part of the hydrology budget that has the most impact directly in economic and social sectors all over the world. For example, Vietnam is shown in the report on Climate Risk from The World Bank Group and the Asian Development Bank that its social and economic losses are mainly attributed to natural disasters including floods, storms, and droughts in Vietnam during 1900-2020 in Figure 1. They indicate in detail that Vietnam is a country with extremely high exposure to flooding - ranked 1st, as well as tropical cyclones and their associated hazards - ranked 8th. Followed by Drought, this exposure is ranked 82nd but is still significant as highlighted by the severe drought of 2015–2017 (worldbank.org, a).

Improvement of our knowledge about precursors of extreme events as well as prediction quality through increasing the range of forecasts is an essential domain of research to improve people's daily lives and contribute to national defence and security. As recorded by the National Hydrometeorology Centre, that drought - the worst drought in 90 years was caused by the strong 2015-2016 El Niño which is one of the longest in the last 60 years as reported by FAO (2016). In 2015, natural disasters were fewer in number but the impact intensity of

some events was at a record high. The central region of Vietnam suffered serious drought over many months and the rains came in late autumn with less than 30-50% of the previous period. This devastated the rice crop as well as gave rise to warnings for capacity in hydroelectric dam basins which decreased by 25% compared with the previous year (FAO, 2016).

Disaster Type	Disaster Subtype	Events Count	Total Deaths	Total Affected	Total damage ('000 US$)
Drought	Drought	6	0	7,860,000	7,399,120
Epidemic	Others	1	16	83	0
	Bacterial disease	1	598	10,848	0
	Parasitic disease	1	200	0	0
	Viral disease	8	395	97,027	0
Flood	Others	16	1,012	2,011,287	160,055
	Coastal flood	6	804	4,353,316	749,000
	Flash flood	13	481	912,607	516,700
	Riverine flood	52	3,644	25,637,158	2,896,407
Landslide	Avalanche	1	200	38,000	0
	Landslide	4	109	40	0
	Mudslide	1	21	1,034	2,300
Storm	Others	10	323	219,280	145,035
	Convective storm	8	160	4,513	10,100
	Tropical cyclone	92	18,869	53,272,568	9,967,657

Figure 1: Summary of Vietnam natural hazard reported in worldbank.org (a)

From the atmospheric science's point of view, the motion occurs at various scales, and different dynamic atmospheric processes can be identified in terms of space and time scales as shown in Figure 2 from Laing and Evans (2011). According to the spatial scale, four categories can be defined. The microscale is the study of atmospheric phenomena on a scale of about 1 kilometre or less. For example, local turbulence caused by buildings and other obstacles (such as individual hills) is presented on this scale. The mesoscale is the study of atmospheric phenomena that have horizontal scales ranging from 1 km to 100 km. Mesoscale systems last from less than a day to several days. The events typically of interest are tornadoes, thunderstorms, fronts, precipitation bands in tropical and extratropical cyclones, and topographically generated weather systems such as mountain waves and sea and land breezes. The Synoptic Scale is focused on the changes at scales up to 1000 km and up to a month in time and space. At this scale, the Coriolis acceleration plays a main role in predictions of moving air masses. The phenomena typically described by synoptic meteorology include events such as extratropical cyclones, baroclinic troughs, and ridges. At the global scale is the study of weather patterns related to the transport of heat or very-large-scale oscillations with the time period in order of months like the Madden-Julian Oscillation or years like El Niño–Southern Oscillation.

Under the seasonal timescale, intraseasonal processes including Madden Julian Oscillation, planetary waves, and Tropical Cyclones are considered typical patterns of variability in this range. These processes have a spatial scale of 10^5 to 10^8 km, and a time-scale range from

weeks to months. It shows that both the timescale and the space scale are quite distinct from seasonal processes. Therefore, extremes are often related to different physical processes than those that govern long-term means. The factors leading to abnormal intraseasonal variability might differ from the seasonal ones, and so need to be investigated further.

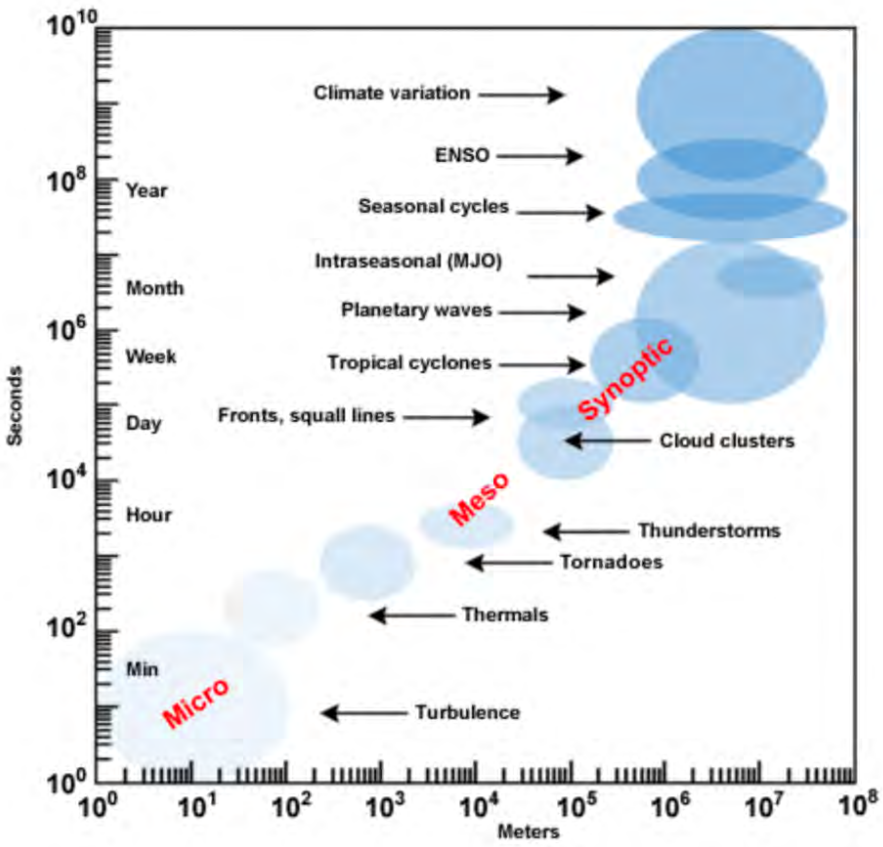

Figure 2: Space and time-scale of dynamical atmospheric processes presented in Laing and Evans (2011)

The variability of climate is then also considered over time and space scales. It is statistical information, a synthesis of weather variations focusing on a specific area for a specified interval with a long enough dataset - usually greater than 30 years. It is different from the weather variability that describes the day-to-day state of the atmosphere and its short-term (from hours to a few days) variations. The total variability of a time series can be decomposed into different timescales (as shown below). Then, the atmospheric processes associated with these timescales can be further investigated according to the objectives of the study.

Total variability = Climate variability + Weather variability (synoptic perturbation)

with: Climate variability = Trends + Annual cycle + Intraseasonal variability

For the hydrology over the whole of Vietnam, dominant trends for annual rainfall are downwards but are not statistically significant (Nguyen et al., 2014). The annual precipitation

cycle is conditioned by the impact of the Asian monsoon circulation and its reversal in wind direction. The annual variability of rainfall is normally attributed to the variability of the monsoon system, the topography, and ENSO (Nguyen et al., 2014). The presence of orography leads to a more diverse climate due to its impacts not only locally but also on a large scale with the monsoon circulation.

The intraseasonal variability of Vietnam's rainfall is of great interest and has been investigated in recent studies. Some studies show characteristics of ISV in specific time intervals associated with intraseasonal processes. These atmospheric processes could be influenced either by the tropics or the extratropics. Some investigate a certain event and then indicate the interaction of tropic-extratropic. All of them show the diversity of regions and the use of different rainfall criteria and timescales of consideration. There is a need to investigate the sensitivity of the conclusions to such considerations. In addition, until now, there is still a lack of research about the hydrology budget associated with intraseasonal variability.

In this context, the main objective of this work is to investigate the hydrology budget and tropical and remote dynamical influences on Vietnam rainfall intraseasonal variability in different scales by different approaches.

The first chapter will introduce the characteristics of Vietnam's rainfall climate including the annual cycle and intraseasonal variability. The annual cycle of Vietnam's rainfall is presented first with the annual patterns, the topography, and the hydrology budget. Then we present the large-scale circulation directly controlling the annual cycle as well as the concept of the linkages to large-scale forcing. Then the intraseasonal variability of rainfall including a statistical description of the timescale and physical characteristics will be shown according to previous studies. This is followed by a literature review about possible influence factors of Vietnam's rainfall intraseasonal variability. Finally, the objectives and approaches of this thesis are listed, followed by the outline of the manuscript.

Figure 3: Dry anomaly event in Gialai-CVN in the period of May - Jul 2020. Source: VOV.vn

Figure 4: Wet Anomaly event in Hatinh-CVN in September 2022. Source: BaoHaTinh.vn

Chapter 1

Introduction of Vietnam Rainfall

Contents

This chapter will introduce the characteristics of Vietnam's rainfall climate including the annual cycle and the intraseasonal variability. The annual cycle of Vietnam's rainfall is present first with the annual patterns, the topography, and the hydrology budget. Then we present the large-scale circulation directly controlling the annual cycle as well as the concept of the linkages to large-scale forcing figured out. After that, the intraseasonal variability of rainfall including the statistical description of timescale and physical characteristics is shown according to previous studies. It is followed by a literature review about possible influence factors of Vietnam's rainfall intraseasonal variability. Finally, the objectives and approaches, followed by the outline of this manuscript are presented.

1.1 Vietnam Rainfall Annual

Vietnam is located between 8°27'N and 23°23'N in the tropics but also extends into the extratropics. It is well known that Vietnam is directly impacted by the Asian monsoon system - a planetary phenomenon - typified by the seasonal reversal of atmospheric circulation and precipitation associated with the thermal contrast in east-west or land-sea heating. Furthermore, it is considered a much more complex character of rainfall than other regions as it is in a transition region between three distinct sub-systems of Asian summer monsoon: India, East Asia, and Western North Pacific (Wang and LinHo, 2002). Vietnam's rainfall shows diversity in the subregional annual cycles.

In this section, the rainfall annual cycle over Vietnam subregions is described. The general characteristics of the hydrology budget and topography complexes are indicated as background. We will also present our current knowledge about the large-scale circulation associated with the rainy season including the Asian Summer Monsoon onset and withdrawal date, and the linkage to the large-scale forcings.

1.1.1 Annual rainfall pattern

The climatological extended winter (November - April) and summer (May - October) rainfall patterns over the Asian Monsoon region including Vietnam are summarized as in Fig 1.1a & b. It is distinct between Vietnam's summer and winter precipitation due to spatial rainfall distribution.

The winter precipitation pattern is mainly located in a narrow band from 15S to 10N with the peak of rainfall over the Maritime Continent and Western South Pacific (Fig 1.1a). It is dry, but not over the whole country. There is a small area along the Vietnam coast which has rainfall of about 4 mm/day. Over the South China Sea, the rainfall is still high intensity with a maximum of 8mm/day. North Vietnam rainfall associated with the south of China has a small amount of rainfall. The summer pattern moves to the North and becomes stronger from 10S to 25N and shows retraction of rainfall spatial scale. It shows the strong peaks of rainfall over the bay of Belgian and Southeast Asia. The summer rainfall patterns

over Vietnam show a stronger rainfall amount over the Southern area - 8mm/day - than the Central and the North 6mm/day.

Based on the Koppen climate classification (Köppen, 2011), Vietnam is usually divided into 8 sub-regions: 7 mainland sub-regions and an island area. The annual rainfall cycle over the subregions shows a great diversity as shown in Fig 1.2 (Nguyen et al., 2014).

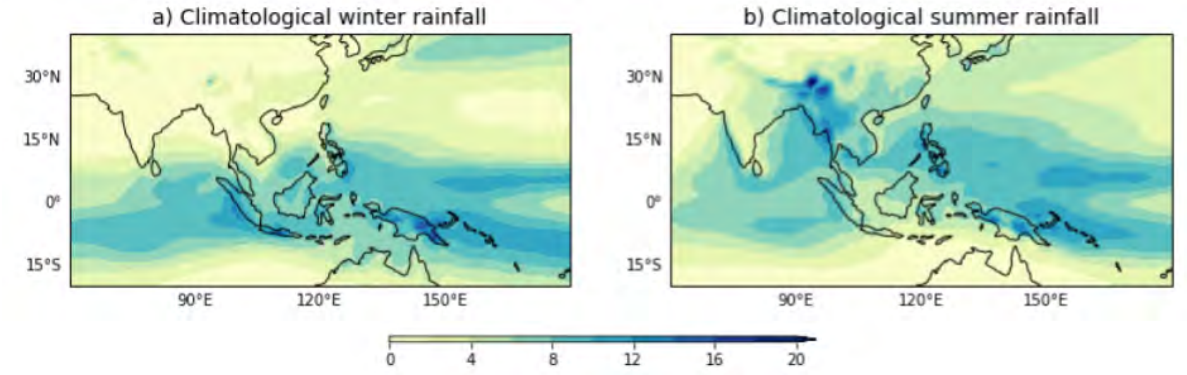

Figure 1.1: Climatological mean precipitation (mm/d) during (a) boreal winter - DJF and (b) boreal summer - JJAS rainfall over Asian Monsoon region. Derived from FROGs - ERAi 1979-2017 resolution 1x1 degree (Roca et al., 2019).

Northeast, Northwest, and Red River Delta (N1-N3) in Fig 1.2 b,c & d subregions show some similarity in the annual cycle of rainfall which peaks in July-August. These subregions have rainfall from May to September. Monthly rainfall varies from 200 to 300 mm per month during the rainy season, while during winter-time from November to February, it is less than 50 mm per month. The peak of rainfall shifts gradually from July to August associated with N1 to N3 (from the west to the east). The rainfall gradually increases from December to the peak in N3 rather than N1 and N2.

Although these regions have an extension of nearly 4 degrees of latitude for each, the North and South Central Coast region (N4 and S1) in Fig 1.2 e,f show similarity with the peaks of rainfall in October with intensive monthly rainfall of nearly 600 mm for N4, 500 mm for S1. These show a great amount of rainfall from August to November, N4 is slightly greater than S2 in all months. From May to July, the monthly rainfall is less than 200 mm, and then it suddenly increases during the summertime. Rainfall totals are greater than for the previous three subregions, both in summer and winter.

Located at the same latitude as the S1 region, the Central Highland region - S2 in Fig 1.2 g shows different characteristics in the monthly rainfall annual cycle with a relatively high rainfall intensity in the period of June-September. Rainfall during wintertime from December to March is very low but grows sharply in May. The annual cycle has two peaks: one in May, and another in October.

Southern Vietnam - S3 region in Fig 1.2 h is located from 8.5N to 12N. The annual cycle shows high-intensity rainfall from May to October. It is not much different from the Red River Delta subregion - N3 in terms of cycle. The dry period only occurs within boreal wintertime

Dec-Feb, then April has a monthly average rainfall of 150 mm.

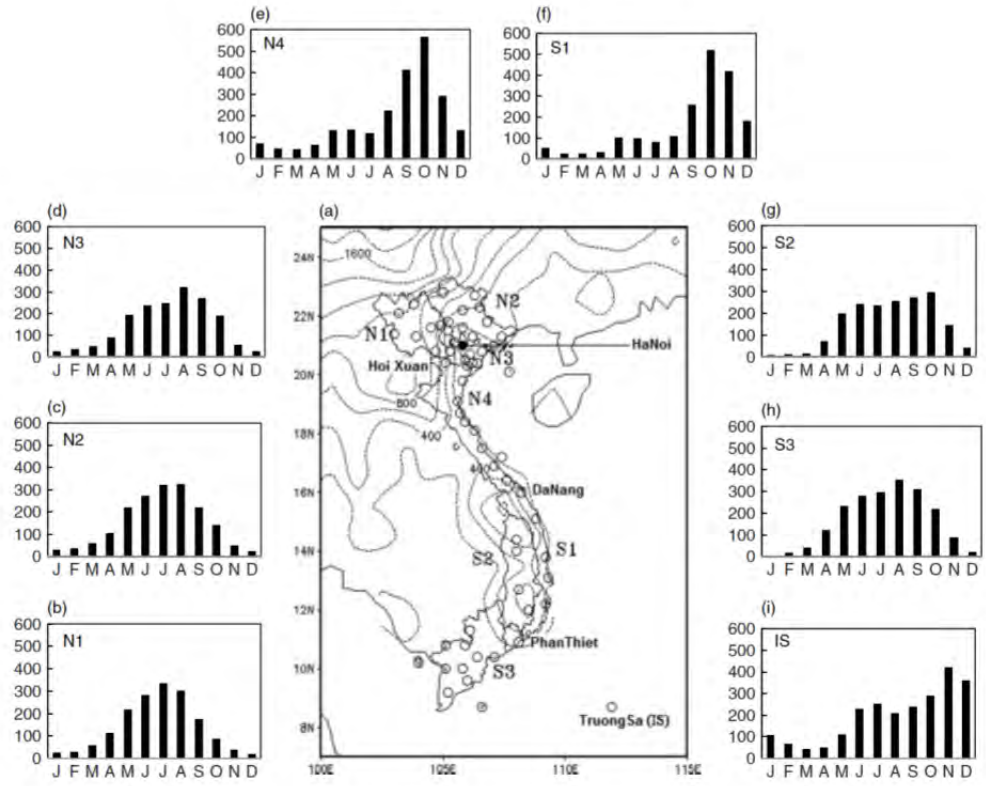

Figure 1.2: Distribution of meteorological station and the elevation in contour line in meters (a) and (b-i) Monthly average of annual rainfall cycle over Vietnam subregions N1, N2, N3, N4, S1, S2, S3 and IS using rain gauge data taken from Nguyen et al. (2014).

The island area in Fig 1.2 i - Nguyen et al. (2014) shows that it is located far away from the mainland - in the central South China Sea close to the equator. It is very different to other subregions. Monthly rainfall averages less than 100 mm per month from February to March. The months with intensive rainfall are from June to December.

The division of Vietnam into subregions for large-scale study has been formalized. Normally, three subregions are considered: North, Central, and South. Particularly, North Vietnam includes N1-3, the Central N4 and S1; and the South Vietnam S3 eg, Truong and Tuan (2018, 2019); Nguyen et al. (2014). Most studies carefully extract the S2 Central Highland and consider it as a specific case due to the local rainfall mechanism. The rainy season over Vietnam subregions is usually considered from May to Oct for North and South Vietnam, but from June to November for Central Vietnam.

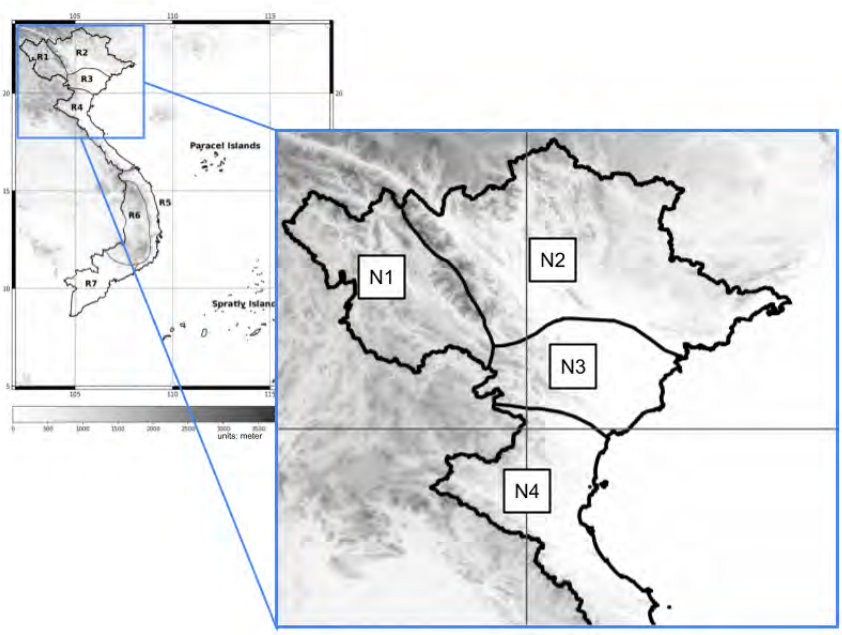

Figure 1.3: The elevation in grey shaded in meters. N1, N2, N3, N4 as in Fig 1.2.

1.1.2 Topography

The complexity of Vietnam's terrain is a major factor leading to differences in rainfall annual cycle between subregions, following research on regional and large scales. Tran (2005) summarized the basic characteristics of Vietnam subregion climate including the topography impact.

It indicates the difference in the terrain between three subregions over the North Vietnam N1-3 that lead to the differences in the peak of the annual cycle and its evolution Fig 1.3. Particularly, the Northwest subregion N1 is the area with the highest elevation on average in Vietnam with ranges of Mountains in the NW-SE direction whereas the Hoang-Lien-Son range has peaks of more than 2000-3000 m and is located in the middle of the subregion. The Northeast N2 subregion has a lower elevation compared with N1, but still high. It has 4 small ranges of mountains with an arc direction opening to the northeast. It could interact with monsoon winds to lead to the latter peak of rainfall in August for N2. For Red River Delta N3, this mostly flat area leads to an annual cycle having variations that do not show rapid changes.

North and South Central Coast regions N4 and S1 have similar terrain. On one side is the South China Sea, and on the other is the Truong Son mountain range which is divided into the northern range and southern range by a small range Bach Ma. The Central Highland S2 is located at the same latitude as S1 but has a higher elevation than S1. Southern subregions - S3 including the Mekong River delta have relatively flat terrain and lower compared with S2.

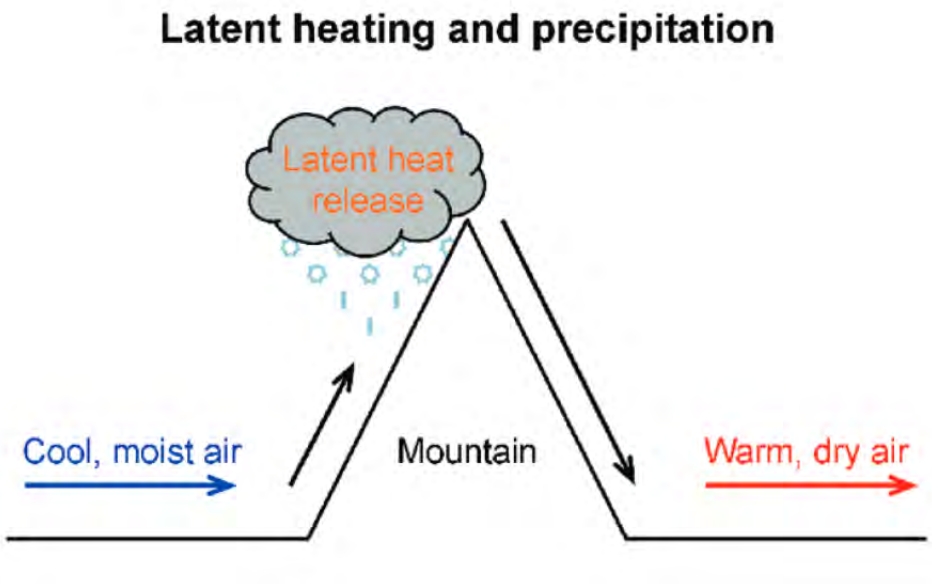

Figure 1.4: Schematic of latent heating and precipitation of winds in the lee of a mountain range. As shown in Elvidge and Renfrew (2016).

The mechanism usually invoked for Central Vietnam subregions to explain the difference in their regional climate and rainfall annual cycle is the Foehn effect. It is summarized in Elvidge and Renfrew (2016) as a warm and dry wind descending in the lee of a mountain range. Fig 1.4 shows a schematic of the winds with cool and moist air blowing from one side of the mountain that leads to warm and dry air winds descending on the other side. This is why during June-July-August over Central regions we have relatively low rainfall amounts. It leads to the delay of the rainy season in Vietnam's Central subregions with the peak of rainfall normally in October.

1.1.3 Hydrology Budget

Precipitation is a dominant term in the hydrology budget for the evolution of water vapour in the atmosphere. The availability of moisture in the air associated with rainfall amount during a season also depends on the large-scale circulation and associated flux of water vapour. Depending on the research problem, the hydrology budget is expressed in terms of various balances. In this study, we follow the conservation of water in the air for the following expression of the hydrology budget. In the sigma vertical coordinates where:

$$\sigma = \frac{p - p_{top}}{p_{surface} - p_{top}} \tag{1.1}$$

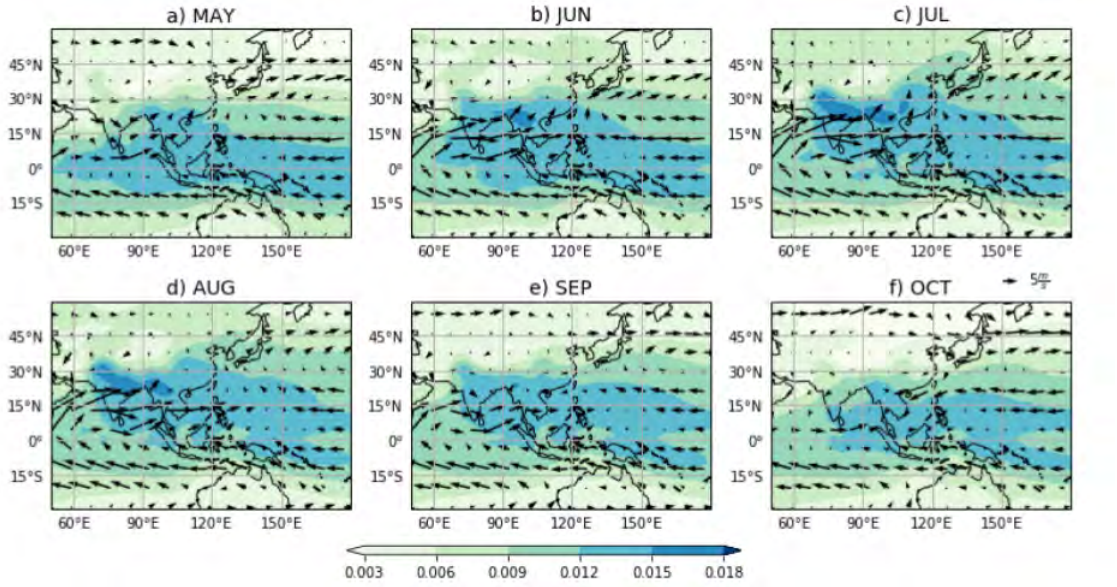

Figure 1.5: Water vapour and winds at 850mb from May to Sep during 1979-2016 ERA-Interim.

We have:

$$\frac{1}{g}\int \frac{dq}{dt}d\sigma + \frac{1}{g}\int \bigtriangledown(q.V)d\sigma = E - P$$

$$TMC = \frac{1}{g}\int \frac{dq}{dt}d\sigma$$

$$VIMC = -\frac{1}{g}\int \bigtriangledown(q.V)d\sigma$$

$$TMC - VIMC = E - P$$

There are four terms in this hydrology budget: the tendency of total moisture in the column, the vertically integrated moisture flux convergence, evaporation, and precipitation. These four terms are balanced at any given time in the atmosphere. The source of water in the air comes from the evaporation processes and the sink comes from precipitation.

Besides evaporation and precipitation, the vertically integrated moisture flux convergence (VIMC) is a scalar quantity computed from winds and moisture. From the mathematical expression, Sohn et al. (2004) states that it could present directly the link between the hydrological cycle and the associated large-scale circulation. Banacos and Schultz (2005) suggests the VIMC could be a good indicator for rainfall in mid-latitude cyclones. For this utility, they have to invoke the assumption that evaporation E is small and the local changes in water vapour content are mainly attributed to synoptic-scale systems. Chansaengkrachang et al. (2018) show that the VIMC has a high positive correlation with the daily rainfall over Thailand, a tropical country with a similar latitudinal extent to Vietnam.

Fig 1.5 shows the monthly climatology of water vapour at 850 mb during the extended summer from May to October. The moisture zone spreads along the Equator and extends up to 25N in May. Vietnam is in a humid tropical zone with climatological southwesterly summer monsoon winds that favour rainfall. Both the winds over India and moisture become stronger and show maximum during June - August. Winds and moisture over the Western North Pacific extend into the South China Sea region mostly in late summer. The Bay of Bengal and the Western Pacific are the main sources of moisture for the rainfall over Vietnam during the summer.

Previous studies also indicate that there is a close relation between rainfall and column-integrated water vapour in the tropics, eg., Holloway and Neelin (2009). It is not unexpected that there is a positive relationship between rainfall and humidity because deep convection and rainfall may both be caused by and result from high humidity. But the expected feedback is in both directions (Holloway and Neelin, 2009). So convection can moisten the column via moisture convergence, detrainment, and evaporation, while the increased column moisture could play a causal role in enhancing convection by allowing entraining plumes to maintain higher buoyancy in the lower-troposphere Holloway and Neelin (2009).

In the intraseasonal timescale, Mapes et al. (2006) demonstrate that the positive moisture anomalies of the moisture column increase at lower levels a few hours before and close to the time of the maximum rainfall, then decrease several hours afterwards. These studies imply that a high moisture column frequently precedes precipitation, and is not passively related to heavy rainfall but involved in the mechanism for producing it. Holloway and Neelin (2009) deduce a mechanism for the column water vapour - precipitation relationship. They demonstrate that a buoyancy increase that leads to deep convection is significantly influenced by the greater lower tropospheric humidity values.

1.1.4 Large-scale Circulation - Asian Monsoon

The Asian Monsoon is characterized by the seasonal reversal of atmospheric circulation and rainfall, and it exerts a controlling influence on the rainfall over Vietnam. Figure 1.6a,c and b,d shows the upper and lower tropospheric circulation associated with winter and summer monsoon seasons, depicting the changes in atmospheric circulation known as the southwest monsoon winds during summertime and northeast monsoon winds during winter time (Lau and Waliser, 2011).

The summer monsoon winds are typically hot and humid. At the low levels, the circulation (Fig 1.6 b) is characterized by the Asiatic Low over the northern Bay of Bengal. The westerly winds at low levels are strong in the tropics, at 850 hPa over the Arabian Sea, known as the low-level westerly jet. There is also large-scale cyclonic vorticity extending from the northern Bay of Bengal to western India known as the monsoon trough. At upper levels, there is an easterly jet (Fig 1.6 d) centred around 5N and the Tibetan anticyclone centred over the monsoon region during northern summer.

In the winter monsoon, the winds at low levels during the winter monsoon season are

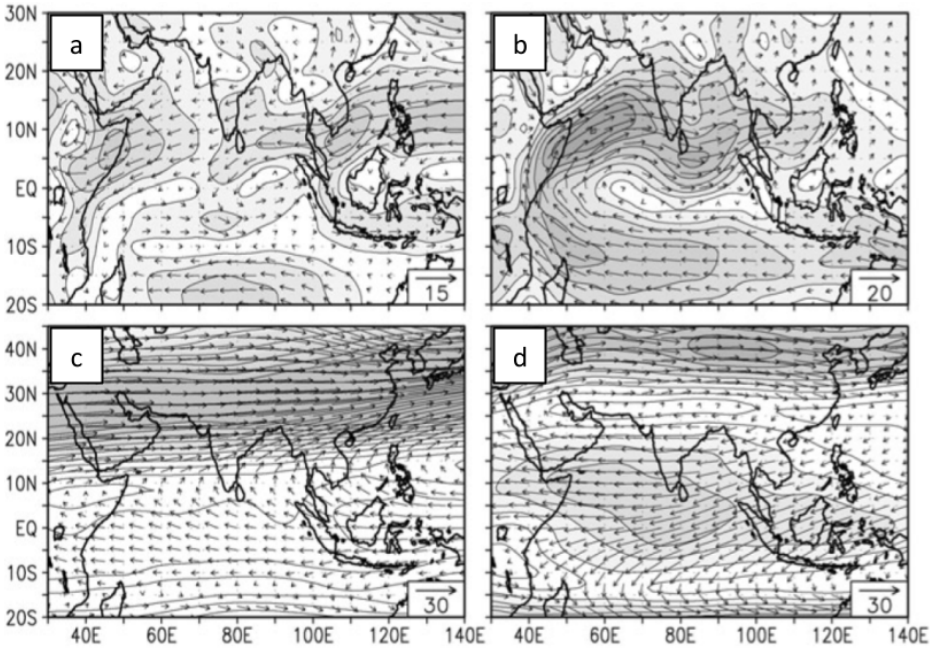

Figure 1.6: Taken from Lau and Waliser (2011)-chapter2- B.N. Goswami: Climatological winds 850mb with isotach IC 2m/s based on CMAP during (a) boreal winter (DJF) and (b) summer (JJAS). (c) and (d) same as (a) and (b) but for winds at 200mb with isotach IC 5m/s.

reversed compared with summer. The low-level circulation pattern changes from cyclonic to anti-cyclonic and the polar front moves southwards. A surface high-pressure system then develops over East Asia. In the upper atmosphere, the equatorial easterlies are weak and confined between 5N and 10S while the subtropical westerlies intrude to 10N during northern winter (Figure 1.6 a). The subtropical westerlies recede to the north of 30N during northern summer and a strong easterly jet characterizes the equatorial upper atmosphere in the region (Figure 1.6 c).

A widely used definition of the rainy monsoon season is presented in Wang and LinHo (2002). Using only rainfall as a uniform criterion for the Asian-Pacific Monsoon region, the domain of the summer monsoon rainy season is defined by the relative pentad mean rate. The relative climatological pentad mean rainfall rate is used to define the onset, peak, and withdrawal of the rainy season.

Fig. 1.7 depicts the start and end dates of the monsoon rainy season over the Asian-Pacific area. The Bay of Bengal's southeast region has the earliest onset, according to the map of the onset date. The pre-mei-yu season then begins over Taiwan, Japan, before moving northeastwards and passes through Vietnam in early May (P25–P26) and the subtropical Western North Pacific by P29 Fig. 1.7 a. A rainband on a planetary scale is then formed. The directions of rain-belt propagation are depicted as grey arrows over the Indian Ocean, the Bay of Bengal, and the North Western Pacific, extending from south to north. Over the Central Pacific, the onset date (P40) is much later with the eastward moving rain belt.

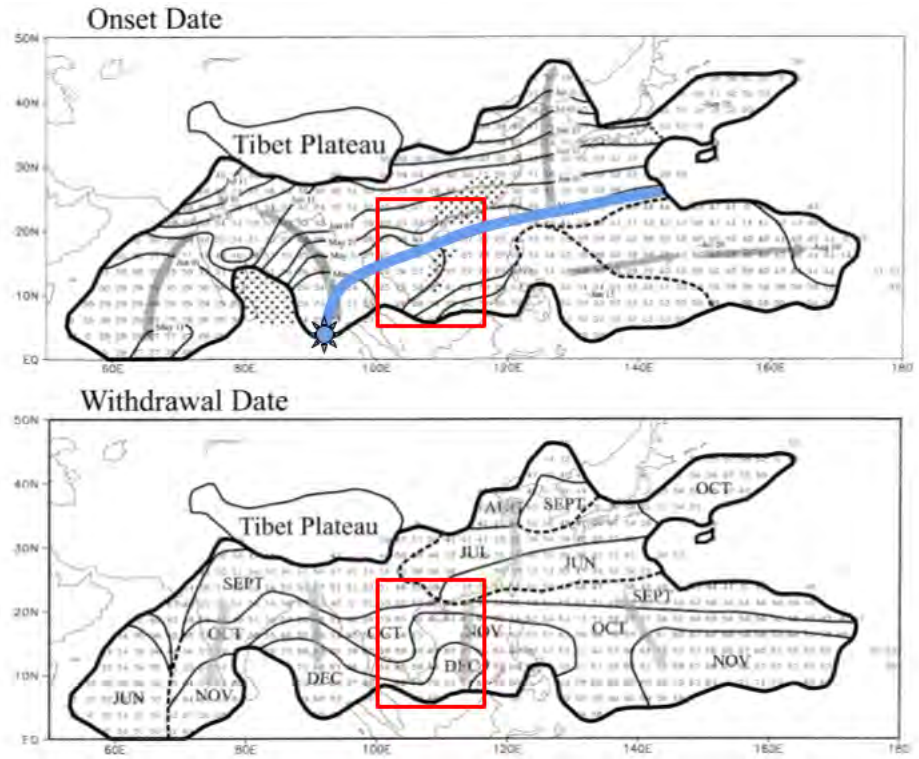

Figure 1.7: The upper- a) Onset date: The thick dashed lines denote discontinuities (merger of three or more contours). The arrows point in the direction of rain-belt propagation. The thin dashed line divides subtropical monsoon and oceanic monsoon regions; and The bellow- b) withdrawal date: The arrows also indicate where the rain belts migrate. Adapted from Wang and LinHo (2002).

The trend of climatological withdrawal date of the monsoon is shown in Figure 1.7 b. Since it is driven by the same onset of the rain belt, the rainy season over the central Arabian Sea ends early. This early end is partly attributable to the Arabian Sea's quick cooling in the west and centre following the breakup of the Somali jet (Wang and LinHo, 2002). In East Asia, the monsoon rainy season retreats in a northward direction that resembles the onset pattern. This distinctive feature arises from the fact that the western Pacific subtropical high and the monsoon front migrate northward during the beginning and end of the East Asian monsoon rainy season, respectively. The rainy season gradually moves southwards across the tropical monsoon zones. It often gets longer as you get closer to the equator. In particular, the southeast Bay of Bengal experiences around 7 months of rainy season.

The peak rainy season generally occurs during four distinct times in Fig. 1.8. The earliest peak occurs between 26 May and 9 June across the southern Arabian Sea, the southeast Bay of Bengal, and in the subtropics from the southeast coast of China to the south of Japan. The second peak occurs in the China-Japan region, the central South China Sea, and the southwestern Philippine Sea in late June. The third phase crosses India and northeastern continental Asia between P40 and P42 in the second part of July. The peak of the rainy season in the Western North Pacific occurs during the fourth phase, which runs from 5 to 19

August (P44-P46). It is consistent with Wang and LinHo (2002) that the convention centres shift from the Indian monsoon zone to the Western North Pacific monsoon region in July and August. Additionally, the rainy season peaks in mid to late September across the southeast part of the Western North Pacific and the northeast of Japan (P52–P55). As highlighted

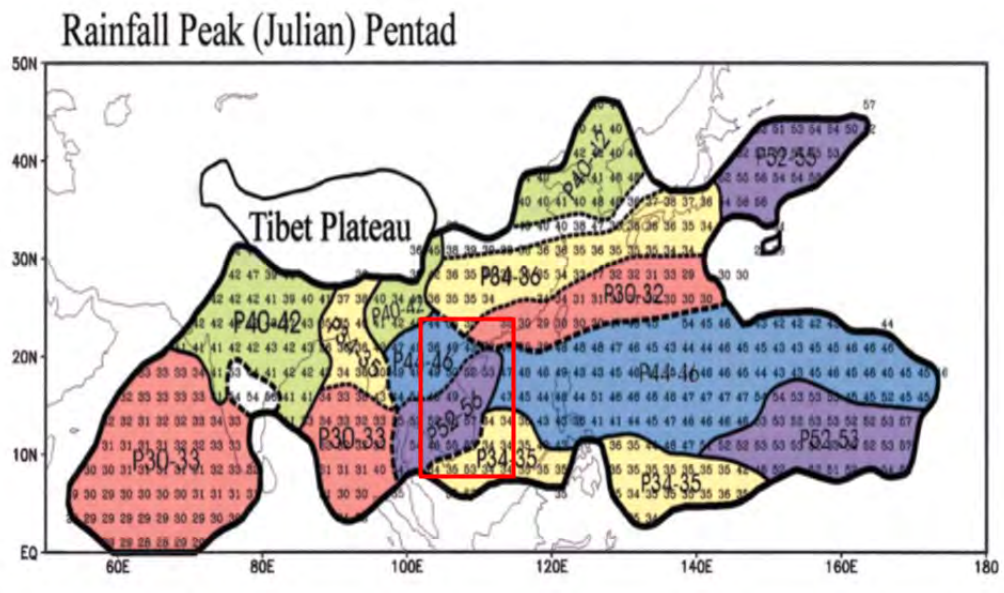

Figure 1.8: The timing of monsoon rainfall peak: the Julian pentad during which the annual maximum rainfall occurs. The thick dotted lines indicate strong discontinuities. The rainfall peak pentads can be divided into four periods in the boreal summer, coloured by light red (p30-33), yellow (p34-36), green (40-42), blue (p44-46), and one period in boreal autumn, purple (p52-56). Taken from Wang and LinHo (2002).

by the red box in Fig 1.7 a,b, the climatological onset and withdrawal of the monsoon rainy season over Vietnam do not progress continuously from south to north as in other nearby regions. Near the coast, the onset is later than inland. For example, South Vietnam has the onset date in P32, while North Vietnam's onset is in P29 and over the Red River Delta the onset is in P32. The withdrawal date over North Vietnam occurs earlier than elsewhere. The northern side of North Vietnam has a monsoon withdrawal in September, and the southern side in October. Central and South Vietnam are in regions with the withdrawal date in November. The monsoon rains peak over North Vietnam in P42-46, while the rest of the country experiences peak monsoon rain in P52-56.

Combining precipitation characteristics of the Asian-Pacific region and the change in circulation between summer and winter, the Asian monsoon systems can be divided into three sub-systems following Wang and LinHo (2002) as shown in Fig 1.9: Indian, East Asia and Western North Pacific summer monsoon. These systems have different rainfall characteristics as well as winds. The low-level winds in the Indian summer and Western North Pacific summer monsoons switch from winter easterlies to summer westerlies. In the Eastern Asian Subtropical Monsoon, low-level winds change from winter northerlies to summer southerlies. The southern edge of the Western Pacific subtropical High shows a notable discontinuity in the

rainy season's start, peak, and withdrawal patterns, but the Western North Pacific summer monsoon retreats equatorward after mid-September, and the East Asia summer monsoon gradually retreats poleward from June to early September.

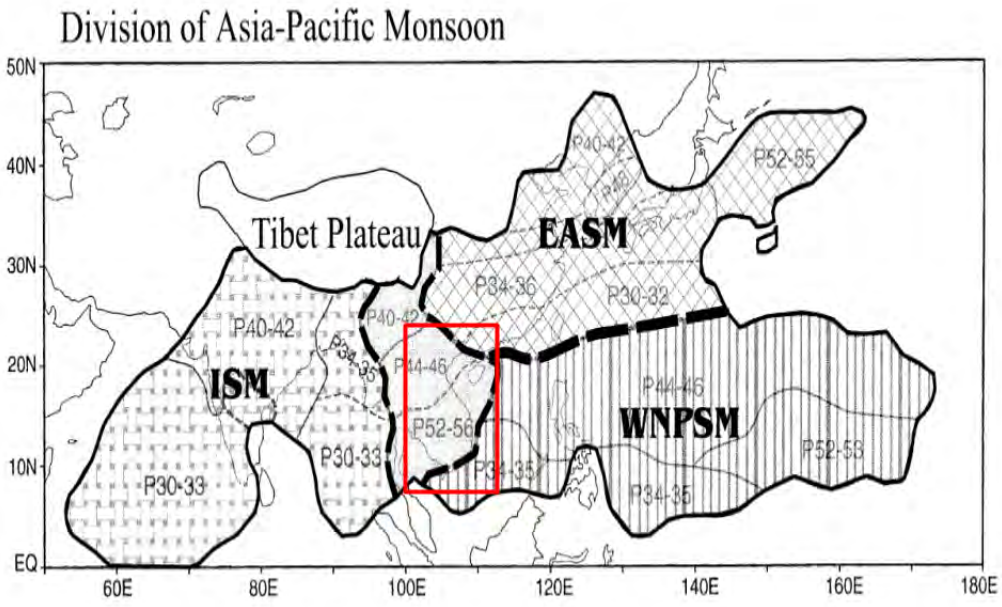

Figure 1.9: This map divides the Asian–Pacific monsoon into three subregions. The ISM and western WNPSM are tropical monsoon regions. A broad corridor in the Indochina Peninsula separates them. The subtropical monsoon region is identified as the EASM. It shares a narrow borderline with the WNPSM. Taken from Wang and LinHo (2002).

In Wang and LinHo (2002), they suggest that the difference in the peak of the rainy season is due to the shifting of the convection and diabatic heat source from the early summer to the late summer from the Indian Ocean to the Western Pacific zone. In addition, the considerable regional differences are primarily caused by the placements of the subsystems concerning the land-ocean arrangement as well as the thermal and dynamical impacts of the Tibetan Plateau. A very active southwesterly monsoon occurs across India as a result of the meridional land-sea thermal difference, enhanced Tibetan Plateau heat source effects, and the inter-hemispheric thermal contrast caused by differential solar radiation. A zonal pressure gradient between the Asian continental low and the oceanic Western Pacific subtropical High is frequently induced in the East Asia summer monsoon area by an east-west, land-sea heat difference.

Following the division above, there is a transition zone that includes Vietnam, where the character of changes in the wind and the timeline of the monsoon is much more diverse. The key distinction between this region and the others is the diversity at the peak of the rainy season and the onset patterns. The peak and withdrawal of the rainy season look like the Western Pacific zone, but the onset is far from resembling the Indian summer monsoon. In Nguyen-Le et al. (2014), the peak rainy month is shown, and the movement from north to south with time coincides with the southward migration of the subtropical ridge and intertropical convergence zone from July to September.

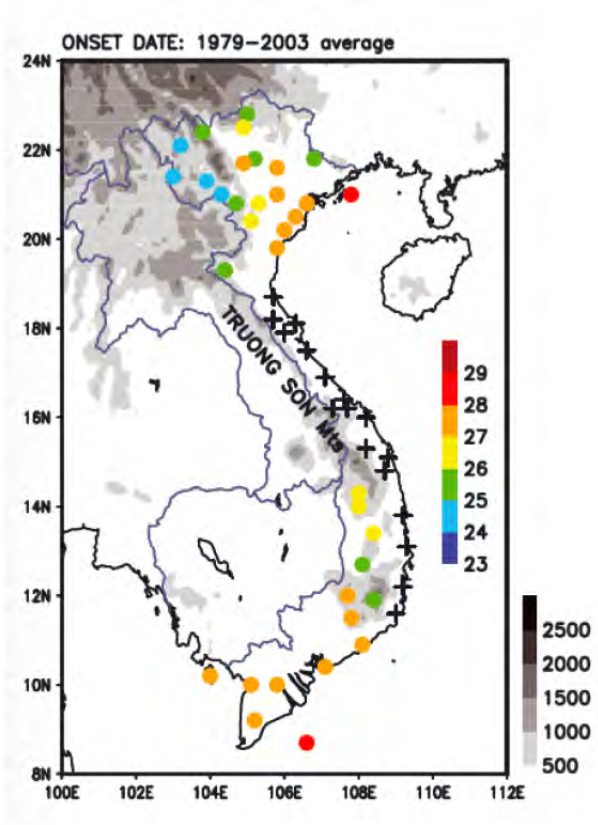

Figure 1.10: Onset date over Vietnam region taken from Nguyen-Le et al. (2014): Topography heigh is greyed (IC-500m) and climatological summer monsoon onset date (coloured dot, pentad number) at 54 stations in Vietnam. The cross denotes stations that have non-typical monsoon rainfall patterns.

Nguyen-Le et al. (2014) made a detailed study of the onset of the summer monsoon by subregion. Fig 1.10 shows the climatological onset date of the SEA monsoon over Vietnam. The subregion located in the northwestern mountains has the earliest onset of the summer rainy season in late April to early May, while the Red River and Mekong River delta in north and south Vietnam have monsoon onset in early to mid-May. Furthermore, they indicate that the rainy season over the central coastal plain is delayed until late autumn to early winter due to the influence of orography on the rainfall as discussed in the previous subsection. They suggest that the Foehn wind plays a role in modulating the monsoon to a dry rather than rainy season in the summer in Central Vietnam. Indeed, the southwest summer monsoon winds from the Bay of Bengal contain a lot of moisture that is blocked by the Truong Son northern range leading to rainfall on the west side of the mountain in Laos and a dry Foehn wind on the east side in Vietnam. The change in winds on one side could lead to impacts on the other side.

The Western North Pacific Subtropical High is known to play a role in modulating the variability of monsoon circulation (Wang and LinHo, 2002) inter. var. This could lead to many extreme weather and climate events such as floods, heat waves, and typhoons [e.g. Wu

et al. (2012); Cheng et al. (2020); Vu-Thanh et al. (2013)]. Wang et al. (2013) indicates the Western North Pacific Subtropical High is strongly associated with the variability of not only the monsoon circulation over East Asia but also tropical storms over the Western Pacific.

Fig. 1.11 shows the monthly climatological stream function and winds at low levels during the extended summer. The Western North Pacific subtropical high is shown in blue shading, and moves during summertime. In May, the subtropical high is strongest and closest to the Southeast Asia circulation. It moves to the east from May to September, then returns in October. The intensity decreases at the same time, but the easterly wind at low levels increases getting closer to the South China Sea.

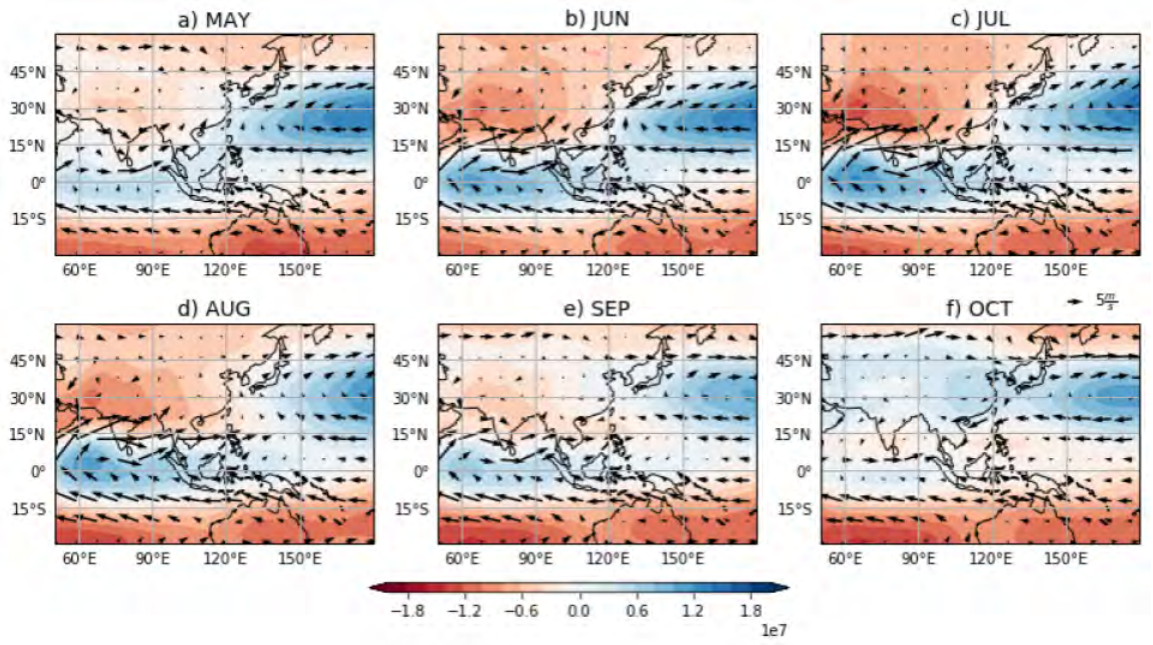

Figure 1.11: Monthly climatological stream function and winds at 850mb ERAi over Southeast Asia (Dee et al., 2011).

1.1.5 Linkages to large-scale forcing

In addition to the space-time scale separation for atmospheric processes discussed above, there is also a complex system of all interactions and feedback, schematized in Fig. 1.12. The consequence of Vietnam's rainfall is the diversity in the subregional annual cycle caused by linkages between the monsoon climate and the large-scale forcing.

As shown in Lau et al. (2000), the inter-linkages of a monsoon climate system have various components Fig 1.12. The monsoon is affected by fast systems which are internal atmospheric processes such as the moisture cycle in the atmosphere. In addition, the fast/slow - slow-intermediate system including the adjacent oceans and land processes also contributes to the variability of the annual cycle via for example SST, and heat fluxes. The "intraseasonal

variability" that links the fast and intermediate subsystems has been connected to the onset, breaks, and retreat of the monsoon.

Remote forcings from planetary scale events like ENSO and other long-term secular fluctuations of the global climate system, from decadal variability to global warming, have an impact on both the fast and intermediate subsystems. These external influences comprise the "slow" subsystem, which is external to the monsoon climate but may still have a significant impact on changing the fundamental characteristics of the monsoon atmosphere, the surrounding waters, and the land surfaces. These altered states may then lead to modulations of the probability distribution of monsoon states within the fast component. It is also plausible that the coupling of the fast and intermediate subsystems may influence the slow system.

Lau et al. (2000) particularly shows that the Southeast Asia monsoon as a component of the Asian summer monsoon acts as a hybrid monsoon system with multiple meridional cells and an extratropical extension of the meridional circulation. The dynamical characteristics are attributed to the strong interaction of the East Asian jet stream with tropical convection and extratropical disturbances. They suggest a role for extratropical dynamics that can impact the circulation on a global scale.

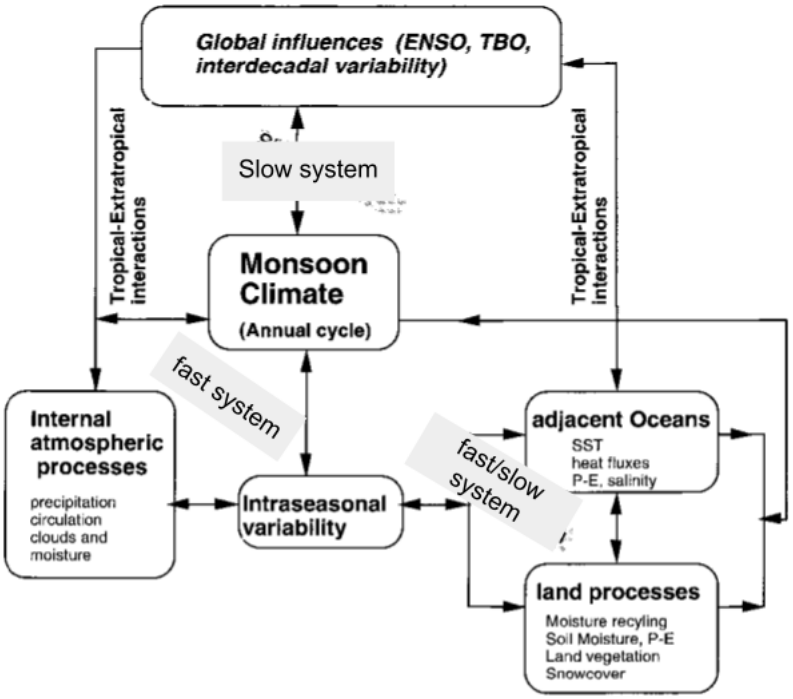

Figure 1.12: Schematic showing the various components and interlinkages of a monsoon-centric climate system. Taken from Lau et al. (2000).

On the annual timescale, ENSO as a large-scale forcing has an impact on the rainfall as well as the temperature over Vietnam, as described by Nguyen et al. (2014). They showed that the linkage between ENSO and the subregional climate is latitude-dependent through a correlation map between annual mean rainfall anomalies, SSTA and MLSP. On the other

hand, Lau et al 2000 found that the SEA circulation has a weak relationship with ENSO-related SSTA and suggested that the coupling of the SSTA in adjacent oceans might have contributed to monsoon processes and the moisture budget.

On the intraseasonal timescale, Wang and Xu (1997) uses a climatological pentad mean time series of OLR and winds, to study climatological intraseasonal oscillations and monsoon singularities: events that occur on or near a fixed date with some regularity. They find that these phenomena, particularly over the Western North Pacific, are connected to the progressive monsoon onset. They also emphasized that extreme phases of climatological intraseasonal oscillation are often related to summer monsoon singularities.

1.2 Vietnam Rainfall Intraseasonal Variability

Moving beyond the annual cycle of rainfall discussed in the previous section, Fig 1.13 gives an overview of the intraseasonal variations of rainfall over Vietnam in terms of the monthly mean. Across the seasonal cycle, the variability of monthly rainfall from 1971 to 2020 over the Vietnam mainland is considerable, especially during May-November - the rainy season. The dispersal is the largest in September and October. In the sub-seasonal timescale, Vietnam rainfall shows a great deal of variation, eg., Truong and Tuan (2018, 2019); Yokoi and Satomura (2005); Yokoi et al. (2007).

In this study, we use the decomposition of all the variabilities of rainfall with a timescale of less than a season - 90 days called rainfall intraseasonal variability. The rainfall intraseasonal variability can include extreme events such as drought, or floods, or longer or shorter periods significantly wetter or drier than the mean. It is often analysed by the statistical separation of intermittent timescales such as quasi-periodic oscillations from 30-60 days, a sub-monthly oscillation of 10-20 days and transient waves of 3-5 days that correspond to well-known atmospheric phenomena.

Generally, the rainfall ISVs are investigated through observational analysis to give a statistical description of the timescale of variation. Power-spectrum analysis is widely used to identify the spectrum of intraseasonal variability in the Vietnam rainfall data. For example, Truong and Tuan (2018, 2019) show two timescales of oscillation that have been previously identified for Vietnam rainfall ISV: 30-60-day and 10-20-day.

Through observation data, recent studies have further investigated the structure, mechanism and forcings according to each oscillation of Vietnam rainfall ISV eg., Truong and Tuan (2018, 2019); Wu et al. (2012); Tuan (2019). Composite techniques and Principal Component Analysis have been used mostly in these studies to describe the associated physical characteristics and also suggest the forcings. Some studies focus on certain extreme events that show atmospheric processes as well as the interaction of those associated with the events as driven factors. The factors of influences indicated to come from both Tropics and Extratropics. Theoretical research and modelling studies have also been used to identify remote sources, eg., Hoskins and Karoly (1981); Hoskins and Yang (2000). Remote sources can influence the

region through the theory of Rossby wave propagation.

In this subsection, the climatological characteristics of Vietnam rainfall ISV in observed analyses are presented. Our current knowledge of the possible influence factors for Vietnam rainfall ISV from observational and modelling studies is summarised.

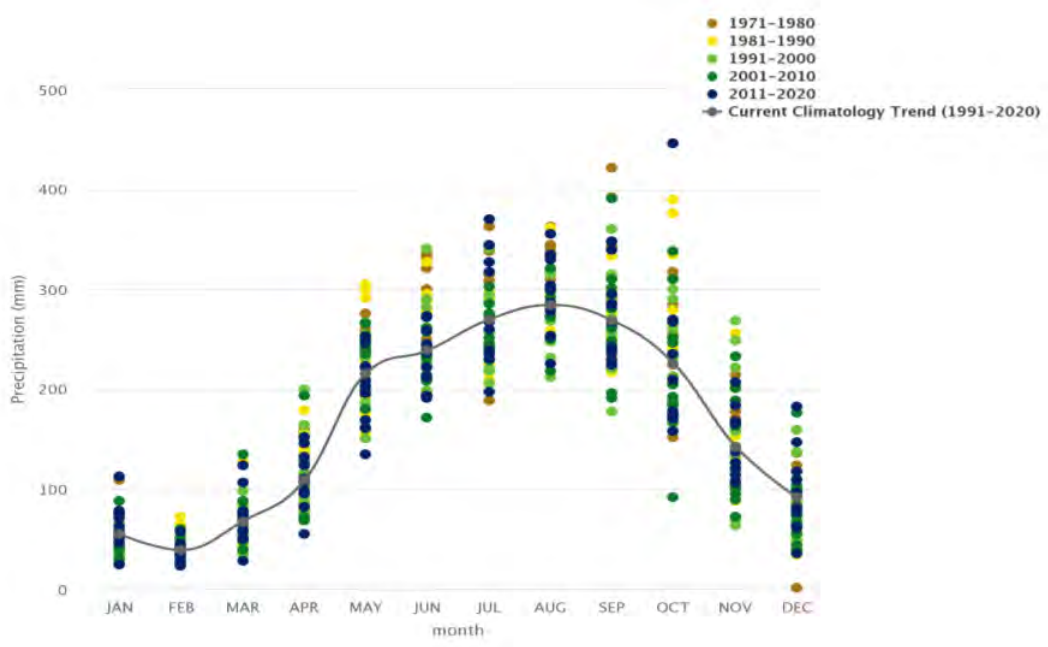

Figure 1.13: Variability of precipitation across seasonal cycle 1971-2020 worldbank.org (b).

1.2.1 Observed climatological characteristics

1.2.1.1 Timescale

As mentioned above, the intraseasonal variability of rainfall over Vietnam can be defined as the variation with a timescale of less than 90 days. The power-spectral analysis is an effective tool to characterise this variability by oscillations of particular periods. A Fourier analysis is applied ascribing the observed variation to the infinite number of small oscillations with a continuous distribution of periods. The plot of power spectral density (PSD) gives information on probable frequencies via peaks. The PDS of rainfall variation depending on the region study usually shows the complexity of the spectrum. The term "variation mode" is often used to refer to probable oscillations with a range of periods that are associated with peaks in the spectrum.

Timescales of 30-60-day and 10-20-day oscillation have been identified by Yokoi and Satomura (2005) and Yokoi et al. (2007) using a wavelet analysis of daily rain gauge data over the Indochina Peninsula inland. Yokoi et al. (2007) introduced an index called the active day ratio that is representative of the intraseasonal variability activity - ISV in a certain period as

the ratio of the number of days when the ISV wavelet power is statistically significant to the number of all days in the period during whole data examined. For the 30-60-day mode Fig 1.14, they indicated that the active day ratio on a bimonthly basis is much stronger during the summertime from May to October than in the winter. The 30-60-day mode is presented over the whole of Vietnam inland strongly from July to October, especially in central Vietnam.

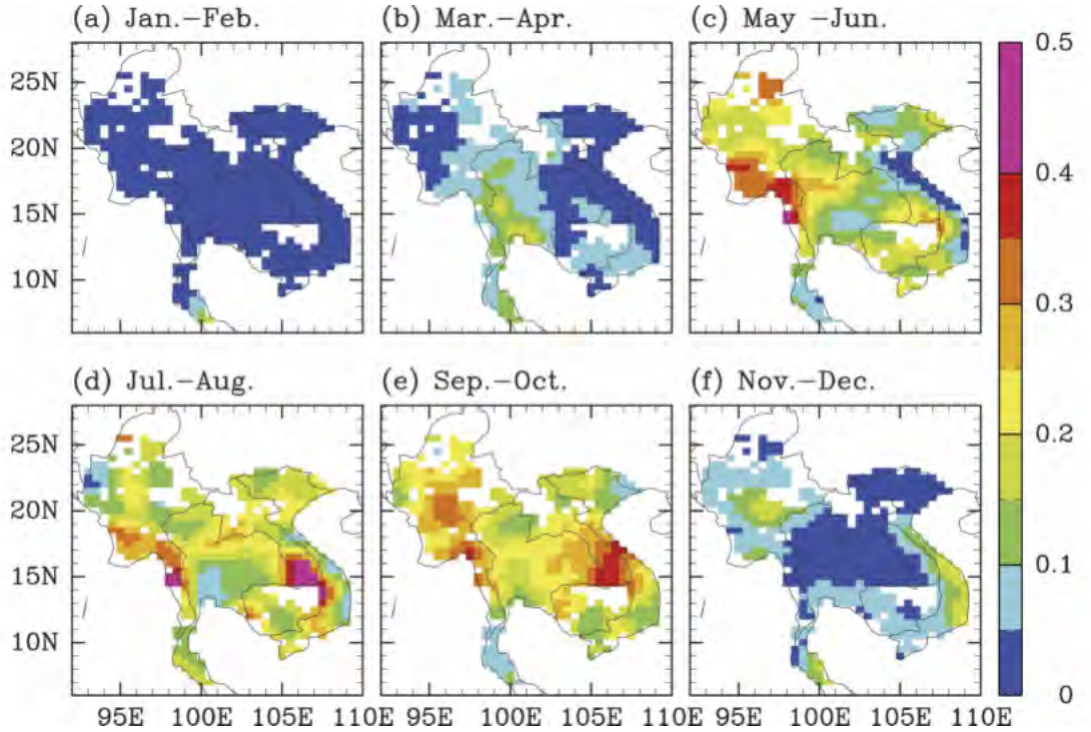

Figure 1.14: Taken from Yokoi et al. (2007): The Active Day Ratio - ADR of the 30-60 day variation on a bimonthly basis, which is defined in section 2c. The periods calculated are (a) Jan–Feb, (b) Mar–Apr, (c) May-Jun, (d) Jul–Aug, (e) Sept-Oct, and (f) Nov- Dec.

For the 10-20-day mode Fig 1.15, the active day ratio on a monthly basis shows strong activity over North Vietnam from May to October, especially in August. Central Vietnam is strongly periodic in October; while only North Central has high values in July - September and South Central in November. South Vietnam shows less active day ratio values over the year but is more active during May-November.

To be more particular, The Vietnam rainfall ISV has previously been characterized as two modes of variation that vary between subregions spatially and temporally. Truong and Tuan (2018) - TT18 and Truong and Tuan (2019)- TT19 have investigated the daily rainfall from selected stations. It displays significant variations on both time scale ranges in all Vietnam sub-regions. The 10-20 and 20-60-day period oscillation through variance spectra is calculated with 95% statistical significance in Fig 1.16.

Over North Vietnam, the spectrum of regional rainfall variance shows 2 groups of peaks, but they are not strongly separated over 10-60 days. The 10-20 day mode has peaks with the same variance as those of the 20-60 mode. Over Central Vietnam, two modes are also

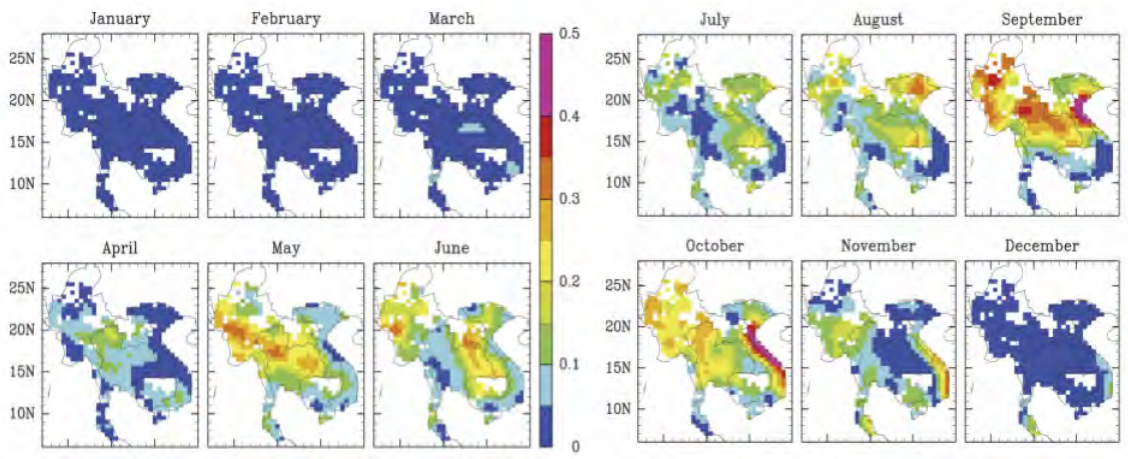

Figure 1.15: Taken from Yokoi et al. (2007): The ADR of the 10–20DV on a monthly basis. A 9-point smoothing has been applied to the ADR.

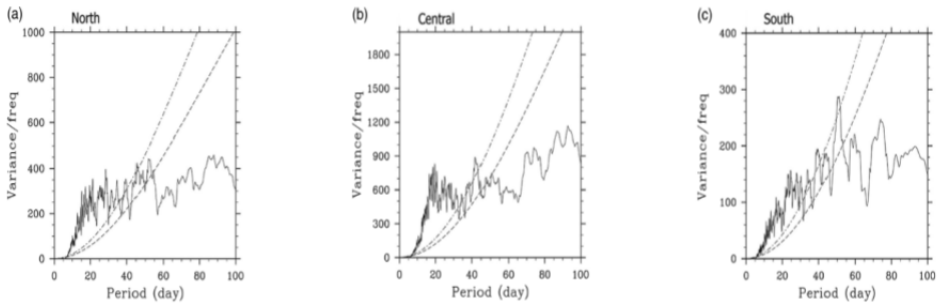

Figure 1.16: Taken from Truong and Tuan (2018): Variance spectra of the regional rainfall in the north (a), central (b), and south (c) Vietnam. The long-short dashed curve is the 95% significance level. The long dashed curve is the Markov red noise spectrum.

significant, but with higher variance according to the scale of the y-axis of variance/freq. Over South Vietnam, it is clear that the 20-60 mode is stronger than the 10-20 mode, although the variance is much less than two other regions. It is worth noting that the selection of stations that represent the sub-regions could influence the relative magnitude of the modes.

1.2.1.2 Spatial patterns

The temporal modes of 10-20 and 20-60-day intraseasonal oscillation (ISO) have been described in TT18 and TT19. The full cycles of oscillations are depicted and assembled to show the evolution of the 3D structure of cycles.

The spatial pattern of 10-20-day ISO has been shown in TT18 as shown in Fig 1.17. The 850-hPa composite analyses of winds and OLR - Outgoing Long wave Radiation as an indicator of deep convection and low-level circulation show the evolution of the 10-20

ISO mode of three subregional rainfall over Vietnam. Fig 1.17a-c stands for the North of Vietnam. The OLR signal and related circulation anomalies initially develop over the northern East China Sea and spread southwards to the sea between the Philippines and Vietnam. Truong and Tuan (2018) proposes the 10–20-day ISO in North Vietnam might originate from the extratropics. On the other hand, the anticyclonic and cyclonic gyres over the Philippines and nearby tropical seas are the principal disturbances responsible for the 10–20-day ISO in South Vietnam Fig 1.17g-i. It implies that South Vietnam has more impact from the tropics even though both subregions show an Equatorial Rossby wave-liked propagation westward. The 10-20-day ISO in Central Vietnam Fig 1.17d-f is controlled by nearly stationary oscillations of enhanced/suppressed convection that are in phase with the alternating presence of convergence/divergence brought on by zonal winds in the tropical western Pacific and meridional winds along the East Asian coast.

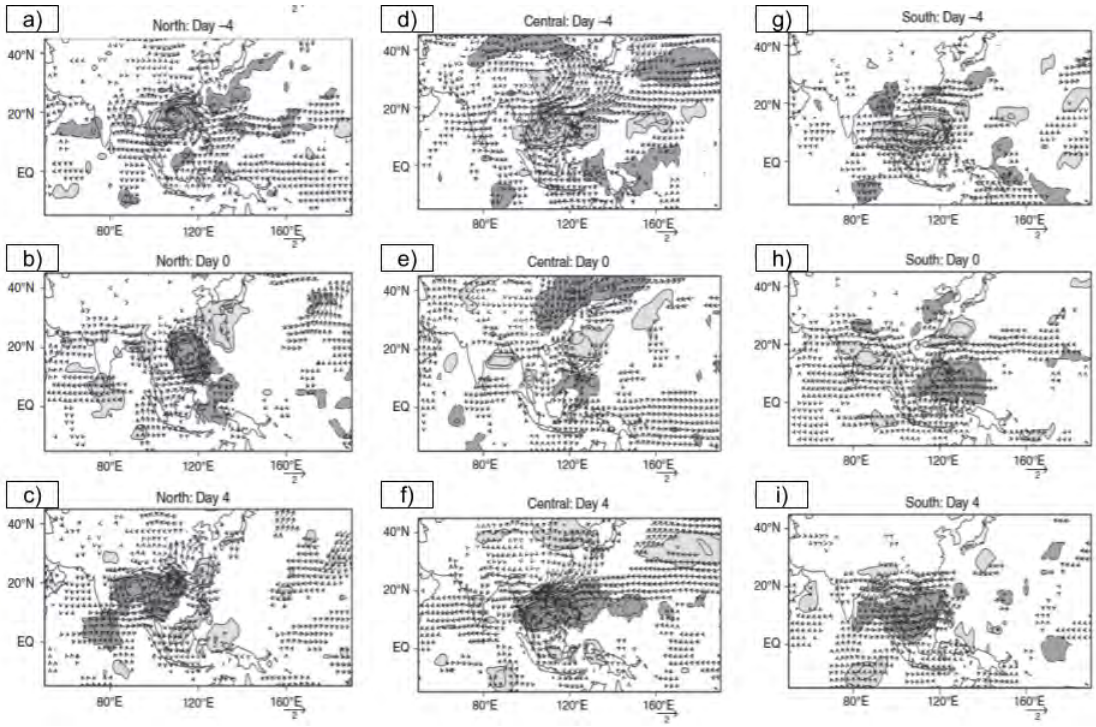

Figure 1.17: Taken from Truong and Tuan (2018): Composites of the 850-hPa wind vector (m/s) and OLR anomalies (contours) associated with the 10–20-day ISO in North-Central-South Vietnam. Solid contours shaded light grey indicates positive values; dashed contours shaded dark grey are negative. Contour interval is 2 W/m2. Only 95% statistically significant anomalies are plotted. (a-c) for North, (d-f) Central and (g-i) for South of Vietnam.

The rainfall anomaly patterns as well as the circulation following the evolution of 20-60 ISO are described over three sub-regions shown in TT19. The authors also used the OLR data to dissect the structure of spatial patterns of the 20-60-day ISO of rainfall over Vietnam subregions - Fig 1.18.

The spatial pattern of the 20–60-day ISO in North Vietnam is assumed by the stationary

oscillation of increased and suppressed convection, according to the composite spatial pattern analysis Fig 1.18-North. Truong and Tuan (2019) signifies an anticyclonic/ cyclonic anomaly that controls rainfall deficits/excesses in the ISO cycle presented across the Philippines and Vietnam concurrently with the large-scale stationary wave structure oriented in the southwest-northeast direction. The authors propose a tropical-extratropical connection or perhaps an inter-hemispheric interaction that supports the presence of the twin vortices crossing Taiwan.

For Central Vietnam, the composite of rainfall anomaly and low-level wind Fig 1.18-Central displays the Northwest Pacific subtropical High extends into the Northwest Pacific and anomalous westerly winds progressively form in the tropical Indian Ocean. The southern intrusion of the anomalous northerly winds from East Asia combines with easterly flow from the tropical Northwest Pacific to cause convergence of the Central Vietnam coast in the wet phase. It depicts the whole East Asian summer monsoon system, including the 20–60–day ISO in Central Vietnam, which is influenced by both tropical and extratropical factors.

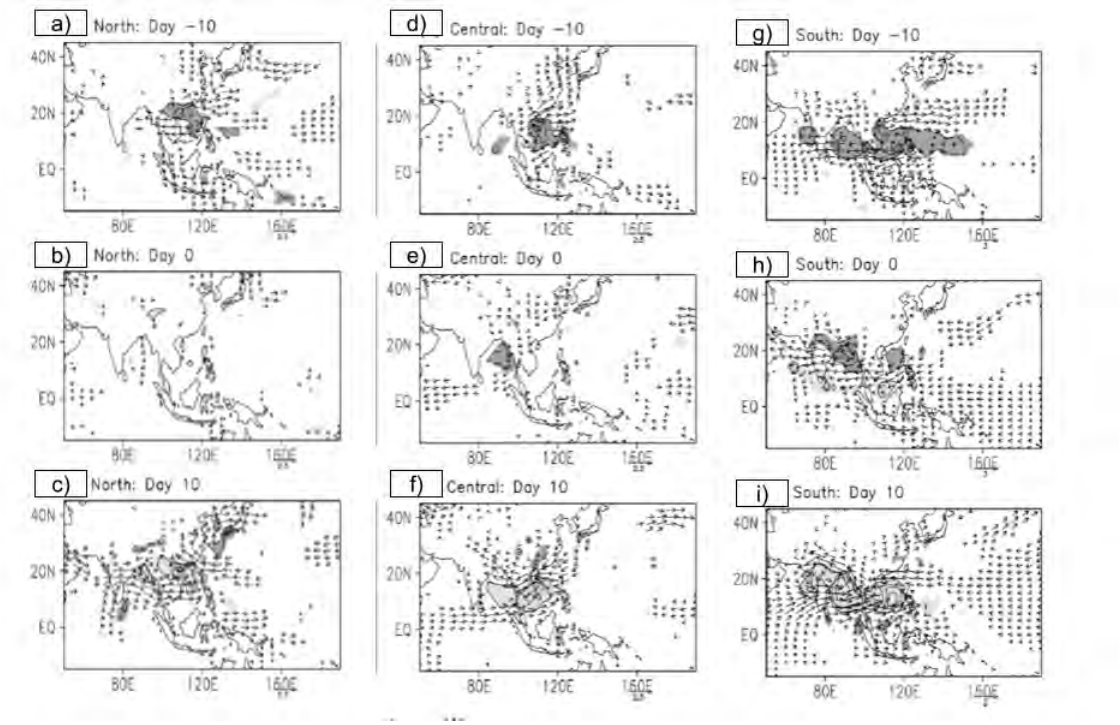

Figure 1.18: Taken from Truong and Tuan (2019): Composites of the 850-hPa wind vector (m.s-1) and ARR anomalies (contours) associated with the 20–60-day ISO in north Vietnam. Solid contours shaded light grey indicates positive values; dashed contours shaded dark grey are negative. The contour interval is 1 kg.m-2.day-1. Only 95% statistically significant anomalies are plotted. (a-c) for North, (d-f) Central and (g-i) for South of Vietnam.

For South Vietnam, Fig 1.18-South exhibits the large-scale pattern, anomalies, and propagation that resemble features of summer-MJO (Madden Julian Oscillation). Among that, the positive/negative OLR and rainfall anomalies roughly extend zonally, and they propagate northeastwards in association with the development of the anomalous easterly/westerly winds

prevailing south from the tropical Northwest Pacific to the Arabian Sea. The onset of the wet phase in South Vietnam is associated with the outbreak of convection in the equatorial central Indian Ocean and its northeastward propagation.

On the other hand, the spatial pattern of rainfall ISV over Vietnam during 1981-2009 has also been classified as principal components using EOF analysis in Tuan (2019). Four leading modes of the rainfall ISO (7-25-day) are portrayed in Fig 1.19 which account for 30.3%, 15.4%, 9.1%, and 5.6% of the total variance with the active and break phases are defined by the standard deviation of the PC time series. The authors diagnose the relations between the rainfall ISO leading modes and heavy rainfall over the subregions using correlation analysis.

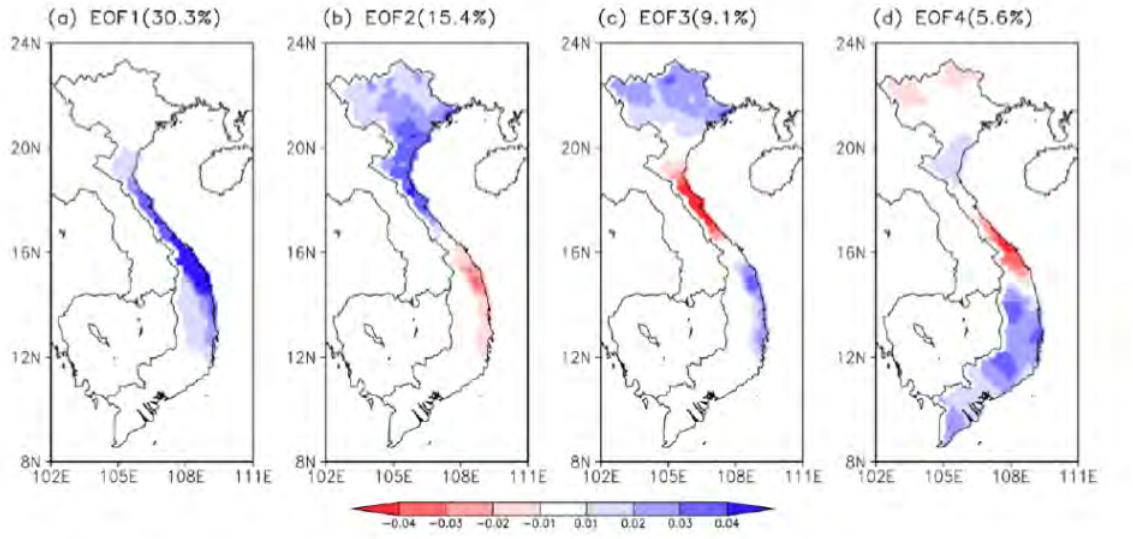

Figure 1.19: Taken from Tuan (2019): First four EOFs of anomalous Vietnam rainfall 1981-2009. Unit is arbitrary.

The first EOF presents a positive value along the central Vietnamese coast as Fig 1.19a, with a clear core over the area with the highest yearly frequency of heavy precipitation. Indicating opposing trends in the rainfall ISO in these regions, EOF2 (Fig 1.19b) exhibits positive values in the North Central and Northern regions and negative values in the South Central region. With significant positive values in Northeastern mountainous regions, a narrow band in the South Central, and big negative values in the North Central subregion, EOF3 (Fig 1.19c) exhibits a tripole pattern. From the north to the south of Vietnam, EOF4 (Fig 1.19d) displays a pattern with opposite big positive and negative values, with positive values largely covering southern Vietnam. In the Central Highlands, where altitudes are comparatively higher than those of the surrounding area, there are two distinct local positive maxima. Tuan (2019) strongly emphasises the orographic effect, in particular, the Truong Son Mountains, as a key factor in boosting the unusual low-level circulation that generates excessive rainfall in the Central subregion.

Tuan (2019) signified the high correlations between the PC time series of EOFs and the anomalous rainfall in certain subregions. Particularly, the PC1 time series is associated with

Mid-Central sub-monthly rainfall variance, PC2 shows the best fit with Red River Delta. PC3 and PC4 time series represent the seasonal variance of the Northeast and Southern Plain, respectively.

1.2.1.3 Mechanism

Following the spatial patterns, via different physical parameters, the mechanisms associated with the spatial patterns of Vietnam rainfall ISO are presented in the previous studies. The asymmetry between wet and dry anomalies of rainfall ISV will also be discussed.

The evolution of conditional instability and moisture flux associated with the 10-20-day ISO over three Vietnam subregions has been considered as a mechanism of the wet/dry spells by Truong and Tuan (2018). They showed that the 10-20 ISO in North Vietnam is associated with the moisture flux divergence/convergence and conditionally unstable/stable anomalies through wet/dry phases Fig 1.20a-c. In particular, the moisture flow divergence controls North Vietnam in the dry phase and is expected to cause surface heating. Together with descending motions, both causes result in a delayed unstable anomaly that is later replaced by a stable anomaly.

For South Vietnam Fig 1.20g-i, the descending movements and stability of the lower troposphere influence the anticyclonic and cyclonic gyres that govern the dry and wet phases in southern Vietnam, over the Philippines and nearby waters. The descent weakens lower tropospheric stability and prevents the growth of anticyclonic circulations, whereas the low-level stability suppresses cyclonic circulations in the wet phase.

The wet phase in central Vietnam is mainly caused by moisture flux convergence without local unstable conditions. The unstable/ stable warm/cold air from the eastern part of China, which has ascending/descending movements within it migrates south. This is associated with descending/ ascending motion in Central Vietnam (Fig 1.20d-f). Truong and Tuan (2018) proposes that local unstable circumstances are not responsible for precipitation processes in Central Vietnam; only the convergence of the moisture flux. They also present composite vertical cross-sections that show that the 10–20–day ISO propagates westward with wet-dry cells. These cells are maintained and divided by broad mountains with the expectation of a stronger signal of the 10–20-day ISO over mountainous terrain than over flat regions. With vertical motions and conditional instability, Truong and Tuan (2018) suggests that the Central Vietnam case is a clear example of extratropical influences on oscillations in the Tropics.

The evolution of the vertical velocity anomaly and the divergent component of anomalous moisture flux associated with the 20-60-day ISO over three Vietnam subregions in Fig 1.21 illustrates the mechanism of regional rainfall anomaly formation.

The instability of the lower troposphere within anticyclonic/cyclonic episodes during dry/wet phases is associated with divergence/convergence of the moisture flux convergence anomaly Fig 1.21-North and South. This is considered the mechanism for 20-60 day rainfall ISO over North Vietnam and South Vietnam. To be more detailed, when anomalous moisture

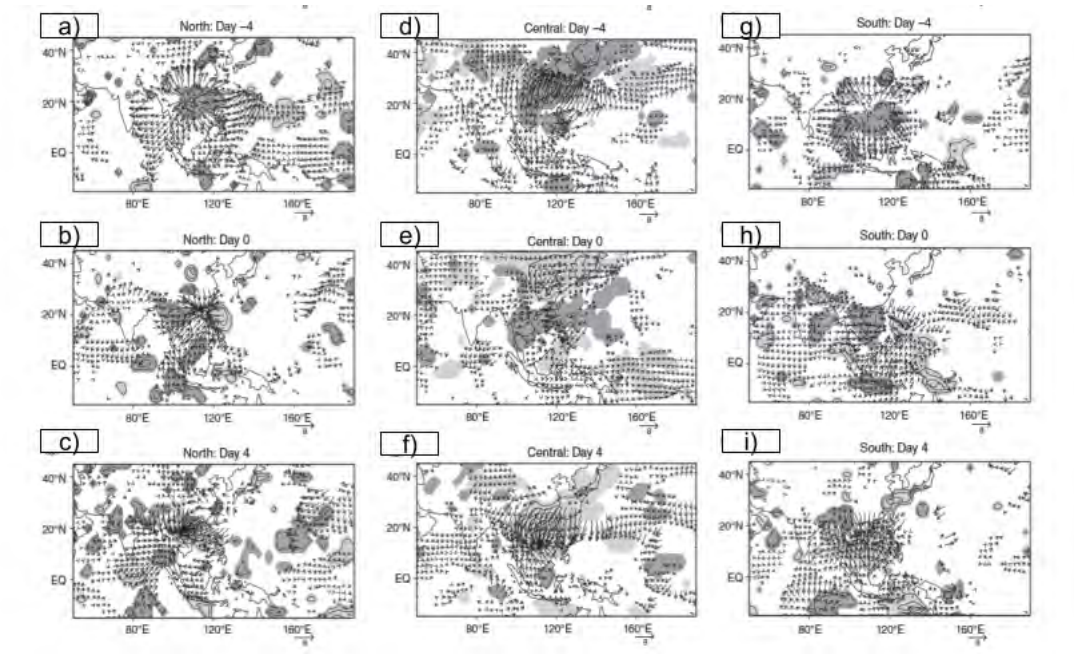

Figure 1.20: Taken from Truong and Tuan (2018): Divergent component of anomalous moisture flux integrated into the layer between 1000–700 hPa (vectors, kg m1.s1) and 1000-hPa temperature anomalies (K, contours). Solid (dashed) contours indicate negative (positive) values shaded by light (dark) grey. The contour interval is 0.1, 0.2, and 0.075 K for North Vietnam, Central Vietnam, and South Vietnam, respectively. Only 95% statistically significant anomalies are plotted. (a-c) for North, (d-f) Central and (g-i) for South of Vietnam.

flux (AMF) diverges, the lower troposphere becomes unstable within the anticyclone in the dry phase, but when AMF converges over the area, it is stable within the cyclone in the wet phase in North Vietnam. Similar to this, the anticyclones from which AMF divergence in the South Vietnam dry phase are colocated with unstable anomalies, and vice versa. However, the local conditional instability does not play a role in rainfall formation over Central Vietnam. Truong and Tuan (2019) indicated that when AMF diverges, the unstable air moves from the Eurasian continent along the northern-eastern margin of the Tibetan Plateau to Vietnam leading to a dry phase over CVN. The CVN wet phase is determined in a reversal way.

It can be seen that although there are symmetrical patterns of 20-60 day rainfall ISO over the three subregions, the divergent component of anomalous moisture flux and the vertical velocity anomalies at the lower level show some asymmetry between the wet and dry phase over North Vietnam and Central Vietnam as in Fig 1.21, but are symmetrical in South Vietnam. The anomaly patterns between wet and dry phases, for example, OLR and low-level winds, show symmetry locally but are asymmetrical at a large scale. In addition, Truong and Tuan (2019) also indicates that the vertical structure in the wet and dry phases over South Vietnam is tilted to the west and symmetrical while North Vietnam and Central Vietnam are vertically developed, and asymmetrical.

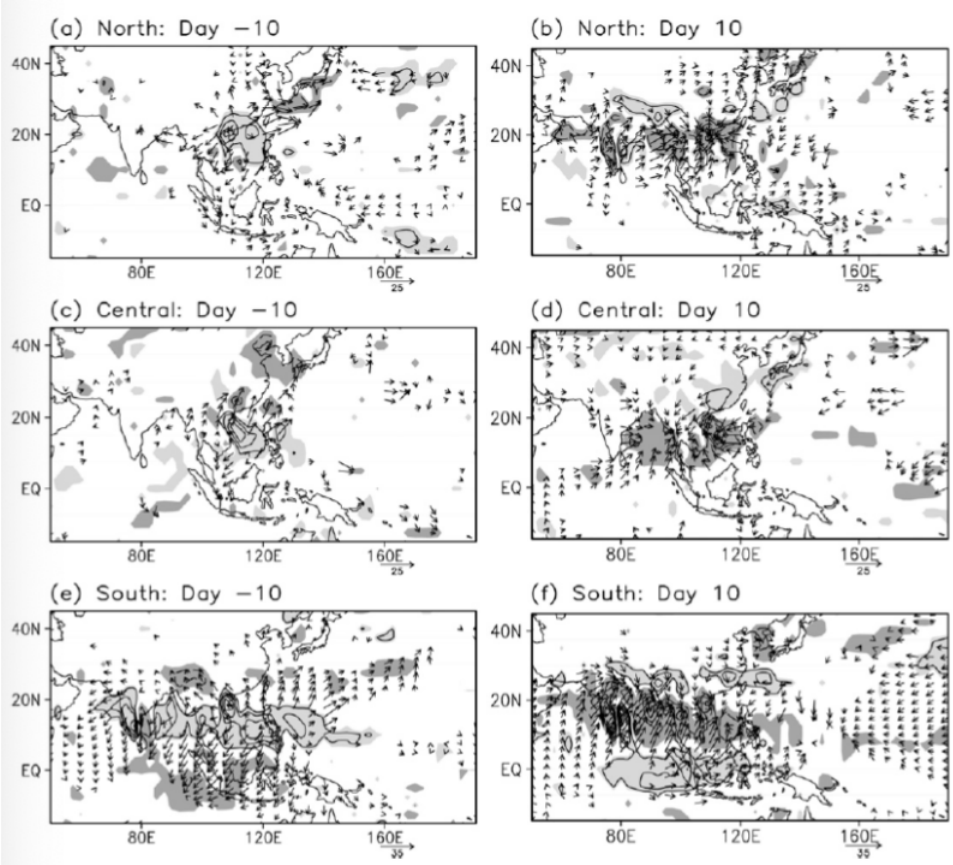

Figure 1.21: Taken from Truong and Tuan (2019): Divergent component of anomalous moisture flux (vectors; kgm-1.s-1) and 850-hPa vertical velocity anomalies (Pa s21, contours) at day (left) 210 and (right) 110 associated with the 20–60-day ISO in (a),(b) north, (c),(d) central, and (e),(f) south Vietnam. Solid/dashed contours indicate positive/negative values shaded by light/dark grey. The contour interval is 0.007, 0.01, and 0.005 Pa s21 for north, central, and south Vietnam, respectively. Only 95% statistically significant anomalies are plotted.

1.2.1.4 Summary

From the observed climatological characteristics of Vietnam rainfall ISV, we have an overview in the form of a statistical description for timescale analysis, with spatial patterns and mechanisms associated with each temporal mode of variation. We summarised from previous studies that two modes of variation of Vietnam rainfall ISV characterise the differences between subregions spatially and temporally.

The EOFs representation from principal component analysis of rainfall ISV gives PCs that capture certain aspects of the ISO but must be combined to represent actual anomalous events over a subregion. It should also be noted that filtering to isolate particular time scale intervals could result in diminished asymmetry in the signal and consequently limit the analysis.

The evolution of spatial patterns of Vietnam rainfall ISV has been explored in previous studies by either compositing onto a cycle following a temporal mode of variation or compositing onto filtered principal component analysis. This approach is necessarily somewhat distanced from the needs of the forecaster, who is interested in local or regional events on all time scales. Further investigations that discriminate between wet and dry events on intraseasonal timescales over Vietnam subregions without pre-supposing the importance of a particular cycle by introducing time filtering, could be of further interest.

Indeed, the description of all variation modes is strongly related to the state, quantity and activity of the moisture field. For example, the divergent component of vertical moisture flux convergence is used in TT18 and TT19; and the cross-section of specific humidity to see the vertical structure of the evolution through dry to wet phases. Further study that includes a more comprehensive treatment of the terms in the moisture budget and their growth associated with rainfall ISV may also be of interest.

The mechanism of ISO cycles in different modes of variations was explored in the two studies of TT18 and TT19. They adhere to a view of opposite phases wet & dry within a full cycle of ISO, for example, day+/-4 for 10-20-day mode or day+/-10 for 20-60-day mode. The convergence/ divergence, the instabilities of the lower troposphere and the anomalous moisture flux convergence are well associated with anomalies. However, the symmetry/asymmetry of the mechanism associated with spatial patterns of opposite phases of variation mode remains unclear. For example, 20-60 ISO North Vietnam displays symmetrical patterns of anomalous rainfall, but asymmetrical large-scale atmospheric patterns. This raises the question of whether the sources of impacts are responsible for that asymmetries. What are the influence factors that come from Tropics or Extratropics? In the next section, the discussion of possible influence factors of Vietnam rainfall ISV and teleconnections are raised. (eg., T18, TT19, Yokoi et al. (2007)).

1.2.2 POSSIBLE Influence factors of Vietnam rainfall ISV

In this subsection, we present our current knowledge about the possible factors of influence on Vietnam rainfall ISV including the related investigations. We will present it following two sources of factors in terms of origins: tropical and extratropical factors. The majority of knowledge comes from observational studies where previous research shows a lot of interesting results about the tropical and extratropical factors that are associated with the rainfall ISV over the Vietnam subregions. There are also some modelling studies and theoretical research about the dynamical influences from sources far away from the target regions.

1.2.2.1 Tropical factors

According to previous studies, the leading tropical factors that affect rainfall ISV over Vietnam include the Madden Julian Oscillation - MJO (Madden and Julian, 1972), and equatorial Rossby and Kelvin waves. These tropical factors mostly affect Central and South Vietnam

more than the North, eg., Yokoi et al. (2007); Van Der Linden et al. (2016).

The MJO - Madden-Julian Oscillation is the dominant mode of intraseasonal variability in the tropics. As outlined in Zhang (2005), the MJO has a global impact because it is a deep convective intraseasonal oscillation with a zonal scale of 12,000 - 20,000 km in the tropics. Enhanced convection occurs over the equatorial Indian and western Pacific oceans with an eastward moving centre of deep convection and intense precipitation. The MJO convection is accompanied by an overturning zonal circulation that extends vertically through the entire troposphere. Eastward propagation is at about 5m/s. The time scale of the MJO is in the range of 30-70 days, typically 48 days (Madden and Julian, 1972). The speed and amplitude vary during its propagation and also between different MJO events.

The impacts of the MJO on global weather patterns are summarized in Fig 1.22 for the summertime -JJA impact on the weather out to 1–3 weeks. The alternating wet/dry conditions over zone 1 are directly attributed to the organization of deep convection of MJO phases that cycle from the Indian Ocean to the Western Pacific flanked by suppressed convection. The phase of the MJO has also been linked to increased frequency and rapid intensification of tropical cyclones compared to the non-MJO over Western Pacific- zone 3, eg.,Liebmann et al. (1994). Moreover, the MJO is related to the modulation of Asian summer monsoon as indicated in zone2 where it favors the anticyclonic anomalies over the subtropical western North Pacific Fig 1.22, eg., Li et al. (2018). The MJO influence can also be affected by the phase of ENSO (Fink and Speth, 1997) and the wind stress anomalies associated with the MJO have been linked to the excitation of oceanic Kelvin waves that modulate the thermocline in the equatorial Pacific (Kessler et al., 1995).

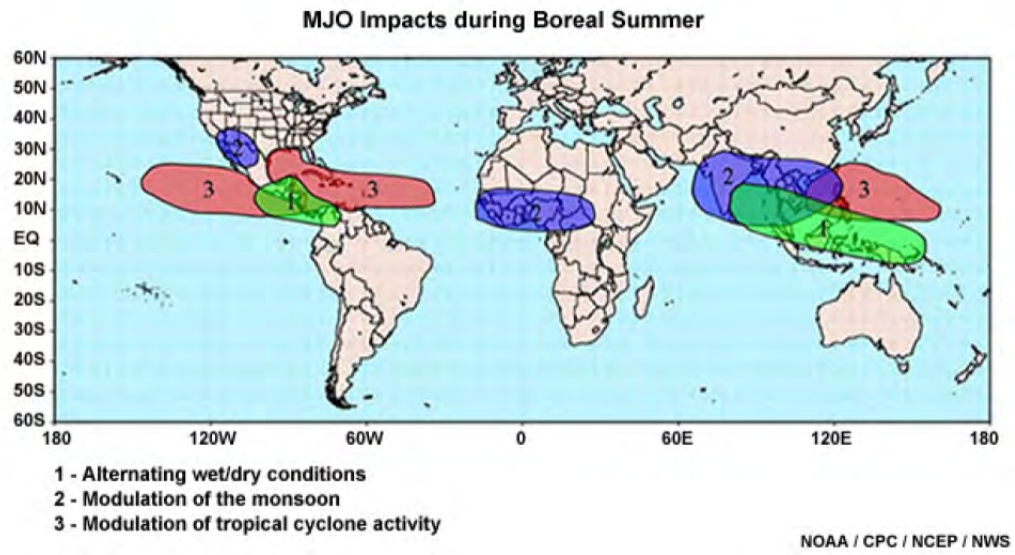

Figure 1.22: Taken from Laing and Evans (2011)- Sources of Intraseasonal Variability: Global pattern of MJO impacts during Boreal summer (JJA). Impacts identified are (1) alternating periods of wetter and drier conditions; (2) modulation of the monsoons; and (3) modulation of tropical cyclone activity.

Kelvin waves exist in the ocean or atmosphere and can be described as a wave that balances the Coriolis force against a topographic boundary pressure gradient. In the tropics, each hemisphere can act as the barrier for a Kelvin wave on the other side, resulting in "equatorially–trapped" Kelvin waves. Kelvin waves are characterized by different phase speeds in different regions of the world. As summarized in the book of Laing and Evans (2011), convectively-coupled tropospheric Kelvin waves have a typical period of 6-7 days when measured at a fixed point and phase speeds of 12-25 m.s-1 Fig 1.20, while dry Kelvin waves in the lower stratosphere have phase speed of 30-60 m.s-1. Kelvin waves over the Indian Ocean generally propagate more slowly at 12–15 m.s-1 than other regions. They are slower, more frequent, and have higher amplitude when they occur in the active convective stage of the MJO (Roundy, 2008).

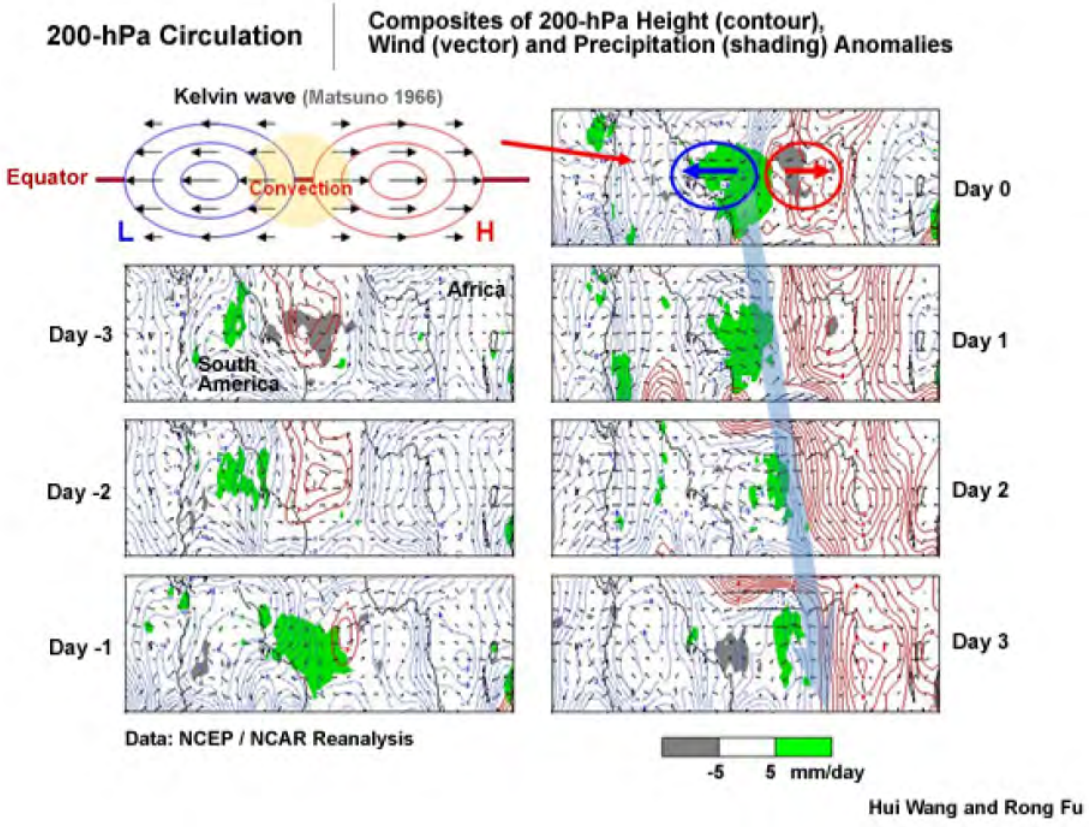

Figure 1.23: Taken from Laing and Evans (2011)- Sources of Intraseasonal Variability: Composite of 200 hPa height (contour), wind (vector) and precipitation (shading) anomalies. The top left shows the theoretical Kelvin wave derived by Matsuno (1966). The light blue arrow shows the eastward movement of the wave.

Fig 1.23 shows the theoretical Kelvin wave derived by Matsuno (1966) on the top left which is caused by the convection in the Equator according to the easterly wind to the west and the westerly winds to the east. Several studies suggest that Kelvin waves are important for the initiation of the El Niño Southern Oscillation -ENSO phenomenon (Li and Clarke, 1994) and maintenance of the MJO (Zhang, 2005). The composite of 200 hPa height (contour), wind

and precipitation anomalies in panels Fig 1.23 also illustrates the link between Kelvin waves and precipitation anomalies in the Tropics.

Equatorial Rossby waves also propagate along the Equator. Rossby waves exist on a varying potential vorticity field and their restoring force can be explained in terms of potential vorticity conservation. The absolute vorticity includes the relative and planetary vorticity, so the latitudinal variation of the Coriolis parameter can provide conditions for Rossby waves. Rossby waves are also known as planetary waves. We can see the spatial characteristics of an Equatorial Rossby wave via observation such as the 850 hPa tropical wind and satellite image. By location of twin vortices, for example, indicated in figure 1.24, the equatorial Rossby waves can have a largest horizontal size up to 10,000 km 100 degrees of longitude (normally greater than 4000 km) and meridional size of 20 degrees of latitude. Equatorial Rossby waves are observed on the order of days to weeks with westward propagation. As in Kiladis et al. (2009) the large waves propagate westwards with speeds on the order of 10-20 m.s-1 for dry atmospheric Rossby waves, 5-7 m.s-1 for convectively-coupled Rossby waves (and 1 m.s-1 for oceanic Rossby waves).

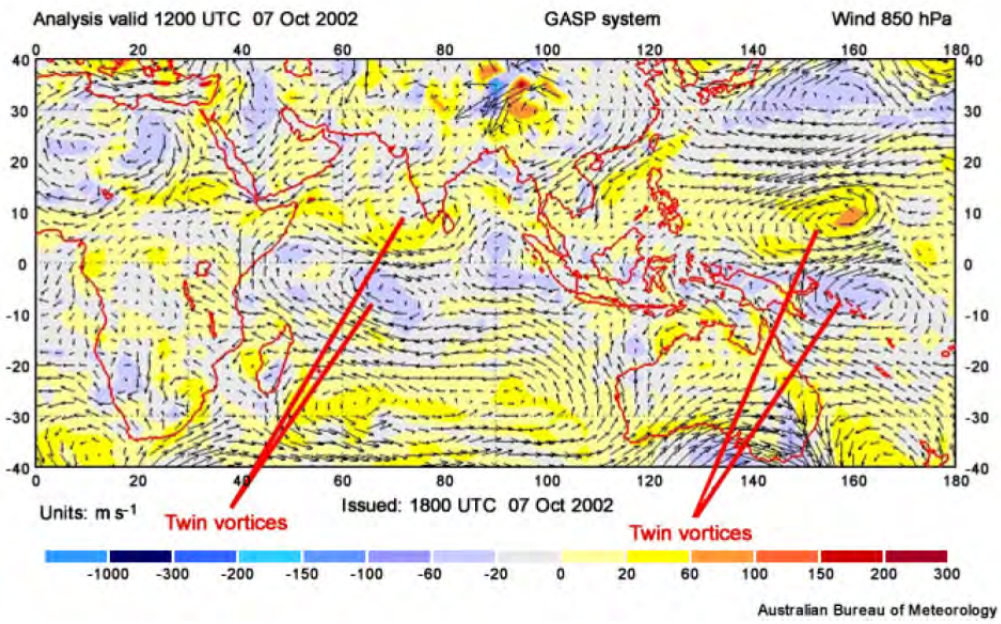

Figure 1.24: Taken from Laing and Evans (2011)- Sources of Intraseasonal Variability: Evidence of equatorial Rossby waves in the Australian Bureau of Meteorology 850 hPa tropical wind analysis for 1200 UTC 7 October 2002.

As mentioned above and reported in Wheeler et al. (2000); Kiladis et al. (2009), the effects of moisture and convection on equatorial waves (both Kelvin and Rossby waves) is to slow them down. This type of wave propagation is called convectively coupled equatorial waves CCEWs. They showed that because of moist processes, the vertical structures of CCEWs are tilted and more complex than linear dry waves. CCEWs have a great impact within the tropics. As seen in Fig 1.25 Kelvin waves have a direct impact on convection only within about 10° of the equator, in particular the central and eastern Pacific oceans. The direct

impact of equatorial Rossby waves is symmetry and strongest over the Asian monsoon region and the West Pacific warm pool regions.

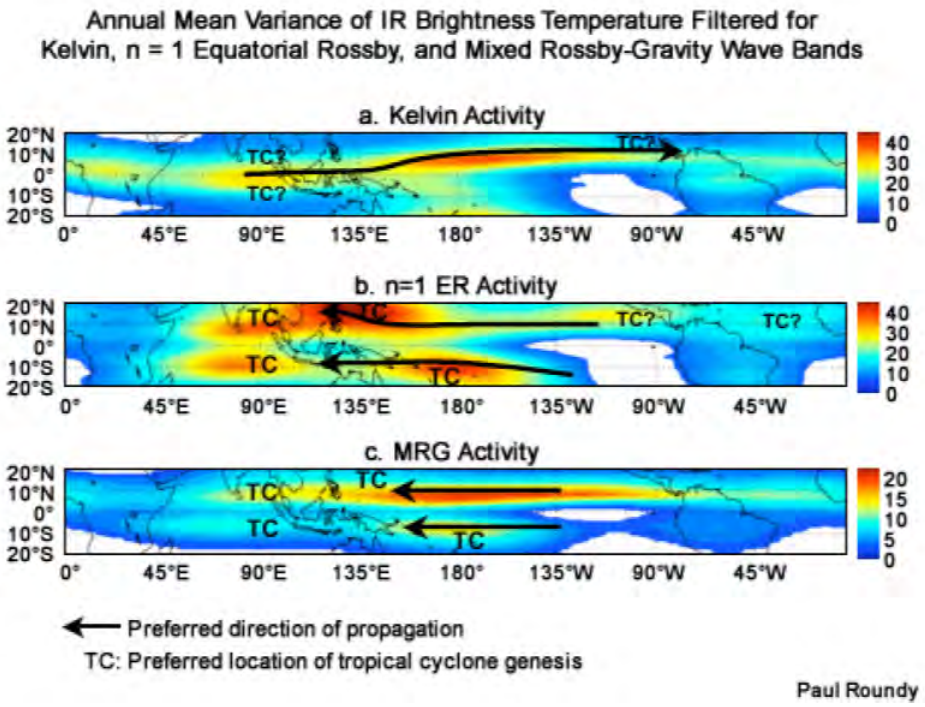

Figure 1.25: Taken from Laing and Evans (2011)- Sources of Intraseasonal Variability: Distribution of annual mean variance of IR brightness temperature filtered for the (a) Kelvin, (b) n = 1 ER, and (c) MRG. Also shown are the preferred direction of propagation and preferred location of tropical cyclone genesis associated with each mode. Adapted from Kiladis et al. (2009).

Finally, Mixed Rossby Gravity waves are also considered an important tropical wave for short-term weather forecasting. MRG waves are identified from a variety of satellite data and numerical model analyses and have a longitudinal scale of 1,000-4,000 km, a period range of 4-5 days and move with speeds 8-10 m s-1 to the west. Two competing restoring forces, PV conservation and buoyancy, control MRG waves. Thus, in the tropics, such waves are strongly modulated by moist convection which slows down the wave propagation and the convection generates cyclonic low–level potential vorticity, eg., Dickinson and Molinari (2002); Kiladis et al. (2009); Takasuka and Satoh (2020).

Related to Vietnam rainfall ISV, as shown by Van Der Linden et al. (2016), the daily rainfall during May-October from the APHRODITE database (Yatagai et al., 2012) shows the association of Vietnamese rainfall with different phases of the MJO and equatorial waves. The MJO has the largest influence in the region of South Vietnam. Equatorial Rossby waves mostly affect Central Vietnam, followed by South Vietnam, while Kevin waves only affect South Vietnam. Van Der Linden et al. (2016) shows that these waves enhance the frequency of intense daily rainfall during the wet phase, and positive interference of these different waves can lead to a strong enhancement of wet or dry events.

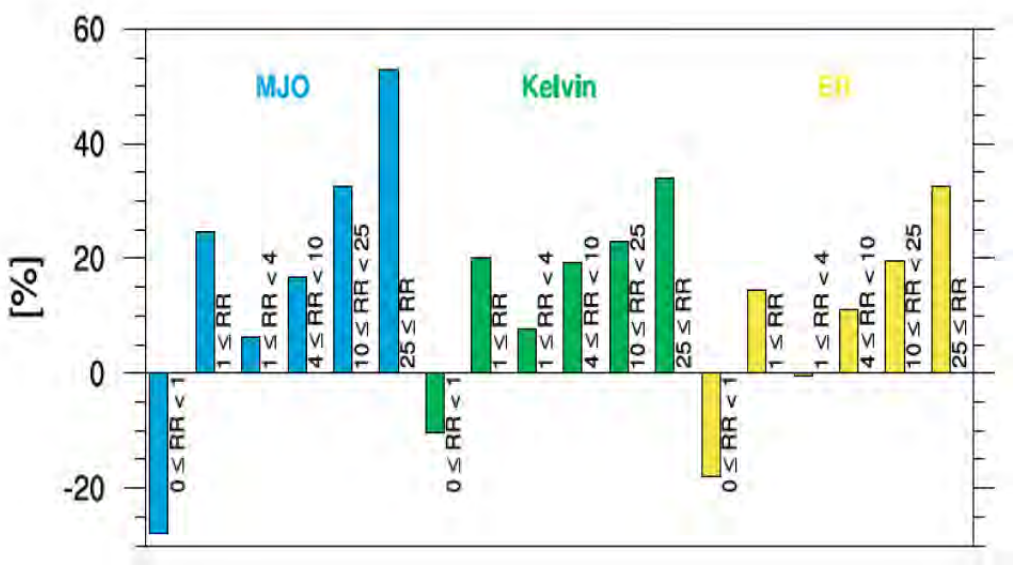

Figure 1.26: Taken from Van Der Linden et al. (2016): Influence of wave phases on the frequency of rainfall (RR) intensities (mm.day-1). Differences in the number of values in the wet phases 4, 5, and 6 are relative to the number of values in the dry phases 8, 1, and 2 for the Madden-Julian oscillation, Kelvin waves, and equatorial Rossby waves during May-October.

Yokoi et al. (2007), TT18 and TT19 agree that large-scale dynamics associated with rainfall variation modes resemble the MJO and tropical wave activity, especially for Central and South Vietnam. TT18 indicates a tropical Indian Ocean mode in the form of equatorial Rossby waves with 10-20-day variations in North and South Vietnam. TT19 shows that MJO activity relates to 20-60-day variations for South Vietnam.

Ferrett et al. (2019) have investigated the link between extreme precipitation in Southeast Asia and equatorial waves including Kelvin Waves, Equatorial Rossby Waves and Westward-moving MRG waves. They state that these waves play a major role in organizing tropical convection on synoptic to sub-seasonal time scales. Particularly, they increase mean rainfall and lead to an increased probability of heavy rainfall. Mainly focused on the Maritime Continents, Ferrett et al. (2019) indicate that Kelvin waves have a large influence on heavy rainfall over Indonesia, WMRG and Kelvin waves impact Malaysia rainfall, while equatorial Rossby and WMRG waves are linked to increased rainfall over the Philippines.

1.2.2.2 Extratropical factors

The extratropics or mid-latitude regions are usually defined between 30-60 degrees of latitude. These regions have a great amount of atmospheric variability due to transient eddies with sequences of cyclones and anticyclones. Stan et al. (2017) summarized the influence of the extratropics on the tropics and indicated that extratropical forcings can lead to further modulation beyond the influence of tropical waves.

As summarized in Stan et al. (2017), the theory of extratropical forcing of the tropics was first presented in Charney (1969) and BENNETT and YOUNG (1971) in terms of meridional propagation of extratropical waves into the tropical zone. They used a zonally averaged basic flow to investigate the extratropical forcings on the Tropics. According to their findings, meridional wave propagation in the presence of mean easterly flow is only conceivable if the midlatitude wave's phase velocity is greater than the easterly mean flow.

Webster and Holton (1982) using a nonlinear shallow water model showed the effects of longitudinal variations in the basic state zonal wind. They concluded that large-scale disturbances generated in the northern middle latitudes may have a significant impact on equatorial regions and the opposite hemisphere only in the presence of a westerly duct in the upper-level winds in the equatorial zone and that the amplitude of the response increases with the strength of the westerlies.

However, Hoskins and Yang (2000) concentrated on creating vorticity and heat sources at 20°N to directly excite equatorial waves in simple linear and primitive equation models. They found that westerly winds are not necessary for the equatorial reaction to extratropical force; instead, the forcing is directly projected onto equatorially trapped waves. In particular, the forcing at higher latitudes with an eastward phase speed effectively triggers an equatorial Kelvin wave.

In Hoskins and Ambrizzi (1993), the response of a barotropic model to localised forcing shows the existence of a strong wave-guide in the Asian jet. They show Rossby wave propagation on a realistic longitudinally varying flow of a climatological winter time-mean flow. Using a variety of perturbation vorticity sources they show the position and spatial features of the waves and show the preferred propagation regions from Europe to Arabian Gulf.

Then Yang and Hoskins (1996) use theoretical analysis, ray tracing and initial value problems in barotropic and baroclinic numeral models to investigate the propagation of Rossby waves with eastward and westward phase speeds. They found that the jets act as wave-guide and the eastward-moving waves have shorter wavelengths and are more meridionally confined than the westward waves.

Hall et al. (2016) conducted numerical experiments with the Weather Research and Forecasting (WRF) model with a tropical configuration (30N-30S) to quantify the influence of the extratropics on simulated tropical intraseasonal variability during winter by modifying the boundary conditions. The boundary effect from the midlatitudes on the same intraseasonal timescale contributes significantly to the intraseasonal variation associated with propagating tropical signals. They indicated that this boundary impact does not alter the structure of the tropical variance but it does change its amplitude, identifying an extratropical trigger that increases the activity of internal tropical modes.

Through observations, extratropical precursors to rainfall ISV shown in previous studies are wave trains along with the North Atlantic- Asian- North Pacific jet and/ or cold surges from the Siberian High, or possibly the interaction between the tropics and the extratropics.

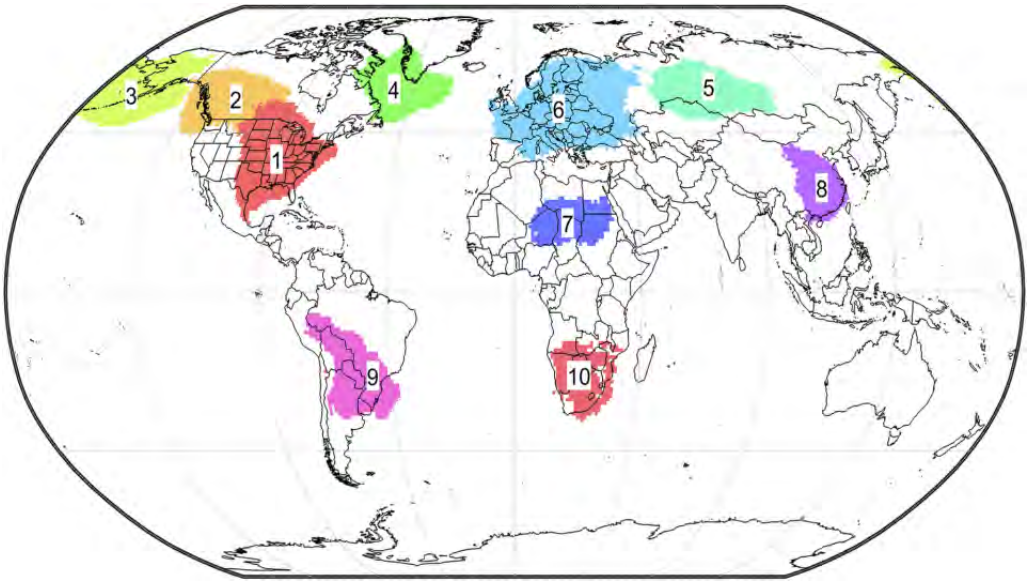

Figure 1.27: Taken from Smith and Sheridan (2020): Regions based on the CAOs produced from the ERA5 data set.

Cold air outbreak or cold surge events are defined as the sudden release of cold air masses from high latitudes and typically lead to rapid temperature drops, high pressure, and strong winds for one to several days that affects weather variability further away. As indicated in Smith and Sheridan 2020, Fig 1.27 shows a map of preferred regions of Cold Air Outbreaks CAOs across a large portion of the Earth mostly during the winter using reanalysis dataset ERA5. Eurasia and East Asia are frequently identified as regions that have cold surges penetrating far into the tropical region, inducing convection and precipitation in Southeast Asian countries, especially around the Eastern Sea (Vietnam) and the Philippines Sea. CAOs can also lead to heavy rainfall and flood events in Vietnam or Malaysia (Yokoi and Matsumoto, 2008; Tangang et al., 2008).

Mechanisms of intraseasonal amplification of the Siberian high have been investigated by Takaya and Nakamura (2005) on the basis of composite anomaly evolution for the strongest events at each of the grid points over Siberia. They found that the interaction between an upper-level stationary Rossby wave train and pre-existing surface cold anomalies is essential for the strong amplification of the surface high. The intensified surface cold anomalies then induce anomalous vorticity advection aloft that reinforces the blocking ridge and cyclonic anomalies downstream of it that constitute the propagating wave train.

In TT19, the change from dry to wet phases of rainfall ISO over North Vietnam is associated with enhanced and suppressed convection which are associated with the dual vortices straddling Taiwan. They suggest that the Taiwan vortex might originate from the extratropics. The wet and dry phases of ISO rainfall over Central Vietnam are associated with the combination of southward intrusion of the anomalous northerly winds from East Asia and the easterly flow from the tropical Northwest Pacific to create convergence in the Central Vietnam wet phase. At the same time, the northwest Pacific subtropical high appears to expand in the

northwest Pacific and the anomalous westerly winds gradually evolve in the tropical Indian Ocean. This suggests that the 20–60-day ISO in Central Vietnam is governed by both tropical and extratropical factors that influence the whole East Asian summer monsoon system.

In TT18, Central Vietnam cases are associated with the southward propagation of cold surges from the Eurasian continent. They also emphasise that topography plays an important role in modulating the 10–20-day ISO, especially in central Vietnam as it helps block northeasterly winds associated with cold air masses.

Tuan (2019) also proposes a schematic diagram illustrating the interaction between the extratropical wavetrain and the Tropical depression for the four leading modes of sub-monthly rainfall ISO as in Fig 1.28. The extratropical precursors to Vietnamese rainfall ISV, are often in the form of wave trains along the North Atlantic-Asian-North Pacific jet. Tuan (2019) shows that pressure surges from the Siberian high and Northeast China are associated with sub-monthly rainfall ISO over North and Central Vietnam. The wave trains originating from the North Pacific at the upper level strengthen the Tropical depression at the lower level through the meridional pressure gradient to lead the wet phases over South Vietnam.

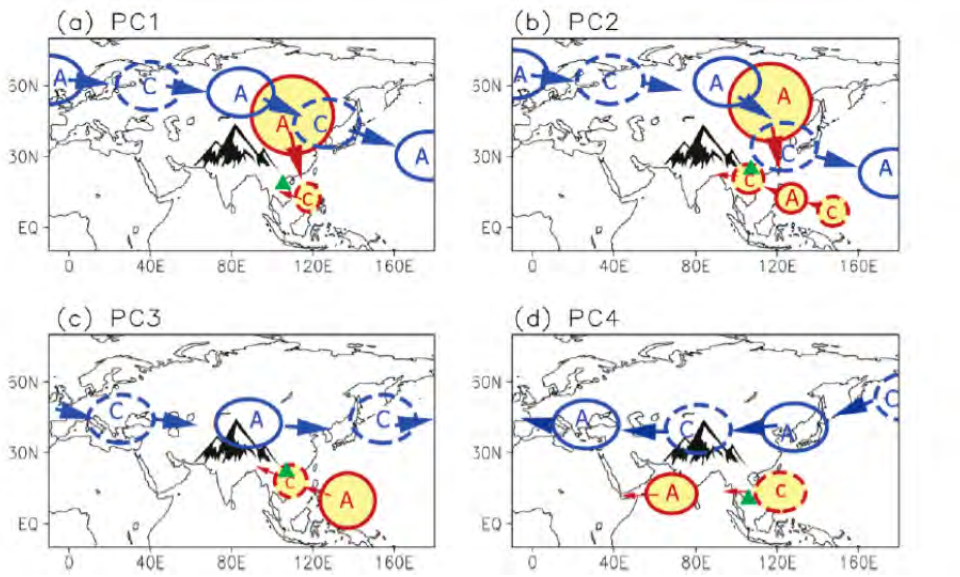

Figure 1.28: Taken from Tuan (2019): Schematic diagram of the interaction between extratropical wave trains and TD-type waves during the active phases of sub-monthly rainfall oscillation determined by first-four Principal Components. The closed/dashed blue circles: upper-level anticyclone/cyclone. The green triangles denote the strong convection over Vietnam subregions.

Abdillah et al. (2021) also indicates the influence of northerly and westerly cold surges induced by Cold Air Outbreaks (CAOs) at high latitudes during wintertime. Abdillah et al. (2021) suggests the pathways of influence that induce subtropical surges over the South China Sea leading to the greatest influence on precipitation over Central Vietnam. Westerly cold surges are associated with precipitation over North Vietnam.

The interaction between tropical and extratropical factors is also discussed in case studies of extreme rainfall events over Vietnam. Wu et al. (2012) show an example of a synoptic-scale tropical wave formed over the South China Sea combined with a surface high extending from western Mongolia to the East China Sea in the presence of a strong MJO over the Indian Ocean leading to heavy rainfall over Central Vietnam. Further examples of combined effects include cold surges associated with the expansion of the Siberian High and tropical depressions associated with the MJO (Yokoi and Matsumoto, 2008; Chen et al., 2012; Abdillah et al., 2018)

1.2.2.3 Summary

We have presented a catalogue of structures that may influence the rainfall ISV over Vietnam subregions from previous studies that come from both modelling and observational studies. This constitutes the substantial background research for this PhD thesis that we would like to focus on the remote dynamical and tropical influence on Vietnam hydrology, particularly the rainfall ISV.

From observational analysis, the influence of extratropical and tropical factors and their interaction, on Vietnam rainfall ISV are seen to be associated with various temporal and spatial modes of variation as well as individual events. This type of combined influence appears to have varying impacts on different regions, so the exact nature of the remote influence is sensitive to how these regions are defined and how the data are processed, including choices about thresholds, time filters, etc. For example, in terms of the temporal variation of rainfall over Vietnam, TT18 indicates that the circulations associated with 10–20-day rainfall ISO in north and south Vietnam are in the form of equatorial Rossby waves, while 20–60-day rainfall ISO in north and south Vietnam is suggested as coming from extratropical- tropical interaction and summer MJO, respectively in TT19. However, we also see that PC2 and PC4 of sub-monthly rainfall of gridded Vietnam daily rainfall in Tuan2019 associated with rainfall anomaly over North and South Vietnam are suggested in association with the southward excursion of the polar air mass and upstream development of the wave train from the North Pacific with TD-type waves, respectively.

The conclusions to the multiplicity of regions, rainfall criteria and timescales need to be further investigated within the extended summer. The interrelation between regional events and sensitivities to the choice of regions and threshold could be a useful feature of a complement investigation. What is the overall large-scale dynamics picture associated with the regional events without the restriction of a narrow band time filter and the associated tacit assumption of oscillatory behaviour? Related to the dynamical influence, we are concerned with the identification of dynamical precursors to ISVs of rainfall over sub-regions of Vietnam and the pathway of influence. In addition, the discrimination between opposite anomaly events on an intraseasonal timescale merits further attention. The nonlinearity of influences could be unpacked partly by considering these events in terms of the moisture budget and associated large-scale precursors.

The background of model studies in terms of possible influence on Vietnam rainfall ISV shows that both GCM and RCM can be used to investigate the dynamical influence on Vietnam circulation. Simple global modelling studies suggest that the extratropical influence that can be simulated in a model as a wave source, can lead to impacts on the tropics. Furthermore, RCMs such as WRF with regional configurations and prescribed boundary conditions can help to examine the impacts of the extratropics on the tropics. This suggests to us a way to do further investigation in this context. It is possible that we can systematically examine multiple model simulations to find the wave sources that can potentially influence the target regions' circulation in a GCM. Then downscaling studies with an RCM can be employed to investigate the influence of extratropical forcing via the boundary conditions, including the local circulation and the humidity budget.

1.3 Objectives

The modeling and observational studies presented in this chapter have shown that the annual cycle and the ISV of Vietnamese rainfall both have considerable amplitude and complexity, with much variation between Vietnam subregions. The timescales, patterns and associated 3D-circulation of Vietnam subregional rainfall ISV has been investigated using a variety of approaches. Specified time-filter and principal component analysis can be quite revealing, but results can be sensitive to definitions so there is also some interest in revisiting an investigation of regional anomaly events, and especially their opposite anomaly events.

The link between the rainfall intraseasonal variation and moisture flux divergence, and moisture transport has been revealed in some studies with a focus on the driving terms in the moisture budget, and it is of interest to accompany our proposed analysis with a consideration of the moisture supply at a regional scale. The overall picture of moisture budget terms associated with ISV needs to be assessed.

The extratropical and tropical factors found to affect the Vietnam rainfall ISV in previous studies show some sensitivity to the choice of regions, timescales and rainfall criteria within the extended summer. In this study, the main objective is to use different approaches to investigate the moisture budget and large-scale dynamical precursors of rainfall ISV events over Vietnam subregions, on different scales. Our specific objectives are as follows;

- Assess the contribution of moisture budget terms to regional events for both positive and negative anomalies separately.
- Identify the large-scale dynamical precursors and pathways of influence.
- Diagnose the nonlinearity of influence through the asymmetry in our results.
- Assess the sensitivity to choices of region, threshold and composited quantity.
- Verify the pathways of influence.
- Qualitatively assesses the extratropical and tropical influences.

1.4 Approaches

To pursue these objectives, we will use a combination of observational analysis and modeling approaches including global and regional scales. First, we will use the global reanalysis dataset - ERA-Interim from 1979 to 2016 including atmospheric variables, rainfall and evaporation data, and for comparison, the rain gauge dataset will also be used.

A composite analysis is performed to gather observational composites of opposite signs of anomalous regional rainfall ISV over Vietnam. Instead of using the precipitation, the index for composite is created over each region based on the vertically integrated moisture flux convergence, which is more directly linked with the circulation. The contribution of moisture budget terms before an event will be described. Precursors are then identified from the composites of large-scale circulation associated with opposite regional rainfall patterns. The asymmetry between Wet and Dry events over a region will be investigated. Then we will also explore the sensitivity of the index in terms of the choice of regions, the threshold and alternative hydrological indices.

A model study approach will then be used to further investigate the pathways of influence. Two different numerical models will be employed: one is a global model - DREAM and the other is a regional model - RegCM4. The global model study is accompanied by a theoretical analysis of potential Rossby wave trajectories using the ray tracing technique.

DREAM is a global spectral primitive equation model, used to investigate the influence of the dry dynamics from remote wave sources on the Vietnam subregion's circulation. A stationary wave configuration is used to systematically find the source which gives the most influence on target regions, by diagnosing the dynamical response to an artificial source. This will be complemented with nudging experiments on this configuration to simulate realistic sources that are extracted from the observed composites.

The raytracing calculation package is based on the dispersion relation of the Rossby plane-wave in a Mercator projection, then used to trace the Rossby wave sources propagation from the Northern Hemisphere to the Vietnam region. Rossby wave ray paths are traced from a set of determined sources, specified wave numbers, and directions of propagation on different states of the atmosphere.

Finally, the regional climate model RegCM version 4.3 (RegCM4) with a non-hydrostatic core and advanced schemes will be used in this study to investigate the influence of the large-scale flow on the regional circulation. The configuration employed will re-use our observational composites to define boundary conditions taken from the same ERAi data, diagnosing simulations taken from the CORDEX - Southeast Asia project. The model output is then investigated to show the impact of the large-scale forcing embedded in the boundary conditions. The three sub-regional indices are used to assemble the RegCM composite. The moisture budget terms in the regional model will be explored in detail.

1.5 Outlines of the thesis

The structure of the thesis is as follows. In this chapter, we have presented an overview of Vietnam's rainfall with particular attention to the rainfall intraseasonal variation. The Vietnam rainfall annual cycle includes spatial patterns, topography, the hydrology budget, the large-scale circulation mainly driven by the Asian Monsoon, and the linkages to the large-scale forcing on different timescales. Then, Vietnam rainfall ISV is described including the observed characteristics and the possible factors of influence.

In Chapter 2, an observational analysis of the moisture budget and large-scale dynamics associated with Vietnam's subregional anomalous hydrological events is presented. It consists of a short introduction, data and methods used in this chapter and the results for composite analysis. The remote influences on Vietnam sub-regional rainfall ISV are shown. Further results are then presented to examine the sensitivity of the composites to alternative rainfall datasets, parameters such as threshold values chosen to define the composites and interannual events such as the ENSO.

Chapter 3 shows the work using DREAM, the global dynamical model study. Following a short introduction, the model description and configuration used in this chapter are outlined, and the output of heating and nudging experiments using the stationary wave configuration are analyzed. Based on the theoretical Rossby wave propagation, the results from the ray-tracing calculation on different basis states are also discussed.

In Chapter 4, the regional climate model RegCM4 and its configuration are described. Then, the model validation and composite techniques are shown. This is followed by a diagnosis of the model about rainfall intraseasonal variation, the impact of the lateral boundary condition and the moisture budget within RegCM for each of the subregions.

In Chapter 5 we present overall conclusions and perspectives for further work.

Chapter 2

Observed Composite

Contents

2.1 Introduction

In section 1.2, we have reviewed rainfall intraseasonal variability over Vietnam including a statistical description and some physical mechanisms and the factors of influence.

For the statistical description of the rainfall ISV over Vietnam, most research focuses on a certain timescale of the variability of the rainfall such as a 10-20-day variation, 20-60-day variation or even shorter 3-20-day variation. The decomposition of the signal onto a timescale of variation has the advantage of being easier to link with well-known atmospheric phenomena on the same timescale, but no single mode of variation can represent the entire variance of rainfall ISV. Tuan (2019) uses principle component analysis to visualize the EOF patterns that explain most of the variance of rainfall ISV for the whole country. EOFs are often determined by a subregion with a higher variance of rainfall ISV. In this case, Central Vietnam patterns show as a first EOF, while the fourth EOF can not capture well the South Vietnam patterns.

The application of a time filter has the disadvantage of constraining the signal and can lead to bias in the observational analysis. In addition, the differences between subregions on the role of each variation mode are different. Furthermore, the linearity due to the principal component analysis applied to the rainfall ISV over Vietnam limits the examination of differences between opposite events. All of these considerations suggest we could study the rainfall ISV on a large scale without applying any time filter to retain all signals on the timescale that allow further examination of opposite events over subregions.

For the hydrology budget, the three components including the moisture flux convergence, the tendency of moisture and evaporation are important to lead precipitation events at a certain time. It includes the circulation activities through the moisture flux convergence, as well as the tendency of the sources of moisture and evaporation that favor the rainfall event. On the intraseasonal timescale, the descriptive study for these terms that contribute to a rainfall ISV event is an aspect we could study.

Instead of using the precipitation as an index to determine the rainfall ISV events, we would like to use the vertically integrated moisture flux convergence, because of its more direct link with the circulation that could give a better representation to investigate dynamical influences. The composite technique is used here to assemble the opposite events called wet and dry events.

This chapter of the study is an extension to the previous research to investigate explicitly the sensitivity of the conclusions to the different regions, rainfall criteria and timescales of consideration. In this study, we will take a regional approach, and investigate the characteristics of the moisture budget, then diagnose remote influences separately for wet and dry composites and pay particular attention to their interrelations.

We will present our investigation in terms of large-scale observed composites associated with opposite events on regional scale rainfall variability over Vietnam with two sub-sections.

The following section is named remote influence on regional scale rainfall variability over Vietnam in the format of a submission to a peer-review journal. It includes detailed methods for the composite technique to gather wet and dry events, a quick examination of the contribution of hydrological budget terms and a deeper investigation into remote influences associated with these events. For the influence on Vietnam sub-regional rainfall ISV, we focus on the extratropical and tropical flows to identify the precursors up to 2-weeks before an event. The asymmetry between opposite events, the interrelation between subregions and the sensitivity of the indexes derived from different kinds of data will be addressed.

Then, we will give further results for the moisture budget terms associated with the rainfall ISV events via composites. The chapter's conclusion is presented.

2.2 Remote influence on regional scale rainfall variability over Vietnam

2.2.1 Precipitation data: ERA-Interim dataset

According to previous studies, several datasets of precipitation are used to analyze the intraseasonal variability of rainfall over either Vietnam or Southeast Asia. The table in Fig 2.1 highlights the findings and the datasets used. The data is either regional or covers Vietnam's mainland only that are treated by a specified time filter then obtain the regression or composite. Among that, the Wet and Dry spell is recognized only in TT18 and TT19 by discriminating the opposite phases of sub-monthly and 20-60-day variation. Besides the main scientific question that will be addressed in this study, the question of which kind of data will be used for the analysis of rainfall particularly.

Study	Data	Data treatment & analysis method	Including Wet/Dry events	Findings
Yokoi et al 2007, 2008	daily rain gauge data 26yr 1978-2003 **Regional**	wavelet analysis **Regression**	NO	10-20-day variation: NVN and CVN during May-Sep 20-60-day/30-60-day variation: CVN during Jul-Oct
Linden et al 2016	APHRODITE: gridded rainfall data: xx rain gauge stations 1979-2007 0.5 x 0.5 grid **Regional**	MJO/wave phases attributed **Composite** per phase	-	MJO: CVN+SVN significantly influence Equatorial Rossby wave: CVN most Kelvin waves: SVN only
Truong and Tuan 2019 a&b	selected rain gauge stations 1981-2009 **Vietnam only**	specified time-filter 10-20 and 20-60 **Composite** for cycle of ISO	YES but wet/dry phases of cycle	summer MJO: CVN + SVN tropical-extratropical interaction: NVN
Tuan 2019	VnGP: gridded rainfall data: 210 rain gauge stations 1981-2009 0.25 x 0.25 grid **Vietnam only**	Principal Component analysis with specified time-filter 7-25 **Composite** Pcs timeseries	NO	CVN + NVN: extratropical wave-trains interact tropical depression

Figure 2.1: Resume of previous studies for investigation precipitation intraseasonal variability.

In this study, we choose the ERA-Interim reanalysis dataset. That includes all atmospheric variables reanalysis and the precipitation as a derived-products with both land and

sea coverage. This dataset has the advantages of periods continuously from 1979 to 2016 as well as consistency with the modeling input. However, it also depends on the quality of the model and that might differ from daily rain gauge data.

Fig 2.2- the first row, presents the histogram of daily rainfall data over North and South of Vietnam - NVN and SVN from reanalysis data - ERAi and gridded data derived from rain-gauge data - APHRODITE during the summertime May-Oct. The regional daily rainfall time series are obtained by averaging over each subregion. In both cases, the ERAi daily rainfall overestimates the rainfall events less than 4 mm/d and underestimates the rainfall with higher intensities. Generally, the distribution of regional daily rainfall is not well captured by ERAi. However, the intraseasonal rainfall variation - ISV of rainfall shows a better presentation (Fig 2.2- second row). Mostly normal distributions are seen in the intraseasonal rainfall variation over both NVN and SVN from APHRODITE and ERAi. Particularly, APHRODITE data show a lower variation than those of ERAi, especially for SVN. In addition, the ERAi rainfall shows more sensitive to the negative rainfall anomalies on the intraseasonal timescale.

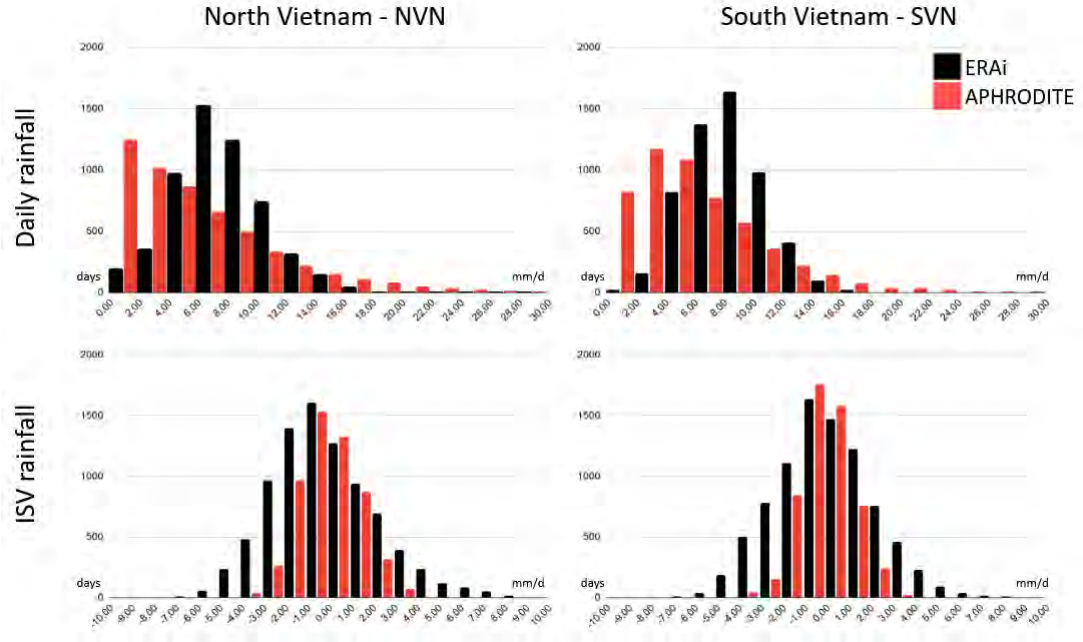

Figure 2.2: The histogram of Daily (first row) and ISV rainfall (second row) over North (left) and South (right) of Vietnam using ERAi and APHRODITE rainfall dataset.

Thus, we acknowledge that the difference between the datasets could influence the analysis of large-scale fields. We will present more comparisons between ERAi and APHRODITE as well as VnGP - a gridded rainfall data dedicated over Vietnam mainland in the next part in terms of correlation and the standard deviation. ERAi-based indices in the following analysis are conducted but we will evaluate sensitivity to the other datasets.

2.2.2 * Summary of paper*

The paper below is submitted to International Journal of Climatology and it is in revision at the time of writing.

In the paper, a short literature review concerning the characteristics and remote influence of ISV of rainfall over Vietnam is pointed out. Rainfall in Vietnam (ISV) is typically described as spatio-temporal patterns that manifest differently in the North, Central, and South of the country. Both extratropical and tropical factors and even their interactions from previous studies are indicated to impact Vietnam rainfall ISV in terms of patterns, intensity and frequency of occurrence.

However, the challenge is sensitive to the choice of location, period, dataset, and analysis approach, and there have been very few analyses that distinguish between wet and dry anomalies over Vietnam subregions on intraseasonal timescales. We rise the importance of investigating how sensitively the results apply at the regional scale considering the variety of areas, rainfall parameters, and timescales of variation.

We aim to identify the dynamical precursors/pathways of influence to anomalous rainfall events over North and South Vietnam with paying attention to asymmetric precursors to Wet and Dry events. The sensitivity of our conclusion is further investigated by choice of regions and hydrological index.

Remote influences on anomalous rainfall over regions that encompass North and South Vietnam are explored using a 38-year (1979-2016) global dataset over the extended summer (May-October). Focuses on anomalous rainfall events during the summertime with a lead time of two weeks, we have used the vertically integrated moisture flux convergence (VIMC) as a link between regional precipitation and large scale dynamics. We displayed that is well correlated with rainfall ISV and can thus be reasonably used as a proxy. For the other moisture budget terms, the tendency of moisture column - TMC and the evaporation - EVP contribute a small part. The TMC develops slightly differently between the regions. EVP anomalies are negative for Wet events and positive for Dry events over all subregions and are mostly symmetrical (see Annex A - moisture budget)

At regional scales, lag composites of VIMC and rainfall anomalies gain significant amplitude at different lead times for the different regions, but in all cases show a reasonable degree of symmetry between Wet and Dry cases. This straightforward situation is not observed at larger scales.

The asymmetrical large-scale dynamics associated with Wet and Dry events are both seen in NVN and SVN including extratropics and tropics. The similarities between SVN events and opposite NVN events are indicated including the rainfall patterns and extratropical precursors. However, the extratropical precursors associated with NVN events show more sensitivity to the choice of the region than SVN, by including overlapping day -CVN. There is fairly consistency in large scale dynamics associated with NVN events between the VIMC index and in-situ rainfall data. We figure out three pathways of influence at lead times of

one to two weeks: a high latitude pathway seen in NVN Wet and SVN Dry; a jet pathway in NVN Dry and SVN Wet; and an equatorial pathway as a signature for both SVN Wet and Dry.

2.2.3 Remote influence on regional scale rainfall variability over Vietnam

Remote influence on regional scale intraseasonal rainfall variability over Vietnam

Hong-Hanh Le* and Nicholas M.J. Hall †

LEGOS - University of Toulouse III - Paul Sabatier, Toulouse, 31400, France

Thanh Ngo-Duc ‡

LOTUS - University of Science and Technology of Hanoi, Vietnam Academy of Science and Technology, 100000, Vietnam

**Corresponding author*: Hong-Hanh Le, Lehonghanh.Lhh@gmail.com

†Nick.Hall@legos.obs-mip.fr

‡Ngo-Duc.Thanh@usth.edu.vn

ABSTRACT

Remote influences on anomalous rainfall over regions that encompass North and South Vietnam are explored using a 38-year (1979-2016) global dataset over the extended summer (May-October). Composites of Wet and Dry events with lags of up to two weeks are assembled for various rainfall indices over the two subregions, including reanalysis products and in-situ data. On the regional scale, the moisture flux convergence correlates well with reanalysed rainfall. The large-scale dynamics associated with these events are described. Rainfall event composites of opposing signs show asymmetrical large-scale precursors and different pathways of influence. Wet and Dry events in North Vietnam are seen to originate from Europe and propagate at high latitudes. The exact nature of the precursors is sensitive to the definition of the composite index. There is also a pathway of influence along the Asian jet, which impacts South Vietnam, especially for Wet events which often coincide with Dry events in the North. South Vietnam is also influenced by tropical divergent precursors, which are again asymmetric between Wet and Dry events.

Keywords: Remote influences; Rainfall; Intraseasonal variability - ISV; Large-scale dynamics; Tropical waves

1. Introduction

The annual cycle of rainfall over Vietnam is controlled by the seasonal South-East Asia monsoon system. However, within a season there are large variations that account for a major fraction of the total rainfall variability (Yokoi et al. 2007). Intraseasonal anomalies during the rainy season from May to October can take the form of prolonged periods of flood or drought, or extreme events of shorter duration, e.g., Wu et al. (2012); Linden et al. (2016a). Such anomalous rainfall can have important consequences for agriculture and water resources. This study focuses on remote influences on rainfall anomalies over Vietnam on regional spatial scales and intraseasonal time scales.

Intraseasonal variations (ISV) of rainfall over Vietnam have previously been characterized as spatio-temporal modes. Yokoi and Satomura (2005) and Yokoi et al. (2007) used a wavelet analysis of daily rain gauge data over the Indochina Peninsula and identified two ISV timescales for different horizontal distributions of rainfall over Vietnam. They showed that a 30-60-day variation is observed in Central Vietnam in July-October, while a 10-20-day variation is observed in North and Central Vietnam in May-September. Truong and Tuan (2018) - TT18 and Truong and Tuan (2019) - TT19, also showed that daily rainfall from selected stations displays significant variability on 30-60-day and 10-20-day time scales.

There have been relatively few investigations that discriminate between wet and dry anomalies over Vietnam subregions on intraseasonal timescales. The problem is sensitive to the choice of region, timescale, dataset and analysis technique.

For example, Tuan (2019) used Principal Component (PC) analysis to extract spatial patterns of sub-monthly rainfall variation using high-resolution gridded precipitation data from 1980 to 2010 over Vietnam (Nguyen-Xuan et al. 2016) with a time-filter of 7-25-day. Four patterns

were identified, each of which covers the entire region. Only the active (Wet) phases of PCs were considered. On the other hand, TT18 and TT19 concentrated on individual regions and isolated time periods of 10-20-day and 20-60-day respectively, using station data, which is mostly concentrated along the coast. They consider wet and dry phases as part of a cycle. Other investigators have looked at individual wet cases over Vietnam subregions, e.g., Linden et al. (2016a); Yokoi and Matsumoto (2008); Wu et al. (2012).

Given the multiplicity of regions, rainfall criteria and timescales to consider, it is worthwhile investigating explicitly the sensitivity of the conclusions to such considerations at the regional scale. In this study, we diagnose remote influences separately for wet and dry composites and pay particular attention to their interrelations across relatively large regions. We will use vertically integrated moisture flux convergence (VIMC) as a proxy for rainfall ISV since it is highly correlated with regional-scale rainfall. VIMC is a quantity that is close to the large-scale dynamics and is available from a consistent dataset.

We then consider two types of remote influence: tropical and extratropical. Tropical phenomena such as the Madden Julian Oscillation - MJO (Madden and Julian 1972), and equatorial Rossby and Kelvin waves are the main factors that influence rainfall ISV over Vietnam, mostly in the central and southern regions. Linden et al. (2016b) show daily rainfall associated with different phases of the MJO and equatorial waves. They also show that these waves enhance the frequency of intense daily rainfall during the wet phase, and positive interference of these different waves can lead to strong enhancement of wet or dry events. Yokoi et al. (2007), TT18 and TT19 also find that large-scale dynamics associated with rainfall variation resemble the MJO and tropical wave activity, especially for Central and South Vietnam. TT18 indicates a tropical Indian Ocean mode in the form of equatorial Rossby waves with 10-20-day variation in North and South Vietnam, and TT19 relates MJO activity to 20-60-day variations for South Vietnam.

Extratropical influence is commonly identified with pressure surges or cold surges from the Siberian High. Tuan (2019) finds that extratropical precursors to Vietnamese rainfall ISV often take the form of wave trains along with the North Atlantic-Asian-North Pacific jet, and that pressure surges from the Siberian high and Northeast China are associated with sub-monthly rainfall anomalies over North and Central Vietnam. Abdillah et al. (2021), also identifies pathways of influence in East Asia and tropical impacts of northerly and westerly cold surges induced by Cold Air Outbreaks (CAOs) at high latitudes during wintertime.

Individual wet events can also arise from an interplay between tropical and extratropical factors. Wu et al. (2012) shows an example of a synoptic-scale tropical wave formed over the South China Sea combined with a surface high extending from western Mongolia to the East China Sea with a presence of strong MJO over the Indian Ocean leading to heavy rainfall. Further examples of combined effects include cold surges associated with expansion of the Siberian High and tropical depressions associated with the MJO, e.g., Yokoi and Matsumoto (2008); Chen et al. (2012); Abdillah et al. (2018).

The main focus of this paper is on the asymmetries in large-scale dynamical precursors to opposite signs of anomalous rainfall: Wet and Dry episodes in selected sub-regions of Vietnam. Our work is intended to complement previous work where regional dependence has been expressed either as sub-regions or spatial patterns. Our choice of sub-regions is deliberately simple and we retain a relatively large scale compared to the linear nature of the country under consideration in order to ease the potential connection with dynamics at a larger scale compared to local phenomena. We will explicitly analyse composites for two large regions that include Vietnam: North and South, and we will also analyse a buffer zone between them in order to address the scale of the anomalies considered. These regions will first be analysed separately and then their interdependencies will be investigated. Specifically, we address the following questions:

- Can we identify dynamical precursors/pathways of influence to anomalous rainfall events over North and South Vietnam?
- How asymmetric are the precursors to Wet and Dry events?
- How much do these precursors extend or overlap from one sub-region to another?
- How sensitive are our conclusions to choices of region, threshold and composited quantity?

Data and methods are presented in Section 2. The regional development of the moisture budget terms associated with event composites are described in Section 3. Section 4 then shows the large-scale dynamics associated with these composites. Discussion and conclusion are given in Section 5.

2. DATA and METHODS

a. Data

We use 38 years (1979-2016) of ERA-Interim global reanalysis (Dee et al. 2011) from May to October. Four-times daily data of atmospheric variables including zonal wind- u, meridional wind- v, specific humidity- q, and geopotential height- gph are used from a dataset that has been interpolated to T42 horizontal resolution on a 128x64 grid and set on sigma levels relative to mean sea level pressure for use in complementary studies with a dynamical model. Daily gridded 1x1 degree data of precipitation (PPT) is used from ERA-Interim reanalysis using the Frequent Rainfall Observations on GridS (FROGS) dataset (Roca et al. 2019).

We also use different sources of precipitation data: APHRODITE and VnGP, to examine the sensitivity to the definition of our index. The APHRODITE-MA V1101EX-R1 is downloaded from `http://aphrodite.st.hirosaki-u.ac.jp` (Yatagai et al. 2012) and the VnGP is published in Nguyen-Xuan et al. (2016). Details of these datasets are given in Table 1.

The data are processed retaining the entire ISV signal. The only filter applied is to remove synoptic timescales. So four-times daily Vertically Integrated Moisture Flux Convergence (VIMC) is calculated using u, v, and q at all levels, and then averaged to daily values for comparison with the PPT. These fields are smoothed with a 10-day running mean, and a smoothed annual cycle is removed based on average by calendar date. Finally, the linear trend is removed to obtain intraseasonal and interannual variations. The geopotential height at 250 mb and u, v and velocity potential at 850 mb are also subjected to the same procedure to investigate the large-scale circulation.

In addition, El Niño Southern Oscillation (ENSO) is known to affect rainfall in Vietnam (Nguyen et al. 2013). Since our focus is on intraseasonal variability, dominant interannual ENSO-related signals are removed using the bi-monthly Multivariate ENSO Index - MEI time series provided by the National Oceanic and Atmospheric Administration (NOAA) at `https://psl.noaa.gov/enso/mei/`.

b. Methods

Signals associated with anomalous rainfall events are constructed using composites. This approach allows us to assess asymmetries in the moisture budget and large-scale dynamics associated separately with wet or dry events. It requires a regional index and a threshold that defines positive or negative episodes over the region.

The regional index is generated from the VIMC anomaly as outlined above. Each regional index is averaged over the domains. To analyze regional dependency (Nguyen et al. 2013; Tuan 2019), and to analyse the encroachment of one region onto another we divided Vietnam into three regions included in the three boxes shown in Fig. 1: North Vietnam - NVN; Central Vietnam and Central Highlands - CVN and South Vietnam - SVN. Note that these regions are relatively large compared

to some previous studies and thus may display temporal characteristics that differ from those of station data. For this reason, we concentrate on NVN and SVN in our composite analysis. A central "buffer" region is also considered for the statistics of the indices. Our CVN sits between NVN and SVN at a similar scale, but it region crosses the central mountain range and so integrates differing local rainfall signatures: rainfall peaks in the winter monsoon season in the eastern side and in the summer monsoon season in the southwestern part of the region, i.e. the Central Highlands. CVN is included to provide information on the extension of NVN and SVN indices into these central latitudes, but does not necessarily provide detailed guidance for rainfall in a given location in central Vietnam. Sensitivity to the definition of these indices and to the rainfall dataset used will be discussed further below.

Thresholds were defined from the Probability Frequency Distribution (PFD) of the daily VIMC index shown in Fig. 2. A value of ±3mm/day is widely used in the hydrology sector to classify rainfall anomalies Haensel et al. (2015). Following our regional PFD, the probability of days having intensity of rainfall anomaly above/below +3/-3 mm/day accounts for about 10% of the rainfall variability in all cases. It can be used as a threshold value in this study to simply present opposite events of anomalous rainfall. We will discuss the sensitivity of our results to this choice below.

The composites are initially constructed from daily VIMC indices exceeding +3mm/d and -3mm/d. Firstly, we concentrate on characteristics exclusive to each region by gathering composites for a given domain only, but not in the other two. This means that the overlapping dates having more than one regional index exceeding the threshold value are excluded from the composites. Further composites are then constructed that include the overlapping events to reveal the level of dependency between regions or the degree of extension of a rainfall signal outside the defined

region. All dates that have regional VIMC anomalies greater than 3mm/d are called Wet events, and those less than -3mm/day are called Dry events.

Details of the numbers of days associated with all possible combinations for the three regions for Wet and Dry events are shown in Table 2. This table forms a symmetric matrix so the redundant upper right triangle is left blank, and impossible Wet-Dry combinations are marked "none". Total numbers of events are recorded, and in parentheses, we show the number of events when multi-region Wet or Dry events are excluded. The number in parentheses can only be non-zero on the leading diagonal and in the lower left quadrant. Specifically, there are 302, 277 and 172 exclusive Wet days for NVN, CVN and SVN respectively, and 282, 267 and 277 exclusive Dry days.

3. REGIONAL DEVELOPMENT

a. Regional climatology

Monthly averaged rainfall and monthly variance of daily anomalies of PPT and VIMC over NVN and SVN domains are shown in Fig. 3. The monthly variance of VIMC and PPT are similar and follow the seasonal cycle of rainfall, especially in NVN. Most of the rainfall occurs over both regions during the summertime (May- October). Monthly rainfall peaks in August in NVN (Fig. 3a)and September-October in SVN (Fig. 3b). The VIMC and PPT anomalies in NVN show maximum variance in line with maximum rainfall.

The annual cycles of rainfall over the three regions show differences from previous regional rainfall studies due to the definitions chosen for the regions and the data used. Note that the seasonal cycle for CVN (not shown) is different from what it would be if data were restricted to the national territory. Our region includes an area to the west that is directly influenced by the summer monsoon in addition to the orographic influence of the Truong son mountains that better

characterises the Vietnamese coastal rainfall signal which peaks in September (TT19). For this reason, we do not present composites for this region but we retain it for information pertaining to the extension of the rainfall signal in the other two regions. For SVN, our selection covers flat terrain and a part of the sea, which is subject to a strong seasonal signal from the summer monsoon (Nguyen et al. 2013). The high rainfall intensity has a relatively low variance during the rainy season compared to two other regions.

Temporal variations in VIMC are well correlated with the reanalysis rainfall product, and thus present a reasonable proxy to investigate directly the link between the hydrological cycle and the associated large scale circulation as previously found by Sohn et al. (2004). Chansaengkrachang et al. (2018) also show that VIMC shows a high positive correlation with the daily rainfall over Thailand.

Further details are shown in Fig. 4 in the form of a Taylor diagram that summarises the standard deviation ratio and correlation coefficient for the daily-time series from May to October, averaged over our three regions for the APHRODITE, VnGP, VIMC and FROGs datasets. The reanalysis product - FROGS/ERA-interim over each box is used as a reference: a black point on the lower axis. The RMS difference from this reference is the linear distance to this black point, the correlation coefficient is the angular distance, and the relative magnitude of the standard deviation is the radial distance from the dashed circle.

We see that the standard deviation of PPT is very similar over our three chosen regions, with 2.43 mm/day for NVN, 2.42 mm/day for CVN and 2.22 mm/day for SVN.

The daily VIMC indices have a high positive correlation to PPT, with coefficients of 0.66 for NVN; 0.76 for CVN and 0.72 for SVN. They are also very close to PPT in standard deviation for all three domains. The VnGP and APHRO indices both show a positive correlation with PPT of

about 0.4 (and APHRO and VnGP indices are very highly correlated with one another: 0.93 for NVN, 0.78 for CVN and 0.85 for SVN).

The APHRO indices show uniform variance, but it is weaker than for PPT with a ratio of 0.5-0.6. On the other hand, the VnGP CVN indices show a spread of variance: stronger than PPT for CVN and weaker for NVN and SVN.

These differences between data can mostly be attributed to the extent of the coverage. It can be seen that the ISV over CVN box is particularly sensitive to the dataset in use, undoubtedly for the reasons already discussed: VnGP covers Vietnam mainland only, thus represents the coastal region - east of the Truong Son mountains.

Since our focus is on large scale precursors, we will proceed with VIMC as a proxy for the diagnosis of rainfall variability over NVN and SVN only, at the regional scale on intraseasonal timescales in the summertime. We will, however, examine the sensitivity to the choice of rainfall dataset for large scale precursors to wet and dry events in section 4 below.

b. Composite precipitation events

The two-week lagged composites of VIMC and PPT anomalies associated with Wet and Dry events over regions are shown in Fig. 5 - 6.

Fig. 5 shows spatial patterns of VIMC and PPT anomalies for Wet and Dry events in NVN. Positive anomalies of VIMC and PPT over the western Pacific can be seen from day-15 to day-0 (Fig. 5 a-d) prior to Wet events, and negative anomalies precede Dry events. VIMC anomalies develop quickly to the northwest to cover NVN at day-9, followed by PPT anomalies. A wet-dry dipole over North-South Vietnam is established from day-9 for Wet events. Dry events are more weakly foreshadowed in the lagged composites (Fig. 5 e-h). The VIMC anomalies occur first over NVN at day-9, while PPT anomalies are well established at day-3. The day-0 regional dipole over

North-South Vietnam for dry events is quite symmetrical between Wet and Dry cases. Both NVN Wet and Dry events have a maximum of VIMC over NVN at day-3, while PPT peaks at day-0.

Fig. 6 shows lagged composites for SVN. Both Wet and Dry events have significant VIMC and PPT anomalies from day-15, especially the Dry events. Wet events in SVN are associated with positive anomalies of VIMC and PPT over the Maritime Continent from day-15 which intensify to cover a large region, from the equatorial Western Pacific to the Indian Ocean (Fig. 6 a-d). At the same time, weaker negative anomalies from the northern Philippines move gradually westwards to cover northern Vietnam. Dry events in SVN on day-15 (Fig. 6e) show significant positive VIMC and PPT anomalies extending from the north of Vietnam to the western Pacific. This broad feature then becomes progressively more concentrated over the north of Vietnam (Fig. 6 e-h). The negative anomalies over the Maritime Continent strengthen and extend at the same time to cover a similar region to the positive anomalies in the Wet events. VIMC and PPT anomalies for Wet and Dry events in SVN show dipole patterns over North-South of Vietnam at day-0 (Fig. 6d and Fig. 6h). The anomaly centers are co-located with anomalies of opposite signs for NVN.

These rainfall anomaly patterns are in broad agreement with the EOF decompositions from 7-25-day rainfall variations produced by Tuan (2019). We also see an agreement between our Wet - Dry events and maxima - minima of the 20-60-day intraseasonal oscillation (ISO) of observed rainfall in Vietnam described in TT19. Our results indicate that there are some asymmetrical features between opposing events, especially for NVN. This was also mentioned in TT19 and Linden et al. (2016b), in which positive anomalous rainfall over Vietnam was attributed to convergent moisture flux, suggesting that VIMC may constitute short term predictive information for large scale rainfall.

4. LARGE-SCALE CIRCULATION

In this section, the large-scale circulation associated with Wet and Dry composites is examined. Precursors will be analysed with attention to the degree of symmetry between Wet and Dry episodes and between regions. Diagnostics have been chosen to highlight both tropical and extratropical factors.

a. Tropical flow

To look at tropical influence, we examine the divergent flow. The following set of figures shows the lower tropospheric velocity potential, together with wind vectors and VIMC, to focus on anomalous moisture transport and its convergence.

Fig. 7a-d shows the divergent flow associated with NVN Wet events. The positive VIMC anomaly over the Western Pacific is associated with a persistent low-level convergence anomaly from day-15 (Fig. 7a) that remains strong over two weeks prior to events. It can be seen as a tropical precursor to Wet events in NVN. It intensifies over NVN from about day-9, assisted by anticyclonic winds over Japan and strong south-westerlies over the Bay of Bengal, leading to a second center of velocity potential and positive VIMC over NVN at day-0 (Fig. 7d). The peak in westerlies separates North and South Vietnam and VIMC is negative over SVN from day-9 (Fig. 7b). The low-level pattern for Dry events over NVN shows no strong precursors in the divergent flow (Fig. 7e-h). There is a persistent equivalent barotropic cyclonic flow off the coast of Japan (also seen in Fig. 9). Only on day-9 do we see the development of large scale low-level divergence. This intensifies rapidly over the following week to form a strong divergent center over the NVN area with negative VIMC and local anticyclonic low-level flow. But this divergent anomaly does not appear to have tropical origins. For NVN, we see an asymmetry in tropical precursors, which

shows little evidence of a propagating signal. In both cases the low-level influence comes from the east, but only NVN Wet is associated with a persistence of convergence.

Low level divergent flow for SVN events is shown in Fig. 8. Here we see a positive anomaly in velocity potential over the eastern Indian Ocean with a slow eastward displacement. From day-9 (Fig. 8b) there is also a weak large-scale divergent anomaly over the Pacific and easterly winds develop across the Philippines into southern Vietnam, associated with a pair of anticyclones straddling the equator. This easterly jet is a potential source of moisture transport and VIMC grows over SVN from day-9 as this easterly flow strengthens and the positive center of velocity potential intensifies and moves over the Maritime Continent. Dry events (Fig. 8e-h) are piloted by large scale convergence over the Western Pacific, followed by a similar slow displacement from the equatorial Indian Ocean to the Maritime Continent. There is a low-level westerly jet which in this case remains mostly east of Vietnam but the associated pattern of VIMC looks quite symmetrical compared to the Wet case.

It is worth drawing attention to some similarities between the divergent flow for NVN Wet and SVN Dry events. They share a convergence area over the Western Pacific and northerly winds from Japan from day-15 associated with the positive VIMC over NVN. However, for SVN-Dry, the convergence area moves to the east which leaves a cyclonic anomaly over NVN with a weaker signal in VIMC and vertical motion on day-3, while for NVN-Wet, it strengthens and develops westward. The negative anomaly of VIMC over the NVN box in NVN Dry events is associated with the local anticyclonic development with descending motion, but there is weaker vertical motion for SVN-Wet.

In summary, these composites are characterized by an eastward displacement of large scale equatorial divergent flow dor SVN. No significant equatorial wave activity is found for NVN Wet

and Dry events. There is some similarity between NVN-Wet/Dry and SVN-Dry/Wet events, but the tropical divergent flow exerts a far greater influence on SVN events.

b. Extratropical flow

For the diagnosis of extratropical teleconnections, we examine the rotational flow at larger scales. The following figures show the upper tropospheric geopotential height to focus on the extratropical geostrophic flow anomalies and their propagation over the two weeks preceding the events.

The Northern Hemisphere extratropical flow for Wet and Dry composites in NVN are shown in Fig. 9 through two weeks of lagged composites of 250 mb geopotential height anomalies. For Wet events on day-15 (Fig. 9a) a positive anomaly is situated over Europe and a negative anomaly over Kazakhstan. This dipole shows slight eastward displacement until day-9 and then dissipates, giving way to a low over Russia that subsequently grows on day-3 and spreads southwards quickly. At the same time, there is a persistent high over Eastern Siberia that extends over Japan. This feature is almost stationary. At lower latitudes a high starts to displace eastwards, south of the Asian jet until day-0 (Fig. 9d) as a low develops over China.

Dry events in NVN are associated with a large-scale negative anomaly over Eastern Europe that strengthens and extends southwards into the jet region from day-15 to day-9 (Fig. 9e-f). During this period there is an equally strong negative anomaly further east over northern China/Mongolia, and there is a persistent high between the two negative centers. This low-high-low structure sits on the Asian jet axis and shows very slight phase propagation to the east. From day-3 to day-0 (Fig. 9g-h) the two low centers merge and spread towards South-East Asia while the positive anomaly dissipates and a new positive anomaly center is established over China-Korea-Southern Japan.

Comparing Wet and Dry precursor developments we see considerable asymmetry. For example, there is no counterpart in the Dry composite to the persistent Siberian high seen for the Wet events.

322 Although both series show alternating signs along the jet, they are not in phase opposition and they
323 have different characteristic scales. The NVN-Wet precursors spread both sides of the jet, while
324 NVN-Dry precursors are more confined to the jet region. However, the ensuing local circulation at
325 day-0 is more symmetrical, consistent with the regional analysis. NVN events appear to comprise
326 predominantly extratropical influences.

327 Fig. 10 shows composites for SVN Wet and Dry events. Both composites are associated with
328 remarkably strong signals compared to NVN and CVN. Wet events are associated with a low
329 over Siberia and a compact high over Japan throughout the preceding two weeks. Further west,
330 precursors take the form of an extended low and high, orientated SW-NE over eastern Europe/Asia.
331 This structure tilts into the Asian jet from day-15 to day-9 (Fig. 10a-b), after which a compact
332 high intensifies in-situ in the jet entrance. Although there is no phase propagation, the increased
333 amplitude of the signal appears to propagate at the latitude of the jet, finally intensifying the high
334 over Japan. The collocation of anomaly centers with mean position of the jet core is reminiscent
335 of the dry composite for NVN.

336 For SVN dry events, precursors are dominated by a persistent Siberian high which is present
337 from day-15 (Fig. 10e). It intensifies on day-9 then spreads southwards over China from day-3 to
338 day-0. There is also a high over eastern Europe and a low over the jet which slightly moves to the
339 east from day-15 to day-9 then intensifies until day-0. This pair of anomalies and the persistent
340 Siberian high are opposite to those seen for SVN Wet events, so in this respect, there are symmetric
341 precursors between Wet and Dry events. The overall patterns of extratropical flow associated with
342 SVN Wet/Dry events shows some similarity to the composites for NVN Dry/Wet, although there
343 are some differences in detail. The high-latitude anomalies over Europe are more stationary for
344 SVN.

345 In summary, we have diagnosed remote teleconnections in terms of extratropical rotational
346 flow and tropical divergent flow. Extratropical influence is probably responsible for disturbing the
347 otherwise symmetric patterns of rainfall anomaly prior to Wet and Dry events. The strongest signals
348 are seen in SVN cases, while the propagation of anomalies from Europe and higher latitudes over
349 Siberia is observed more clearly in NVN cases. Symmetric patterns for NVN Wet and Dry events
350 are associated with extratropical influence, while SVN events are subject to additional influence
351 from the tropics.

352 *c. Regional interdependency*

353 The analyses presented up to this point have been based on composites in which days, where
354 the threshold is exceeded in more than one region, have been excluded. This operation has been
355 carried out separately for Wet and Dry events so the prominent Wet-Dry opposition between NVN
356 and SVN is retained. But there are many excluded days where, for example, wet conditions extend
357 from the NVN as we have defined it, into our artificial CVN region to the south. In this section,
358 we examine how the results are affected by including such events in the analysis.

359 Table 2 shows that the CVN zone often shares Wet or Dry events with NVN or SVN. Generally,
360 about half the Wet events and about one-third of the Dry events in either NVN or SVN extend
361 into CVN. On the other hand, NVN and SVN are relatively independent from one another. They
362 rarely share Wet events, but they are more commonly in opposition, consistent with some of the
363 symmetries in composite patterns we have seen. And exclusion of the overlap with CVN makes
364 very little difference to the frequency of NVN-SVN opposition.

365 How do the composite patterns change when shared events are permitted? Events in a given
366 region are of practical interest, regardless of how unique they may be. The extratropical flow
367 associated with anomalous events shared by more than one region are shown here and compared

with the isolated cases. The differences between these figures serve to illustrate how dependent these precursor diagnostics are on the definition of the regional index.

Fig. 11 shows the large scale precursors when both NVN and CVN are wet (Fig. 11a-d) or dry (Fig. 11e-h). So patterns for all NVN Wet events (not shown) will be very close to an average of figs 9 and 11. The final state at day-0 shows a stronger signal, consistent with stronger and larger scale rainfall events. The pattern is largely in phase with the isolated NVN pattern. Negative height anomalies are more prominent, and this is even more evident at earlier lags, where a large-scale depression occupies a region over western Siberia whereas the signal is weak in the isolated case. Dry composites show more consistency between extended and isolated events with a slight phase shift in perturbations that essentially travel along the latitude of the jet, and this time more prominence is given to the positive geopotential anomaly. The set of all NVN Dry events (not shown) is weighted towards the isolated pattern.

A similar exercise can be carried out for common events between SVN and CVN and the resulting composites are shown in Fig. 12. In this case, there is more consistency for Wet events, especially for the long term precursors over Eurasia (Fig. 12a-c). Differences are apparent at smaller scales, for example, the disappearance of the high over Japan on day-0 compared to the isolated SVN case. Patterns for all SVN Wet events (not shown) are again essentially an average of figs 10 and 12, resulting in fairly weak precursors over eastern Asia but consistent dipole patterns over eastern Europe / western Asia. For Dry events (Fig. 12e-h) shared by SVN and CVN a different picture emerges. There is a complete reversal of sign for the large scale patterns and when the two are combined in the correct proportions (table 2) only the Siberian high remains, moving southwards from day-9 (Fig. 12j). The high over China is the main common feature between isolated and extended Dry events.

391 In all cases, the tropical divergent circulation shows much less sensitivity to the definition of the
392 index for NVN and SVN, for both Wet and Dry composites. Events that extend into the CVN zone
393 are almost identical with a slightly stronger signal in most cases.

394 Finally, it is of interest to examine cases where NVN and SVN have opposite rainfall anomalies.
395 Fig. 13 shows large scale composites from the 87 cases of NVN-Wet/SVN-Dry and the 31
396 cases with NVN-Dry/SVN-Wet. Recall that there is a close resemblance between composites for
397 exclusive NVN-Wet and SVN-Dry. Fig. 13a-d again shows a similar pattern but with much higher
398 amplitude, implying that although the NVN-Wet/SVN-dry pattern represents a relatively small
399 number of events, they are among the strongest in terms of large scale precursors. Interestingly,
400 no such amplification is seen for the tropical divergent flow (not shown) which appears much like
401 the stronger SVN Dry cases except for a local convergent feature over NVN. The NVN-Dry/SVN-
402 Wet composite is also shown in Fig. 13e-h looks like a strongly amplified version of SVN-Wet,
403 which was already somewhat stronger than NVN-Dry. This is even more apparent for the tropical
404 divergent flow (not shown). Both cases apparently show the propagation of anomalies over Eurasia,
405 more likely those of NVN cases.

406 *d. Sensitivity to index definition*

407 In this section we present a brief summary of results for alternative indices, APHRO and
408 VnGP, to see how sensitive our results are to the type of rainfall data used. As presented in
409 the data comparison, we note that the threshold for regional indices varies with the variance on
410 the intraseasonal timescale, so in the following the thresholds have been chosen so that these
411 composites account for a similar fraction of the variance.

412 For NVN, the threshold value for VnGP is 3 mm/day as it is for VIMC, but for APHRO it is
413 1.6 mm/day. Composites are assembled by applying the same process as for VIMC. The NVN

Wet/Dry composites include 302/282 days for VIMC, 372/222 days for APHRO, 303/199 days for VnGP. For SVN, the threshold value for VnGP is 1.5 mm/day, and for APHRO it is 1.6 mm/day. The SVN Wet/Dry composites include 172/227 days for VIMC, 267/123 days for APHRO, 315/192 days for VnGP.

Fig. 14 shows composite large scale geopotential height anomalies for 9-day lead times for NVN events. These plots can be compared with the second row of Fig. 9 for ERAi. For wet events over NVN we see the 9-day precursors for these two datasets are in broad agreement. They share a north-south low-high dipole over western Asia and a double-high structure over northern Siberia extending over Japan. This latter feature is also present for the ERAi composite but further to the west the structures differ. For dry events, the very broad low over central and western Asia is recovered for all three indices, although it is weaker for ERAi. The high over Europe is also common to the three datasets, while there is some difference in the placement of smaller-scale positive anomalies. The broad agreement of phase for the three indices persists to day-0 (not shown).

Fig. 15 shows the results for SVN (to be compared with the second row of Fig. 10). In this case for wet events there is quite a good agreement between APHRO and ERAi, but the VnGP composite is somewhat weaker and does not produce the same phase over northern and eastern Europe, or the high over eastern China - Japan. VnGP gives higher amplitude precursors for dry events which are in phase at a large scale with those from APHRO, at least for eastern Asia. For dry events, the ERAi composite differs, with the dominant large-scale high further north. Over western Asia and Europe there none of the indices show much consistency. As the lag progresses to day-0 the inconsistency between the three indices remains (not shown).

In general, the composites are fairly consistent for NVN, and as might be expected the APHRO and VnGP products are more similar to one another than they are to ERAi. For SVN we see a

different story, with less consistency between any of the datasets. We conclude that precursor anomalies can be sensitive to the definition of index, especially in SVN.

5. DISCUSSION and CONCLUSION

In this study, we have considered intraseasonal rainfall anomalies over three regional scale zones centerd on Vietnam and explored remote dynamical influences. The investigation focuses on anomalous rainfall events during the summertime with a lead time of two weeks. We have used the vertically integrated moisture flux convergence (VIMC) as a link between regional precipitation and large scale dynamics, after first establishing that it is well correlated with intraseasonal rainfall variability on these time scales and can thus be reasonably used as a proxy. At regional scales, lag-composites of VIMC and rainfall anomalies gain significant amplitude at different lead times for the different regions, but in all cases show a reasonable degree of symmetry between Wet and Dry cases. This straightforward situation is not observed at larger scales.

The main focus of this work is to record the larger scale dynamical environment associated with anomalies in regional hydrology. Vietnam is subject to diverse influences and we have seen that they combine in a variety of ways depending on the region. Previous studies have often taken a regional approach to diagnosing the atmospheric state associated with precipitation anomalies. One of the difficulties in assigning causes to anomalies in a given region is the dependency between neighboring and even distant regions. Another difficulty is the clear asymmetry often recorded between Wet and Dry events. These two difficulties are the main theme of this paper, and for this reason, we have chosen to treat Wet and Dry events separately, using composites rather than regressions, and avoiding time filtering that might hide non-periodic components of the variability. We have paid particular attention to the interdependency between regions by explicitly considering them in isolation and in combination.

When we break down the large scale composites and examine them for Wet-Dry, North-South and Tropical-Extratropical symmetries, a complex picture emerges, as follows.

- Wet events in NVN are essentially influenced by the extratropics, but in a highly asymmetric way and also in a way that is very dependent on whether the anomalies in VIMC also spread south to the intermediate CVN zone. Isolated NVN events are associated with a western Siberian high and a depression over China, consistent with cold surges diagnosed by Abdillah et al. (2018). For events that also spread to CVN the precursors are quite different but still essentially north of the mean latitude of the Asian jet, with a Siberian low developing into a three-pole large-scale low-high-low structure.

- Isolated Dry events in NVN are highly asymmetrical compared to the Wet case. They are influenced by anomalies that line up along the latitude of the Asian jet, leading to a high over Japan. For anomalies that extend into the CVN zone, we recover a large-scale high-low-high pattern over Asia that is quite symmetrical with the corresponding Wet cases.

We conclude that for NVN there are two extratropical pathways of influence: large scale quasi-stationary patterns at high latitudes in the Wet case and smaller scale perturbations along the jet in the Dry case. However, it must be stressed that for NVN the large scale precursors are quite sensitive to the index considered and can show a great deal of asymmetry for Wet and Dry anomalies.

- Wet events in SVN are associated with a sequence of sign reversals along the mean position of the Asian jet, somewhat similar to Dry NVN but not perfectly asymmetric. In fact, the SVN Wet composites have greater amplitude than the NVN Dry ones, and precursors over western Asia are quite different. Furthermore, SVN is distinguished from NVN by the strong influence of a slowly moving buildup of low-level convergence over the Indian Ocean towards

484 the Indonesian region, reminiscent of the MJO (Linden et al. 2016b). When SVN Wet is
485 combined with NVN Dry the resulting composites are particularly intense but dominated by
486 the SVN Wet pattern. Such a combination is perhaps selecting the strongest SVN Wet events.

487 • Dry events in SVN resemble Wet events in NVN quite closely, and this is where table 2
488 reveals the greater overlap. Precursors are dominated by a western Siberian high, which
489 spreads southwards, although the depression over China is absent. The combined composite
490 is again more intense than either of the isolated composites. The equatorial influence for
491 SVN Dry is not the opposite of the Wet case. This time the influence builds up in the east in
492 the form of West Pacific convergence at considerably longer lead times before giving way to
493 slowly eastward propagating low-level divergence over the region.

494 Although the overall picture is complicated, some patterns emerge from this analysis. There are
495 essentially three conduits of influence at lead times of one to two weeks:

496 1. A high latitude pathway where large scale quasi-stationary equivalent barotropic patterns
497 slowly build and then spread southwards to influence the region, particularly for NVN Wet
498 and SVN Dry.

499 2. A pathway along the Asian jet, with smaller-scale baroclinic anomalies of alternating sign,
500 showing eastward group propagation to influence NVN Dry and SVN Wet events.

501 3. An equatorial pathway with slow eastward propagation of the asymmetric precursors in the
502 divergent flow influencing SVN Wet and Dry events.

503 A consideration of the differing roles of these three pathways and the different combinations of
504 influences for Wet and Dry events can lead to better classification of the asymmetries associated with
505 precursors for the two regional scale target areas selected in this study. The associated mechanisms

differ with the pathways outlined above and will be explored in a subsequent contribution using a global dynamical model. Extratropical pathways are consistent with Rossby wave propagation on the climatological extratropical flow, with some sensitivity to the basic state as it changes throughout the season. Variations in waveguide impact on both propagation and growth characteristics of the precursors, as well as the latitude selected for the teleconnections. The southern region is directly influenced by tropical wave propagation, and there is also potential for interaction with the extratropics, providing for a link between the precursors. Further work is underway to account for the causality of teleconnections documented in this study, in this highly diverse and sensitive region.

Acknowledgments. Hong Hanh Le was funded by a PhD contract from the French Ministry of Education and Research. ERA-interim data are available at `www.ecmwf.int`. FROGs dataset are available at `ftp://ftp.climserv.ipsl.polytechnique.fr/FROGs/`. We would like to thank Pascal Roucou and Marine Herrmann for helpful discussions.

Data availability statement. The data that support the findings of this study are available on request from the corresponding author.

References

Abdillah, M. R., Y. Kanno, and T. Iwasaki, 2018: Tropical–extratropical interactions associated with east asian cold air outbreaks. part II: Intraseasonal variation. *Journal of Climate*, **31 (2)**, 473–490, doi:10.1175/jcli-d-17-0147.1, URL https://doi.org/10.1175/jcli-d-17-0147.1.

Abdillah, M. R., Y. Kanno, T. Iwasaki, and J. Matsumoto, 2021: Cold surge pathways in east asia and their tropical impacts. *Journal of Climate*, **34 (1)**, 157–170, doi:10.1175/jcli-d-20-0552.1, URL https://doi.org/10.1175/jcli-d-20-0552.1.

528 Chansaengkrachang, K., A. Luadsong, N. Aschariyaphotha, and Coauthors, 2018: Vertically
529 integrated moisture flux convergence over southeast asia and its relation to rainfall over thailand.
530 *Pertanika J Sci & Technol*, **26 (1)**, 235–246.

531 Chen, T.-C., M.-C. Yen, J.-D. Tsay, N. T. T. Thanh, and J. Alpert, 2012: Synoptic development
532 of the hanoi heavy rainfall event of 30–31 october 2008: Multiple-scale processes. *Monthly*
533 *Weather Review*, **140 (4)**, 1219 – 1240, doi:10.1175/MWR-D-11-00111.1.

534 Dee, D. P., and Coauthors, 2011: The era-interim reanalysis: configuration and performance of
535 the data assimilation system. *Quarterly Journal of the Royal Meteorological Society*, **137 (656)**,
536 553–597, doi:https://doi.org/10.1002/qj.828.

537 Haensel, S., A. Schucknecht, and J. Matschullat, 2015: The modified rainfall anomaly index
538 (mrai)—is this an alternative to the standardised precipitation index (spi) in evaluating future
539 extreme precipitation characteristics? *Theoretical and Applied Climatology*, 1–18, doi:10.1007/
540 s00704-015-1389-y.

541 Linden, R. V. D., A. H. Fink, T. Phan-Van, and L. Trinh-Tuan, 2016a: Synoptic-dynamic analysis
542 of early dry-season rainfall events in the vietnamese central highlands. *Monthly Weather Review*,
543 **144 (4)**, 1509 – 1527, doi:10.1175/MWR-D-15-0265.1.

544 Linden, R. V. D., A. H. Fink, J. G. Pinto, T. Phan-Van, and G. N. Kiladis, 2016b: Modulation
545 of daily rainfall in southern vietnam by the madden–julian oscillation and convectively coupled
546 equatorial waves. *Journal of Climate*, **29 (16)**, 5801–5820, doi:10.1175/jcli-d-15-0911.1, URL
547 https://doi.org/10.1175/jcli-d-15-0911.1.

548 Madden, R. A., and P. R. Julian, 1972: Description of global-scale circulation cells in the tropics
549 with a 40–50 day period. *Journal of Atmospheric Sciences*, **29 (6)**, 1109 – 1123, doi:10.1175/

550 1520-0469(1972)029⟨1109:DOGSCC⟩2.0.CO;2.

551 Nguyen, D.-Q., J. Renwick, and J. McGregor, 2013: Variations of surface temperature and rainfall
552 in vietnam from 1971 to 2010. *International Journal of Climatology*, **34 (1)**, 249–264, doi:
553 10.1002/joc.3684, URL https://doi.org/10.1002/joc.3684.

554 Nguyen-Xuan, T., T. Ngo-Duc, H. Kamimera, L. Trinh-Tuan, J. Matsumoto, T. Inoue, and
555 T. Phan-Van, 2016: The vietnam gridded precipitation (VnGP) dataset: Construction and
556 validation. *SOLA*, **12 (0)**, 291–296, doi:10.2151/sola.2016-057, URL https://doi.org/10.2151/
557 sola.2016-057.

558 Roca, R., L. V. Alexander, G. Potter, M. Bador, R. Jucá, S. Contractor, M. G. Bosilovich,
559 and S. Cloché, 2019: Frogs: a daily 1x1 gridded precipitation database of rain gauge,
560 satellite and reanalysis products. *Earth System Science Data*, **11 (3)**, 1017–1035, doi:
561 10.5194/essd-11-1017-2019.

562 Sohn, B.-J., E. A. Smith, F. R. Robertson, and S.-C. Park, 2004: Derived over-ocean water
563 vapor transports from satellite−retrieved e−p datasets. *Journal of Climate*, **17 (6)**, 1352 – 1365,
564 doi:10.1175/1520-0442(2004)017⟨1352:DOWVTF⟩2.0.CO;2.

565 Truong, N. M., and B. M. Tuan, 2018: Large-scale patterns and possible mechanisms of 10-
566 20-day intra-seasonal oscillation of the observed rainfall in vietnam. *International Journal of*
567 *Climatology*, **38 (10)**, 3801–3821, doi:10.1002/joc.5534, URL https://doi.org/10.1002/joc.5534.

568 Truong, N. M., and B. M. Tuan, 2019: Structures and mechanisms of 20–60-day intraseasonal
569 oscillation of the observed rainfall in vietnam. *Journal of Climate*, **32 (16)**, 5191–5212, doi:
570 10.1175/jcli-d-18-0239.1, URL https://doi.org/10.1175/jcli-d-18-0239.1.

571 Tuan, B. M., 2019: Extratropical forcing of submonthly variations of rainfall in vietnam. *Journal*
572 *of Climate*, **32 (8)**, 2329–2348, doi:10.1175/jcli-d-18-0453.1, URL https://doi.org/10.1175/
573 jcli-d-18-0453.1.

574 Wu, P., Y. Fukutomi, and J. Matsumoto, 2012: The impact of intraseasonal oscillations in the
575 tropical atmosphere on the formation of extreme central vietnam precipitation. *SOLA*, **8 (0)**,
576 57–60, doi:10.2151/sola.2012-015, URL https://doi.org/10.2151/sola.2012-015.

577 Yatagai, A., K. Kamiguchi, O. Arakawa, A. Hamada, N. Yasutomi, and A. Kitoh, 2012:
578 APHRODITE: Constructing a long-term daily gridded precipitation dataset for asia based on a
579 dense network of rain gauges. *Bulletin of the American Meteorological Society*, **93 (9)**, 1401–
580 1415, doi:10.1175/bams-d-11-00122.1, URL https://doi.org/10.1175/bams-d-11-00122.1.

581 Yokoi, S., and J. Matsumoto, 2008: Collaborative effects of cold surge and tropical depression–type
582 disturbance on heavy rainfall in central vietnam. *Monthly Weather Review*, **136 (9)**, 3275–3287,
583 doi:10.1175/2008mwr2456.1, URL https://doi.org/10.1175/2008mwr2456.1.

584 Yokoi, S., and T. Satomura, 2005: An observational study of intraseasonal variations over southeast
585 asia during the 1998 rainy season. *Monthly Weather Review*, **133 (7)**, 2091–2104, doi:10.1175/
586 mwr2967.1, URL https://doi.org/10.1175/mwr2967.1.

587 Yokoi, S., T. Satomura, and J. Matsumoto, 2007: Climatological characteristics of the intraseasonal
588 variation of precipitation over the indochina peninsula. *Journal of Climate*, **20 (21)**, 5301–5315,
589 doi:10.1175/2007jcli1357.1, URL https://doi.org/10.1175/2007jcli1357.1.

LIST OF TABLES

TABLE 1. Data information.

DATA	Database	Spatial Coverage	Period	Resolution
APHRODITE	ground based product ≥ 100 station over Vietnam	Land only Monsoon Asia area 60E-150E x 15S-55N	1979 - 2007	grid 0.5 degree
VnGP	ground based product 481 station over Vietnam	Land only Vietnam mainland map	1980 - 2010	grid 0.5 degree
ERAi - FROGs	reanalysis product	Global coverage Monsoon Asia area	1979 - 2016	grid 1 degree

595 TABLE 2. The number of days happened over regions N (North), C (Central) and S (South) of Vietnam
596 with/without overlapping days shown out/in parentheses. Wet/Dry means exceeded +3mm/day and −3mm/day
597 of VIMC.

	N wet	C wet	S wet	N dry	C dry	S dry
N wet	624 (302)					
C wet	322	745 (277)				
S wet	53	199	371 (172)			
N dry	none	0 (0)	34 (31)	493 (282)		
C dry	2 (0)	none	3 (0)	211	619 (267)	
S dry	93 (87)	4 (0)	none	29	170	447 (227)

LIST OF FIGURES

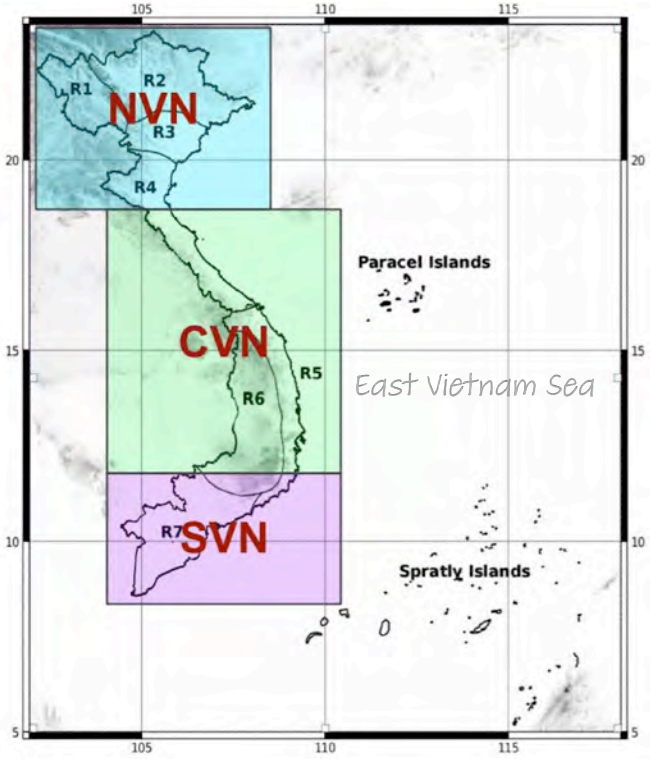

FIG. 1. Vietnam map and selected regions: North Vietnam - NVN, Central Vietnam - CVN, South Vietnam - SVN.

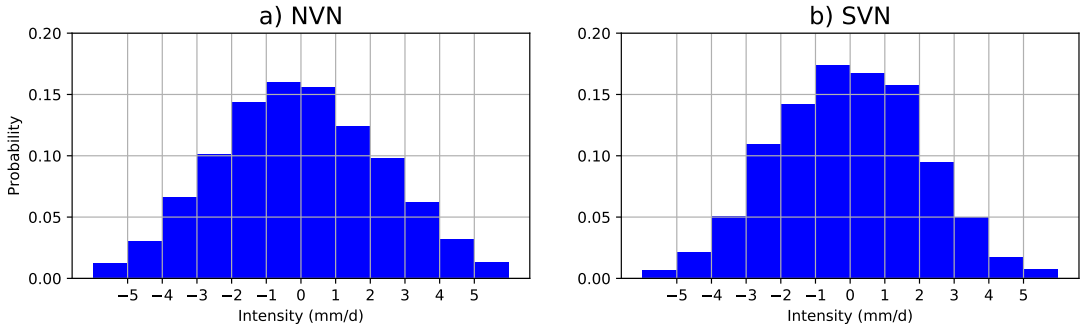

FIG. 2. PFD of VIMC index over (a) NVN, (b) SVN.

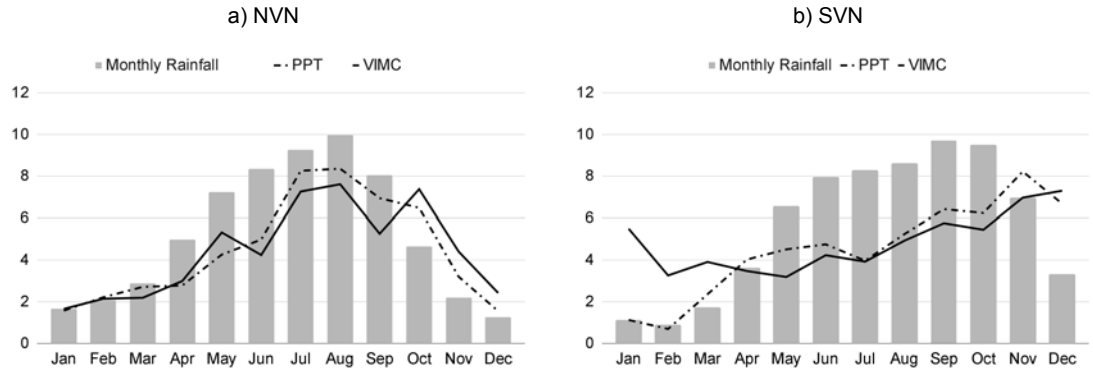

639 FIG. 3. Monthly average of rainfall (grey bars) (mm/day) and monthly variance of daily time-series regional
640 VIMC anomaly (solid line) and PPT anomaly (dashed line) (mm2/d2) over (a) NVN, (b) SVN.

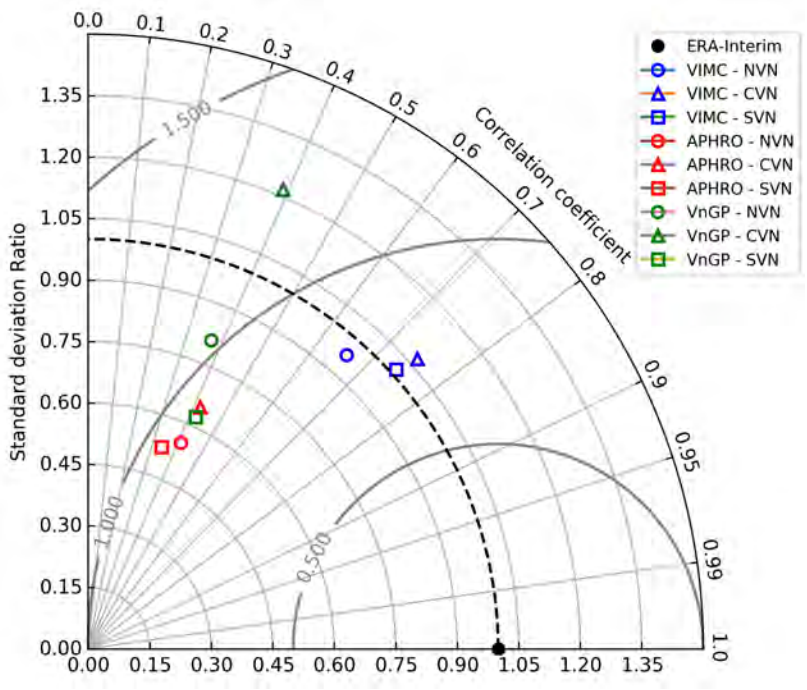

641 FIG. 4. Comparision between regional daily-time series from May to October obtained from APHRODITE,
642 VnGP, VIMC and FROGs.

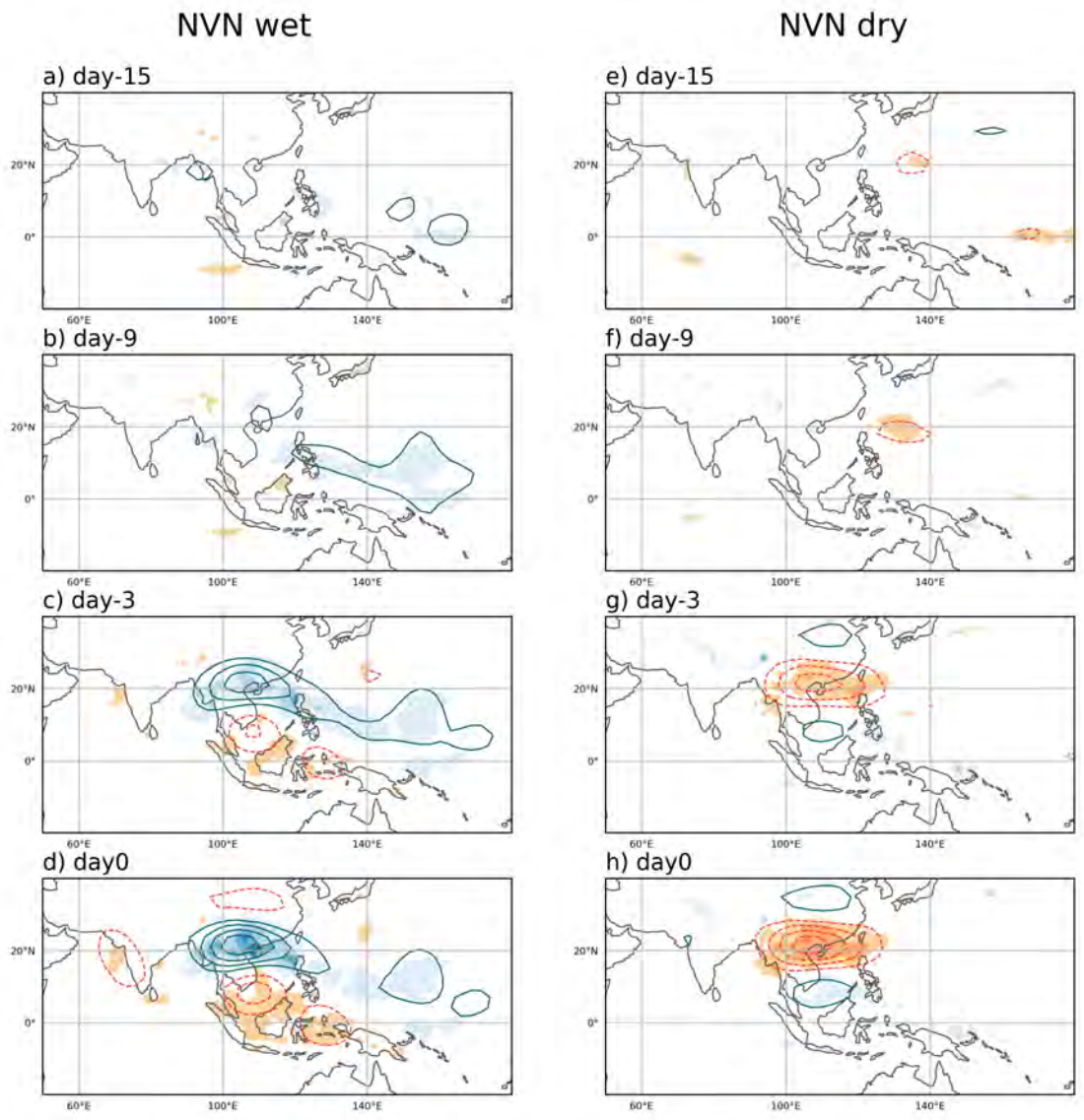

643 FIG. 5. Composites of RAINFALL ANOMALY (shaded color) and VIMC ANOMALY (contour) associated
644 with Wet (a-d) and Dry (e-h) events in NVN. Blue is positive. Red is negative. The contour (color) interval is
645 1mm/day. Plotted signals are statistically significant at 95% for each composite compared to the observation in
646 a two-sided t-test.

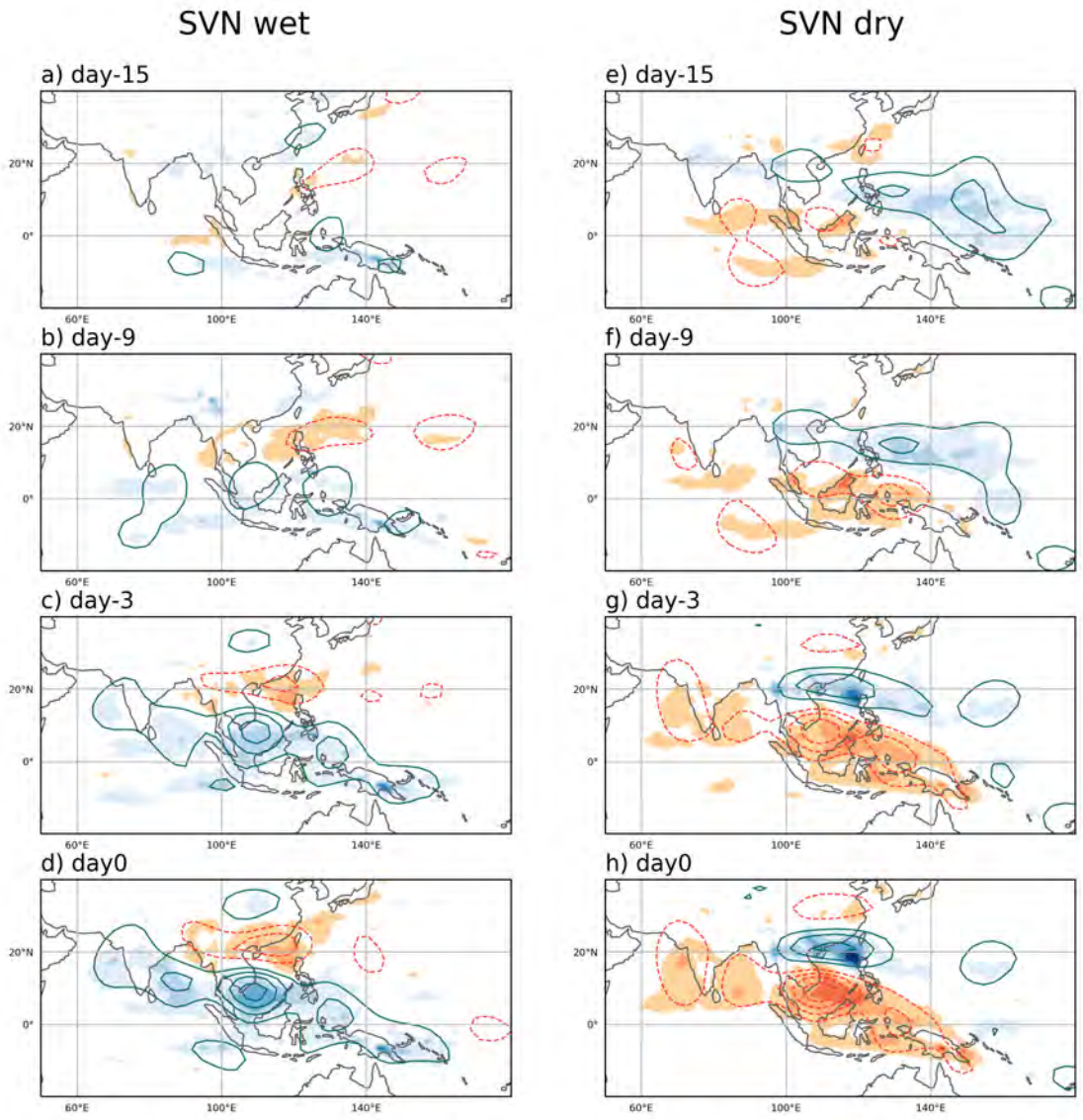

FIG. 6. as Fig. 5, but for SVN

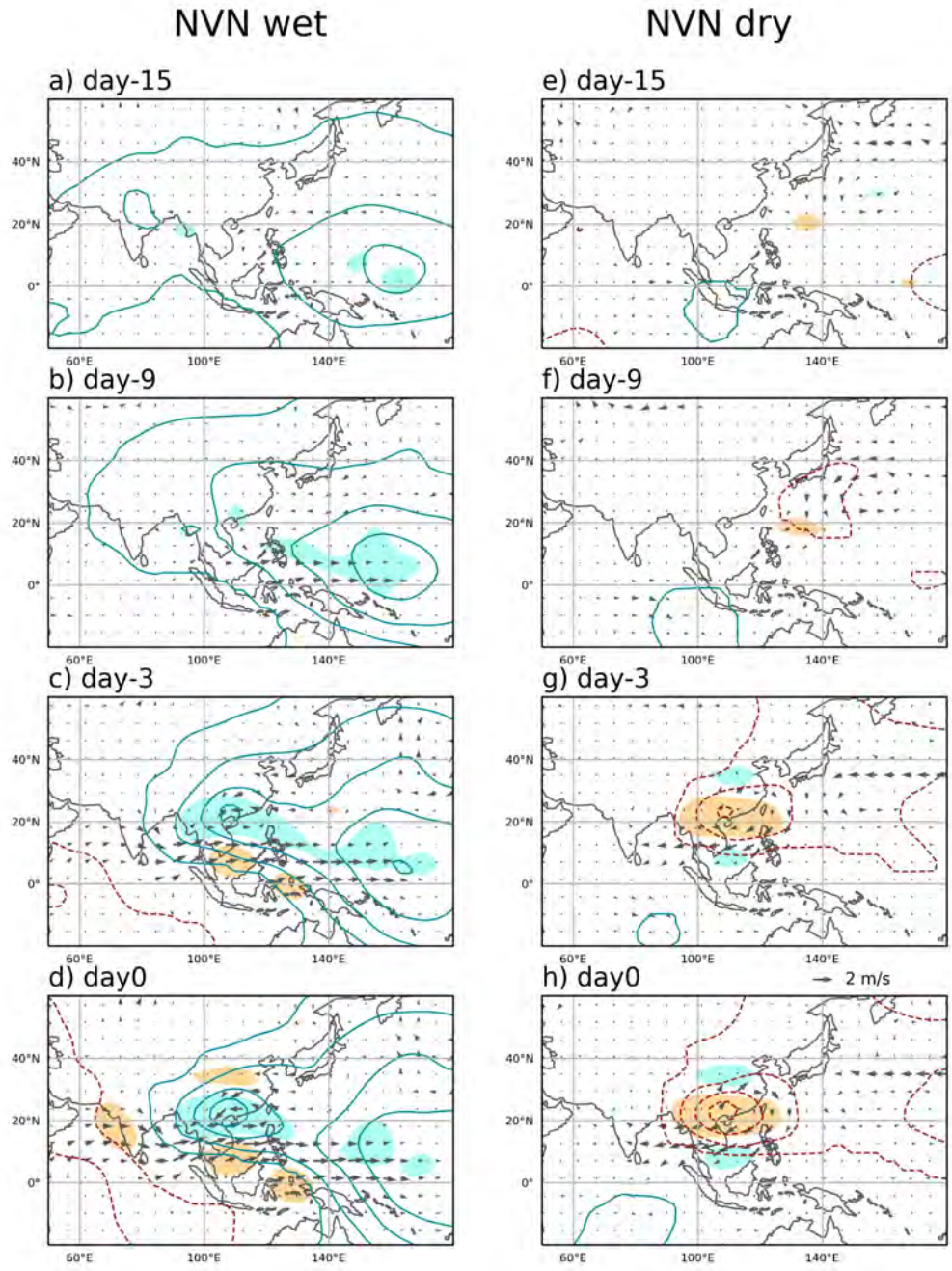

FIG. 7. Composites of velocity potential (contour) and horizontal wind (vector) at 850mb anomalies associated with Wet (a-d) and Dry (e-h) events over NVN. Red is negative. Blue is positive. The contour interval is 2e5 m2/s. Plotted signals are statistically significant at 95% for each composite compared to the observation in a two-sided t-test. VIMC greater than 1 mm/day is plotted (color shading) as Fig. 5.

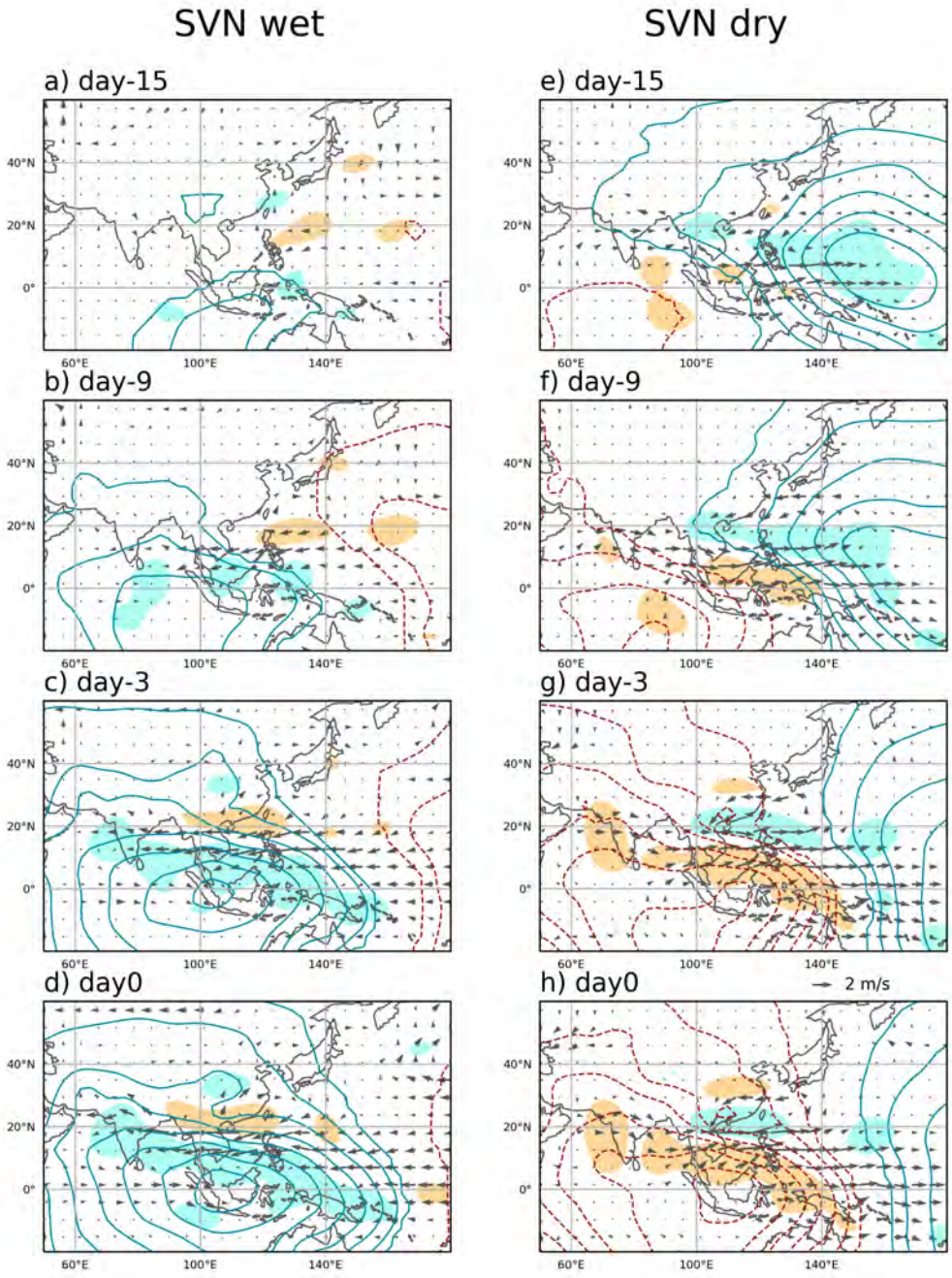

FIG. 8. as Fig. 7, but for SVN.

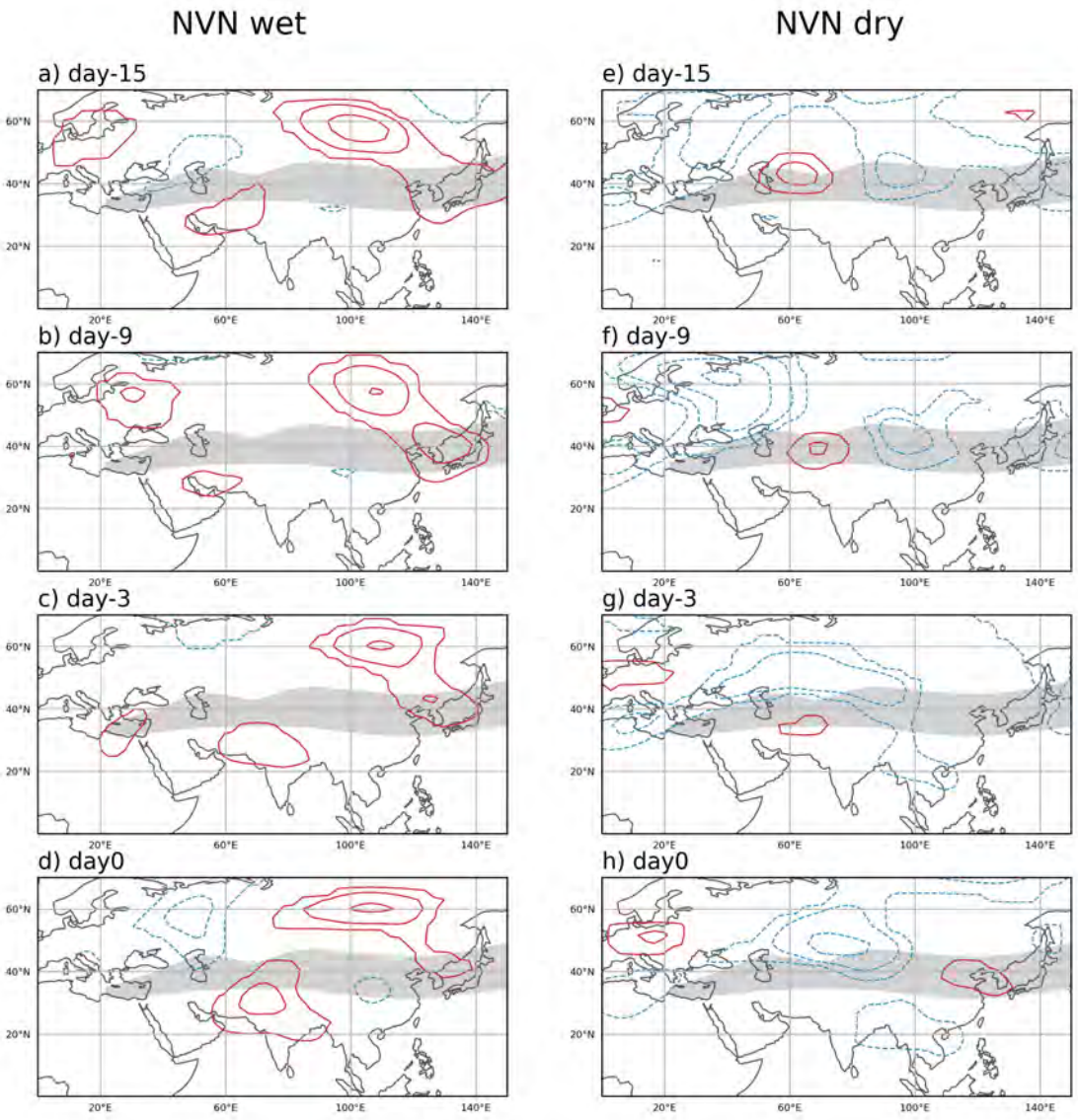

651 FIG. 9. Composites of geopotential height (contour) and Jet stream (color shading) at 250 mb associated with
652 Wet (a-d) and Dry (e-h) events over NVN. Red is positive. Blue is negative. The contour interval is 8 m. Plotted
653 signals are statistically significant at 95% for each composite compared to the observation in a two-sided t-test.

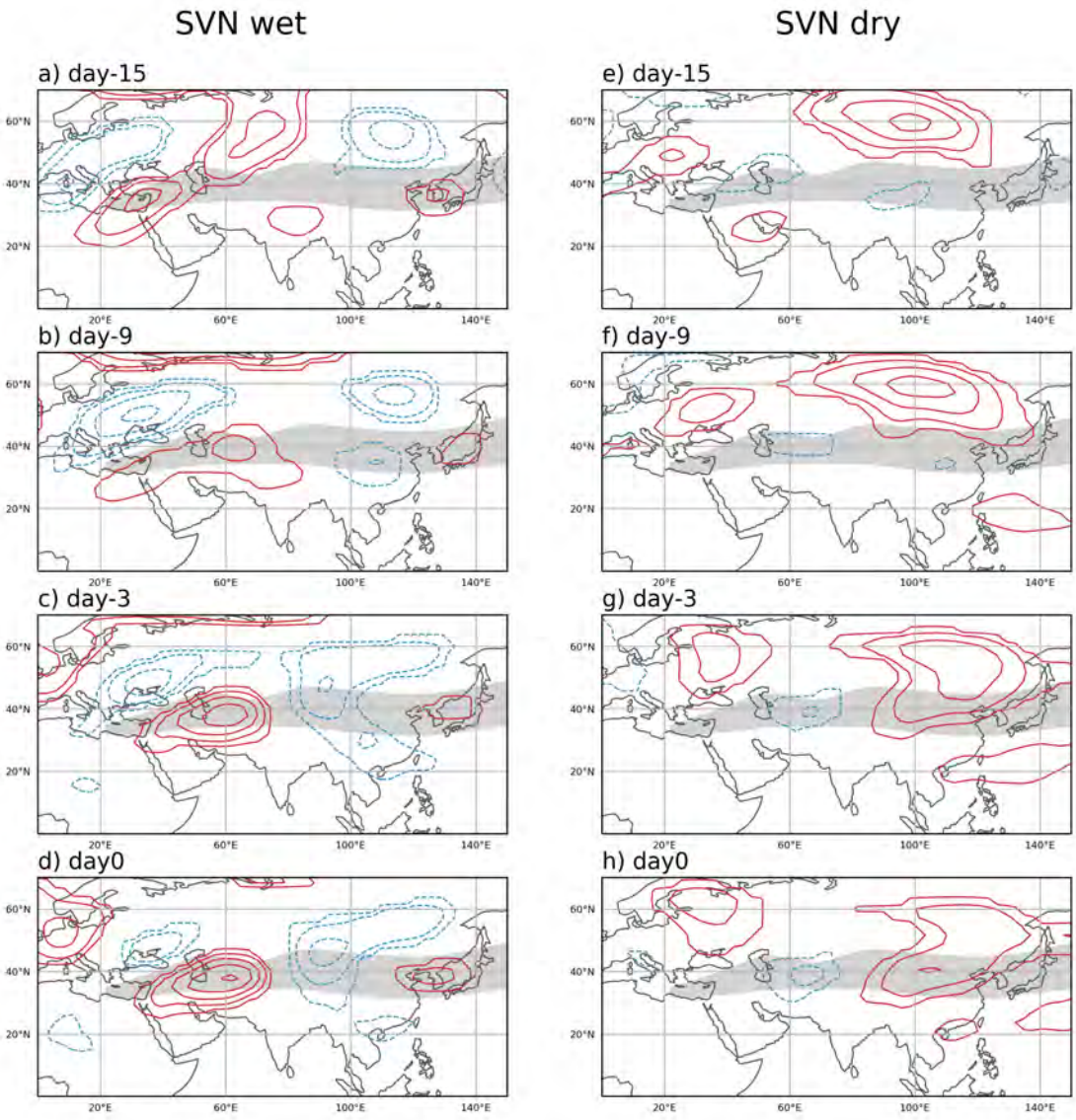

FIG. 10. as Fig. 9, but for SVN.

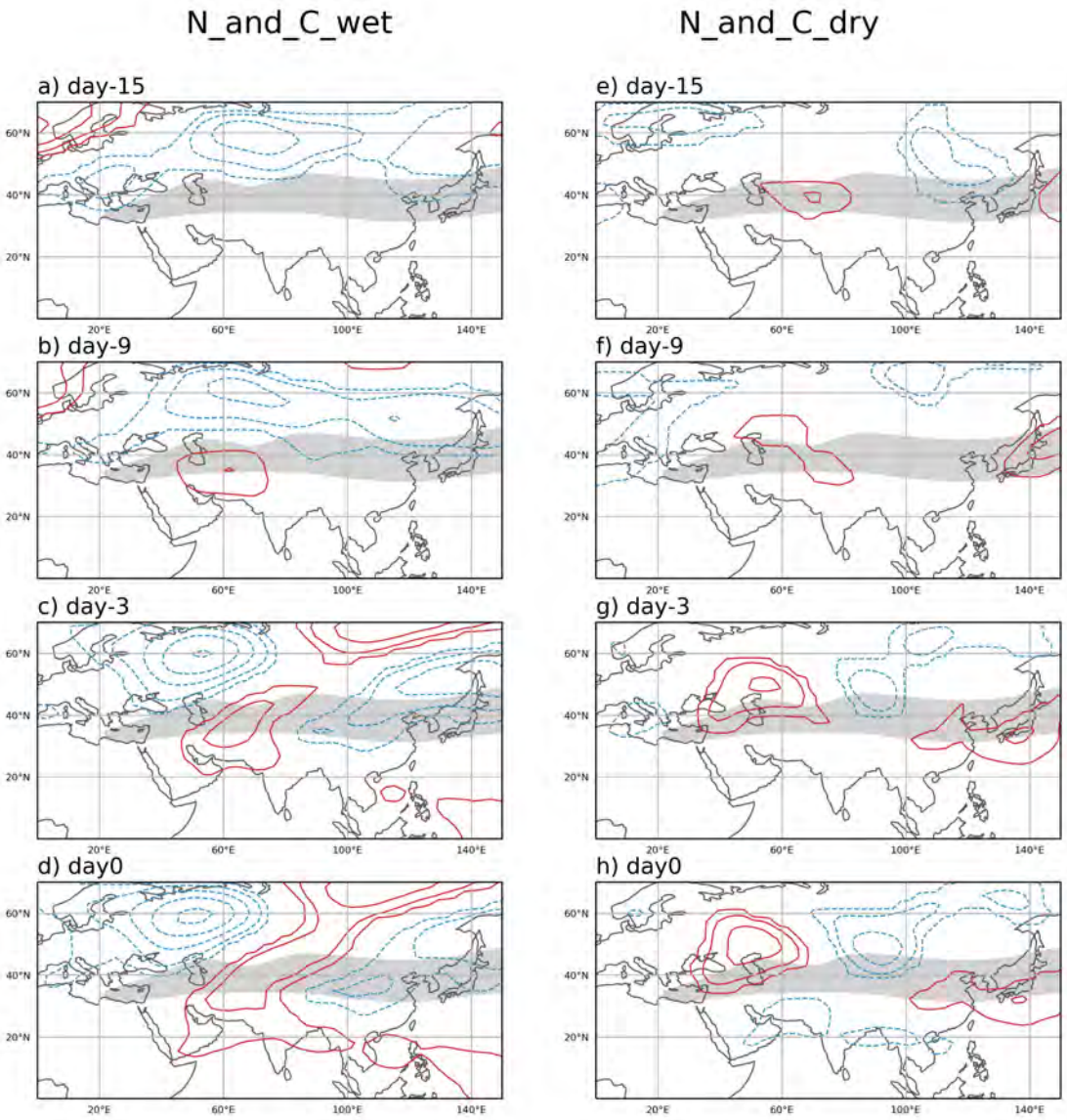

FIG. 11. as Fig. 9, but for the overlapping of North and Central (N_and_C) events.

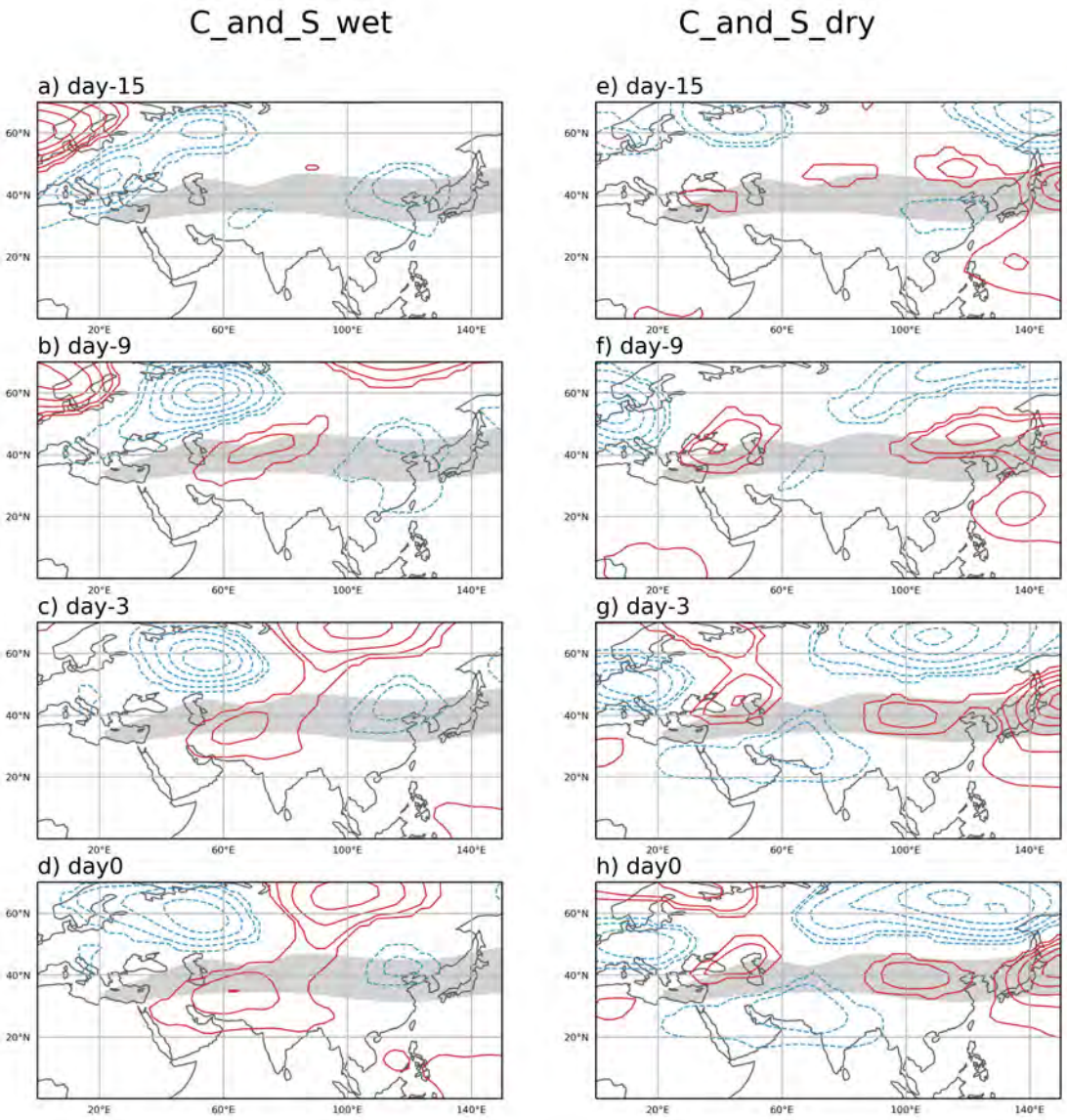

FIG. 12. as Fig. 9, but for the overlapping of Central and South (C_and_S) events.

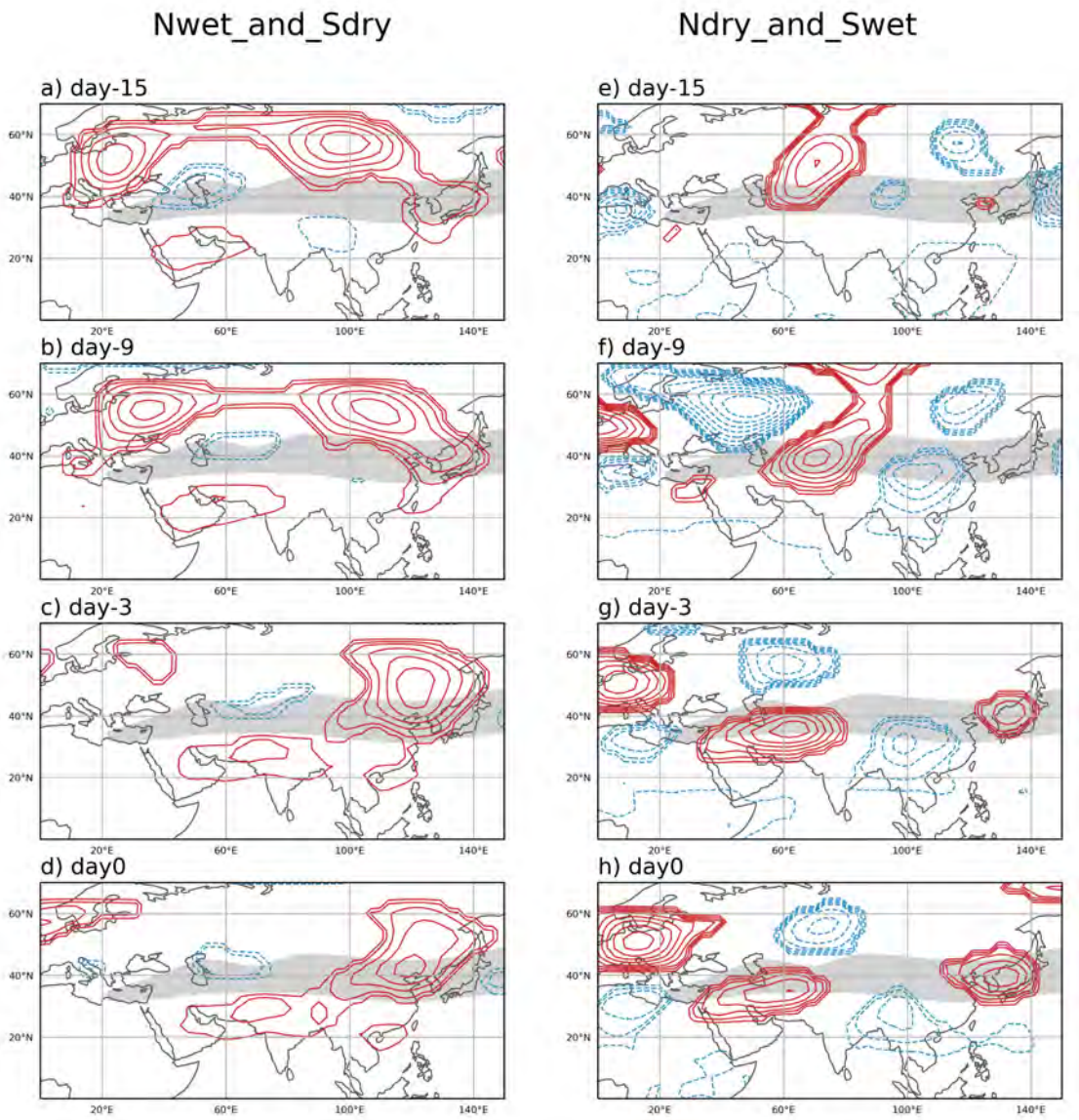

654 FIG. 13. as Fig. 9, but for the overlapping of Wet-NVN/Dry-SVN (Nwet_and_Sdry) (a-d) and Dry-NVN/Wet-
655 SVN (Ndry_and_Swet) events (e-h).

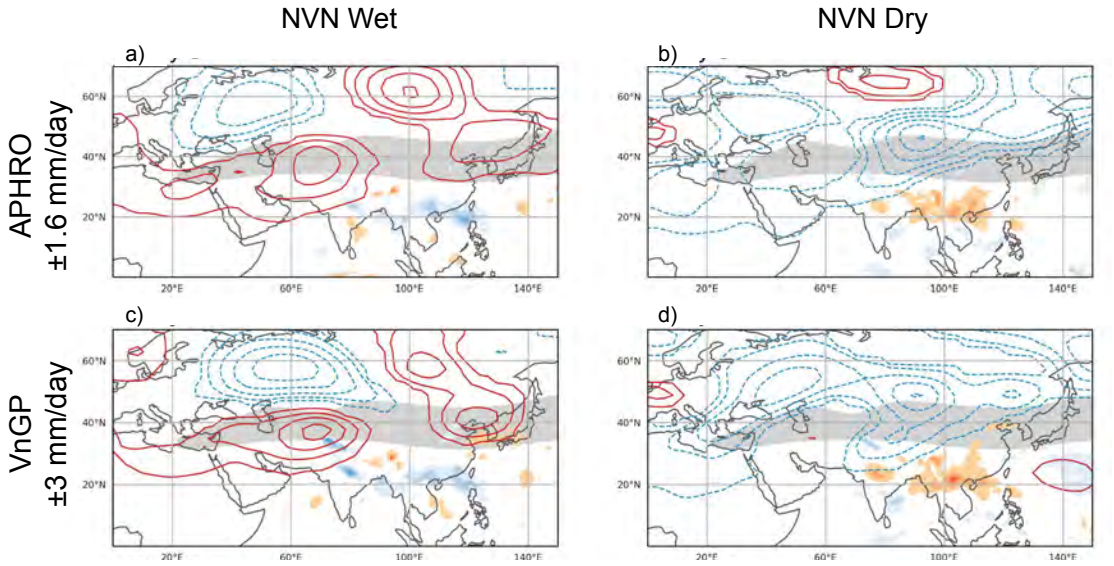

656 FIG. 14. Composite of day-9 of geopotential height anomaly (contour lines) and precipitation anomaly (color
657 shaded) associated with the NVN wet (left column) and dry (right column) events that assembled from APHRO
658 (a - 372days, b - 222 days) and VnGP (c - 303 days, d - 199 days) indexes. The contour line interval is 8m with
659 red/blue is positive/negative. Color shaded interval is 1mm/day with blue/orange is positive/negative.

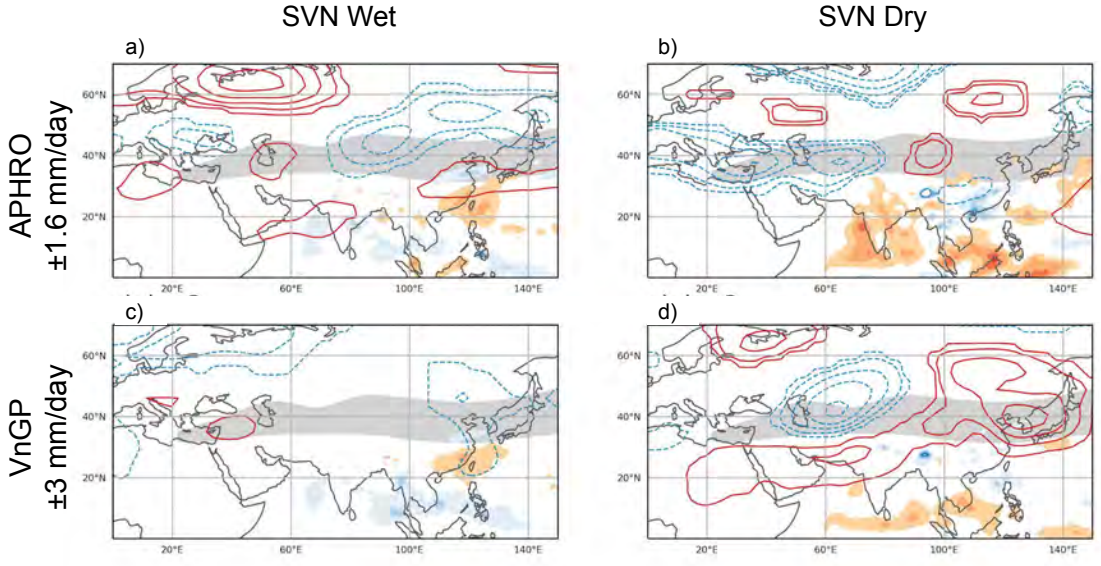

660 FIG. 15. Composite of day-9 of geopotential height anomaly (contour lines) and precipitation anomaly (color
661 shaded) associated with the NVN wet (left column) and dry (right column) events that assembled from APHRO
662 (a - 267 days, b - 123 days) and VnGP (c - 315 days, d - 192 days) indexes. The contour line interval is 8m with
663 red/blue is positive/negative. Color shaded interval is 1mm/day with blue/orange is positive/negative.

Chapter 3

Global Dynamical Model Study - DREAM

Contents

3.1 Introduction

In the chapter 2, the remote influence on the regional rainfall ISV over Vietnam investigated via reanalysis composite suggests different pathways of influence at the lead time of 1-2 weeks. It could be at high latitude, along an Asian jet to influence the rotational flow or even equatorial eastward propagation to modify the divergent flow that is associated with the moisture flux convergence - a proxy of rainfall ISV over Vietnam. The results also indicate that the precursors and pathways are highly diverse and sensitive to the Vietnam subregions. The similarity between the rainfall patterns of Wet and Dry events over North and South Vietnam is associated with not only similarity in the extratropical precursors but also a great difference in tropical divergent flow. Thus, the question of the roles of these pathways in the influences for Wet and Dry events over different Vietnam subregions still needs to be investigated further. In this chapter, we present a large-scale investigation with a dry-dynamical model to help unravel the remote dynamical influence of the circulation associated with the rainfall ISV over Vietnam subregions.

Remote dynamical influence refers to the impact that large-scale atmospheric circulation patterns can have on local weather and climate which is also called teleconnection. That is usually indicated by the correlations between climate time series and remotely forced responses in the observational analysis. It could seem like spooky action-at-a-distance. Indeed, these occur because the Earth's atmosphere and oceans are connected and influence each other, through processes such as ocean-atmosphere interactions, atmospheric circulation patterns, and atmospheric wave propagation Kucharski et al. (2010). Teleconnections through atmospheric wave propagation are a key mechanism for the remote influence of one region's climate on another region's climate.

The influences of extratropical Rossby waves on tropical areas are discussed in many previous studies. That is investigated using the simple model since Charney (1969); BENNETT and YOUNG (1971). They used a zonally averaged basic flow to show the extratropical forcings on the Tropics and show that disturbances with phase speeds more westward than the mean flow may be free to propagate into the Tropics, providing their wavelengths are not too short. Then Webster and Holton (1982) using a nonlinear shallow water model showed the effects of longitudinal variations in the basic state zonal wind. They concluded that the presence of a westerly duct in the equatorial zone is necessary for large-scale disturbances generated in the northern middle latitudes to have a significant impact on equatorial regions and the amplitude of the response increases with the strength of the westerlies. However, Hoskins and Yang (2000) indicates that higher-latitude forcing gives a significant tropical response in both easterly and westerly tropical flow in the context of a dry atmosphere. They showed that the forcing is directly projected onto equatorially trapped waves, particularly, the forcing at higher latitudes with an eastward phase speed can effectively trigger an equatorial Kelvin wave.

Some early work on the remote forcing of a time-independent tropical atmosphere took the form of a nudging experiment by WEBSTER (1973), who used a linear two-layer primitive-equation model in spherical coordinates with parameterized dissipation and realistic basic

flows. The influence of the midlatitudes is included by applying conditions at the lateral boundaries of the model near 40°N and 40'S. WEBSTER (1973) showed that the response near the Equator is found to depend on both the basic state (DJF or JJA) and the magnitude of the forcing, although generally, the midlatitude effects dominate the subtropics, whereas local forcings including latent heating and orography are of greater importance in low latitudes. Further investigation of remote influence on tropical regions is employed by adding an extratropical wave source to examine the impact on a target region, e.g., Hoskins and Karoly (1981); Hoskins and Yang (2000). Hoskins and Karoly (1981) presented the 5-layer baroclinic model used to study the linear response of a spherical atmosphere to thermal and orographic forcing. The fixed heating source was added to present a subtropical forcing and mid-latitude forcing as well. The authors demonstrated that the substantial perturbations are restricted to the source's immediate vicinity and that, for midlatitude thermal forcing, these perturbations critically depend on the vertical distribution of the source at low levels. The sources in the upper troposphere produce wavetrains that closely resemble those predicted by barotropic models. Long wavelengths substantially propagate pole ward as well as eastward for a low-latitude source. The wave-trains separate at this latitude with shorter wavelengths confined to equatorial regions.

Hoskins and Ambrizzi (1993) studied the response of a barotropic model to localized forcing to show the existence of a strong wave guide in the Asian jet. They analyze Rossby wave propagation on a realistic longitudinally varying flow of a climatological winter time-mean flow. Using a variety of perturbation vorticity sources they show the position and spatial features and show the preferred propagation regions from Europe to the Arabian Gulf.

In Hoskins and Yang (2000), the equatorial response to higher-latitude forcing was investigated by adding a localized higher-latitude forcing with eastward or westward phase speed at 40N-0E. The authors use different flows to investigate further the global response in a resting atmosphere, with zonally symmetric and asymmetric basic states. Fig 3.1 shows the solution after 6 days of model integration in DJF zonally asymmetric flow. Both the lower-tropospheric zonal wind (a) and the mid-tropospheric temperature (b) exhibit zonal elongated equatorial structures in the equatorial African-Indian Ocean region. The authors also indicated that the strong equatorial response is associated with a deep Kelvin wave response to forcing in midlatitudes and suggest the possible organization of large-scale, deep tropical convection and the initiation of the Madden–Julian oscillation.

The wave sources added in the perturbation experiment could be diabatic heating associated with convection or a vorticity anomaly, with either a fixed or moving source that leads the global atmospheric circulation response. For example, Jin and Hoskins (1995) showed the direct extratropical response to tropical heating. The 15-level primitive equation model adding heat source shows a Gill-type response in the lower troposphere, while the Rossby wave source and the Rossby wave propagation are strongly influenced by the ambient flow that is generally established within a week.

A more realistic approach to the response to an idealized propagating MJO is presented in Hall et al. (2020). There the MJO was simulated as a heat source moving with spatial patterns derived from OLR data and the vertical structure of deep tropical convection. Hall

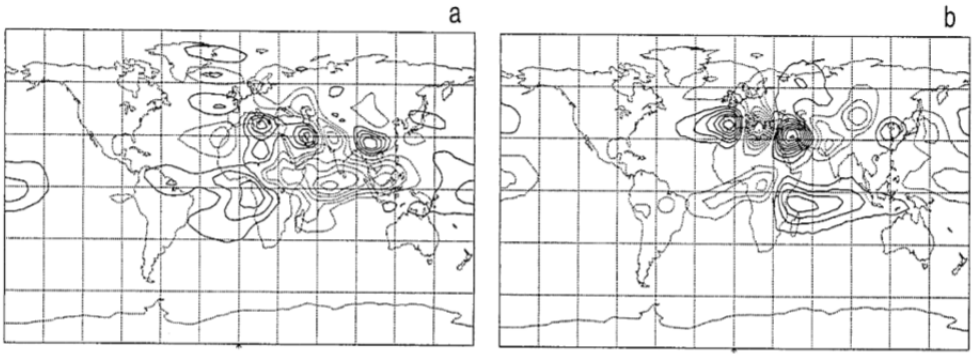

Figure 3.1: Taken from Hoskins and Yang (2000): Baroclinic model day6 solutions for the vorticity forcing at 40N,0E with a period of 4 days in the DJF zonally asymmetric flow: (a) u' at $\sigma = 0.887$ and (b) T' at$\sigma = 0.477$. The contour intervals are (a) 0.1 m/s and (b) 0.05 K.

et al. (2020) show that there are modifications due to the MJO phase cycles at the same timescale on which extratropical response is established. Rossby wave teleconnections are also seen that project onto the PNA pattern

In an alternative approach known as ray tracing, the propagation of theoretical Rossby waves can be tracked, as introduced by Hoskins and Karoly (1981); Karoly (1983); Hoskins and Ambrizzi (1993). The ideas of ray tracing from geometrical optics and wave propagation in a slowly varying medium are used for Rossby waves propagating in a barotropic atmosphere. In Hoskins and Karoly (1981), in agreement between the observational and linearized barotropic models results, authors indicated the rays along which wave activity propagates, the speeds of propagation, and the amplitudes and phases along these rays are determined for a constant angular velocity basic flow as well as a more realistic jet flow.

Then in Karoly (1983), the propagation of Rossby waves in a basic state with zonally varying middle latitude or low latitude jets is studied. This ray tracing approach, as described in Hoskins and Karoly (1981); Karoly (1983), offers a quick and affordable way to examine the spread of driven planetary waves in various fundamental states. For example, Fig 3.2 is taken from Karoly (1983) showing rays and propagation speed for sources at 30°N and 30°S on a JJA stationary wave flow. The propagation speed is lower and phase variation is larger in the Northern Hemisphere than in the Southern Hemisphere due to the basic flow being weaker, as seen in a plot of ray paths for different wave numbers from 1 to 6. Karoly (1983) argued that this two-dimensional ray tracing may be utilized to give ideas on the speed and direction of horizontal wave dispersion from a local source in several basic states relevant to the atmosphere.

Yang and Hoskins (1996) then used the raytracing method, combined with theoretical analysis to investigate the propagation of Rossby waves of positive and negative frequency, corresponding to eastward and westward phase speeds, respectively. They indicated that

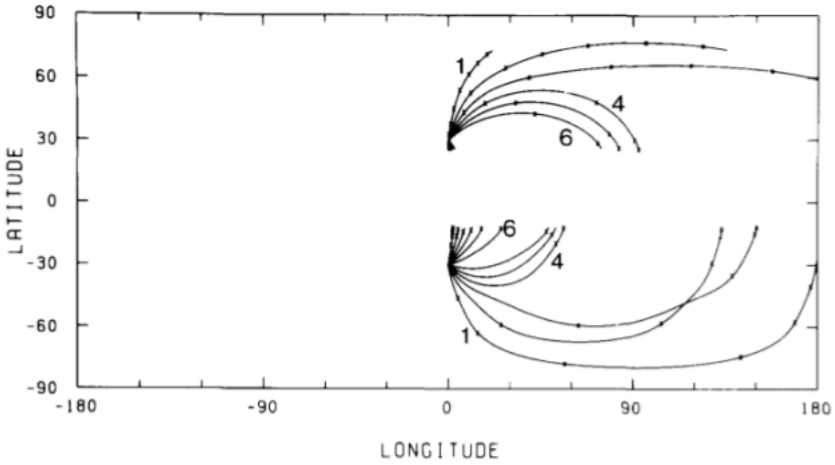

Figure 3.2: Taken from Karoly (1983): Rays and propagation speed shown by crosses at 2-day time intervals, for sources at 30N ans 30S in the JJA stationary wave flow. Zonal wave numbers 1-6 are used.

Rossby waves with positive and negative frequencies can vary greatly in form from one another and stationary waves with zero frequency. Larger total wavelengths and higher meridional group velocities are typical characteristics of negative frequency waves. In both barotropic and baroclinic models, westward-moving sources exhibit enhanced meridional propagation and even cross-equatorial propagation.

In a dry atmosphere, propagation induced by the heating/vortices anomaly is well explained based on wave propagation theory. Thus, adding a heating source as doing a perturbation experiment on a global scale is the easiest way to examine the dynamical influence on Vietnam circulation. The question now is where is the best place to put the heat source to influence that target region? It could be solved by doing a lot of experiments all around the world to find that. This is the first time the dynamical influence on Vietnam circulation is investigated in this way.

To continue from the remote dynamical influences on Vietnam rainfall ISV from observational analysis in chapter 2, we would like to further investigate dynamically the influences to the Vietnam rainfall ISV on a global scale by using a global circulation model called DREAM combined with the ray tracing technique. DREAM includes a three-dimensional structure with a dry-dynamical core and a simple physical scheme of the atmosphere. It is used here to examine the influence on the Vietnam subregion circulation. This will be complemented by ray tracing applied to Rossby wave propagation.

With specified target regions, we focus on the two Vietnam sub-regions North and South Vietnam and address the questions:

- At what position does a wave source give the most influence in terms of wave propagation within two weeks? Can we identify the pathways of influence?

- Is it possible to use DREAM to reproduce the impacts of a real source?
- What are the Rossby wave sources that can reach the NVN SVN circulation in different basic states?

In this chapter, DREAM will be used in stationary wave configuration. The model description as well as the configurations are described in the next section. Then, the results are presented respectively following the problems addressed. An influence function from a set of artificial heating sources employed on the stationary wave configuration is presented to investigate systematically the possible wave-like sources of influence. Then, a nudging experiment for a specific region is applied to the same configuration to attempt to reproduce more realistic sources obtained from the observed composite described in the previous section. Finally, the results from ray-tracing calculations on different basic states are presented. The last section is the chapter's conclusion.

3.2 Model and Methods

3.2.1 DREAM Model

Dynamical Research Empirical Atmospheric Model (DREAM) is a global spectral primitive equation model. It can be used to simulate global atmospheric circulation as introduced first as a dry model in Hall (2000). The source code is mainly based on the spectral primitive equation model first developed by Hoskins and Simmons (1975). Because of the various ways its forcing can be manipulated, DREAM is considered a hierarchy of models designed to work with the reanalysis data and empirical forcing. The latest DREAM User Manual from Hall and Leroux (2022) presents various aspects of DREAM including the model description and the different configurations. In this part of the manuscript, I would like to briefly present again the model basis and the configuration used.

3.2.1.1 Model Basics

a) Model dynamics

DREAM uses primitive equations expressed in terms of vorticity and divergence. The non-dimensional equations of motion for an inviscid, adiabatic, hydrostatic, perfect gas surrounding a rotating, spherical planet are represented in sigma coordinate as shown in Hoskins and Simmons (1975) in Fig 3.3.

The variable names used in the model are also shown: spectral variables in blue and grid point variables in red. These equations also describe the development of the temperature deviation from a reference value which in DREAM is set to 250K, the surface pressure, which in DREAM is calculated as the mean sea level pressure and the geopotential. The semi-implicit time-stepping approach is used to filter gravity waves, by discretizing the equation so

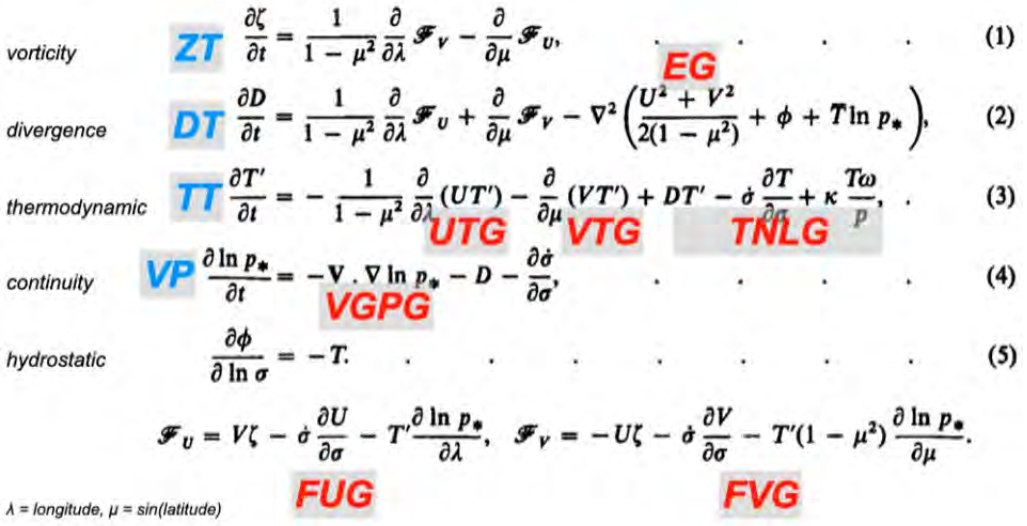

Figure 3.3: Taken from Hall and Leroux (2022): The primitive equations as presented in Hoskins and Simmons (1975). Spectral variables are in blue and grid point variables are in red.

that the wave equation operator acts on the centered average divergence, effectively filtering the fast gravity modes and allowing a longer time step. This development is summarised in Fig. 3.4, including some more variable names from the code.

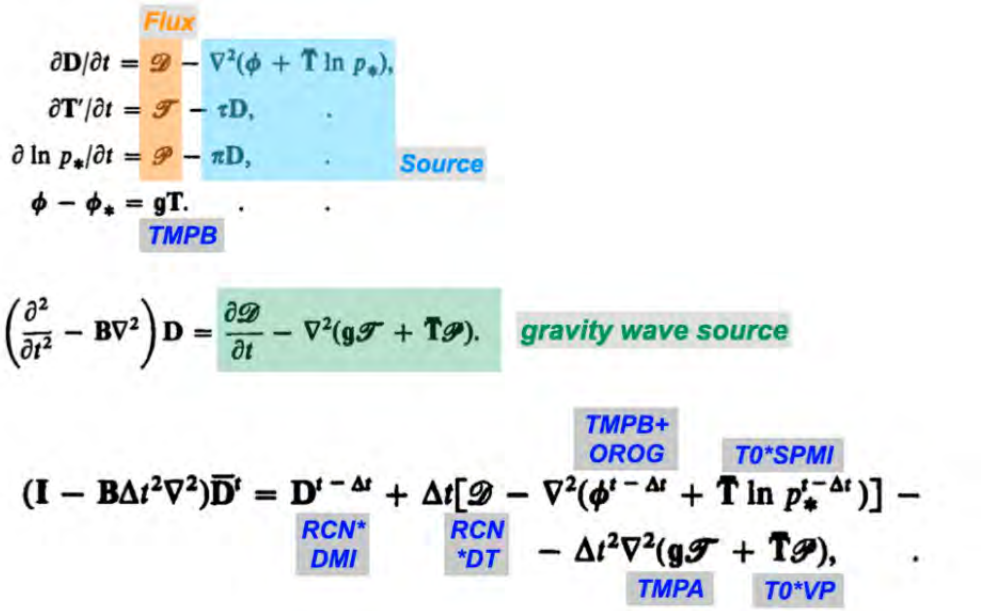

Figure 3.4: Taken from Hall and Leroux (2022): Some more equations taken from Hoskins and Simmons (1975), outlining the semi-implicit timestep

The model proceeds by calculating tendencies and then applying these tendencies to the model state to find the next model state using a semi-implicit centred difference timestep. Linear calculations for the tendencies are carried out directly in spectral space. Spatial derivatives are calculated as part of the transformation between spectral and grid space. Nonlinear advective terms are calculated in grid space. Model state variables, therefore, have both spectral and gridpoint arrays assigned to them.

b) 3D structure

Model variables are projected onto Fourier transforms in the zonal direction and Legendre polynomials in the meridional direction as below:

$$X = \sum X_n^m P_n^m(\mu) e^{im\lambda}$$

where m is the zonal wave number, and n is the meridional wave number (i.e. the number of zeros between the poles). Jagged triangular truncation is applied to limit the number of coefficients. DREAM data is set up to be run at T31 or T42. When the model variables are transformed to grid space they are stored on a Gaussian grid in latitude pairs, closing in towards the equator from the most polar latitudes to the most equatorial. Equally spaced longitude points are used around the globe, with the first one situated on the Greenwich meridian and Gaussian latitudes in each hemisphere are situated between the pole and the equator. The model uses the Simmon and Burridge angular momentum conserving vertical scheme (Simmons and Burridge, 1981).

DREAM currently uses 15 sigma levels in the vertical. They are referenced to the mean sea level pressure, as calculated from temperature and pressure at the 1000 hPa level as shown above. So model levels in DREAM are quite close to pressure levels because there is no explicit orography. The sigma levels used in DREAM have been chosen to be as close as possible to the ECMWF standard pressure levels on which the data was originally provided, minimising interpolation errors. The layer boundaries in DREAM have been chosen with model sigma levels centred at the following fifteen values:

$$\sigma * 1000 = 37.5, 100, 150, 200, 250, 312.5, 400, 500, 600, 700, 791.67, 850, 883, 925, 975$$

c) Model variables

The model variables are vorticity (s^{-1}), divergence (s^{-1}), temperature (degrees Celsius), Surface pressure (Pa), and Q specific humidity kg/kg. These quantities as well as time intervals are non-dimensionalised.

d) Dissipation

Scale selective hyper-diffusion is applied in spectral space to all the model's 3-d state variables (Z, D, T, Q) independently of the vertical level. The default horizontal diffusion is set to 12-hour ∇^6. Further level-dependent vertical diffusion and damping are added in grid

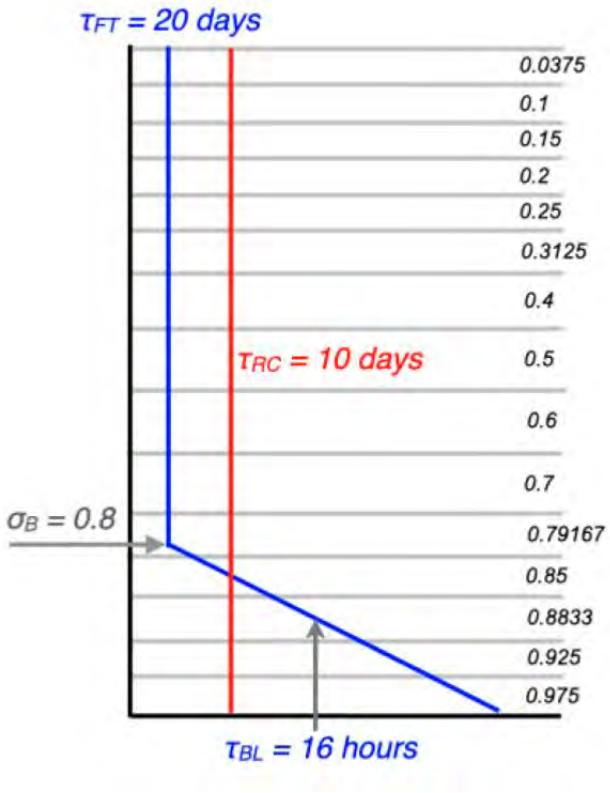

Figure 3.5: Taken from Hall and Leroux (2022): Vertical profiles of diffusion and damping with associated time scale.

space to all 3-d state variables (U, V, T, Q). Linear diffusive vertical fluxes are calculated from vertical gradients at sigma-level boundaries. The damping rate follows a linear profile from the surface to a specified boundary layer height fig 3.5. The mean rate in the boundary layer corresponds to a time scale of 16h. There is level-independent linear damping on temperature only, with default time scales of 10 days (T31) and 12 days (T42). This is intended as the crudest radiation scheme imaginable. In principle, simple in-situ linear damping like this could be added either in spectral or grid space.

3.2.1.2 Stationary waves Configuration

The concept of the stationary wave model is presented here by considering the instantaneous time evolution of an observed atmospheric state - the state vector Φ in reality is:

$$\frac{\mathrm{d}\Phi}{\mathrm{d}t} = N(\Phi) + F(t) \tag{3.1}$$

where N is a nonlinear operator and depends on Φ, $F(t)$ is external forcing and independent of Φ. It is like the presentation of a perfect model where N includes all physical

processes and F is prescribed as boundary forcing.

For the DREAM presentation, we have model state Ψ developing as:

$$\frac{\mathrm{d}\Psi}{\mathrm{d}t} = N(\Psi) + G \tag{3.2}$$

where G is a constant vector, N is prescribed as dry primitive equations plus some damping and all other processes or interactions of the system are as external forcing added to F. With a semi-implicit scheme, the model time step is specified at 22.5 mins. This configuration of DREAM was first shown in Hall (2000); Hall and Derome (2000).

We would like to use here DREAM T42 with the set-up to investigate the deviation of the summer climatology state. This state is derived from 38 extended summers May-Oct of the ERA-Interim 1979-2016 dataset - denoted as $\bar{\Phi}_{summer}$. The basic state is introduced into the model as spectral coefficients of Z, D, T, Q.

As in eq. 3.2, the G is specified in order to investigate the growth of anomalies on a time-independent basic state. By setting up the initial condition as a basic state and G is to maintain that state, we can examine the deviation from that state by putting a perturbation forcing. This approach is introduced by Jin and Hoskins (1995), in which, forcing G associated with the $\bar{\Phi}_{summer}$ is derived by the running model unforced for 1-timestep. With $G = -N(\bar{\Phi}_{summer})$, it maintains the basic state against its own advective tendencies and damping without any forcing added. In this configuration, G represents the sum of diabatic forcing and transient-eddy flux convergence. Therefore, the model does not develop following the eq. 3.3 called Stationary wave model.

$$\frac{\mathrm{d}\Psi}{\mathrm{d}t} = N(\bar{\Phi}_{summer}) + G_{\bar{\Phi}_{summer}} = 0 \tag{3.3}$$

Then if a perturbation forcing is imposed on the right-hand side of eq. 3.3, we have perturbation mode. There are two kinds of perturbation forcings are applied on stationary wave configuration in this study.

$$\frac{\mathrm{d}\Psi}{\mathrm{d}t} = N(\bar{\Phi}_{summer}) + G_{\bar{\Phi}_{summer}} + F_{perturbation} \tag{3.4}$$

a) Heating sources

The heating source is prescribed with a fixed vertical profile as fig 3.6 and prescribed spatial extension, the magnitude of the centre point is 2.5K/day. This source is used as an artificial wave source adding onto the model's basic state as $F_{perturbation}$ in eq. 3.4. This thermal forcing is applied only on temperature for 2 days and then switched off. The model develops freely after this pulse of heating and runs for 15 days in total. The heating anomaly file is prescribed in grid space, and then transformed into a spectral field as an input to the model. The vertical profile is $Z(L) = -\pi/2. * cos(\pi * \sigma(L))$. The spatial pattern uses the

cosine bell function.

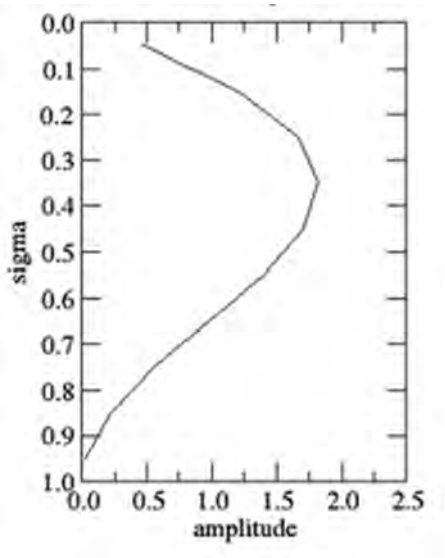

Figure 3.6: Taken from Lin and Brunet (2018): Vertical profile of the heating: $Z(L) = -\pi/2. * COS(\pi * \sigma(L))$.

The heating source is set all over the map one by one following a grid array of 10*10 degrees. In total, we do 648 experiments. Then the examination of the sources which give the most influence associated with the prescribed target regions (Vietnam sub-regions) is then described.

b) Nudging technique

To attempt to create a more realistic source, we would like to nudge the area that gives the most influence from heating experiments to the two-week lagged precursor state deduced in the last chapter - Nudging experiments. This means that, instead of putting thermal forcing, we nudge the model state toward the day lag-15 state over a given region. It is applied to all model variables as in:

$$\frac{\mathrm{d}\Psi}{\mathrm{d}t} = N(\bar{\Phi}_{summer}) + G_{\bar{\Phi}_{summer}} + \frac{1}{\tau}(\Phi_{ndg} - \Psi) \tag{3.5}$$

In other words, if the difference between day lag-15 states and the summer climatology is considered as an observed anomaly forcing, this experiment is a perturbation mode with a realistic anomaly source. This realistic source is maintained for 4 days. The two lag-15day states associated with the NVN-Wet and dry obtained from the observed analysis in chapter 2 are used in these experiments.

Furthermore, observed anomaly forcings derived from two day lag-15 states associated with the NVN-Wet and dry are applied also on different basis sate - monthly climatology state from May to October. The model response on varying basic sates is investigated.

3.2.2 Ray Tracing

The tool for Rossby wave tracing used here is the package "raytracing" written in the R language, provided by Rehbein et al. (2020), trace Rossby wave ray paths from a determined source, specified wave number, and direction of propagation. "Ray tracing" can be employed as a set of experiments changing these parameters, enabling the identification of Rossby wave sources automatically. The theory used in the package is based on classical studies: Hoskins and Karoly (1981); Karoly (1983); Yang and Hoskins (1996).

The ray theory with the solutions of the non divergent barotropic vorticity equation on the sphere is presented firstly in a Mercator projection of the sphere by Hoskins and Karoly (1981); Karoly (1983). Then the basic Rossby wave theory was presented in Hoskins and Ambrizzi (1993) starting with the dispersion relation of Rossby plane-wave with discussion applied on the winter climatology basic state.

In summary, on a given basic state, the zonal wind can be used to derive the dispersion relation for barotropic Rossby waves on a westerly flow $\bar{U}$: $\omega = \bar{U}k - \frac{\beta_* k}{K^2}$ with β_* is the meridional gradient of absolute vorticity and the K is total wave number. The consideration of stationary Rossby wave ($\omega = 0$ and the phase speed $c = \omega/k = 0$) leads the conclusion that wave number K_s is possible if the flow is positive (westerly) and the β_* is positive. Then the wave activity propagates with the speed of $2\bar{U}cos\alpha$ depending on the alpha - the angle of the wave crests and troughs with the x-axis - eastward direction.

Considering in a 2D field, the basic flow varies slowly in latitude compared with the scale of the waves, thus the wave number in the x-axis - k - is constant but in the y-axis, the wave number - l - varies but follows the local dispersion relation. So the Rossby ray paths are refracted according to the procedure detailed in Appendix 4.4

- The wave moves with group velocity c_g at the start point. The wave numbers in the x and y direction are k and l.
- The meridional variation of K_s leads to changes in the y-axis wave number l.
- The angle of crests and troughs with x-axis changes → the Rossby ray thus changes direction

Hoskins and Ambrizzi (1993) show a schematic of stationary Rossby wave number profiles and tray path refraction (Fig 3.7). The Rossby rays are always refracted towards latitudes with larger K_s shown in Fig 3.7a. There is a turning latitude Y_{LT} at which $K_s = k$ and $l = 0$ shown in Fig 3.7b beyond which decay is predicted. The latitude Y_B at which $K_s = 0$ in Fig 3.7c indicates all rays return before that. The critical latitude Y_{CL} at which $\bar{U} = 0$ and K_s becomes infinite is shown in Fig 3.7d where rays are refracted normally into such a line but with meridional scale and group velocity tending to zero. Fig 3.7e shows a local maximum of K_s that indicates waves with zonal wave number in a certain range are trapped. This case is associated with a strong westerly jet that can act as a Rossby wave guide.

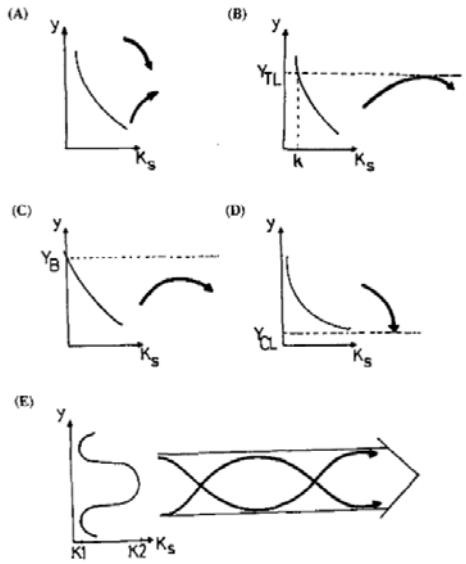

Figure 3.7: Taken from Hoskins and Ambrizzi (1993): Schematic stationary Rossby wave number K_s profiles and ray path refraction. K_s versus y in each panel and Ray paths are shown by heavy lines with arrowheads: (a) simple refraction, (b) reflection from a turning latitude Y_{LT} at which $K_s = k$; (c) reflection from a turning before a latitude Y_B at which $\beta_* = 0$; (d) refraction into a critical latitude Y_{CL} at which $\bar{U} = 0$; (e) wave guide effect of a K_s maximum.

The ray calculations in the 'raytracing' package employ Mercator coordinates in order to account for the effect of spherical geometry as presented in Hoskins and Ambrizzi (1993). With the zonal wind of a basic state (eg. the time-mean zonal wind - u), the function can transform it into Mercator coordinates (U_m); calculate the meridional gradient of the absolute vorticity (β) in Mercator coordinates (β_m), then calculate the stationary wave number (K_s) in Mercator coordinates ($K_s m$). β_m and U_m are independent of the zonal direction. Thus, the ray track is drawn by integrating the differential equation using the second-order Runge-Kutta scheme for a given initial position, total wave number and frequency.

Rossby wave ray paths (lat/lon) can be traced from one or more initial sources (x0, y0) for one given total wave number (K), and one initial direction set up when invoking the function. There is also a function for $wave_arrival$ that ingests the ray paths to filter by a determined target region. It is applied in Coelho et al. (2015) to show the extratropical teleconnection between the Pacific and the Atlantic through stationary Rossby waves that are in agreement with their observed analysis.

We would like to use this package to investigate the Rossby ray paths that can influence the Vietnam subregions for various basic states. The basic states are derived from the reanalysis dataset including summer climatology, and lag-composites of Vietnam subregion wet and dry events as in chapter 2.

All the Rossby wave sources in the Northern Hemisphere are traced in the band 30-50N

at each 10 degrees of longitude. We consider three total wave numbers of Rossby waves $K = 1to3$. With the target region being rectangular 104-110E and 8-23N, all the ray tracings that can reach the target region within a 15-day integration (6 hours per time step) are presented.

3.3 DREAM Results

3.3.1 Heating experiment on Summer Climatology basic state

3.3.1.1 A single experiment

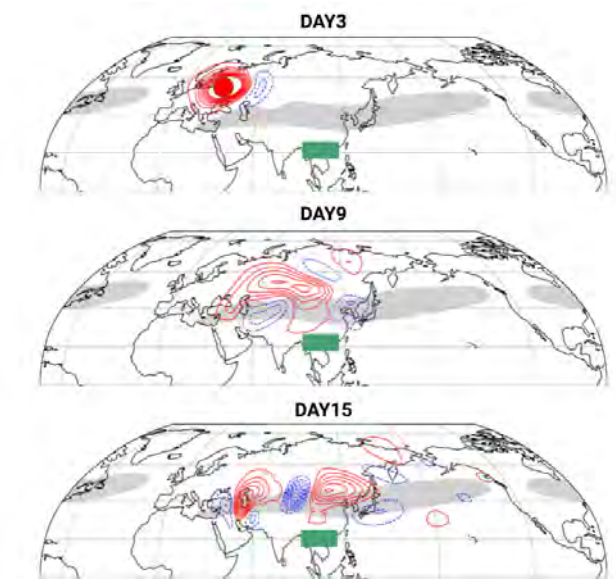

Figure 3.8: The development of geopotential height at 250 mb from an individual experiment on a summer climatological basic state Red point: heat source added. Red is positive. Blue is negative. The contour interval is 8m. Green rectangle: the target area.

Fig 3.8 shows the development of geopotential height at 250 mb from day 3 to day 15 of a perturbation experiment using DREAM on a summer climatological basic state, adding a 2-day perturbation heat source. The geopotential height anomalies continue to develop after the source is switched off on day 3. They propagate downstream along the Asian jet and give rise to a negative anomaly over Japan after 9 days of model integration. Following this, the anomalies along the Jet strengthen.

This individual experiment illustrates the development of an anomaly in the basic state, but it does not inform us of the location of the heat source that would give the most influence on the Vietnam subregion compared to other sources. To see this we construct an influence map, in which we measure the change in a target variable over a target region with time, then plot it at the location of the heat source. We choose mid-tropospheric vertical velocity as

the target variable, as it is potentially indicative of moisture convergence in a dry dynamical model. The construction of an influence map from a large number of experiments allows us to visualize the development over the target region caused by heating at all the different locations, for a given moment in the model integration. Two separate target regions are considered: NVN and SVN for the set of heating experiments described below.

3.3.1.2 Influence map for NVN circulation

The set of 648 experiments including the same heat source added but in 648 different locations all around the world are presented as an influence function map. Following the model integration, the influence at a certain time over the target region either NVN or SVN is recorded and plotted at the position of the heat source. In that way, we can examine the sources giving the most influence following model running time. The value of omega at 500mb from model output is presented here with an interval of 3 days. Each map consists of 648 points represented for 648 experiments. Blue means that there is an ascending motion over the target region. Two target regions, NVN and SVN, are investigated separately.

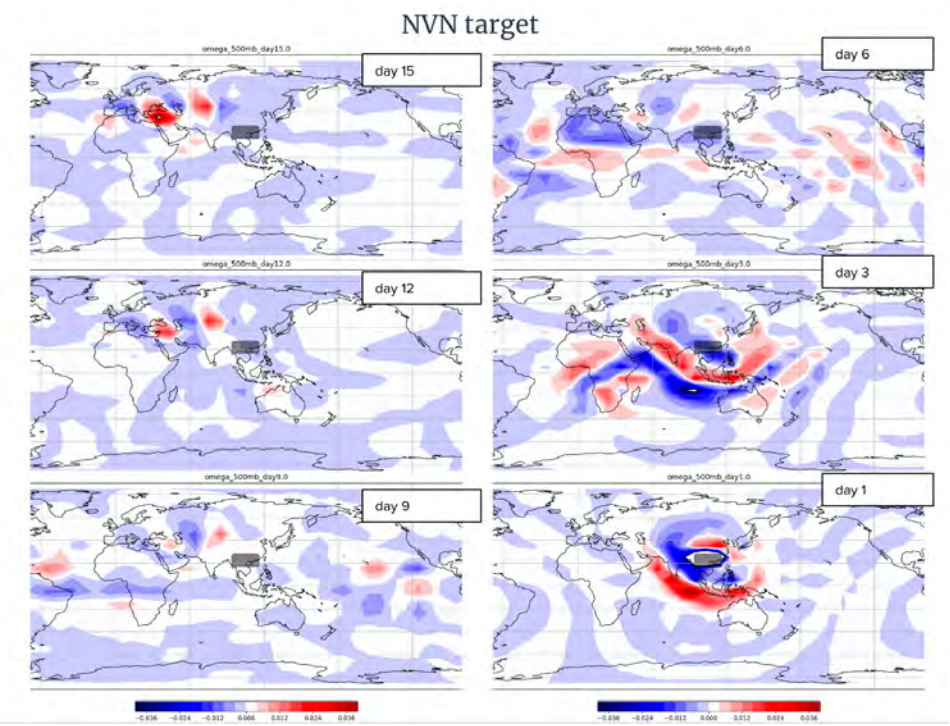

Figure 3.9: The influence function map on vertical velocity over NVN. Mid-tropospheric pressure vertical velocity Omega 500mb is shown in mb/hour. Blue denotes *ascent* over the target region after the specified running time, red denotes *descent*.

Fig 3.9 shows the influence function map of vertical velocity with the target region of NVN. It shows the impact on NVN's circulation from a 2-day pulse of heating in a way that depends on the location of the source and the time in the integration. Diagnostics are

presented in reverse order, with panels that are further into the integration presented first, to ease comparison with the composites presented in chapter 2.

After 1 day of the model run (fig 3.9-day1), it is clear that heat sources that are close to NVN are still switched on giving direct influence to NVN. Heat sources located 0-35N; 70-120E give the upward velocity over NVN, while the sources over the Indian Ocean lead the downward motion over NVN. After 3 days of model running time (fig 3.9-day3), when the heating is switched off 1 day before, the effective sources are further from NVN, with sources as far away as Africa starting to have an impact on the vertical velocity over NVN 3 days later. The influence from sources close to NVN is very different from day 1. Particularly, the sources to the southwest of NVN and around the Equatorial Indian Ocean lead the opposite direction of vertical motion. Moreover, in the band of 20S-20N, the sources on the western side of NVN show faster propagation than those on the eastern side. Particularly African sources compared to the sources over the Philippines that can go nearly 100 degrees of longitude from Greenwich longitude to NVN target region.

The following panel after 6 days of model integration (fig 3.9-day6) shows mainly tropical sources giving rise to vertical motion anomalies over NVN. Sources located on the south of the Indian Ocean no longer impact the NVN circulation. Only North Africa and Eastern Pacific sources are effective at this lead time. This is probably due to strong tropical damping for the wave propagation here.

When the model runs 9 days (fig 3.9-day9), we see clearly that two regions separately influence the vertical velocity over NVN: Tropical and Extratropical sources. The tropical sources are located in the western tropical Atlantic Ocean and tropical Eastern Pacific, while the extratropical sources are located over Iran -Kazakhstan. Thus, waves emanate from heat sources that can reach NVN from both the west and the east.

It is interesting that after 12 days (fig 3.9-day12), the sources over extratropics in Europe - Iran - Kazakhstan show increasing influence on the vertical velocity over NVN. The sources are aligned along the 40N latitude, slightly to the north compared to the results from 9 days of model development. This shows the sensitivity to the longitudinal location of the heat source, around the location of the summer climatological Asian jets. There is no tropical heat source now that can give an impact on NVN vertical velocity 10 days after switching off.

After 15 days running (fig 3.9-day15), the influences due to extratropical sources look to be reinforced during the 3 days following. The source very close to the Asian jet can also influence the NVN circulation. In particular, a heat source over Iran can give the most influence of descending motion vertically over NVN, while the European and Kazakhstan sources lead to slightly weaker ascending motion over NVN.

By plotting the influence of NVN vertical velocity at the position of the heat source, following the influence function map from 15 days to 1 day, the extratropical sources located in the range 0-80E around 40N can lead the influence on NVN circulation for about 10 days after pulsing a heat source (12 days integration). The influence strengthens with time (15 days integration).

On the other hand, the tropical sources show the influence is limited to 1 week (9 days of integration). It looks like the extratropical wave trains induced by the heating sources over Europe - Kazakhstan trapped by the Asian jet then give the influence on NVN that is located to the south. The tropical sources from 9-days to 1-day running suggest the propagation of Kelvin waves along the Equator via the tropical western sources that propagate eastward to the NVN region. There are also tropical eastern sources in the Eastern Pacific that also can influence NVN with westward propagation possibly via Equatorial Rossby waves.

Compared to the composite from observational analysis, the extratropical sources here resemble the anomalies that originate from Europe associated with the NVN events, that propagate at high latitudes and then influence NVN circulation. The tropical sources show less connection with the composite, except for the quick development (about 6 days) of tropical divergent flow from the east side of NVN.

3.3.1.3 Influence map for SVN circulation

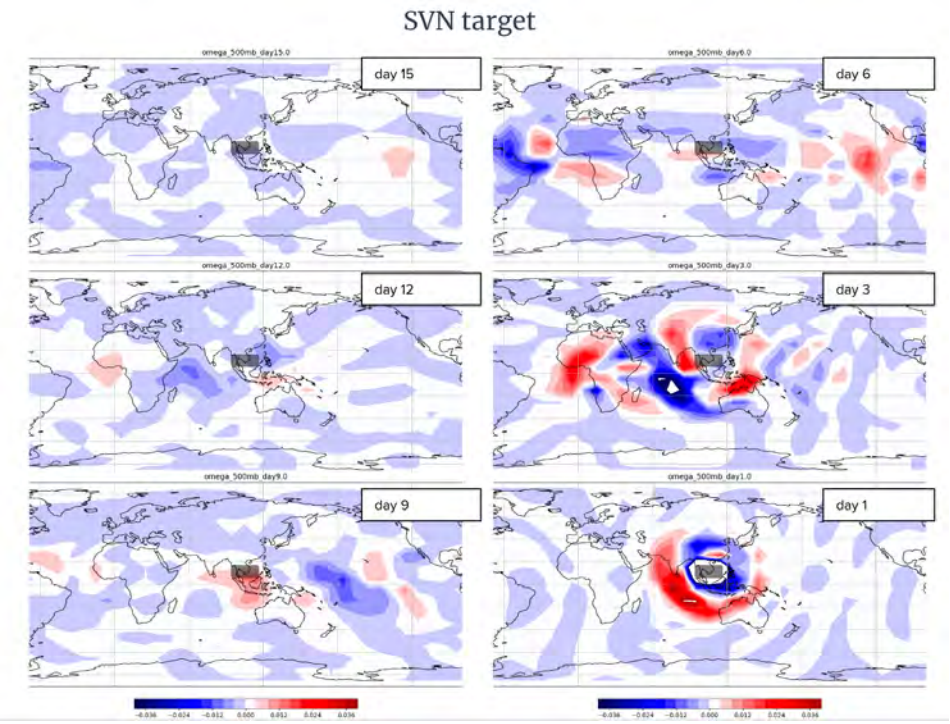

Figure 3.10: as Fig 3.9 but for SVN target region.

Influence function maps of vertical velocity averaged over SVN made from 648 individual perturbation experiments on the summer climatological basic state with up to 15 days of running are shown in Fig 3.10. The pulse of a 2-days heat source shows the impact on SVN's circulation that is shorter lead-time, but stronger. As with the NVN target region, after 1 day's model run, only sources close to SVN are effective. The sources giving downward motion are located to the west of SVN, rather than to the south as for NVN.

After 3 days running (fig 3.10-day3), the distribution of sources giving impacts to SVN circulation changes and is different from the NVN case. Particularly, the 2-day sources over the Maritime Continent and the north of Australia lead to descent over SVN, while giving upward motion to the NVN target. The sources over the equatorial of western Africa give downward motion over both NVN and SVN, but stronger in SVN. However, the sources over Mongolia - North China give the opposite impact for NVN and SVN after 3 days of model run.

When the model runs for 6 days (fig 3.10-day6), the sources over the Tropical Atlantic and Eastern Pacific strongly influence SVN circulation downwards, while the sources over Eastern Brazil lead to upward motion. Compared with the NVN case, the tropical heat sources are similar in generating an influence on the Vietnam subregion. In particular, the sources located on either the western or eastern side raise more influence on SVN than NVN. This is not a surprise because SVN is closer to the Equator than NVN. However, after 9 days of model running (fig 3.10-day9), the influence map of SVN shows a clear difference from the NVN. Only the sources along the Equator give influence, especially the Maritime Continent and the Central Pacific. Then, after 12 days or even 15 days of model runs, there are no sources outside the Tropics giving the influence on SVN circulation (fig 3.10-day12-15).

The influence on the vertical velocity of SVN plotted in place of the 2-day heating source for various model running times shows that only tropical heat sources (within 20S-20N) lead to an influence on SVN circulation in the limit range of 12 days integration. For longer model integration, no heat source shows a significant impact. Following the influence maps forwards in model running time from 1 day to 9 days (i.e. backward on the figures), it looks like a wave source that starts from SVN, then generates "anti-Kelvin" waves that propagate westwards along the Equator talking about 9 days to pass the Pacific Ocean. Interpreting the plot forwards on the figure, shows consistency with the observational composites, from the reanalysis dataset. In which, the strong tropical wave activities are associated with the SVN events that propagate slower.

To sum up, within a 2-week model run using ERAi summer climatology as a basic state, a set of artificial heat sources in different locations around the world in perturbation mode, we get influence function maps with 2 different target regions as NVN and SVN. The pure-dry dynamics of the model set-up show the difference in the heating sources that can influence NVN and SVN circulation. For NVN, the extratropical sources exhibit the impact after 12 days and the tropical sources lead to the modification of vertical velocity within the first 9 days of the model run. For SVN, only tropical sources can modify the circulation. It suggests two pathways of influence on Vietnam subregions circulation: tropical waves in both regions and extratropical only for NVN. For NVN the heat sources over Europe give the most influence after 15 days. For SVN, the influence map suggests the most significant precursors resemble Kelvin wave sources.

Other diagnoses of the Vietnam subregion's circulation are also considered in this PhD work such as the divergence and the stream function in the upper level (Annex 4.4). They show consistency with omega in the middle level and indicate clearly that the European sources can lead to a strong stream function anomaly in the upper level over the NVN domain, but

do not impact SVN.

3.3.2 Observed Precursors

3.3.2.1 Nudging experiments: European Precursors

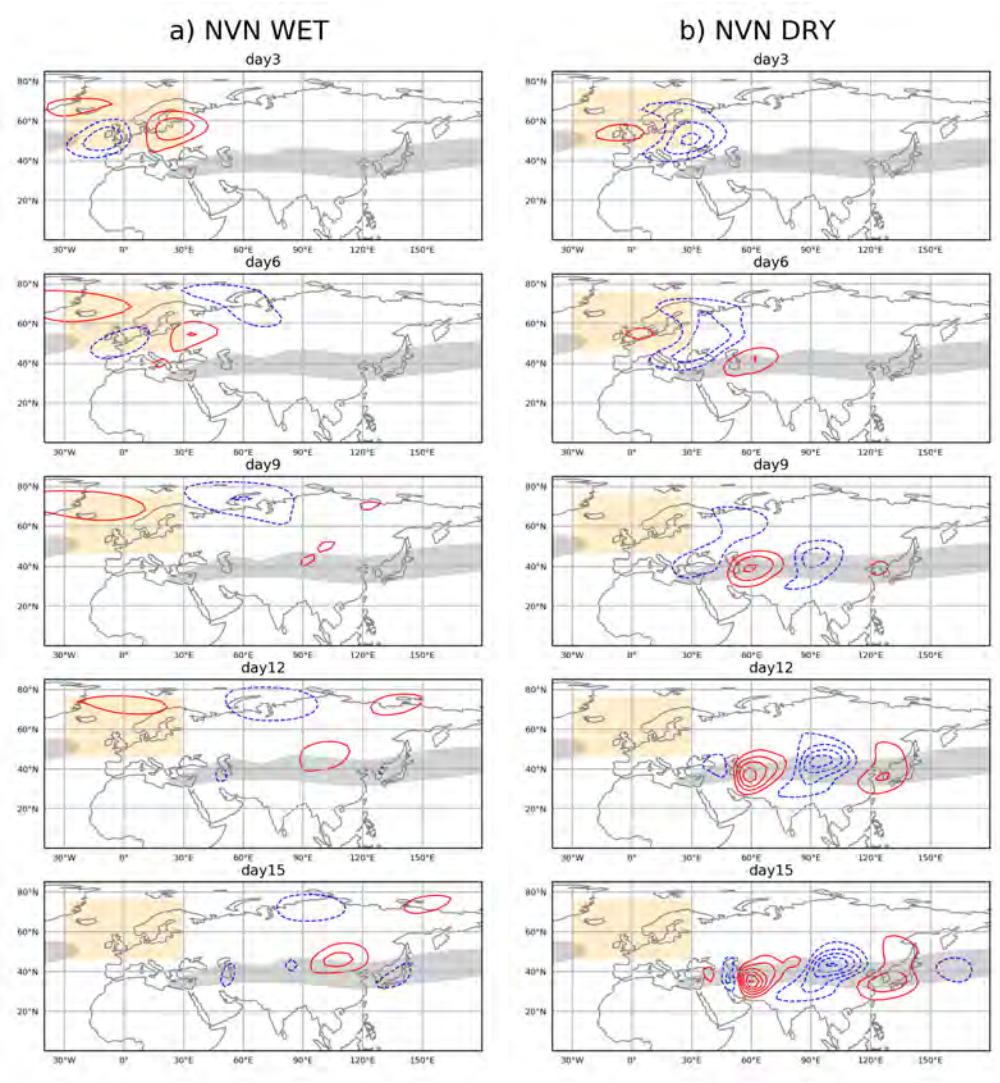

Figure 3.11: Geopotential height anomaly at 250 mb for nudging experiments on the summer climatology basic state by nudging the domain towards the lag-15day composite of (a) NVN-Wet and (b) NVN-Dry. The grey shading indicates the jet stream where the zonal wind is greater than 20m/s. The orange shading indicates the nudging domain.

We have seen that European heat sources can have a strong influence on NVN circulation through the influence map of heating experiments and the observed composites. Thus, to attempt to simulate a realistic anomaly source of influence from extratropics, we present here the results from nudging experiments conducted using the lag-15 composite from chapter 2

as the nudging field. Over the nudging domain pre-prescribed, all parameters are nudged toward the lag 15-day composite associated with NVN-Wet and dry events for 4 days. The nudging is then switched off. The model development is presented below.

On the summer climatology basic state, by nudging the domain - yellow area - towards the observed precursors from the lag-15day composite associated with the NVN-Wet and NVN-Dry, the developments of geopotential height anomaly at 250mb from day 3 to day 15 of the model running are shown in Fig 3.11.

The NVN-Wet precursors are recreated as a dipole anomaly aligned longitudinally over the nudging area at day3 out of 4 days of nudging (Fig 3.11a-day3). It consists of two equal anomalies of geopotential height: negative over Western Europe and positive over Western Russia. Two days after switching off the nudging, the anomalies start to propagate to the east with a decrease in the magnitude of the dipole and the development of a negative anomaly at higher latitudes, in the north of Russia (day 6). Then after 9 days, the dipole disappears, while the anomaly over North Russia grows. Day 12 shows the growth of a positive anomaly over North China which is located on the north side of the Asian jet and another positive anomaly over northeast Russia (Fig 3.11a-day12). There is an eastward propagation of anomalies over north Russia clearly from day 12 to day 15. At the same time, anomalies develop along the jet, particularly the positive anomaly over North China and the negative one over Japan. Compared with the observed composite, although the nudging field leads to an eastward propagation at high latitudes, it leads to a positive anomaly over China instead of a negative one. Other signatures that have been seen in the NVN-Wet composites, such as the Siberian positive anomaly and the positive over Japan are not simulated by this experiment.

The NVN-Dry precursors show reversed anomaly signs compared to NVN-Wet cases, but the dipole anomaly is asymmetric. In particular, the negative anomaly over Europe-Russia covers a larger area and is stronger than the positive one (Fig 3.11b-day3). This dipole on the summer basic state leads to a strong anomaly development far from the source after 15 days run compared with the NVN case. After a 6-day run, when the source area is free from nudging, anomalies propagate to the east that are quickly trapped by the jet, then a positive anomaly appears over the jet (Fig 3.11b-day6). These anomalies quickly develop downstream (day 9 and day 12). The anomalies on day 12 along the jet are reinforced after 3 days with no change of patterns (day 15). The propagation of the precursors, the negative anomaly over China and the positive over Japan look like those in the observed composite. In this experiment, it appears that the jet acts as a wave guide. The similarity between this nudging experiment and the observed composite suggests the important role of European precursors and Asian jets associated with the NVN-Dry events.

European precursors associated with opposite events over NVN are simulated by the nudging technique on the summer basic state. Although the precursors are symmetrical in sign, they are asymmetrical in spatial pattern. The model responses are quite different between these two precursors. The NVN-Wet case shows propagation at high latitudes which then goes further to the south where the anomaly grows quickly afterward (Fig 3.11a). The NVN-Dry precursors are quickly trapped by the jet and the anomaly grows very quickly until day 12 (Fig 3.11b)and is then reinforced. The nudging experiment reproduces a relatively

good geopotential height anomaly associated with the NVN-Dry event, but not for NVN-Wet. This might suggest a role for other precursors, for example, Siberian High, in association with the NVN-Wet events. In any case, the existence of two different pathways can be seen in the summer basic state due to the two kinds of precursors introduced. The Asian jet plays an important role in the anomaly growth associated with the NVN-Dry precursors.

3.3.2.2 Linear response and Growing mode

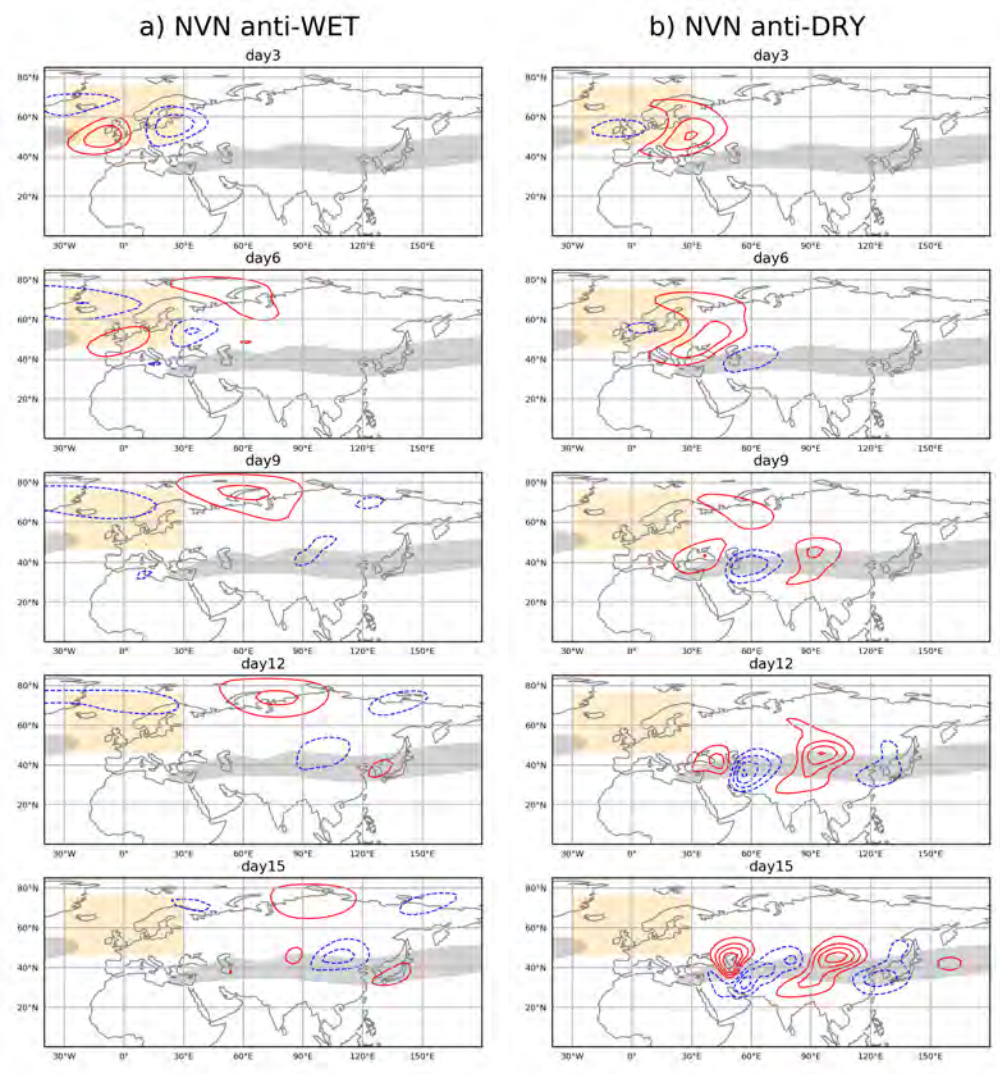

Figure 3.12: as Fig 3.11, but nudging the domain towards the **negative** of lag-15day composite of NVN events: (a) NVN anti-Wet and (b) NVN anti-Dry.

We employ further nudging experiments to investigate the linearity of the model response to the European precursors. Fig 3.12 shows the extratropical response to anti-nudging sources via geopotential height at 250 mb. The anti-Wet source that has an exact inverse dipole structure as NVN-Wet at day 3, gives the extratropical response at high latitudes. After 15 days,

the model shows a linear response by reappearing China-Japan anomalies and propagation over high latitudes. For the anti-Dry source, the model response is almost linear. The anomalies are quickly developed along the jet as in the NVN-Dry source, slightly weaker from day 12. The opposite patterns of anomalies over China-Japan again are located in the same place as in Fig 3.11 after 15 days.

Thus, the model shows a linear response to the European sources that suggest the mechanism of propagation of teleconnection in NVN events is linear. In addition, the response shows a difference due to the difference in sources. Particularly, the response to the NVN-Dry sources seems to be directly projected onto growing baroclinic mode.

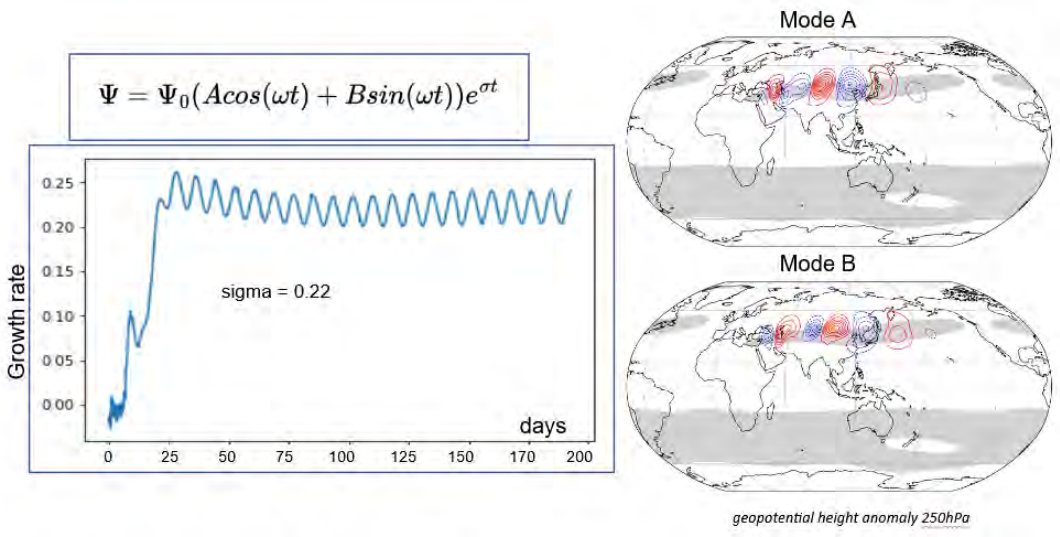

Figure 3.13: Presentation of Growing mode of Summer Climatology Basis state. The grey shading indicates the jet stream where the zonal wind is greater than 20m/s.

By adding noise and running the model on the summer climatology basis state used for the nudging experiments during 200 days, we present the fastest growing mode in Fig 3.13. Following the expression of the model state from the initiation, the plot of growth rate versus time and two principal modes A and B are shown. The model state shows exponential growth with sigma=0.22 stably after almost 100 days. The response to NVN-Dry forcing events projects onto these modes after 15 days of model run to compare the modes and the model response to European precursors. Thus, it suggests the transition mechanism of model response to NVN-Dry experiments, as well as the different pathways between NVN-Wet and NVN-Dry experiments is needed to be explored.

3.3.2.3 On different basic states

We continue our examination of the extratropical precursors extracted from the observed composites for different monthly climatological basic states derived from the reanalysis dataset. Within the summer extended from May to October, we conduct six monthly climatological basic states.

Fig 3.14 presents the development of geopotential height anomaly at 250mb from day3 to day 15 by adding the precursors extracted from lag-15-day composite associated with NVN-Wet events on different basic states. Generally, although the same precursors are added, the development of anomalies is different from case to case. On the May basic state - Fig 3.14a, from day3 to day6, the anomalies not only propagate to the east at high latitude but also develop to the south where the Asian jet is located. The propagation over Russia is decaying from day 9 to day 12, but the anomalies along the jet grow strongly. From day 12 to day 15, the anomalies are strengthened at the same place. On the June basic state - Fig 3.14b, the propagation of anomalies is similar to in the May basic state from day 3 to day 12. After that, the high latitude anomaly continues to propagate eastwards, while the anomaly over the jet only develops in the African region. On the July basic state - Fig 3.14c, there is only propagation over high latitudes seen that can extend further as in June basic state. The development along the jet is at a smaller scale. The jets from May to July are retracted both to longitudinal and latitudinal extents and become the most compact in July. The African part of the jet appears to have an important role in initiating anomaly development along the jet.

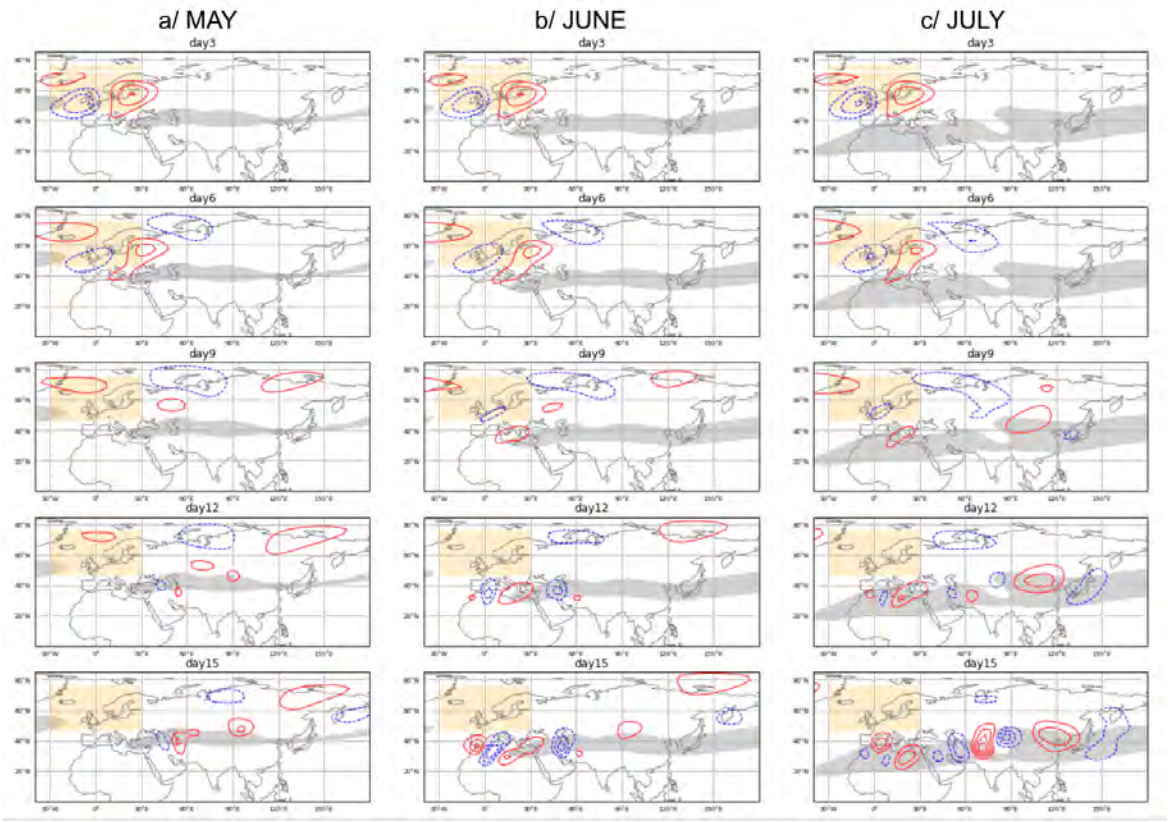

Figure 3.14: Geopotential height anomaly at 250 mb of nudging experiment by nudging domain toward to lag-15day composite of NVN-Wet on monthly climatology basic state (a) May, (b) June, (c) July, (d) August, (e) September and (f) October. The grey shading indicates the Jet stream where the zonal wind is greater than 20m/s. The orange shading indicates the nudging domain.

On the August basic state - Fig 3.15d, the model response shows the propagation of the anomaly over high latitudes to the east from day 3 to day9, then there is some growth on the jet on day9. The anomaly over the Asian jet develops slightly downstream and quickly grows. On the September basic state - Fig 3.15e, the anomalies develop in the same way as for August. This state seems to favor high latitude propagation with the presence of the Atlantic jet. The anomaly over the Asian jet has a greater spatial extension than for the August basic state. This is clearer for the October basic state (fig 3.15f) with the Atlantic jet at 40-60N and an extension of the Asian jet over Eastern Asia. The positive anomaly that is just above the Atlantic jet propagates and strengthens quickly to the east from day 6 to day 12. The high latitude anomalies then extend into the Asian jet.

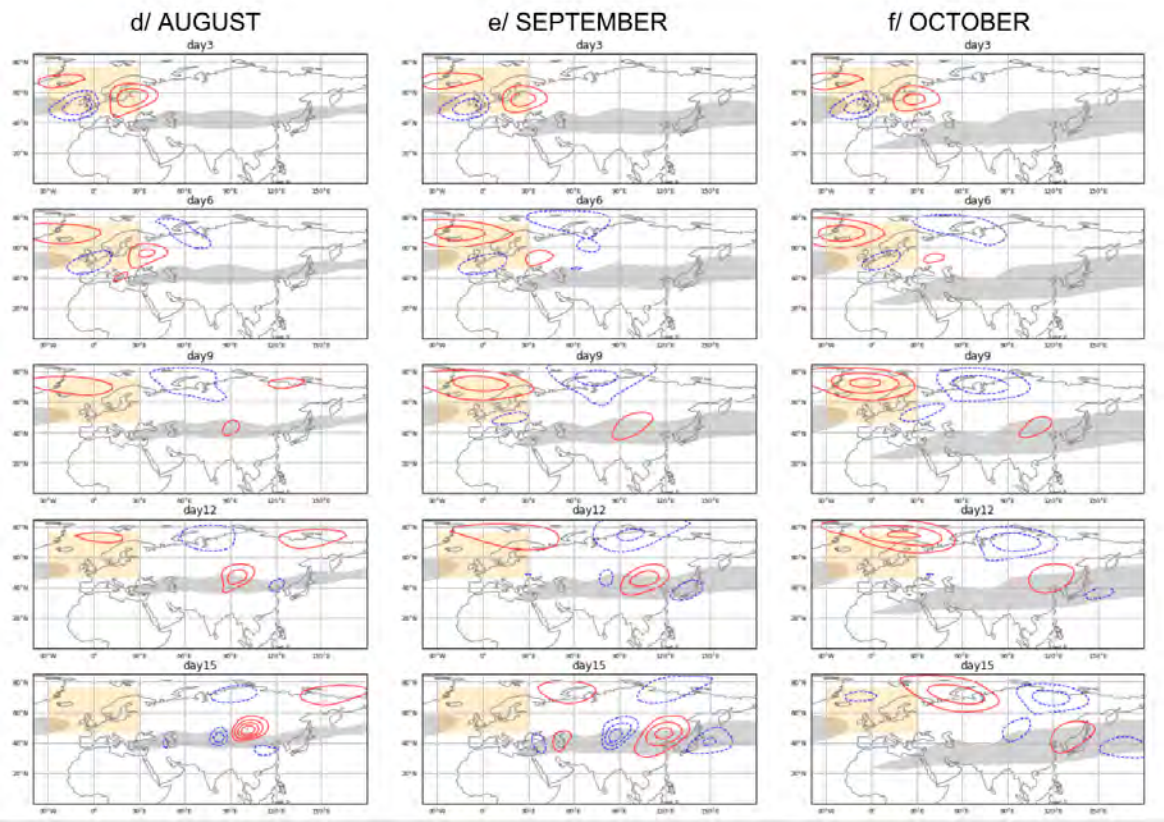

Figure 3.15: Fig 3.14 continued.

The model responds to NVN-Wet precursors in different ways that are strongly dependent on the basic state jet. There still are two main pathways of propagation. One is at high latitude with eastward propagation then the anomaly extends into the Asian jet leading to an impact on NVN circulation (AUG-OCT). The other is the development of the anomaly that is quickly trapped by the jet leading to rapid growth, reaching East Asia (MAY). The Atlantic jet plays a role in favoring the propagation of the former pathway, while the state of the Asian jet has an influence on both pathways.

Fig 3.16 presents the development of the geopotential height anomaly at 250mb from day3 to day 15 on six monthly basic states by adding precursors extracted from lag-15-

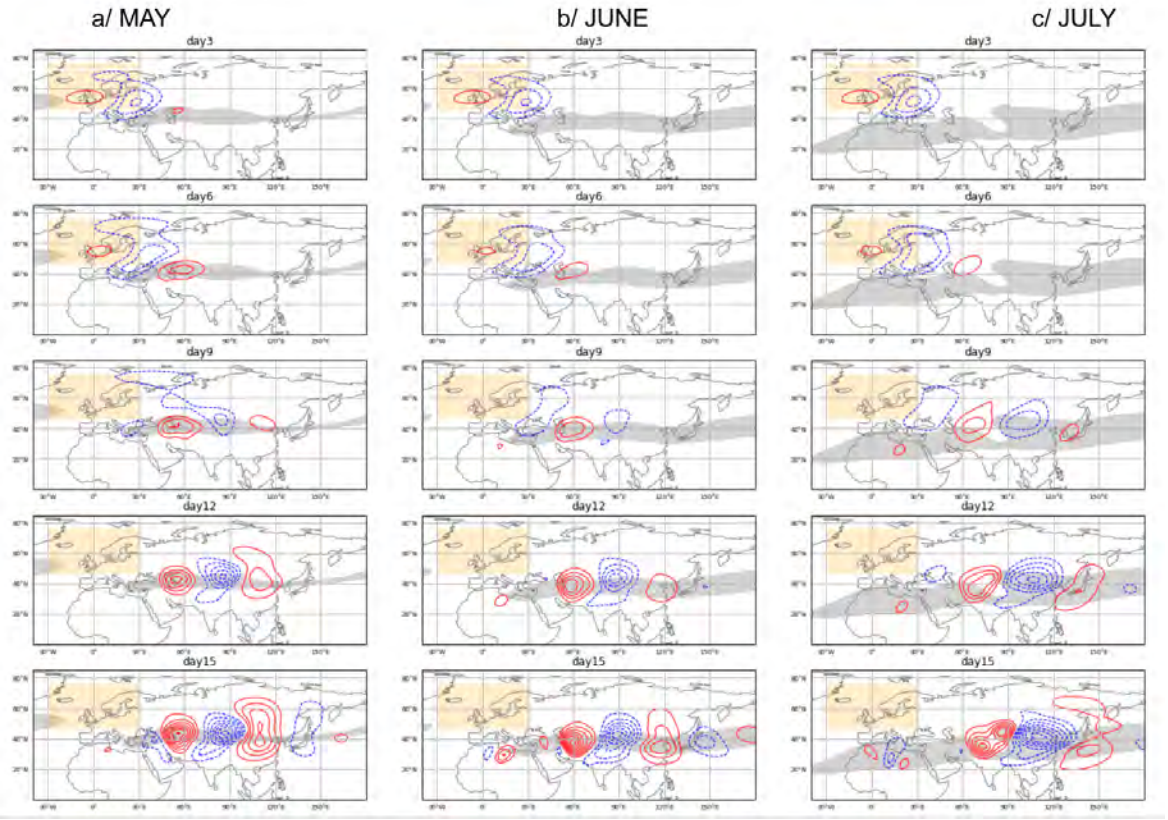

Figure 3.16: Geopotential height anomaly at 250 mb of nudging experiment by nudging domain toward to lag-15day composite of NVN-Dry on monthly climatology basic state (a) May, (b) June, (c) July, (d) August, (e) September and (f) October. The gray shaded indicates the Jet stream where the zonal wind is greater than 20m/s. The orange shaded indicates the nudging domain.

day composite associated with NVN-dry events. The development of anomalies induced by the NVN-Dry precursors all have very similar pathways of influence. For the May basic state (Fig 3.16a), the anomalies extend into the Asian jet from day 6 to day 9. These are strongly enhanced by the jet and slightly propagate along the jet from day 9 to day 15. The same development is seen in the June and July basic state (Fig 3.16b-c). The Asian jet is more compact in June and July which leads to anomalies that develop at the same location resembling an exponentially growing mode in spatial pattern. This could lead to a very different impact on the NVN circulation associated with anomalies over China and Japan.

The development of anomaly induced by the NVN-Dry precursors on the August -October basic state (Fig 3.17) is not sensitive to the presence of the Atlantic jet. The responses are all projected onto the Asian jet. Thus, the spatial extension of the Asian jet plays the most important role in anomaly growth.

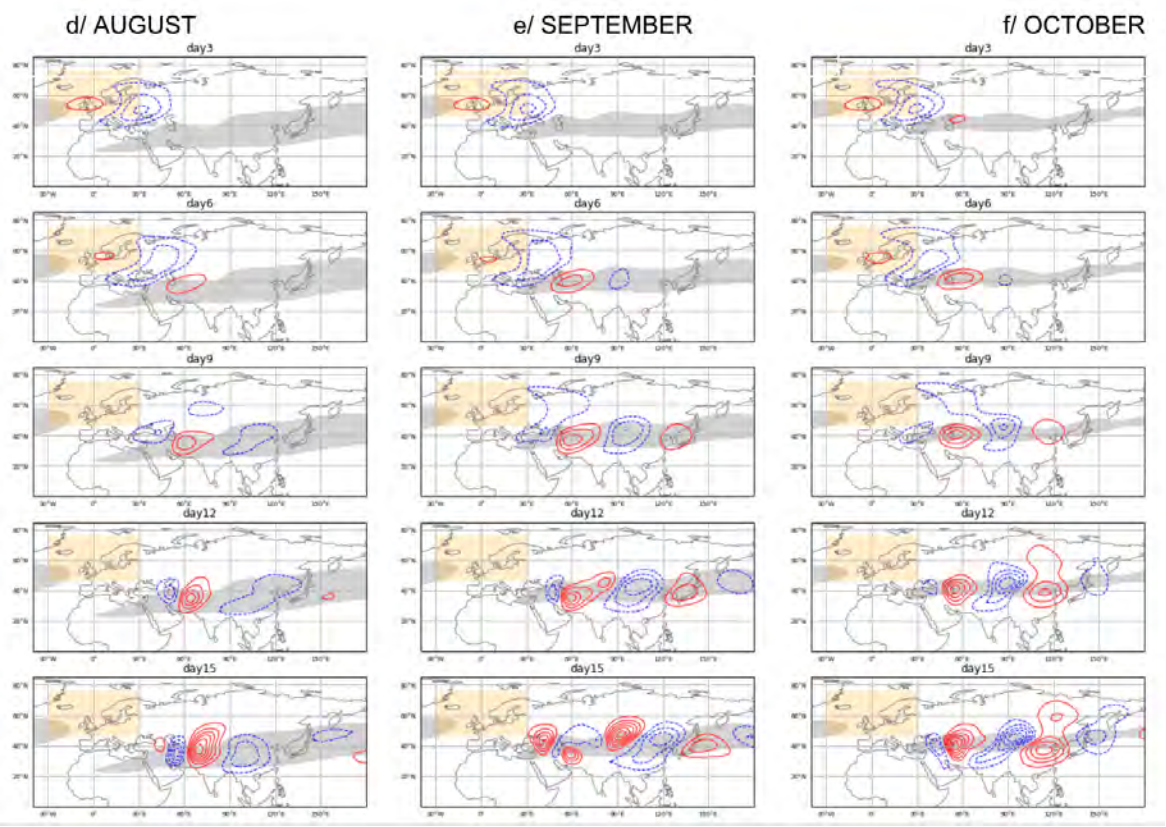

Figure 3.17: Fig 3.16 continued.

3.4 Rossby wave: Ray-tracing

In this subsection, the ray tracing technique is applied to different basic states. We focus on the Northern Extratropical influence on the Vietnam region. Thus, all the Rossby wave sources over the extratropical band 30-50N are tested to indicate the possible propagation of extratropical Rossby waves to impact Vietnam circulation in different basic states. The total wave number for stationary Rossby waves associated with the chosen basic states is shown.

3.4.1 Summer Climatology

Fig 3.18 shows the 250mb stationary wave number for the climatological basic state and rays traced from northern extratropical sources with different wave numbers that can influence the Vietnam region. The value of Ks decreases with increasing latitude. The highest values of stationary wave numbers are located mostly around the negative regions where the Ks value is up to 10. The stationary wave number shows negative values over the Tropics from the eastern Atlantic to the Western Pacific and over the north of South America, where there is a strong easterly zonal wind (not shown). According to the formula for the stationary wave number, Rossby wave propagation is not possible in these regions. For this distribution of Ks

values, there are two possibilities for Rossby wave propagation from the northern extratropics to the tropics (Fig 3.7a): one is to go northeast and then to the south, the other is to go directly to the tropics.

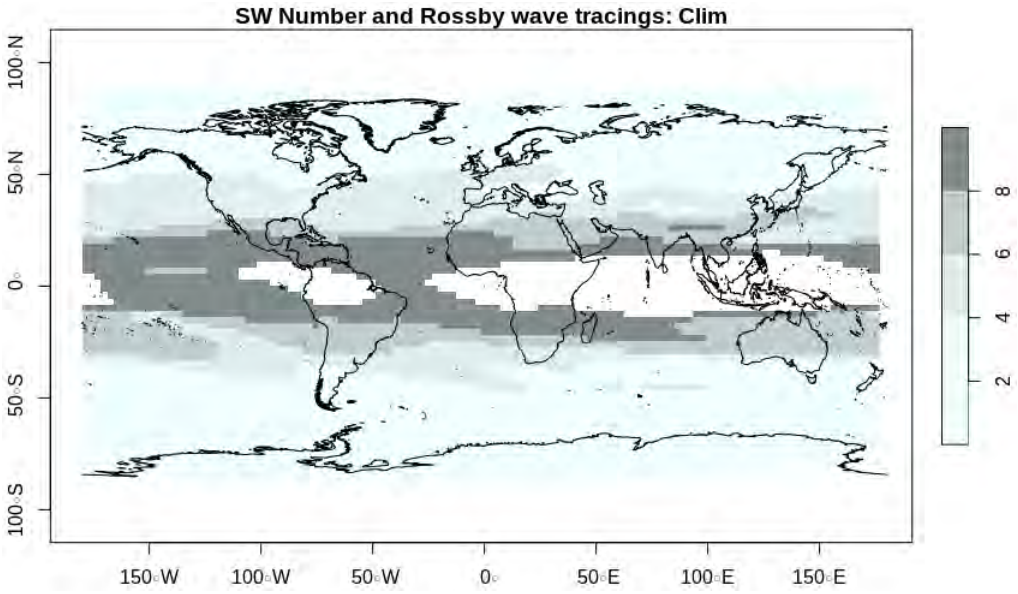

Figure 3.18: Stationary wave number for the Climatological basic state.

As an example of one extratropical source at 40N-15E, the propagation of different Rossby wave numbers on the summer climatology basis state during 15 days are shown in Fig 3.19. There are six different wave numbers from K=1 to K=6 that show two distinct kinds of propagation. First, wave numbers K=1, K=2 and K=3 with a larger scale that can propagate in the higher latitude, then reflect toward the South. While, with smaller scale, K4, K5 and K6 propagate to the south directly.

We then examine all extratropical sources over the Northern Hemisphere (with a latitude band of 30-50N and a longitude separation of 10 degrees from 5E) with six different wave numbers to find all possible sources that can propagate to the Vietnam region within 15 days. Several rays of different wave numbers are indicated in Fig 3.20 and Fig 3.21 that indicate clearly two kind of pathways discussed in Fig 3.19.

The Rossby waves with K=1 (blue lines in Fig 3.20) located at 30N-45E and 40N-45E show a ray that goes to the north nearly 80N and then propagates southeastwards towards Vietnam within 15 days. The Rossby wave with K=1 over Mongolia also impacts directly onto Vietnam but in just 2 days, then it can not go further due to the presence of the easterly wind. The Rossby wave with K=2 (green lines in Fig 3.20) initiates from the 30N-15E and shows great circle propagation to reach the North Vietnam region in 7 days subsequently passing over the whole country. The K=2 sources at 30N-105E and 40N-95E take only 1 day to reach the target region. Rossby waves with K=3 (purple lines in Fig 3.20) initiate from 30N-35E and 40N-35E passing over the North Vietnam region quickly in about 4 days to reach the South China Sea afterwards.

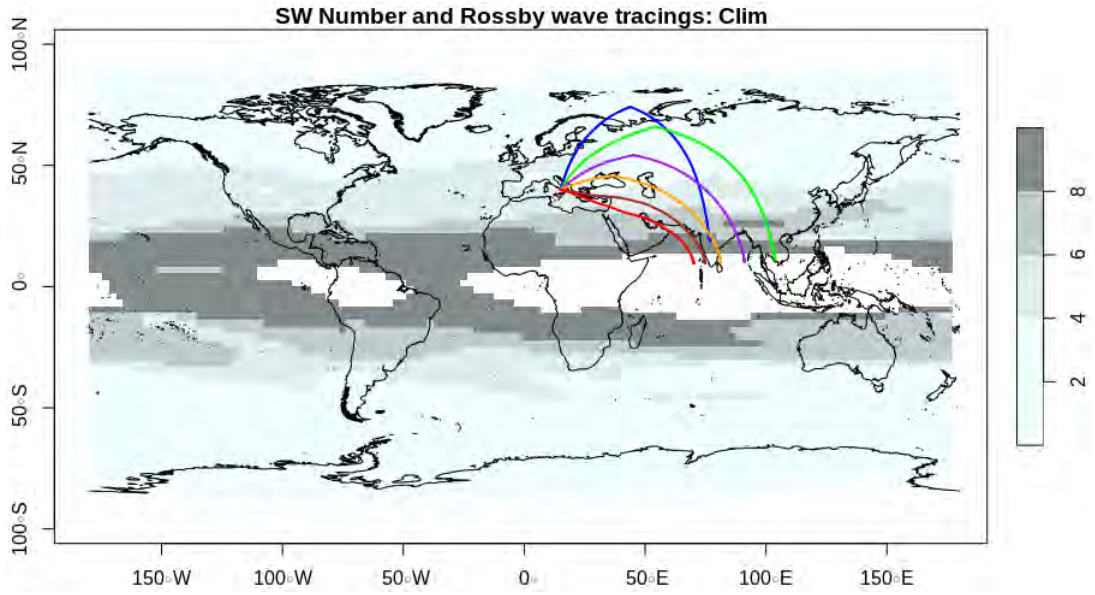

Figure 3.19: as in Fig 3.18 with the ray tracings of one sources with different Rossby wave number: K=1 (Blue), K=2 (Green), K=3 (Purple), K=4 (Orange), K=5 (Brown) and K=6 (Red).

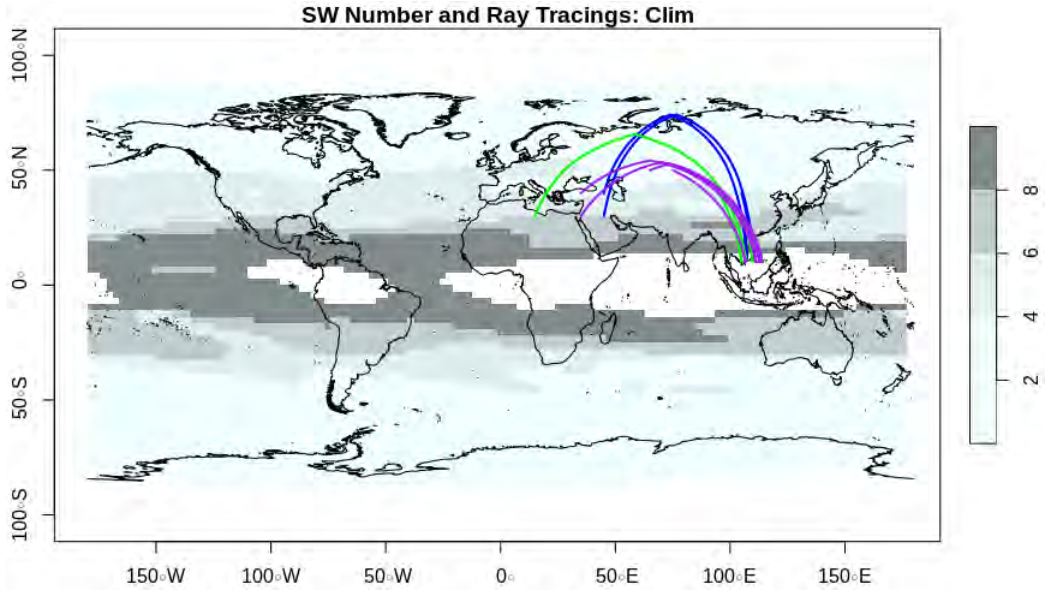

Figure 3.20: as in Fig 3.18 with the ray tracings of extratropical sources with different Rossby wave number propagating toward Vietnam region: K=1 (Blue), K=2 (Green)and K=3 (Purple)

The Rossby waves with K=4 (orange lines in Fig 3.21) from 50N propagate to Vietnam directly, while the source at 30N - same longitude shows an arc that reflects at about 45N then pass North Vietnam. These rays take about 2 - 2.5 days to reach Vietnam region. The Rossby wave with K=5 (brown lines in Fig 3.21) initiates from the 50N (from 15E-25E) and

propagates a long distance to reach the Vietnam region in 3.5 days subsequently passing until South Vietnam. The K=5 sources at the lower latitudes 30-40N take less than those of 50N a half of a day to reach the target region. Rossby waves with K=6 (red lines in Fig 3.21) show similarities with K4 and K5, but much faster. K6 with a smaller scale, it passes the Vietnam region quickly after about 1.5 - 1.75 days to reach the Eastern Sea afterward.

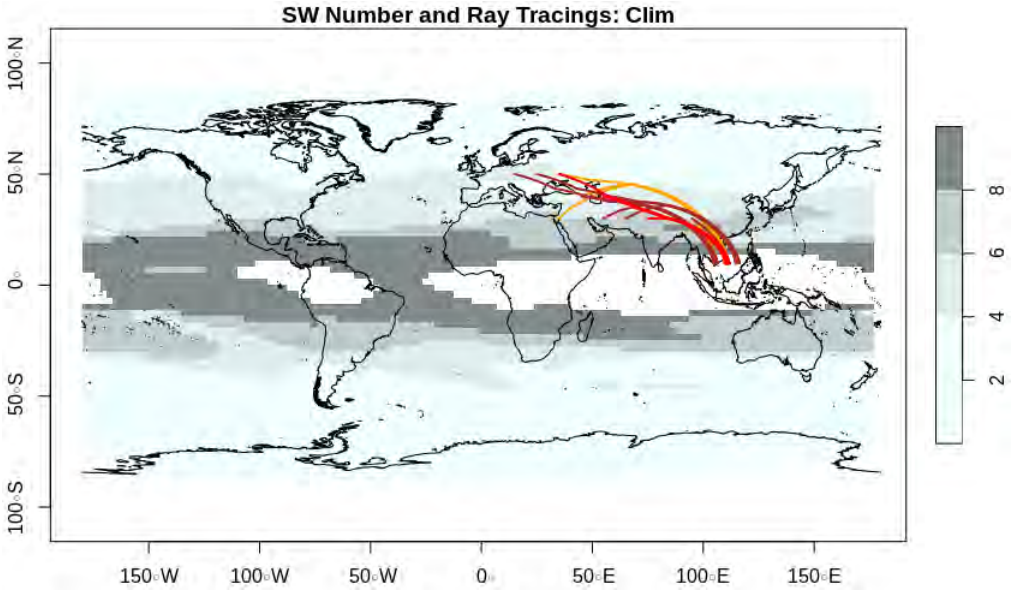

Figure 3.21: as in Fig 3.20 but for K=4 (Orange), K=5 (Brown) and K=6 (Red).

Testing for extratropical sources of the Northern Hemisphere during 15 days indicates trajectories of different Rossby wave numbers (K1, K2 and K3) that propagate to the Vietnam region in 2 weeks on the climatological basic state. Sources in the region of 30-50N and 15-45E show northeast propagation towards higher latitudes that then reflect towards the tropical region in a range of 1-2 weeks. Sources in place of the Asian jet at 30N over Mongolia 95-105E can quickly reach the Vietnam region within 1-2 days. The trajectories of Rossby wave numbers K4, K5 and K6 with a smaller scale, that propagate into Vietnam region much faster, in 3 days. Particularly, sources at higher latitude propagate directly southwards that blend following the Asian jet.

There are two separate pathways of propagation for Rossby wave sources using the ray tracing technique. The northern pathway of the sources (K123 - wave with a larger scale) is initiated from Eurasia: it propagates northeast, reflects at its critical latitude then propagates towards Vietnam. The southern pathway is from the Mongolia region that propagates directly to the Vietnam region through the Asian jet (K456 - wave with a smaller scale). These pathways resemble those in the observed composite over the Northern Hemisphere as well as nudging experiments on the same basic state. Particularly, the later pathway is seen after the downstream development of the anomaly along the Asian jet.

The same results but for the states associated with opposite events over Vietnam sub-regions as presented in chapter 2 are described below. These states consist of the anomaly

and precursors associated with the regional events that can also influence the propagation of Rossby waves.

3.4.2 On various states

Fig 3.22 shows the 250mb stationary wave number for the composite associated with North Vietnam - NVN-Wet (a) and Dry (b) events and the ray tracing for extratropical sources with different wave numbers that can influence the Vietnam region. The Ks map shows a slight difference from the climatological basic state. The negative Ks over Peru - Eastern Pacific are recovered in NVN-Dry but have a more longitudinal orientation in NVN-Wet events. There is also an effect that leads the Ks map to have a small area with negative values over the Northern Hemisphere.

The propagation of Rossby waves at different total wave numbers that have the same target of the Vietnam region is shown in Fig 3.22. All three Rossby wave numbers exhibit a northern pathway to influence Vietnam on NVN states. Rossby waves K=1 have to be initiated from a higher latitude (50N for NVN-Wet and 40-50N for NVN-Dry) instead of 30N as in the Climatology state to reach the Vietnam region. This could be due to the presence of a negative area that is formed by the meridional gradient of absolute vorticity β_* that is unfavorable for Rossby wave propagation. Rossby waves with K=2 show a great difference in propagation from an extratropical source. They are initiated from 40-50N 25-35E on NVN-Wet state to reach Vietnam after 7 days, while those starting from 40-50N 5W-5E on NVN-Dry state take 8 days. The Rossby wave with K=3 initiates from various locations in the range of 25-45E showing propagation that takes from 2 to 4 days to arrive in Vietnam. For the southern pathway, the sources are the same as for the climatological basic state.

These results are in accord with the nudging experiments for NVN-Dry precursors that show relatively good agreement with the observed composite. Ray tracing illustrates the northern pathway of propagation induced by the nudging field that can reach the Vietnam region. The nudging field covers the location of Rossby wave source K=2 which includes the dipole precursors over Eurasia.

The stationary Rossby wave number for 250mb zonal wind associated with CVN-Wet and Dry states are presented in Fig 3.23. The negative Ks value covers tropical zones and some places over the extratropics. Regions of negative Ks over the Eastern Pacific in CVN-Dry are smaller compared to those of CVN-Wet that have a large longitudinal extension. Both CVN-Wet and dry show Ks negative over Turkey and north Japan.

Extratropical Rossby wave sources over the Northern Hemisphere with three different total wave numbers that can influence the Vietnam region are traced in Fig3.23. Two states associated with opposite events over CVN show a slight difference in the location of Rossby wave sources. Rossby waves with K=1 have a source located 50N-55E and propagate to Vietnam following the northern pathway after 12 days for the CVN-Wet state. For the CVN-Dry state, the same wave number Rossby wave initiated from 50N-45E takes about 13 days to arrive in Vietnam. The Rossby wave K=2 sources take about 7 days to propagate to the

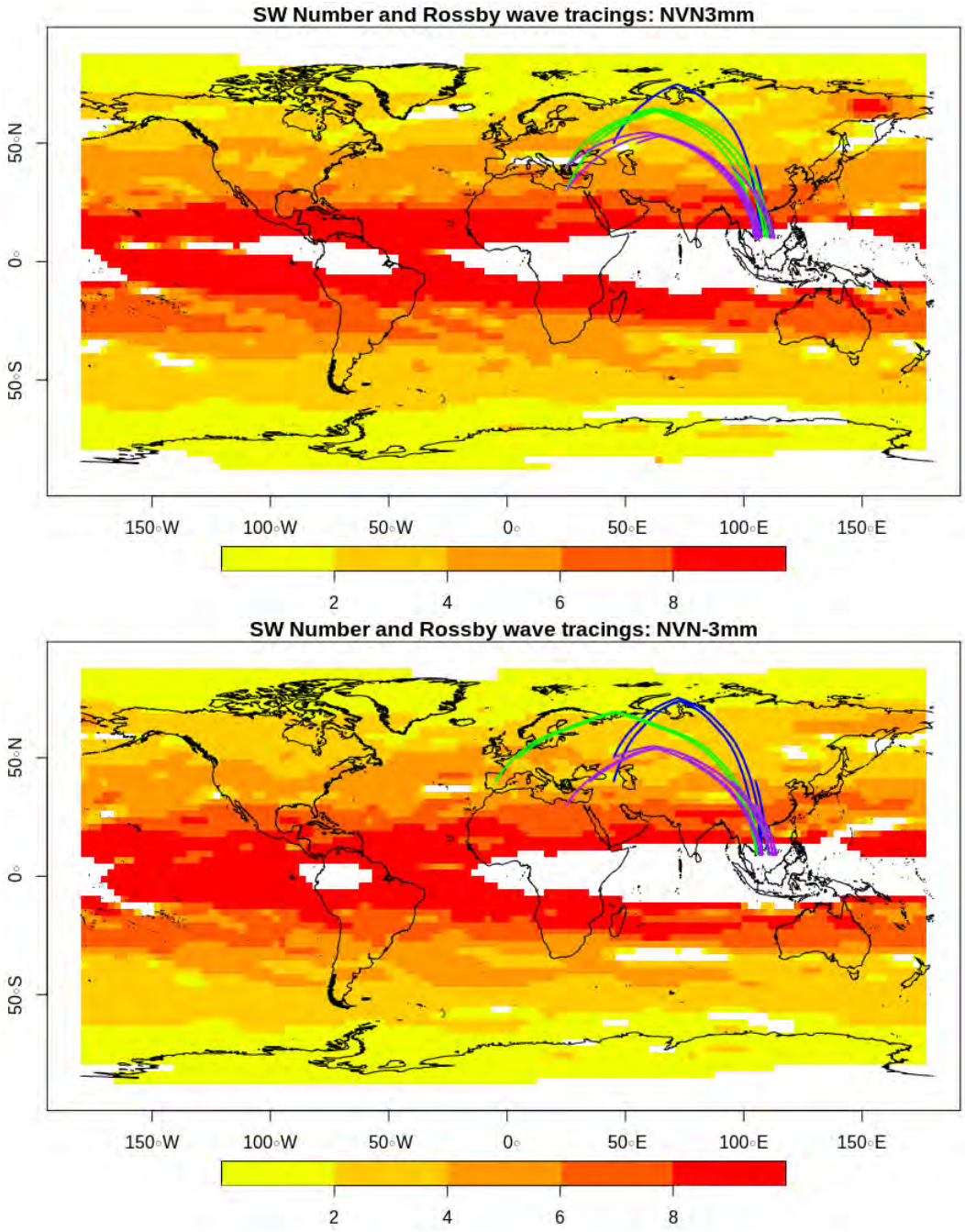

Figure 3.22: as Fig 3.18 but for NVN-Wet (a) and Dry (b) events.

Vietnam region in both CVN-Wet (initiated at 30-40N 15E) and dry (30N-5E). The wave number K=3 ray tracks are relatively similar in CVN events. The sources directly giving an impact on Vietnam following the southern pathway resemble those in the climatological basic state.

Fig 3.24 shows the 250mb stationary wave number Ks for the composite associated with

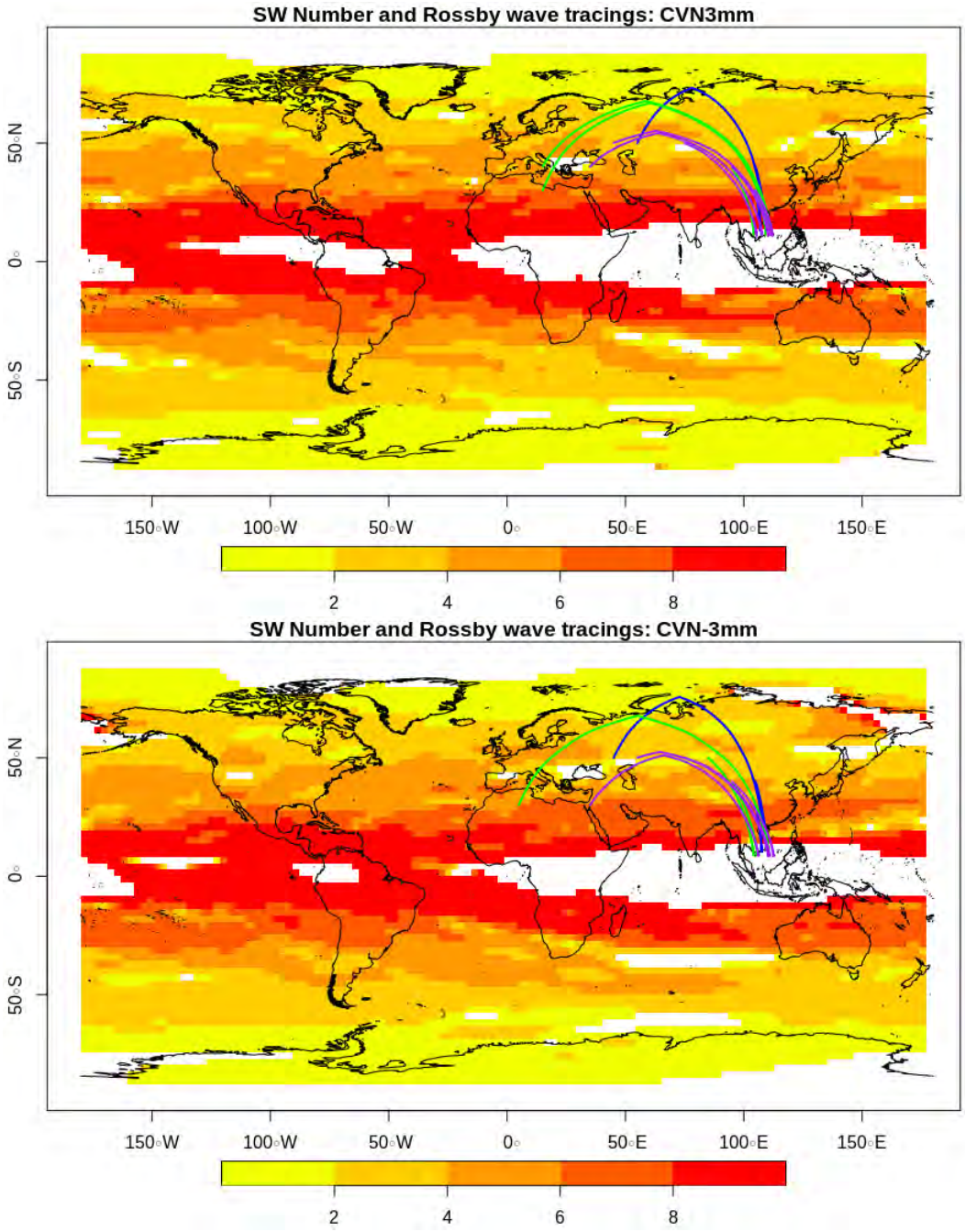

Figure 3.23: as Fig 3.18 but for CVN-Wet (a) and Dry (b) events.

South Vietnam - SVN-Wet (a) and Dry (b) events. The Ks map shows more negative areas over Extratropics compared to the climatological state, especially at high latitudes over Eastern Asia.

Rossby wave propagation with different wave numbers is plotted in Fig 3.24 for the states associated with the opposite events over SVN. There is no recorded propagation of Rossby

wave K=1 from the northern extratropics to Vietnam regions. On the SVN-Wet state, the Rossby wave with K=2 propagates from initiation at 30N-15E and takes 8.5 days to arrive in Vietnam, while from 50N-15E it takes 7 days. The wave number K=3 wave exhibits two sources, 30N-45E, and 40N-25E, that take 4 days to propagate to the Vietnam region. In the SVN-Dry state, ray tracing from extratropical locations for Rossby wave number K=2 is initiated at 30-50N 15-15E and is slightly different from SVN-Wet in that it takes 7 days to reach Vietnam. The distance between sources is large due to the presence of negative Ks. The Rossby wave with wave number K=3 shows propagation from an initial point different from SVN-Wet. The source is at 30N-35E and the wave takes 4 days while from 40-55E it takes 3 days to arrive in Vietnam.

3.5 Chapter's conclusion

In this chapter, the spectral global model DREAM in stationary wave configuration and the theoretical analysis of Rossby wave -Ray tracing have been used to investigate pathways of remote influence in the Vietnam region. A set of 648 experiments with heat sources that act as an artificial wave source with different locations has been conducted on fixed basic states to find the best place to influence the Vietnam subregion circulation. In a range of 2 weeks, pure-dynamical model responses to 2-day sources are examined via influence maps with two separate target regions: North Vietnam - NVN and South Vietnam- SVN.

Tropical heat sources have an influence on both NVN and SVN within 9 days. However, there is no extratropical source found that can influence SVN. Extratropical heat sources over Europe can influence only the NVN circulation after 12 days, then the responses are reinforced in the following 3 days. The European region is suggested as an important site of precursors to NVN events which can trigger upstream influence on the circulation over Vietnam. Extratropical wavetrains and Kelvin waves are suggested from influence maps, and they resemble some of the teleconnections between Vietnam's subregion circulation and remote influence sources.

The European region is further investigated with the nudging technique on different basic states to simulate the precursors associated with opposite events over NVN. Precursors derived from a composite of 15-day lagged of NVN-Wet and dry events are applied to the climatological basic state, and the model response exhibits two different pathways of influence. NVN-Wet precursors propagate at high latitudes and then develop southeastwards. NVN-Dry precursors develop downstream along the Asian jet. The model response after 15 days of running is quite similar to the observed composite at day 0 in NVN-Dry, but not for NVN-Wet. These precursors are also imposed on six monthly-mean basic states from May to October. The results show the model response is very dependent on the basic state jet. It suggests that Asian jets play an important role as a wave guide.

The application of ray tracing on the climatological basic state as well as other states associated with regional events reveals two pathways of theoretical Rossby wave propagation that are also in accordance with the observed composite and the nudging experiments. By

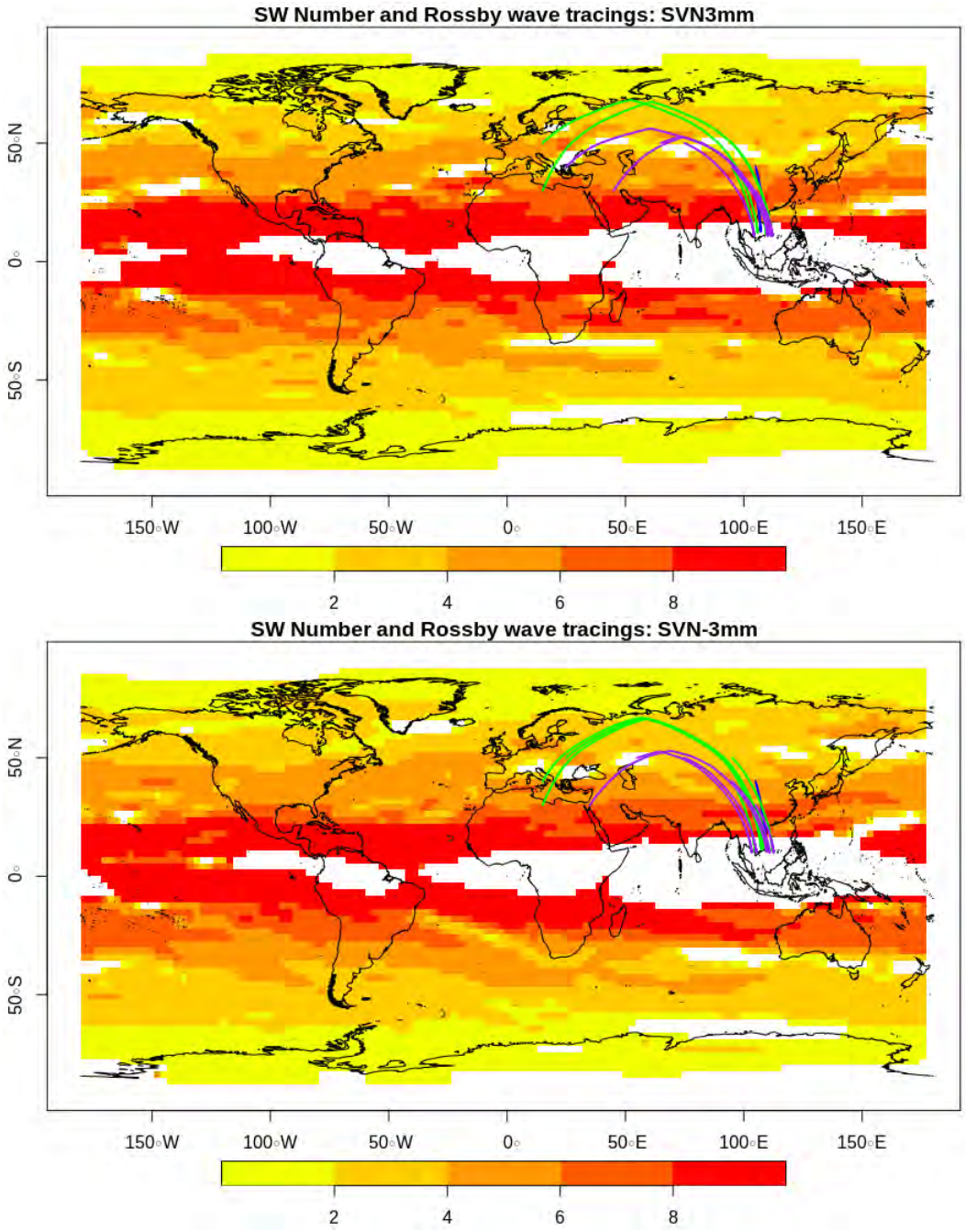

Figure 3.24: as Fig 3.18 but for SVN-Wet (a) and Dry (b) events.

testing all the sources over the northern extratropics that can influence the Vietnam region, the ray tracing calculation confirms two distinct pathways of Rossby wave propagation that can arrive in the Vietnam region. The northern pathway includes a trajectory from extratropical sources located in Europe -Eastern Asia. It is directed northeastward to the pole, then reflects at the high latitudes that then continue towards the Vietnam region. This takes about two weeks with wave number K=1, one week with K=2, and three to four days with

K=3. A Rossby wave also originates from the Mongolia region that propagates directly to Vietnam within about 1-2 days. The propagation of the Mongolian sources seems not to be sensitive to the basic state. However, sources in Eurasia are sensitive to the basic state. Particularly, wave number K=1 is not active in SVN events. Wave number K=2 is very sensitive to the basic states associated with NVN-Wet and dry events, with a change in the initiation point of 20 degrees of longitude. The propagation of wave number K=3 differs between NVN and SVN events. The K456 with a smaller scale, that propagate much faster following the jet pathway from mid-latitudes with only two-three days.

Chapter 4

Preliminary work: Regional model - RegCM4

Contents

4.1 Introduction

Global Climate Models -GCMs have frequently been used to estimate large-scale climate. However, it is difficult for GCMs to reflect the effectiveness of local to regional scale forcings, including complex topography and land-surface characteristics, because of the limitations of low-resolution climatic data Eden et al. (2014). Additionally, GCMs provide limited in-depth information on the atmospheric processes at small scales connected to land-surface dynamics, cumulus convection, and cloud radiative forcing Luca et al. (2011). To address these limitations, Regional climate models -RCMs have been used as a dynamical downscaling approach since the late 1980s Dickinson et al. (1989); Giorgi and Bates (1989). In general, RCMs were designed to address smaller-scale atmospheric phenomena that were entangled with large-scale forcings. This approach offers a more detailed representation of small-scale processes such as convective precipitation and the increased accuracy in capturing stationary elements like topography and coastlines, leading to more precise climatic data, eg., Inatsu and Kimoto (2009); Lorenz and Jacob (2005).

That is in fact that RCMs are driven by GCMs or reanalysis datasets as indispensable inputs with initial conditions (ICs), lateral (LBCs) typically wind components, temperature, water vapor, and surface pressure. The models' prognostic equations across a lateral border area, or buffer zone, employ relaxation techniques (Davies and Turner, 1977) Thus, each prognostic equation is basically given a relaxation term that pushes the model solution in the buffer region toward the enforced LBC, e.g., Marbaix et al. (2003)). As summarized in Giorgi (2019), most of the studies used the standard relaxation technique in Davies and Turner (1977)

The RCM receives input from the GCM on large-scale driving conditions, but not the other way around, which is why this downscaling method is sometimes referred to as one-way nesting. In the second generation of regional climate model RegCM2, Giorgi et al. (1993) indicated that, depending on the size of the domain and season, equilibrium might be reached after a spin-up period of the order of 5–10 days. Giorgi et al. (1993) indicate that the nested RCM typically inherits large-scale defects in the boundary forcing fields. The nested RCM offers accurate sub-GCM grid-scale information. However, Laprise et al. (2008) argues that the large domains might have less boundary forcing effects. in which, the model has more free to develop its climatology and perhaps alter some large-scale structure.

Although high-resolution RCM experiments through multiple nesting can lead to grid intervals as small as 10-50 km, there are limitations firstly caused by the employed one-way nesting approach. It means that the ICs and the LBCs are just downscaled from the GCMs to RCMs, without considering regional-to-global feedback. Secondly, the nesting technique can also introduce biases into RCMs, such as those related to the domain, the LBCs downscaling procedure, and internal physics.

The utilization of RCMs is significantly impacted when the boundary force limitation is present because the systematic biases in the input boundary conditions can be propagated into the RCM domain. Thus, as the protocol simulation, the RCM is used in the perfect LBC

mode for given simulation periods, and the results are validated against the actual observed climate of the simulated years. This result enables one to detect faults mostly linked to the regional model dynamics, physics, and configuration and ultimately enhance the model performance through a customization process since the LBC comes from reanalysis data, which combines observations and models (e.g., testing different physics schemes and selecting the best performing over the given domain) (Giorgi, 2019).

A downscaling study with an appropriate configuration is considered a complemented step in this PhD work, following the two previous chapters, to investigate the impact of the large-scale forcing from LBCs on Vietnam subregional rainfall on intraseasonal timescale. Indeed, both large-scale observational analysis and global model study indicate that the remote precursors of Vietnam subregional rainfall are different from wet and dry events, as well as North and South events. Particularly, although the resemblance in the rainfall anomaly patterns between North-wet and South-dry, as well as North-dry and South-wet, are associated with the similarities in extratropical precursors, the tropical propagations are significant only in SVN events. Chapter **??** shows the results of the global model study accompanied by Rossby wave tracing in stationary waves based on only dry-dynamics core with no convection scheme for rainfall formation. An RCM with an optimal configuration forced by the same observational analysis dataset that has an experimental domain including the Vietnam region needs to be figured out.

Southeast Asia is a region including Vietnam highly vulnerable to hazards, thus it is crucial to have a comprehensive climate modeling system to assess extreme events including those related to temperature and precipitation, and climate change impacts. Recently, several multi-institutional international projects known as the Coordinated Regional Climate Downscaling Experiment (CORDEX) have been established to produce regional climate scenarios using RCMs over multiple CORDEX regions (Giorgi et al., 2012), including Southeast Asia - SEA (Tangang et al., 2020). Specifically, the downscaling experiments over the CORDEX-SEA domain were investigated in previous research within the region, providing a substantial background of the SEA climate, eg., Juneng et al. (2016); Ngo-Duc et al. (2016); Cruz et al. (2017); Tangang et al. (2020); Herrmann et al. (2020); Tibay et al. (2021); Nguyen et al. (2022). The RegCM4 version, developed by the Earth System Physics section of the Abdus Salam International Centre for Theoretical Physics (ICTP) Giorgi et al. (2012), is employed under this framework.

The RCM simulations for Southeast Asia generally reproduce rainfall climatology well. However, these simulations are highly sensitive to the representation of certain physical parameterization schemes (Juneng et al., 2016; Cruz et al., 2017). Indeed, deep convection and air-sea flux parameterization are considered crucial in modeling the regional climate over this region, given the extensive ocean coverage within the CORDEX-SEA domain and the convective nature of the region's rainfall processes.

With various options for physical parameterization schemes available, the sensitivity tests by Juneng et al. (2016) showed the optimal combination of parameterization for simulating rainfall over Southeast Asia. In Juneng et al. (2016), the performance of the RegCM4 model in simulating rainfall over Southeast Asia was evaluated for different combinations of

deep-convection and airsea flux parameterization schemes. They introduced a comprehensive scoring system to rank the individual experiments based on their ability to simulate various aspects of rainfall criteria. The ranking was based on the following factors: (1) spatial root mean square error (RMSE), (2) spatial correlation coefficient, (3) the amplitude of the annual cycles over 20 sub-regions, (4) the variation of the annual cycles over 20 sub-regions 4.1, (5) the strength of interannual variability as measured by the coefficient of variation and (6) the actual year-to-year variability in terms of time-series correlation coefficients between simulated and observed annual rainfall; that compared with the different observational gridded data products.

Juneng et al. (2016) claimed that simulations using the MIT (Emanuel and Živković-Rothman, 1999) scheme performs better in reproducing the patterns of seasonal rainfall in 20 subregions, as shown in Fig. 4.1 below. They found that air-sea flux schemes had a minimal impact on the simulations. In comparison to observed data, all simulations revealed more inter-annual variation in rainfall patterns. Additionally, all simulations produced an exaggerated amount of rainfall over the mainland of Southeast Asia. The authors attribute this to the absence of summer airsea interactions in the model, which might result in positive rainfall anomalies.

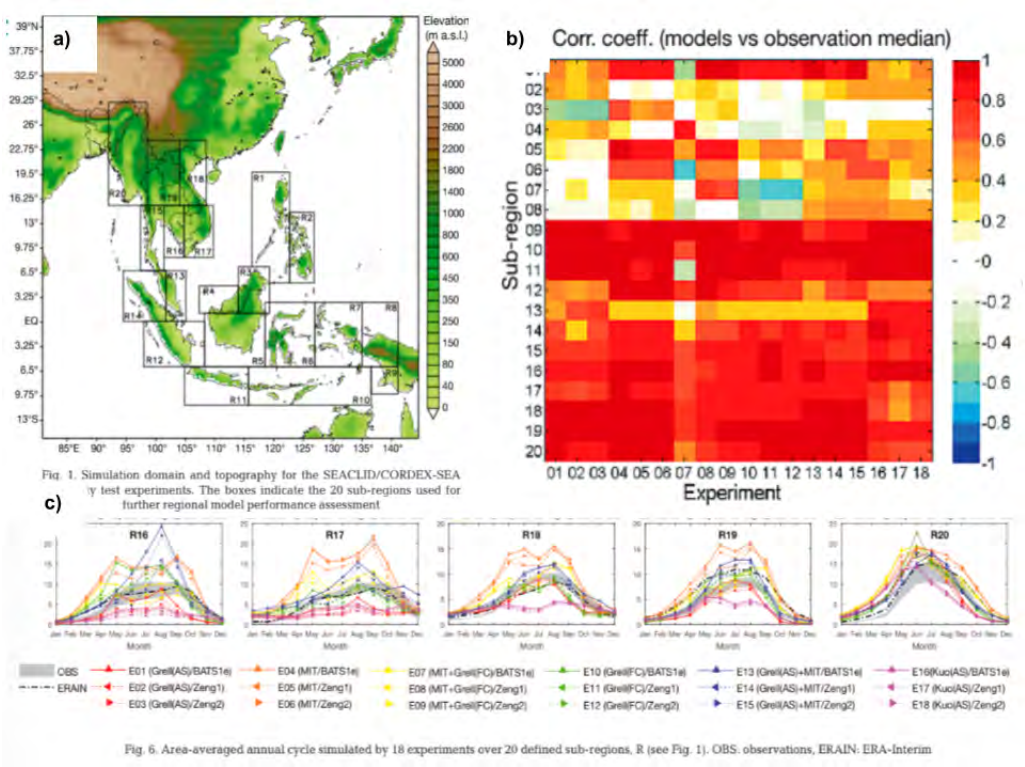

Fig. 1. Simulation domain and topography for the SEACLID/CORDEX-SEA ...y test experiments. The boxes indicate the 20 sub-regions used for further regional model performance assessment

Fig. 6. Area-averaged annual cycle simulated by 18 experiments over 20 defined sub-regions, R (see Fig. 1). OBS: observations, ERAIN: ERA-Interim

Figure 4.1: a) The Southeast Asia domain; b) correlation coefficient between simulated rainfall in the model experiments and the observation median; c) observed, reanalysis and model simulation annual cycle of rainfall over the subregions 16–20 as defined in Juneng et al. (2016) and shown in (a).

Figure 4.1, adapted from Juneng et al. (2016), depicts the annual rainfall cycle in Vietnam, reproduced by different combinations of convection and air-sea flux schemes. Vietnam's mainland and surrounding area are covered by the subregions R16–19. Specifically, R18 mostly represents North-Central Vietnam, and R17 represents Central Highland and South Vietnam. It can be seen that the annual cycle over the Vietnam subregions demonstrates a strong positive correlation coefficient in most of the experiments, with low root mean square error.

Ngo-Duc et al. (2016) used the same simulation as Juneng et al. (2016) and conducted an analysis of 12 extreme indices for rainfall and temperature at 52 meteorological stations in the SEA region. The authors focused on the rainfall indices of Rx1day (maximum 1-day precipitation) and RX5day (maximum consecutive 5-day precipitation), as well as R10mm (number of days with rainfall greater than 10 mm), and R20mm (number of days with rainfall greater than 20 mm) to evaluate monthly and yearly biases in the model output.

Using the omega statistical index (Ω) to measure the degree of similarity between different members of an ensemble in both phase and shape, the authors found the low similarity patterns of Rx1day and Rx5day over the Vietnam regions, implying the dominant role of convective rainfall; the near-equatorial region was highly sensitive to the cumulus parameterization schemes. The study emphasized that RegCM4 overestimated the number of rainy days with a low threshold (R10mm) but underestimated the number of rainy days with a higher threshold (R20mm). The model underestimated Rx1day and Rx5day.

Ngo-Duc et al. (2016) also indicated that the frequency distribution of the 18 experiments' means is matched to that of ERAi via the probability density function of precipitation from observation and model output over the 52 stations in the SEA region. The experiments (Exp04, Exp05, and Exp06) using the MIT-Emanuel scheme showed significant improvements in high-intensity rainfall events, especially for the events with rainfall greater than 20 mm day1 (Figure 4.2). While the rainfall frequency distribution was well captured by the simulation using the MIT scheme, the investigation for Vietnam rainfall variation less than the seasonal timescale has not been done yet. As similar work done over Europe in Giorgi et al. (2004), Ngo-Duc et al. (2016) suggested that the variability of rainfall over Southeast Asia may be attributed to boundary conditions.

To this end, we will use the RegCM4 model forced by ERAi with optimal configuration over the Southeast Asia domain following the previous fine-tuning studies Juneng et al. (2016), to consistently address the question:

- Can we attribute different subregional Wet and Dry events to Boundary Conditions which come from the large scale?
- How are the moisture budget terms associated with the ISV of Vietnam rainfall?

In this chapter, the regional daily indexes gathering reanalysis observed composites in chapter **??** are used again to gather the composite from RegCM output. The next subsection, Model and Methods, will present the model description of RegCM4 forced by ERAi over the

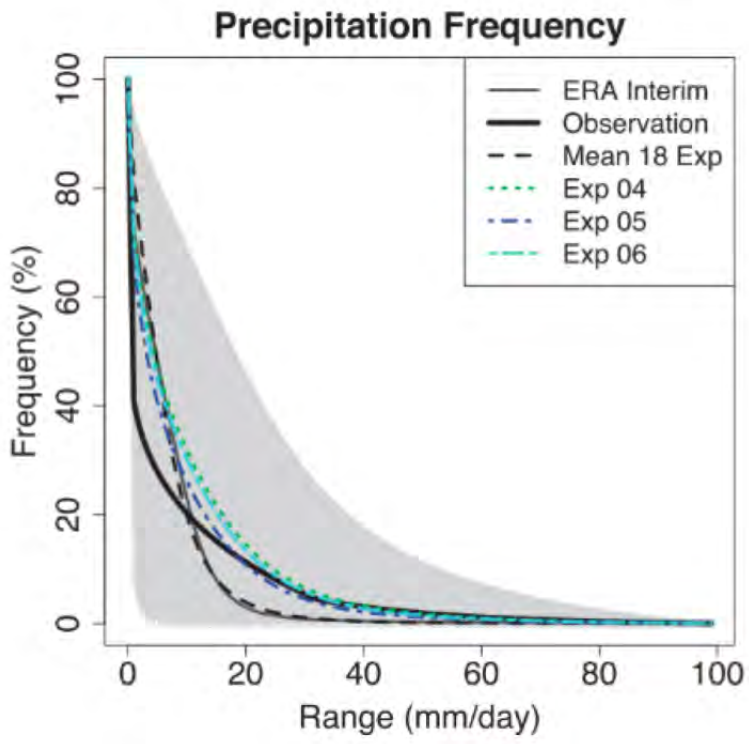

Figure 4.2: Taken from Ngo-Duc et al. (2016): Probability density function of precipitation from observation and model outputs over 52 stations in the Southeast Asia region. Range of values from the 18 experiments is shaded in gray.

Southeast Asia domain and the composite technique. It includes a comparison between the rainfall annual cycle produced by the RegCM4 model and the reanalysis data forcing. In the Results subsection, we will present some statistics of the RegCM output concerning the intraseasonal variation. Composite of all hydrologic budget terms, including rainfall, vertically integrated moisture flux convergence - VIMC, the tendency of vertically integrated moisture column -TIMC, and Evaporation -EVP, associated with subregional events in Vietnam will be explored thereafter. A summary of the chapter's findings will be finally presented.

4.2 Model and Methods

4.2.1 RegCM4 - Model description

The model has significantly evolved except for dynamic core-hydrostatic since the release of RegCM3 Pal et al. (2007). In terms of both software code and physics representations, the fourth version of the model RegCM4.0, was created and released by the ICTP in June 2010 as a prototype version and in April 2011 as the first complete version - RegCM4.1. This version is highlighted by various physics options available listed in Fig 4.3. In this study,

we use RegCM4.3 with a single configuration and would like to describe shortly the options used. The model description provided herein includes basic references for RegCM4 as shown in Giorgi et al. (2012).

Model aspects	Available options
Dynamics	• Hydrostatic, σ-vertical coordinate (Giorgi et al. 1993a)
Radiative transfer	• Modified CCM3 (Kiehl et al. 1996)
PBL	• Modified Holtslag (Holtslag et al. 1990)
	• UW-PBL (Bretherton et al. 2004)
Cumulus convection	• Simplified Kuo (Anthes et al. 1987)
	• Grell (Grell 1993)
	• MIT (Emanuel & Zivkovic-Rothman 1999)
	• Tiedtke (Tiedtke 1989)
Resolved scale precipitation	• SUBEX (Pal et al. 2000)
Land surface	• BATS (Dickinson et al. 1993)
	• Sub-grid BATS (Giorgi et al. 2003)
	• CLM (Steiner et al. 2009)
Ocean fluxes	• BATS (Dickinson et al. 1993)
	• Zeng (Zeng et al. 1998)
	• Diurnal sea surface temperature (Zeng & Beljaars 2005)
Interactive aerosols	• Organic and black carbon, SO_4 (Solmon et al. 2006)
	• Dust (Zakey et al. 2006)
	• Sea salt (Zakey et al. 2008)
Interactive lake	• 1D diffusion/convection (Hostetler et al. 1993)
Tropical band	• Coppola et al. (2012, this Special)
Coupled ocean (not in public version)	• MIT (Artale et al. 2010)
	• ROMS (Ratnam et al. 2009)

Figure 4.3: Taken from Giorgi et al. (2012): Model options in RegCM4.

4.2.1.1 Model Dynamics

Hydrostatic model equations are based on the hydrostatic version of the fifth-generation Pennsylvania State University-National Center for Atmospheric Research (PSU-NCAR) Mesoscale Model (MM5; Grell et al. (1994)). The model uses the vertical sigma coordinate, defined in terms of pressure. Sigma is equal to 1 at the surface and has zero value on the top of the troposphere: $\sigma = \frac{p-p_t}{p_s-p_t}$ where p_s and p_t are the surface and top pressures of the model; where p_t is a constant.

The model equation are given by the following, where: $p^* = p_s - p_t$

- Horizontal momentum:

$$\frac{\partial p^* u}{\partial t} = -m^2 \left[\frac{\partial p^* uu/m}{\partial x} + \frac{\partial p^* vu/m}{\partial y}\right] - \frac{\partial p^* u\dot{\sigma}}{\partial \sigma} - mp^* \left[\frac{\sigma}{\rho}\frac{\partial p^*}{\partial x} + \frac{\partial \phi}{\partial x}\right] + p^* fv + D_u$$

$$\frac{\partial p^* v}{\partial t} = -m^2 \left[\frac{\partial p^* uv/m}{\partial x} + \frac{\partial p^* vv/m}{\partial y}\right] - \frac{\partial p^* v\dot{\sigma}}{\partial \sigma} - mp^* \left[\frac{\sigma}{\rho}\frac{\partial p^*}{\partial y} + \frac{\partial \phi}{\partial y}\right] + p^* fu + D_v$$

- Temperature:

$$\frac{\partial p^* T}{\partial t} = -m^2 \left[\frac{\partial p^* uT/m}{\partial x} + \frac{\partial p^* vT/m}{\partial y} \right] - \frac{\partial p^* T\dot{\sigma}}{\partial \sigma} + p^* \frac{\omega}{\rho c_p} + p^* \frac{\dot{Q}}{c_p} + D_T$$

  where the D terms represent the vertical and horizontal diffusion terms and vertical mixing due to the planetary boundary layer turbulence or dry convective adjustment. The heat capacity for moist air at constant pressure is given by $c_p = c_{pd}(1 + 0.8q_v)$, where q_v is the mixing ratio for water vapor and c_{pd} is the heat capacity for dry air.

- Surface pressure is computed from:

$$\frac{\partial p^*}{\partial t} = -m^2 \left[\frac{\partial p^* u/m}{\partial x} + \frac{\partial p^* v/m}{\partial y} \right] - \frac{\partial p^* \dot{\sigma}}{\partial \sigma} \tag{4.1}$$

  which is used in its vertically integrated form:

$$\frac{\partial p^*}{\partial t} = -m^2 \int_0^1 \left[\frac{\partial p^* u/m}{\partial x} + \frac{\partial p^* v/m}{\partial y} \right] d\sigma$$

  Then the vertical velocity in sigma-coordinates,$\dot{\sigma}$, is computed from by vertical integration:

$$\dot{\sigma} = -\frac{1}{p^*} \int_0^\sigma \left[\frac{\partial p^*}{\partial t} + m^2 \left(\frac{\partial p^* u/m}{\partial x} + \frac{\partial p^* v/m}{\partial y} \right) \right] d\sigma'$$

  where σ' is a dummy variable of integration and $\dot{\sigma}(\sigma = 0) = 0$.

  The vertical motion: $\omega = p^* \dot{\sigma} + \sigma \frac{dp^*}{dt}$

  with $\frac{dp^*}{dt} = \frac{\partial p^*}{\partial t} + m \left[u \frac{\partial p^*}{\partial x} + v \frac{\partial p^*}{\partial y} \right]$

The hydrostatic equation is used to compute the geopotential heights from the virtual temperature T_v:

$\frac{\partial \phi}{\partial ln(\sigma + p_t/p^*)} = -RT_v \left[1 + \frac{q_c + q_r}{1+q_v} \right]^{-1}$

where T_v is given by$T_v = T(1 + 0.608q_v)$, and q_c and q_r are the mixing ratios of cloud water and rainwater.

The 2 fastest gravity modes are isolated from the model solution first, and then integration with smaller time steps is performed using a time-splitting explicit integration approach. This enables the remainder of the model to use a larger time step.

4.2.1.2 Model Physics

The table below summarizes the model options available in RegCM4. Besides the hydrostatic dynamics core and numerous parameterizations, we would like to highlight here the most

important schemes that have been modified/ added or tested in this RCM version to successfully simulate regional climate. These schemes include radiative transfer, planetary boundary layer, cumulus convection, resolved scale precipitation and air-sea flux exchange.

- Radiative transfer

  Radiative transfer is a fundamental energy process taking place in the Earth-atmosphere system that involves the transfer of energy between the Earth and the Sun, between the atmosphere and the underlying surface, between different layers of the atmosphere, as well as between different components in the atmosphere such as greenhouse gasses.

  The radiative transfer methodology of the global model CCM3 (Kiehl et al., 1998) with modifications made by Giorgi et al. (2012), is used to calculate radiative transfer in RegCM4. This covers calculations for both atmospheric gasses and aerosols as well as the short-wave and infrared portions of the spectrum. The scheme accounts for contributions from major greenhouse gasses, including H2O, CO2, O3, CH4, N2O, and CFCs. The scheme also accounts for solar radiative processes Briegleb (1992). and the scattering and absorption of solar light by aerosols, based on their optical characteristics, including absorption coefficient and single scattering albedo.

- Cumulus convection

  As presented in Giorgi et al. (2012), there are multiple options for representing cumulus convection in RegCM4. In RegCM4.3, three cumulus schemes are available, namely Kuo-type (Anthes, 1977), Grell (Grell, 1993) and MIT (Emanuel, 1991; Emanuel and Živković-Rothman, 1999), with two additional combinations of schemes.

  The Kuo-type scheme (Anthes, 1977) is considered as the simplest which activates convection when the column moisture convergence exceeds a threshold value. The Grell scheme (Grell, 1993) is a mass flux deep convection parameterization in which clouds are seen as two steady state circulations, including an updraft and a penetrative downdraft. When a package lifted in an updraft ultimately reaches the moist convection level, the scheme is activated. The MIT scheme is the most complex of the three (Emanuel, 1991), assuming that cloud mixing is episodic and inhomogeneous. According to Emanuel and Živković-Rothman (1999), convection begins when neutral buoyancy reaches a level above the cloud base and is governed by an updraft and downdraft model at the sub-cloud scale.

  There are various factors in both the Grell and MIT schemes that may be used to enhance the model's performance under different climatic conditions. As mentioned in Giorgi et al. (2012), the Grell and MIT schemes are now the most popular, but their performance varies with geographic locations, particularly over land versus ocean areas. The MIT scheme has a tendency to create excessive precipitation across geographical regions via the occurrence of extremely powerful individual precipitation events. On the other hand, the Grell scheme frequently results in weak precipitation over tropical oceans. Giorgi et al. (2012) advise using a hybrid convection technique. Over Southeast Asia, as depicted in the introduction of this chapter, the MIT scheme is considered

as the most effective scheme to reproduce rainfall according to the rankings in Juneng et al. (2016) and Ngo-Duc et al. (2016).

- Resolve scale precipitation

  The scheme is essentially based on the SUBEX parameterization of Pal et al. (2000) and includes a prognostic equation for cloud water. In the cloudy portion, cloud water is converted into precipitation using an autoconversion and an accretion term in a bulk formulation of the Kessler type. Based on the local relative humidity and an evaporation rate coefficient, the

- Air - Ocean exchanges

  Two options for airsea flux schemes, BATS (Dickinson et al.) and Zeng (Zeng et al., 1998), are introduced and investigated for their sensitivity in controlling the oceanatmosphere turbulent exchanges of heat, momentum and moisture in Giorgi et al. (2012). The BATS1e scheme uses a constant roughness length of 2×104 m, whereas the roughness lengths for both Zeng schemes are dependent on friction velocity. As reported in Giorgi et al. (2012), the Zeng scheme improves the excessive evaporation over warm tropical oceans found in the BATS option.

- Planetary boundary layer

  For the planetary boundary layer (PBL) processes, in this study, RegCM4 uses that of Holtslag et al. (1990) with modifications. In the Holtslag scheme, a PBL height is first diagnostically calculated based on an iteration procedure employing a bulk critical Richardson number formulation. Then a non-local vertical profile of eddy diffusivity for heat, moisture, and momentum is specified from the surface to the PBL height, and a countergradient transport term is added for temperature and moisture. The eddy diffusivity depends on the friction velocity, height, Monin-Obhukov length, and PBL height. It is worth noting that Giorgi et al. (2012) stated that this scheme tends to produce relatively strong, and often excessive, turbulent vertical transfer.

- ICs anf BCs

  Practically, RegCM4 calls for the lateral boundary conditions (LBCs) for the meteorological initial and time-dependent wind, temperature, water vapor, and surface pressure components. These can be acquired by running GCMs or reanalyzing observational data. The influence of the initial conditions cannot be sustained over a long time, making the LBCs crucial in determining the area climate. The observational reanalysis data is considered as perfect LBCs for RegCM as it is corrected and balanced by forecast models and data assimilation to be consistent data.

  Following the Userguide of RegCM4.2, the LBCs are added in the RegCM through the relaxation/diffusion technique. It consists of: 1. selecting a lateral buffer zone of n grid point (nspgx in model seting) 2. interpolating the driving large-scale fields onto the model grid 3. applying the relaxation +diffusion term:

$$\frac{\partial \alpha}{\partial t} = F(n)F_1 * (\alpha_{LBC} - \alpha_{mod}) - F(n)F_2 * \Delta_2(\alpha_{LBC} - \alpha_{mod})$$

where α is a prognostic variable (wind components, temperature, water vapor, surface pressure). The first term on the right-hand-side is a Newtonian relaxation term which brings the model solution (mod) towards the LBC field (LBC) and the second term diffuses the differences between the model solution and LBC. F(n) is an exponential function given by: $F(n) = exp\left(\frac{-(n-1)}{anudge(k)}\right)$

Where n is the grid point distance from the boundary (varying from 1 to $nspgx$): n1 is the outermost grid point,$n = 2$ the adjacent one etc. The anudge array determines the strength of the LBC forcing and depends on the model level k. In practice,$F(n)$ is equal to 1 at the outermost grid point row and decreases exponentially to 0 at the internal edge of the buffer zone ($nspgd$) at a rate determined by *anudge*. Larger buffer zones and larger values of *anudge* will yield a greater forcing by the LBC.

In the model *anudge* has three increasing values from the lower, to the mid and higher troposphere. For example for $nspgx = 10$ we use *anudge* equals to 1, 2,3 for the lower, mid and upper troposphere, respectively. This allows a stronger forcing in the upper troposphere to insure a greater consistency of large scale circulations with the forcing LBC while allowing more freedom to the model in the lower troposphere where local high resolution forcings (e.g. complex topography) are more important. As a rule of thumb, the choice of the maximum anudge value should follow the conditions: $\frac{nspgx-1}{anudge(k)} \geq 3$

4.2.1.3 Model Configuration

In this study, the model configuration was already set up and run as in the Exp05 experiment presented in the studies of Juneng et al. (2016); Ngo-Duc et al. (2016). The Exp05 experiment is picked up to investigate the question that we have introduced earlier in this chapter. Detailed information for the model configuration and running is presented in the Table below:

The model domain covers Southeast Asia with a domain size of 256*194 points in longitude* latitude, centered at 6.5N,118E. Fig 4.4 shows the domain including the buffer zone and the inner domain. The grid size is 25km. The simulation runs from 01-01-1979 to 31-12-2008. The radiation is recalculated every 30 minutes and the outputs are saved at 6-hour intervals.

In addition, it is worth noting that sea surface temperatures (SST) are prescribed every 6 hours using temporally interpolated weekly or monthly SST products from default inputs in RegCM. However, actual SSTs can differ significantly from these mean temperatures. Thus, to improve the calculation of diurnal fluxes over the ocean, the prognostic SST scheme described by Zeng and Beljaars (2005) was implemented in RegCM4 and switched on for this study. The scheme is based on a 2-layer, 1-dimensional heat transfer model, with the top layer representing the upper few millimeters of the ocean, which is cooled by net longwave radiation loss and surface fluxes. The bottom layer, 3 m thick, is warmed by solar radiation and exchanges heat with the top layer. This diurnal SST scheme appears to provide significant, although not major, effects on the model climatology, mostly over tropical oceans (Zeng and Beljaars, 2005).

The atmospheric initial condition is taken from the ERAi reanalysis - the same data used

Domain Configuration	
Grid points long*lat	256*194 points
Grid size	25 km
Vertical layers	18
Timestep	60 seconds
Radiation re-calculation	30 mins
Frequency of Atmospheric output	6 hours
Period of study	01-01-1979 to 31-12-2008
Large scale forcing	ERA-Interim 01-01-1979 to 31-12-2008
Physical Parameterizations	
Cumulus convection scheme	MIT Emanuel (1991)
Ocean flux scheme	Zeng1
Simulate diunal sst cycle	yes
Boundary Parameterizations	
Buffer zone nspgx	12 points
Nudge value high range	3
Nudge value medium range	2
Nudge value low range	1
Relaxation boundary conditions	exponential method

Table 4.1: Information for RegCM configuration.

in the observed composite analysis in chapter **??**. ERAi, the global atmospheric reanalysis produced by the European Centre for Medium-Range Weather Forecasts (ECMWF), is widely used as the perfect LBCs in RCM simulations. This data has a large coverage period. Dee et al. (2011) described the forecasting model, data assimilation method, and input datasets used to create ERAi, They also discussed the performance of the system, including improvements in the representation of the hydrological cycle, the accuracy of the stratospheric circulation, and the consistency of the reanalyzed fields over time. RCM simulations were also performed using various GCMs such as CNRM-CM5, HadGEM2, GFDL, etc. (Tangang et al., 2020). These GCMs participated in the Coupled Model Intercomparison Project Phase 5 (CMIP5) (Taylor et al., 2012).

4.2.2 Rainfall Annual Cycle

The validation for a set of experiments in the same configuration including our study experiment has been extensively evaluated in terms of rainfall in Juneng et al. (2016); Ngo-Duc et al. (2016). The validation, using various rainfall observational datasets, analyses of climatology, annual cycle, and interannual variations, had been made for the whole domain as well as 20 selected subregions. According to these various aspects of rainfall characteristics, this experiment demonstrates relatively good performance over the Indochina mainland.

Concerning how the RegCM model reacts with the lateral boundary conditions with a focus on Vietnam subregion rainfall, we would like to present here again the climatology of

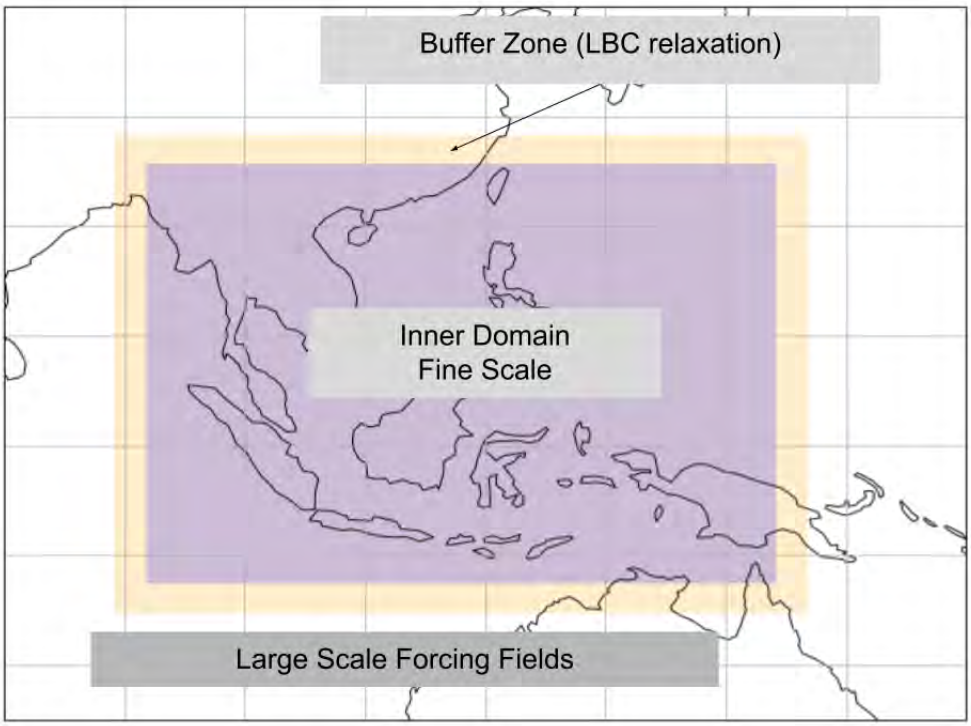

Figure 4.4: SEA Domain for RegCM4 experiment.

rainfall and circulation during the extended summer from model output and compare it with the ERAi reanalysis data.

Figure 4.5 shows the extended-summer climatological precipitation derived from the ERAi reanalysis dataset and the RegCM4 output from 1979 to 2008. The model generally produces high precipitation over land compared to the reanalysis data. In Figure 4.5b, white areas indicate rainfall greater than 20mm/day, which appears to be associated with high-elevation areas as shown in Figure 4.1a. The rainfall over land looks to be exaggerated. The model performs less well over the ocean near the equator. Rainfall seems to be suppressed over the Maritime Continent.

The summer climatology of low-level wind from ERAi and RegCM4 output are shown in Fig 4.6. The wind component is relatively well reproduced by the model over the domain. The zonal wind pattern is well simulated with the northeast low-level wind over the Bay of Bengal crossing the Indochina mainland, which is a signature of the summer monsoon during this period. However, it appears stronger than in reanalysis, as also reported in Juneng et al. (2016).

Nevertheless, the wind is clearly blocked by the model orography, especially the zonal wind. In Figure 4.6c, at the places of high elevation in Thailand, Vietnam, and New Guinea island, the low-level zonal wind can not cross and is blocked by the mountain ranges. In addition, the spatial coverage of zonal wind over the South China Sea and the eastern Indian

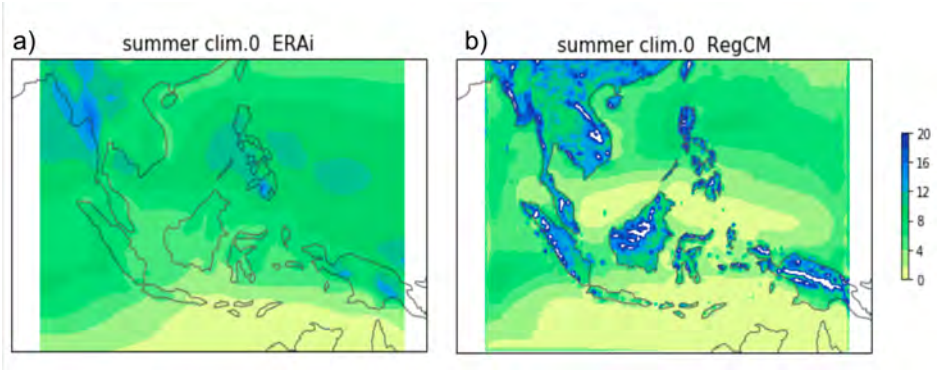

Figure 4.5: Extended- summer climatological precipitation (May-Oct) a) using reanalysis dataset ERAI and b) from RegCM4 model output 1979-2008.

Ocean is not simulated further to the east as in the reanalysis. Otherwise, the simulated meridional wind is strongly amplified on the northwestern side of the domain but not on the southern side near the Equator.

In this domain, along the Equator, it is noted that several tropical wave activities were found from the observed analysis that could be a factor influence on Vietnam rainfall intraseasonal timescale. For example, the MJO propagates from the Indian Ocean and cycles between enhanced and depressed convective phases until the Western Pacific 6 days per phase (Madden and Julian, 1972). It has prominent northeastward propagation during the summertime with a much slower speed than other tropical waves, such as Kelvin and MRG waves as discussed in the chapter **??**.

Juneng et al. (2016) investigated the correlation between the summertime rainfall time series and surface air temperature and the 850 hPa circulation, and the surface heat fluxes in the simulation compared with those of ERAi reanalysis. They indicated that mainland rainfall produced by this configuration is positively and strongly associated with the surface temperature over the South China Sea and the eastern Indian Ocean, while ERAi has less negative correlations over these regions. Juneng et al. (2016) suggest that is attributed to the lack of air-sea coupling in the model, especially over the western Pacific.

* Summer precipitation over subregions

Over Vietnam's subregion, figure 4.7 shows the monthly climatology of the rainfall from May to October taken from RegCM4 output and ERA-Interim. The consideration of Vietnam subregions is slightly different from Juneng et al. (2016) - shown in fig 4.1a. We make the consistency in the choice of subregion as in chapter 2 for the comparison.

For NVN and CVN, the monthly averages of rainfall reproduced by the model and ERAi have the same monthly peaks in August and September, respectively. Both rainfalls over CVN and NVN show much higher intensity in RegCM4 than in the reanalysis data, except for October. For SVN, although the intensity of monthly rainfall between the regional model and reanalysis data has not much difference, the peak of summer climatology of rainfall is not

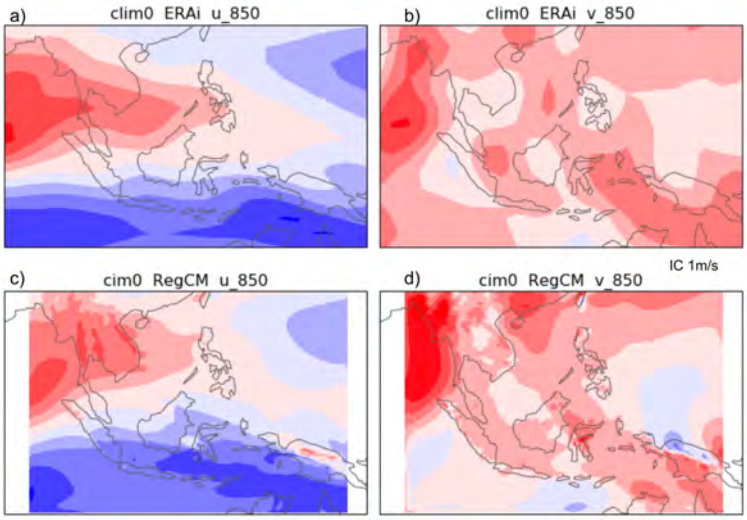

Figure 4.6: Extended- summer climatological wind components u and v (May-Oct) using reanalysis dataset ERAi: a) and b); and from RegCM4 model output: c) and d).

reproduced. The temporal correlation between regional daily rainfall time series reproduced by the model and ERAi shows a positive correlation coefficient: 0,40 for NVN, 0,31 for CVN, and 0,25 for SVN.

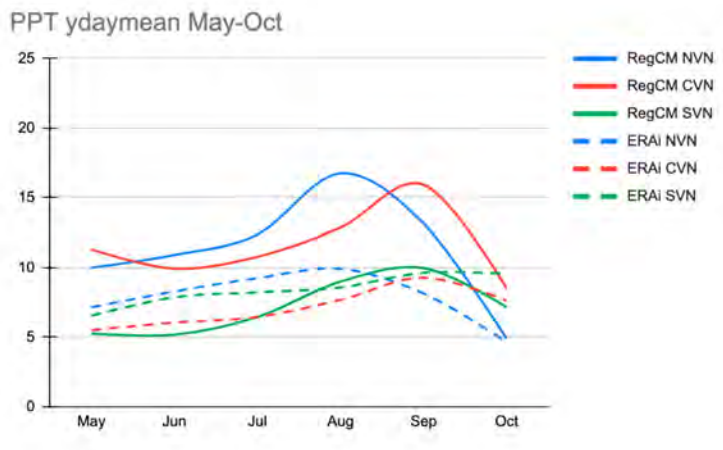

Figure 4.7: Monthly average of rainfall over three Vietnam boxes as defined in Fig1 in section (2.2.3).

Ingest ERAi as lateral boundary conditions, RegCM4 shows the reproduction of rainfall over Southeast Asia with intensity exaggerated over land, but not in the ocean under the effects of sub-grid scale forcings. It suggests the rainfall formation might be too sensitive to the area with high elevation, especially mountain ranges in Vietnam and Indonesia. Over the ocean region, the rainfall along the Equator in the range of 105-140E is not reproduced. As shown in Juneng et al. (2016) (Exp5), in this region, the latent heat flux shows a high positive correlation with the summertime rainfall time series, and the sensible heat flux is

strongly negatively correlated with summer rainfall. However, the ERAi dataset shows a low negative correlation between both latent heat flux and sensible heat flux and summer rainfall. Furthermore, the summer rainfall cycles over the SVN subregion are not reproduced where the high rainfall intensity is strongly affected by the tropical waves propagation (eg., Van Der Linden et al. (2016); van der Linden et al. (2016)). Therefore, we note here that RegCM4 might lack air-sea coupling in the model Juneng et al. (2016) that can suppress the waves propagation over Maritime Continent as a consequence.

Based on Juneng et al. (2016) study that compared various scheme combinations, we decided to use this output as a reasonable downscaling experiment to do the investigation of rainfall variability on the intraseasonal timescale in the context of the impact of large-scale lateral boundary condition on the regional scale.

4.2.3 Composite Analysis

4.2.3.1 Output processing

To analyze the intraseasonal variability of rainfall over the domain, we apply the same processes as presented in Chapter 2 for the rainfall derived from ERAi - FROGs (Roca et al. (2019)).

Besides rainfall, the different terms of moisture budget are also considered in this chapter. The vertically integrated moisture flux convergence (VIMC), and the tendency of vertically integrated moisture (TMC) are computed from the model output. Evaporation is taken directly from the atmospheric output. All the data computed and collected have a frequency of 6 hours. After the treatment to obtain those intraseasonal signals, we convert 6-hourly data into daily data for all terms analyzed in this investigation.

We apply the same processes to all daily moisture budget terms as shown in chapter **??** to make the comparison with the large-scale index used in chapter **??**. The data are processed to retain the entire ISV signal. The only filter applied is to remove synoptic timescales. The daily data are smoothed with a 10-day running mean, and a smoothed annual cycle is removed based on average by calendar date. Finally, the linear trend is removed to obtain intraseasonal and interannual variations.

4.2.3.2 Index for composite

The composite will be assembled using the regional indexes of VIMC derived from the reanalysis dataset used in Chapter 2 - hereafter, reanalysis index. This reanalysis index is used to assemble the composite from RegCM output including 4 terms in the moisture budget. The reanalysis composite gathering by reanalysis indexes including large-scale dynamics as well as moisture budget terms is reminded in this chapter as well. The analysis will focus on how the regional events communicated with the large-scale forcing.

4.3 Results

4.3.1 Statistics of Intraseasonal variation

The intraseasonal signal in Vietnam's rainfall variation is isolated and then compared with those derived from the ERAi reanalysis dataset in the aspects of temporal correlation, variance and probability distribution over three Vietnam subregions.

* Correlation

The temporal correlation between the timeseries of rainfall ISV over three subregions from model output and those derived from ERAi have been calculated. Positive correlation coefficients of 0.33, 0.33, and 0.21 are found over NVN, CVN, and SVN, respectively. Temporal was also estimated for the ISV of rainfall from RegCM and the large-scale index of rainfall ISV, which will be used for composite assembly. We also obtained positive correlation values of 0.28 and 0.32 for NVN and CVN, respectively. However, for SVN, there is no relation found between the timeseries due to the low correlation value of 0.06.

* Variance

The variance of rainfall ISV reproduced by the regional model (Fig 4.8) is much higher than those of reanalysis data over all three subregions (Fig 3 in 2.2.3 - twice times approximately. The North Vietnam box shows the highest variance throughout June - August, indicating a big difference from the monthly variance of rainfall ISV computed from ERAi. However, the Central and South Vietnam domains have a similar variance evolution during the summer. The peak of variance occurs in September.

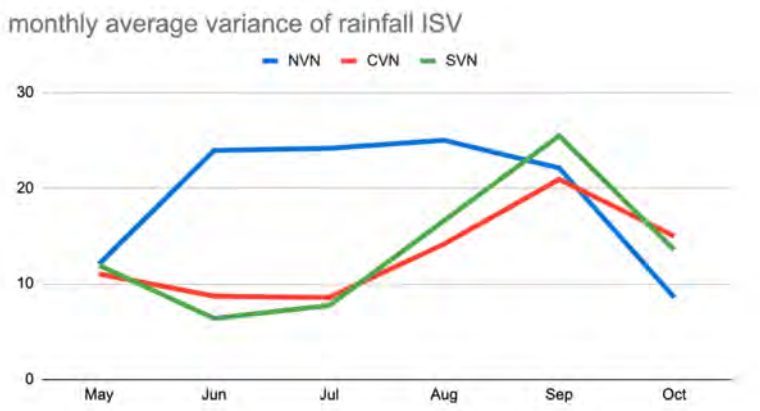

Figure 4.8: Monthly variance of rainfall ISV over NVN, CVN and SVN from RegCM4 output.m2.day-2.

* Distribution

Following the high variance of regional rainfall ISV over Vietnam, Figure 4.9 shows the probability distribution of rainfall ISV taken from RegCM forced by ERAi (Figure 4.9d-f)

over three Vietnam subregions in comparison with those of ERAi as presented in Chapter 2 (Figure 4.9a-c). Generally, the distributions have the dry branch (left side) more uprise than the wet one over all three subregions. Otherwise, the regional distribution from reanalysis shows relatively normal distribution in NVN and SVN, less in CVN. It suggests that the model configuration could be more sensitive in leading to extreme wet anomalies than dry. The rainfall anomaly events exceeding ±3 mm/day are shown according to the red lines. RegCM4 using the ERAi LBCs reproduces the intensive rainfall with much higher frequency compared to reanalysis data, especially in the NVN region.

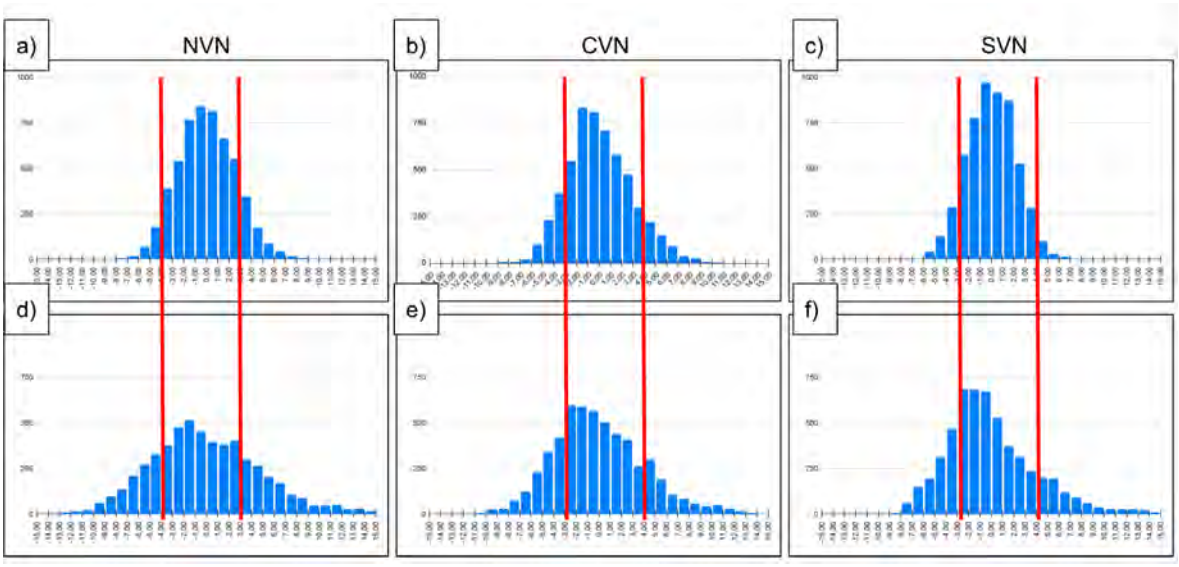

Figure 4.9: Probability distribution of rainfall ISV over three Vietnam subregions: NVN, CVN and SVN was taken from ERAi(a-c) and RegCM(d-f) output 1979-2008, respectively. Red lines indicate the threshold values of -3 and 3 mm.day-1.

4.3.2 Composite of Rainfall ISV

4.3.2.1 North Vietnam - NVN

The 2-week lag-composite of rainfall anomaly from the RegCM4 output forced by ERAi is assembled using the index derived from the reanalysis dataset in the figures below. These figures are described with a comparison with those assembled from ERAi rainfall using the same index. In addition, the composite of extratropical flow (as in chapter 2) associated with these events is recalled. We would like to indicate the model ability of rainfall reproduction and then unravel the association between the RegCM composite and its driven large-scale forcing. We present the development of lag composite followed by the comparison with the reanalysis composite of rainfall anomaly and large-scale dynamics for all regional events.

Figure 4.10.I show the composite of rainfall anomaly assembled by reanalysis index associated with NVN Wet events exceeding 3mm/day from RegCM4 forced by ERAi large-scale

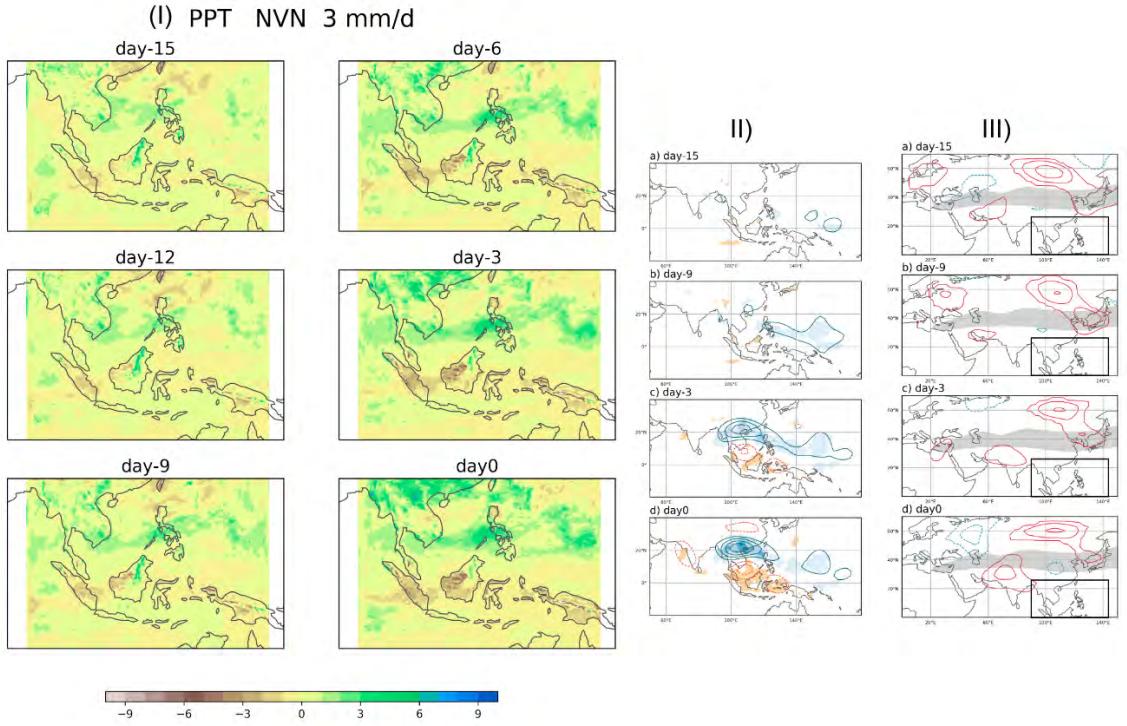

Figure 4.10: Composite of rainfall anomaly of RegCM4 output (I) and ERAi reanalysis (II) assembled by reanalysis index associated with NVN Wet events exceeding 3mm/day. The contour interval (color shaded) is 1mm/day. (III) as (II), but for geopotential height anomaly with the contour interval is 8m. The box indicated RegCM4 Southeast Asia domain that was forced by ERAi. (II) and(III) taken from chapter 2.

forcings (fig 4.10.III). The 15-day lag composites of rainfall anomaly show a significant increase over the North Vietnam region in association with North Western Pacific rainfall anomalies. Positive anomalies appear over NVN - Red River delta region since day-15 and are associated with the wet area over the South China Sea (SCS) and the North Western Pacific. These are intensified at their place until day-9. On day-6, the anomalies over the sea increase but retract to have less spatial extension over the South China Sea. On day-3, the wet area over North Vietnam and the Philippines expands quickly. At day 0, rainfall anomaly over the land on the Northern side of the domain is then intensified.

Compared to the composite of rainfall anomaly from reanalysis ERAi Figure 4.10II using the same index as Figure 4.10.I, RegCM4 configuration can reproduce well the wet pattern over NVN in association with the wet over the North Western Pacific. The large-scale dry area over Indonesia is also well reproduced. Otherwise, the RegCM lag-composite with higher resolution shows the separation of wet anomaly over North Vietnam and the northern SCS, while the southern SCS has a positive anomaly instead of a negative one in the reanalysis composite. The dipole pattern, including wet over NVN and dry over SVN, is not seen here.

The lag-composite of extratropical flow is associated with reanalysis rainfall anomaly in

Figure 4.10.II shows in Figure 4.10.III, that forces the RegCM domain to reproduce rainfall anomaly in Fig 4.10.I. The development of rainfall anomaly over North Vietnam produced by RegCM is associated with the development of the negative geopotential height anomaly over North China that gradually increases over time. As discussed in chapter 2, the large-scale forcing associated with the reanalysis of NVN wet events is typified by the low geopotential height anomaly over North China and the high over Japan. Both anomalies persist along the 2-week lag of the reanalysis composite, despite changes in intensity, which are considered as the precursors directly linked with the observed positive rainfall anomaly over NVN.

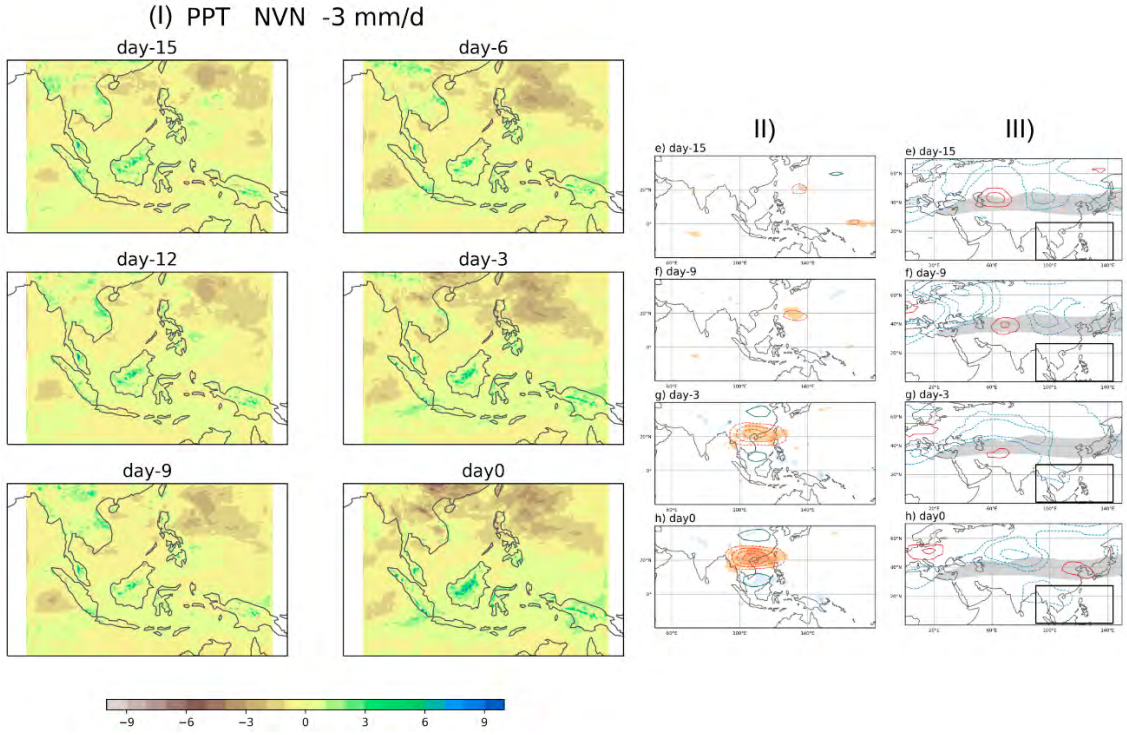

Figure 4.11: as Fig 4.10 but for NVN Dry events exceeding -3mm/day.

The composite of rainfall anomaly assembled by reanalysis index associated with NVN Dry events exceeding -3mm/day from RegCM4 forced by ERAi large-scale forcings (Fig 4.11III) is shown in Fig 44.11.I. Following the 15-day lag composites of rainfall anomaly, there is a sudden change over the North Vietnam region from slightly wet to dry areas in association with negative rainfall anomalies over the North Western Pacific. On day-15, the signal over the whole domain is not strong as in Wet events. The rainfall is slightly wet on the western side of the NVN box and in North Central Vietnam. These anomalies are strengthened until day-9 with small spatial extension. On day-6, these are decayed and replaced by negative rainfall anomalies. Finally, on day 0, NVN is covered by negative anomaly areas. Although the change in the western side of the domain, a negative area over the North Pacific at day-15 develops to the west and becomes stronger during the 2-week lag.

The quick development of negative anomaly over NVN through RegCM Fig 4.11.I composite of rainfall anomaly is similar to the one of reanalysis composite Fig 4.11.II, but with

less spatial coverage. The negative over the North Western Pacific is well reproduced. As in wet cases, the pattern of dry-wet over north-south is not seen even the positive rainfall anomaly covers Maritime Continent.

The lag-composite of RegCM4 rainfall anomaly shows a strong association with the composite of geopotential height of reanalysis extratropical flow. The model composite suggests the role of an anomaly on the northern side of the regional domain using the large-scale forcing as LBC. Indeed, the pattern of high-low-high over the northern side leads to the wet event over NVN that persists during the time of lag-composite, while the low-high-low pattern quickly developed from day-3 to day 0 which leads to the dry anomaly over NVN. In the place of the climatological Asian-Pacific Jet stream, it could suggest the role of this jet in the development of the anomalies that directly show the impact on the NVN regions. Although the mechanism is still unclear, the symmetry of rainfall over the North Western Pacific between wet and dry events over NVN is strongly associated with the symmetry of the development of Japan anomalies.

To sum up, the model is quite successful in reproducing the local wet and dry events over NVN in association with the rainfall anomaly over the northwest Pacific. We note that there is no significant tropical wave activity found in large-scale dynamics associated with NVN events shown in chapter 2. The NVN rainfall anomaly produced by RegCM shows consistent with the development of large-scale extratropical forcing. For large-scale patterns of rainfall anomaly, the dipole over North-South Vietnam symmetrically seen in the reanalysis composite is not simulated, over South Vietnam. In both NVN events, there are no significant signals over the equatorial South China Sea reproduced in the RegCM composite.

4.3.2.2 Central Vietnam - CVN

The composite of rainfall anomalies reproduced by RegCM4 assembled using large-scale dry events exceeding -3mm/day over Central Vietnam are shown in Fig 4.10I. The evolution of rainfall anomalies over CVN is strongly correlated with the development of anomalies over the Philippine Sea following the lag composites of two weeks before the wet events. On day-15, the weak signals of negative rainfall anomaly appear over the South of China and North Western Pacific and the positive one over the Gulf of Tokin. From day-16 to day-6, these anomalies over land become stronger locally, while the oceanic anomaly displays a change of the sign into a positive anomaly on day-6. The anomaly of rainfall over the ocean strongly increases from day-6 to day-3, especially over the South China Sea. At the same time, the positive rainfall anomaly is spread to cover a large area Vietnam-Thailand- Myanmar. The sign change of anomalies over Indonesia, reversely compared to the North Western Pacific one, is recorded in association with the increment of positive rainfall over CVN.

Compared to the composite of rainfall anomaly from the reanalysis dataset using the same index, it is clear that the RegCM can reproduce the rainfall anomaly patterns associated with large-scale wet events over CVN on the intraseasonal timescale. Most of the features are interesting to mention, such as the dipole pattern of rainfall anomaly on day 0 and the link

with the North Western Pacific.

Looking at the large-scale forcing associated with the RegCM lag-composite of rainfall anomaly, the model composite is associated not only with the development of geopotential height anomalies at high latitudes but also with changes in anomalies in the location of the climatological jet stream. The decay of a large-scale negative geopotential height anomaly over Mongolia - Japan is followed by the growth of a positive anomaly along the jet, which is attributed to the development of the circulation on the northern side of the domain.

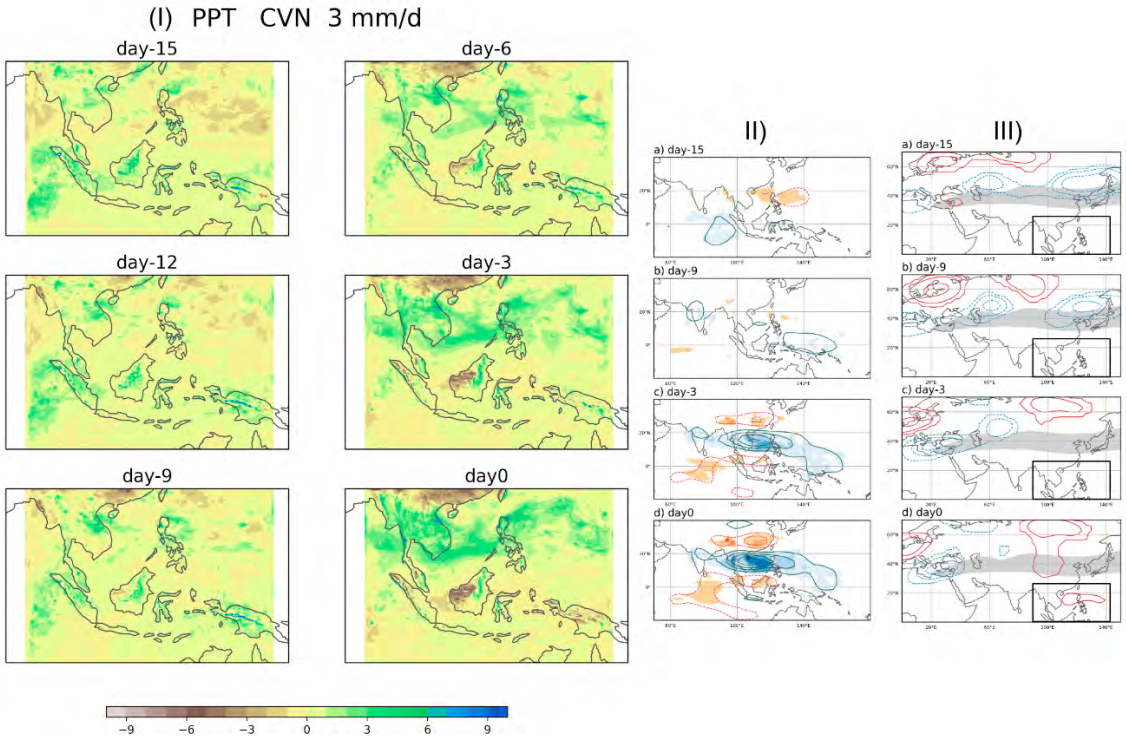

Figure 4.12: as Fig 4.10 but associated with Large-scale Wet Events exceeding 3mm/day in CVN

Figure 4.13 shows the RegCM lag-composite of rainfall anomalies associated with large-scale dry events exceeding -3mm/day over CVN. The signals in the lag composite are much weaker than those of the wet events (Fig 4.12). The composite of rainfall anomalies on day-15 shows large-scale positive rainfall from the North Western Pacific to the south of the South China Sea and Central Highlands Vietnam. The dry is patchy over North Vietnam, expanding until the Philippine Sea on day-15. The positive anomaly gradually decays from day -15 to day-9, then seems to disappear on day-6. The negative anomaly slightly develops into a thin band on day-9, which further slightly expands to the southeast on day-3, then decays over the Philippine Sea on day 0. The dry events are observed with small coverage over the north of CNV.

The similarity of the development of RegCM rainfall anomaly patterns following the lag composites and reanalysis composite is patchy and on a large scale. The dry band from the

north of CVN to the Philippine Sea is reproduced by the model, but not for the whole CVN region as in the reanalysis composite. This band covers only north of the South China Sea and the dipole pattern of large-scale dry/wet over Vietnam/Indonesia is somehow rewritten. Especially, the change of negative rainfall anomaly from day-15 over the Maritime Continent to positive rainfall anomaly on day-3 as in the reanalysis composite is well reproduced.

The RegCM composite of rainfall anomaly shows a strong association with the development of low-high anomalies over Mongolia - North Pacific via a composite of geopotential height anomalies in the extratropics. The wet over Western Pacific appear at the same time with the presence of the positive geopotential height over Japan, then disappear when the anomaly over Japan decay. That is similar to the RegCM composite associated with NVN wet large-scale forcing. The development of a dry band from the north of CVN to the Philippine Sea looks to be associated with the intrusion of the low geopotential height that is intensified by the Asian jet.

The large-scale dynamics associated with the CVN events presented in Chapter 2 showed not only extratropical precursors with the same suggested high-latitude pathway but also tropical wave propagation that is symmetrically significant to both wet and dry events. However, the rainfall anomaly patterns reproduced by the RegCM under ERAi large-scale forcing show a difference between Wet and Dry. The RegCM4 model simulates the rainfall anomaly on a large scale for both CVN event, but CVN Dry show a much weaker signal than CVN Wet. The rainfall anomaly is locally reproduced well only for CVN wet. This suggests that for CVN-wet, extratropical forcing could contribute to the rainfall anomaly patterns and could be more important than the tropical propagation influence. For CVN dry, extratropical precursors might be attributed to the rainfall anomaly patterns, but not to significant anomaly locally.

4.3.2.3 South Vietnam - SVN

Fig 4.14 show the RegCM lag-composite of rainfall anomalies Fig 4.14.I associated with large-scale dynamics Fig 4.14.III of SVN Wet events. The two-week lag composite of rainfall anomalies reproduced by RegCM4 shows no significant development of rainfall anomalies over the whole domain. There are a negative anomaly over the South China Sea - Philippines Sea and the positive anomaly covering Maritime Continent. The rainfall anomalies change slightly in intensity and retract from day-15 to day 0 over Western Pacific. Over NVN, the negative anomaly persists from day-15 to day-6, then decays afterward to become relatively neutral. The center of CVN has a positive rainfall anomaly that gradually increases since day-15. Over SVN, the anomaly remains negative from day-15 to day 0.

Compared to the reanalysis composite of rainfall anomalies using the same index, the patterns of dry and wet over the North Pacific and Maritime Continent, respectively, are reproduced. However, the RegCM composite does not reproduce the expected anomaly over SVN and the South China Sea. In addition, the large-scale positive rainfall anomaly reproduced by the model over Indonesia is relatively stable over the 2 weeks lagged instead of

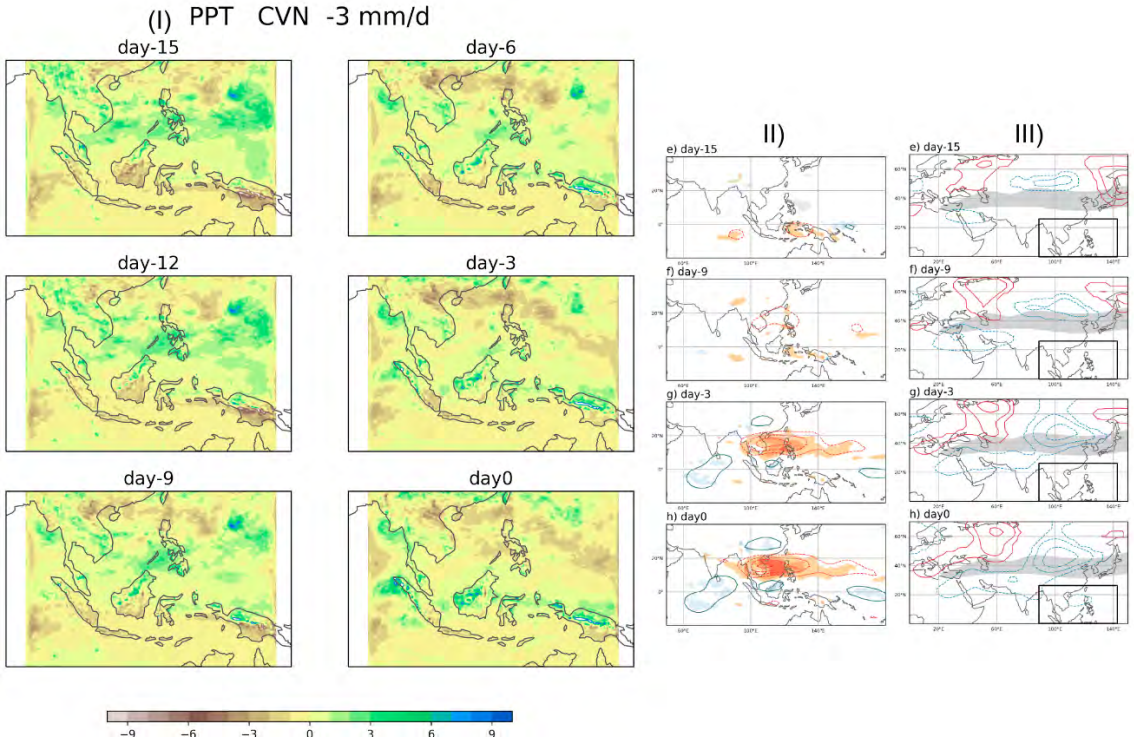

Figure 4.13: as Fig 4.10 but for CVN Dry events exceeding -3mm/day.

strong intensity development in the reanalysis composite.

The large-scale forcing associated with the RegCM composite of rainfall anomalies shows the relation between extratropical precursors and the rainfall anomaly in the same way as NVN Dry, but stronger. The negative rainfall anomaly over the north Western Pacific is strongly associated with the positive geopotential height anomaly, which is a persistent feature since day-15. On the other hand, the negative geopotential height anomaly over Siberia together with the development of other anomalies along the jet show more association with the rainfall anomaly over North Vietnam.

Figure 4.14 show the RegCM lag-composite of rainfall anomalies (I) associated with reanalysis of rainfall anomaly (II) and large-scale dynamic (III) of SVN dry events. Symmetrically to the case of SVN-wet, the patterns of wet anomaly over the north Western Pacific and dry over the Maritime Continent remain stable from day-15 to day 0. These anomalies are associated with the 2 weeks of wet anomalies over NVN, SVN and the South China Sea. The anomaly over the Philippines peaks on day-9. Then that rainfall peak moves to the South China Sea on day-3.

Compared to the reanalysis composite of SVN Dry, the RegCM fails to reproduce a composite of rainfall anomaly locally but the large-scale pattern over the whole domain looks similar to the observed reanalysis. The patterns of rainfall anomaly over the whole domain are fairly symmetrical to the Wet case and highly similar to the NVN wet patterns but with stronger. The dry anomaly over Indonesia reproduced by the model is limited in land and

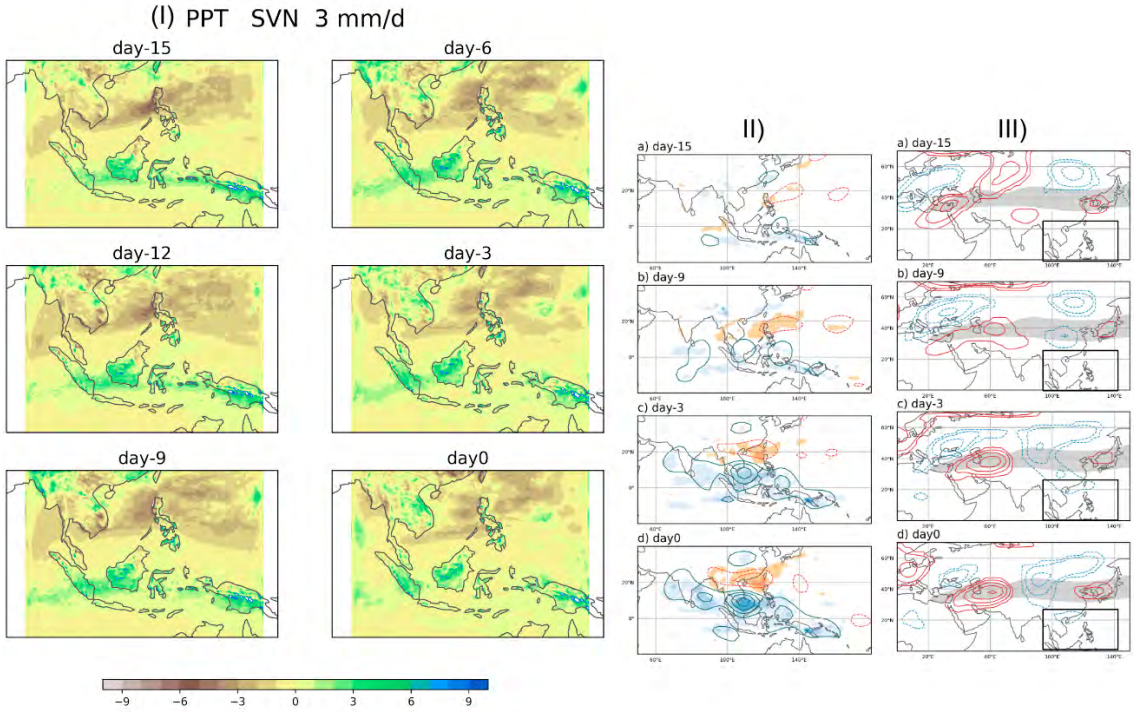

Figure 4.14: as Fig 4.10 but associated with Large-scale Wet Events exceeding 3mm/day in SVN

there is no significant signal over south of the South China Sea.

The large-scale forcings, including the extratropical precursors associated with the RegCM composite of rainfall anomaly, show a strong relation with the patterns of rainfall anomaly and is reversal with the case of SVN-wet. The positive anomaly over Siberia remains for 2 weeks, developing further to the south, and is associated with this rainfall anomaly pattern. The same pattern of anomaly is also seen in the case of NVN-wet which shows the same reproduction of wet over NVN by the model. The pattern of anomalies along the Asian jet indicates a reversal sign except over Japan.

By looking at the two cases of the SVN regional model composite, the large-scale dynamics associated with the SVN events using the reanalysis data suggest the role of extratropical precursors and tropical influence separately. It can be seen that both large-scale patterns of rainfall anomaly over the whole domain are created, while the South China Sea signals are missing in both cases. We note that the tropical wave activities have a strong signal in SVN cases, and are symmetrical to both wet and dry events, which are strongly associated with enhanced/suppressed convection in the equatorial region 100E-140E. This suggests the role of these tropical precursors generated in the equatorial domain in creating rainfall anomalies locally for SVN dry cases.

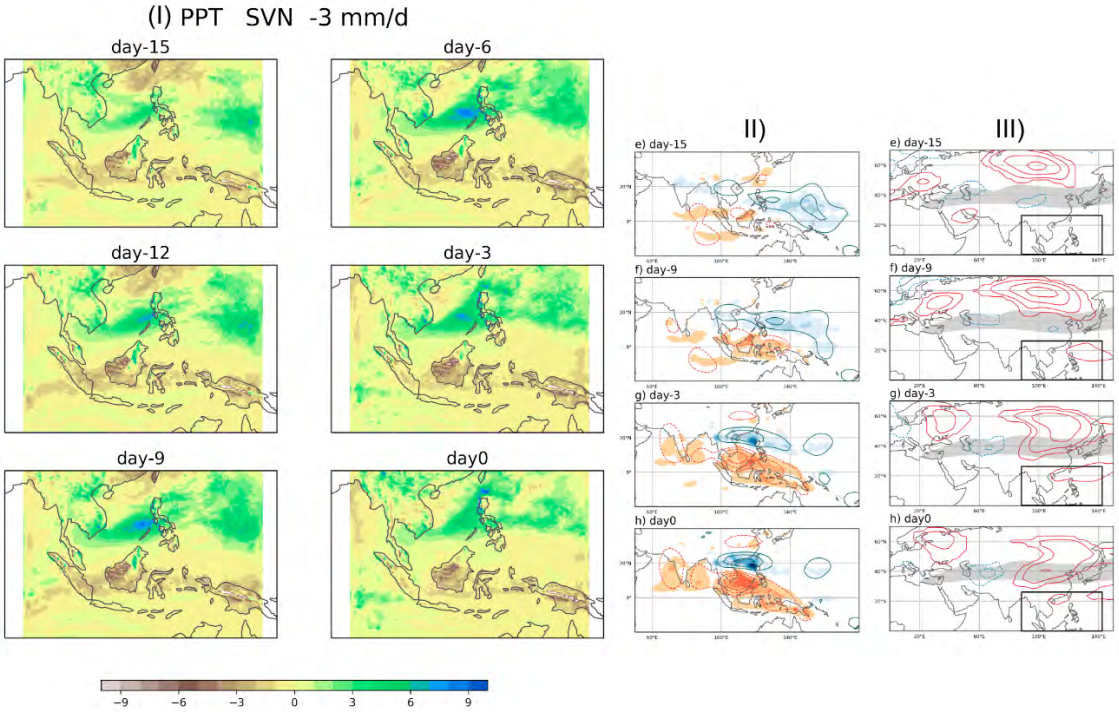

Figure 4.15: as Fig 4.10 but for SVN Dry events exceeding -3mm/day.

4.3.2.4 Summary and Discussion

To sum up, the RegCM4 simulation using reanalysis data -ERAi as LBCs can reproduce the rainfall anomaly on the intraseasonal timescale over Vietnam subregions. The large-scale patterns over Southeast Asia are well represented, especially over the North Western Pacific and the Maritime Continent. Particularly, the symmetrical large-scale forcings on the northern side of the domain are consistent with the relatively symmetrical rainfall patterns over the whole domain. Extratropical forcings derived from ERAi reanalysis, play the main role in the reproduction of the ISV rainfall over the Vietnam subregion such as in NVN wet and dry, and CVN wet events.

The RegCM4 does not reproduce local rainfall anomalies for South Vietnam's Wet and Dry events and dry events over CVN. Besides, RegCM4 shows a lack of equatorial signals particularly over the South China Sea in association with the development of rainfall anomaly over SVN wet-dry and CVN-dry events. It suggests that the model configuration could be a failure in simulating tropical propagation within the domain, especially over the South China Sea which is surrounded by land. It also implies that the tropical influence might be attributed to the local rainfall anomaly formation in these cases.

The pattern of rainfall anomaly suggests us reevaluating the convection scheme used in the configuration that drives the process to decide the rainfall events in the domain. Particularly, rainfall anomalies both wet and dry, mostly occur in places of high elevation and less often

in the equatorial ocean - specifically, the South China Sea. The MIT scheme focuses on the microphysics of the convective process instead of the large-scale moisture convergence, which is mainly driven by buoyancy. Chow et al. (2006) indicated that adding convection suppression criteria to the MIT cumulus parameterization scheme significantly improved Asian Summer Monsoon precipitation in 1998 compared to observed rainfall data. They suggested that the influences of large-scale atmospheric conditions such as moisture convergence, relative humidity, and relative vorticity needed to be taken into account. In particular, convection over the South China Sea is usually suppressed by the Northwestern Pacific subtropical high (WNPSH).

On the other hand, Juneng et al. (2016) indicated a temporal correlation between Southeast Asia mainland rainfall time series from RegCM4, ERAi and the Climatic Research Unit of the University of East Anglia (CRU) dataset with their respective surface variable fields, namely the surface air temperature, 850 hPa circulation and surface heat fluxes. They showed positive and strong positive correlations between RegCM4 mainland rainfall and surface temperature over the South China Sea and eastern Indian Ocean, but moderate negative correlations for ERAi and CRU. The main reason is believed to be the lack of air-sea interaction in the RegCM4 simulation.

Regarding the influence of large-scale forcings from extratropics and tropics on rainfall anomalies over Vietnam subregions by RegCM4 with ERAi configuration, as well as the lack of regional model representation of rainfall, other terms of the moisture budget need further investigation. Indeed, moisture flux convergence (VIMC) and the tendency of moisture column (TIMC) are two aspects of convection that provide a view of moisture driven by the interaction of large-scale forcings from GCMs and the model configuration. In addition, evaporation is an aspect related to the air-sea flux that needs clarification in this context.

4.3.3 VIMC and TIMC - Moisture Budget

4.3.3.1 VIMC

Figure 4.16 shows the composite of VIMC anomaly reproduced by RegCM4 associated with observed Wet and Dry Events exceeding +/- 3mm/day in NVN. For both NVN wet and dry events, the development of the VIMC pattern is consistent with the rainfall anomaly patterns shown in the previous section (Figs 4.10 and 4.11), especially over the ocean. The VIMC anomaly over land shows very detailed values, particularly high elevation areas. There are also symmetrical anomalies over the Philippine Sea - north Western Pacific. In terms of intensity, the VIMC signal is stronger than the rainfall anomaly. The strong difference in the VIMC anomaly over land may be attributed to the topography interaction with the winds or moisture. However, it is clear that although the VIMC anomaly is not always associated with the rainfall anomaly, its signal is stronger and shows more predictability in this RegCM4 configuration. For example, the strong positive signal along the CVN coast is associated with no significant rainfall anomaly. Indeed, this could be attributed to the MIT scheme that mainly relies on instability.

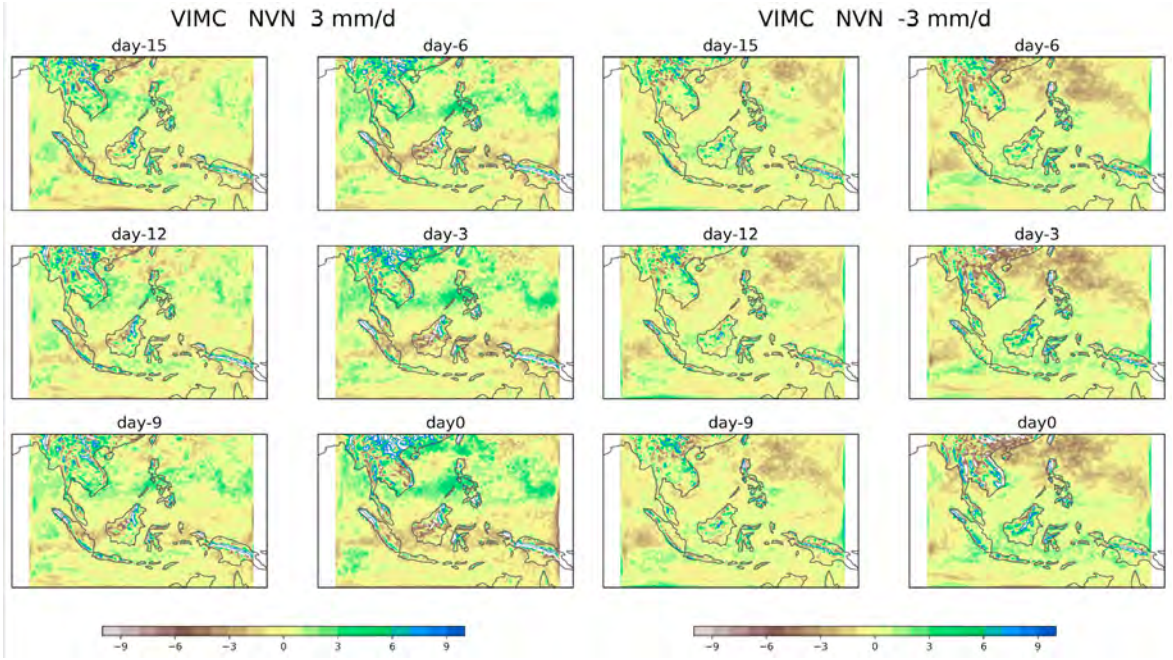

Figure 4.16: Composite of the VIMC anomaly reproduced by RegCM4 associated with Large-scale Wet and Dry Events exceeding +/- 3mm/day in NVN. The contour interval is 1mm/day.

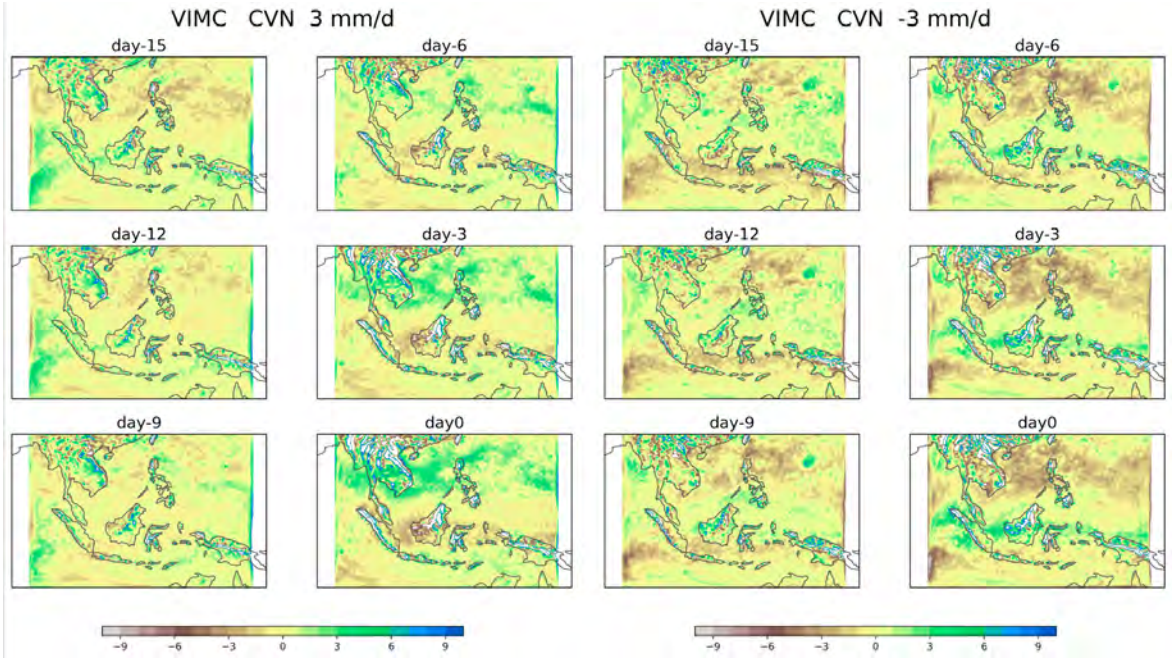

Figure 4.17: as Fig 4.16 but for CVN.

Figure 4.17 displays the RegCM4 composite of the VIMC anomaly associated with re-analysis of wet and dry events exceeding +/- 3mm/day in CVN. The development of the VIMC pattern following a 2-week lag in both wet and dry events is consistent with the rain-

fall anomaly patterns shown in Fig 4.12 and 4.13. The CVN case exhibits the sensitivity of the convection scheme to the high-elevation place in leading the VIMC anomaly. Strong anomalies appear mixed between positive and negative over North and Central Vietnam. We can see the Foehn effect in the CVN wet case, where the western side of Truongson mountain tends to be wetter, causing the eastern side to become drier.

Besides the amplification due to the topography effect seen in NVN cases, the VIMC anomaly over the ocean area shows differences in association with the rainfall anomaly. The VIMC anomaly is present over the South China Sea, even in the lack of rainfall anomaly reproduced by the model over there. Therefore, it is more likely that the atmospheric instability over the South China Sea is not enough to trigger the rainfall anomaly than the criteria of moisture convergence.

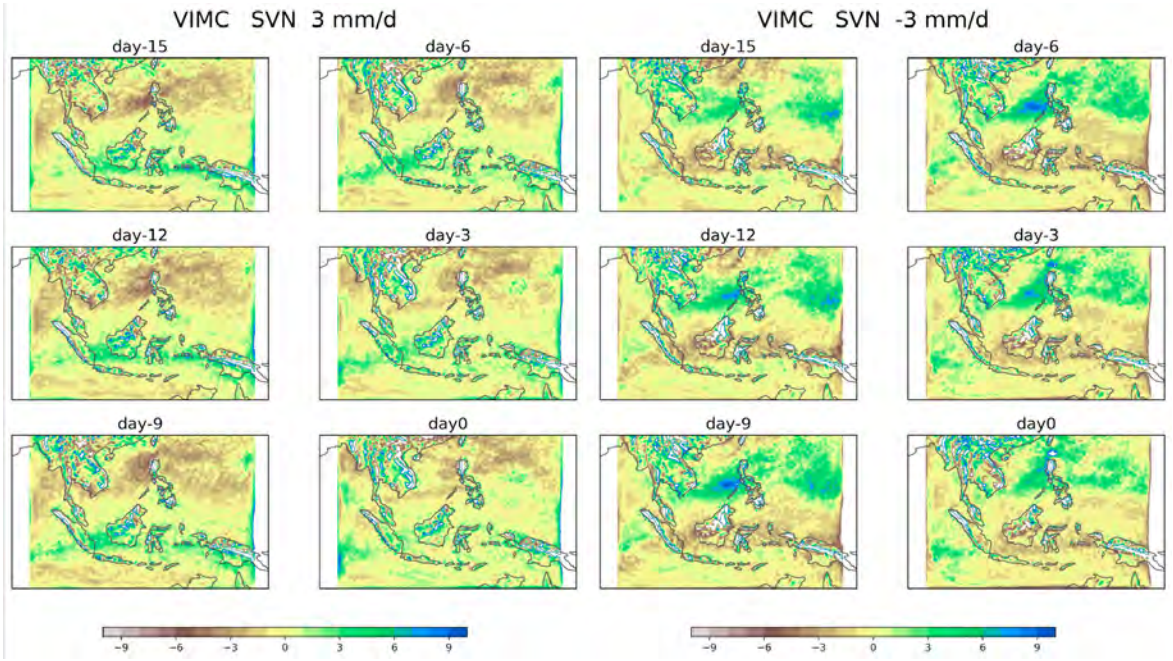

Figure 4.18: as Fig 4.16 but for SVN.

The RegCM4 composite of VIMC anomaly associated with reanalysis wet and dry events exceeding ±3mm/day in SVN is shown in Figure 4.18. The development of VIMC patterns in both wet and dry events is strongly associated with the rainfall anomaly patterns shown in Fig 10 and 11 from day -15 to day 0, especially over ocean regions. Both VIMC and rainfall anomalies reproduced by RegCM4 show less representation along the Equator than the reanalysis composite. Over the SCS and Northwestern Pacific, the VIMC is well matched with the rainfall anomaly in both spatial coverage and intensity.

Thus, all three Vietnam subregions show a strong relationship between VIMC and rainfall anomaly, although small differences exist. The differences mostly appear due to the topography, which directly impacts the low-level winds as well as the low-level moisture in the air. Others might come from the parameterization of convection and/or air-sea flux, or even the lack of representation of tropical waves, for example. Other terms of moisture budget need

to be investigated.

4.3.3.2 TMC

Figure 4.19 shows the composite of the tendency of moisture column anomaly reproduced by RegCM4 associated with Large-scale Wet and Dry Events exceeding ±3mm/day in NVN. The intensity of TIMC, as shown by the color scale, is smaller than that of VIMC and rainfall anomalies. Following the lagged composite of RegCM4, the development of TIMC anomaly over NVN is strongly associated with the rainfall over there in both sign and intensity. The moistening atmosphere first covers the Gulf of Tokin and then spread to the west. At the same time, the Maritime Continent gradually becomes dry. With less predictability, the NVN atmosphere starts to be dry on day-9 and then quickly develops into Dry events. TIMC shows some asymmetries from day-15 to day-9. Although it is much smaller than rainfall or VIMC that could contribute to the asymmetric of rainfall patterns via the balance within moisture budget terms.

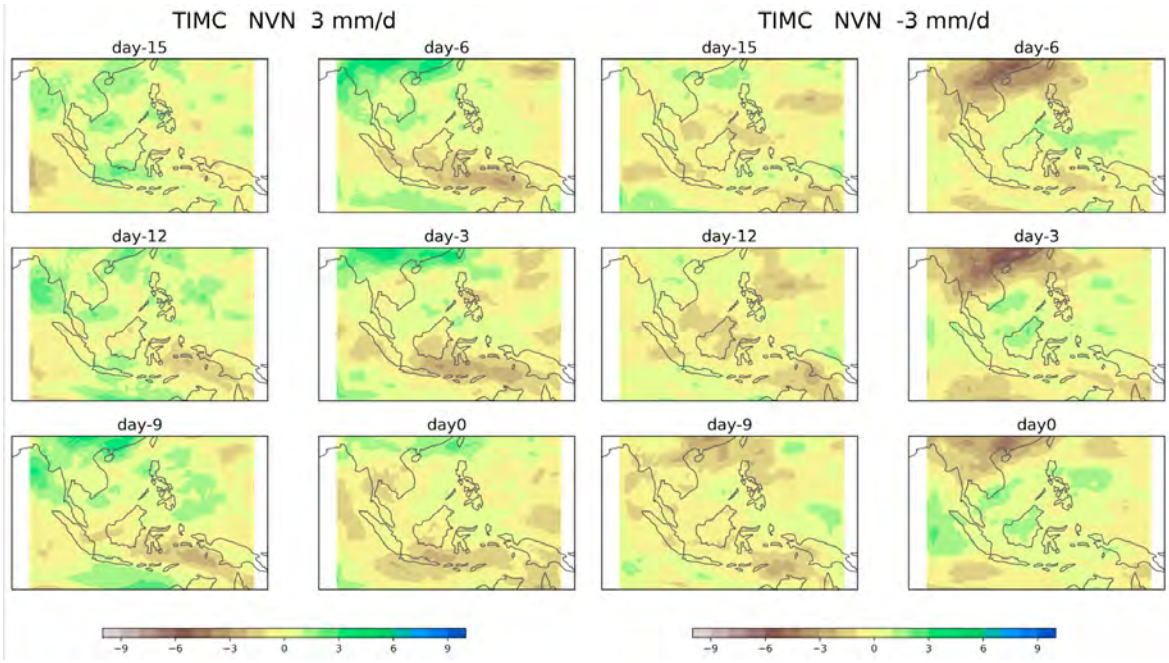

Figure 4.19: Composite of the TIMC anomaly reproduced by RegCM4 associated with Large-scale Wet and Dry Events exceeding +/- 3mm/day in NVN. The contour interval is 0.1mm/day.

Fig 4.20 displays the composite of the tendency of moisture column anomaly reproduced by RegCM4 associated with Large-scale Wet and Dry Events exceeding ±3mm/day in CVN. As the color scale is 10 times smaller than that of the rainfall anomaly, the intensity of TIMC is smaller than VIMC and rainfall anomalies. However, the RegCM4 lagged composite TIMC anomaly develops from the eastern side of CVN in both events, and then the moistening atmosphere covers the entire CVN region. There are significant asymmetries between the

CVN events in terms of TIMC spatial patterns. It is noteworthy that the TIMC signals over SCS, as well as over Equatorial regions, are presented in both events.

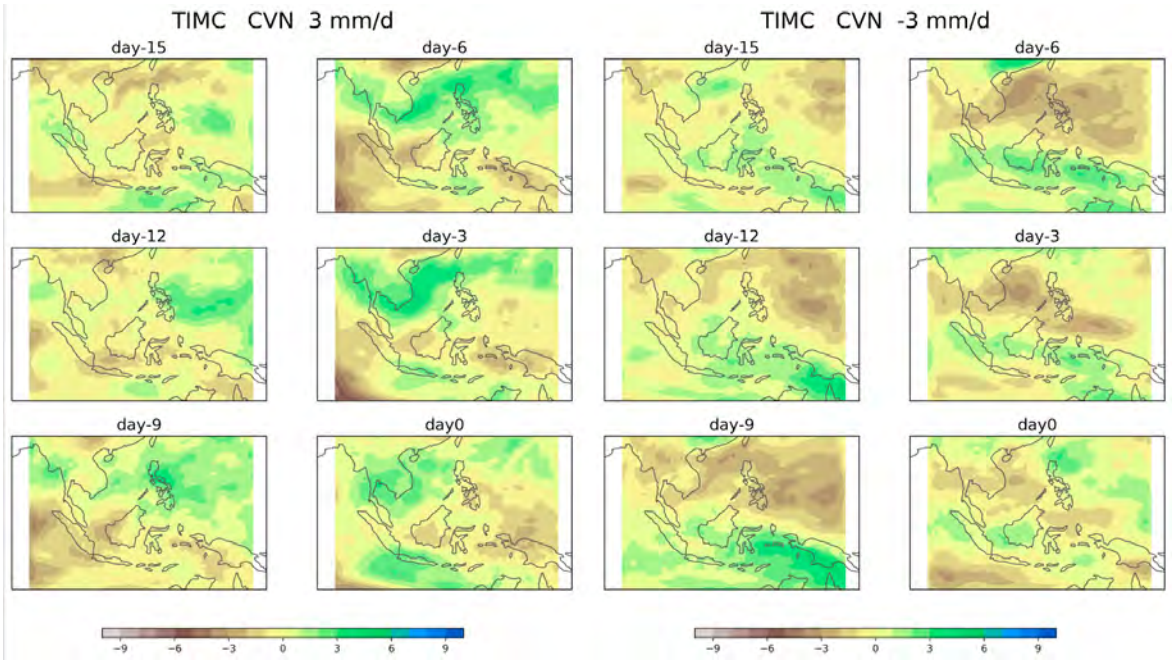

Figure 4.20: as Fig 4.19 but for CVN.

The composite of the tendency of moisture column anomaly reproduced by RegCM4 associated with Large-scale Wet and Dry Events exceeding ±3mm/day in SVN is indicated in Fig 4.21. The RegCM4 lagged composite TIMC anomaly, following the 2-week lagged composite, develops in a similar style to the CVN and NVN cases. In particular, the atmosphere becomes moistened in wet events and dehydrated in dry events, even when the rainfall anomaly shows no local relevance with the reanalysis composite. In wet events, the TIMC anomaly comes from SCS from day-15, while in dry events, the negative TIMC suddenly appears locally on day-6 and then spreads over southern SCS.

4.3.3.3 Summary and Discussion

The composite of VIMC and TIMC from RegCM4 output associated with the reanalysis of the regional event of Wet and Dry provides a more detailed understanding of the moisture budget that is strongly related to the rainfall anomaly events by the model reproduction. The composite of VIMC shows relatively similar patterns with the rainfall anomaly, but the TIMC - the change in the moisture added or lost - provides more information on the atmosphere from day-15 of the events.

For NVN, the composite of VIMC shows the best match with the oceanic rainfall anomaly reproduced by the model in both events, although there is an exaggeration of the VIMC amount due to the topography effect. The atmosphere is moistened locally since day-15 for

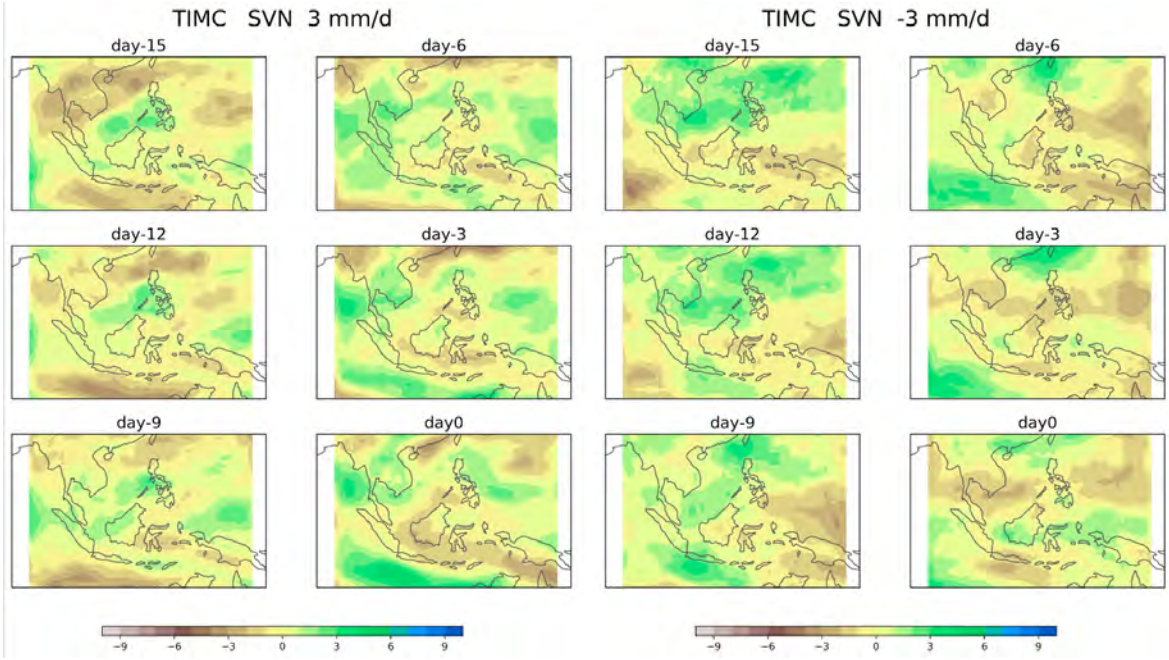

Figure 4.21: as Fig 4.19 but for SVN.

wet events, but later for dry events on day-9.

The composite of VIMC highlights the role of mountains in reproducing rainfall anomalies for the CVN region. The VIMC anomaly signal over SCS that does not lead to rainfall anomaly here, suggests the relevance of the convection scheme. The lack of air-sea flux could lead to inadequate instability of the atmosphere to create an anomaly of rainfall. The composite of TIMC shows that the moistening/drying atmosphere is associated with wet and dry events. It also suggests the sources of moisture associated with CVN events that come from the Western Pacific.

For SVN events, the VIMC is associated with those rainfall anomalies reproduced by the model that does not well represent the local rainfall anomaly over SVN. However, the composite of TIMC shows the same association with the wet and dry events. It suggests the role of tropical wave propagation in rainfall anomaly formation, which may not be well represented in RegCM4.

4.3.4 Evaporation - EVP

4.3.4.1 North Vietnam - NVN

The composite of evaporation anomalies reproduced by ERAi and RegCM4 using the reanalysis index of large-scale rainfall are shown in Fig. 4.22 and Fig. 4.23 for wet and dry events in NVN, respectively. The ERAi composite illustrates the reversal development of evapora-

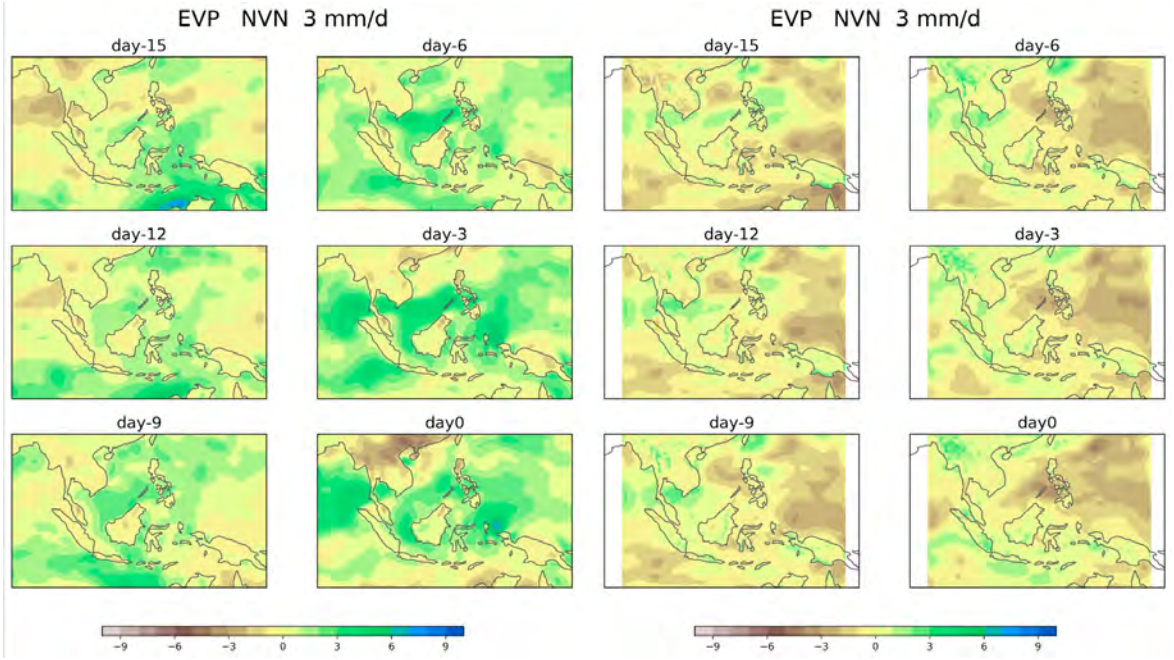

Figure 4.22: Composite of Evaporation anomaly reproduced by ERAI and RegCM4 associated with Large-scale Wet Events exceeding +3mm/day in NVN. The contour interval is 0.1mm/day.

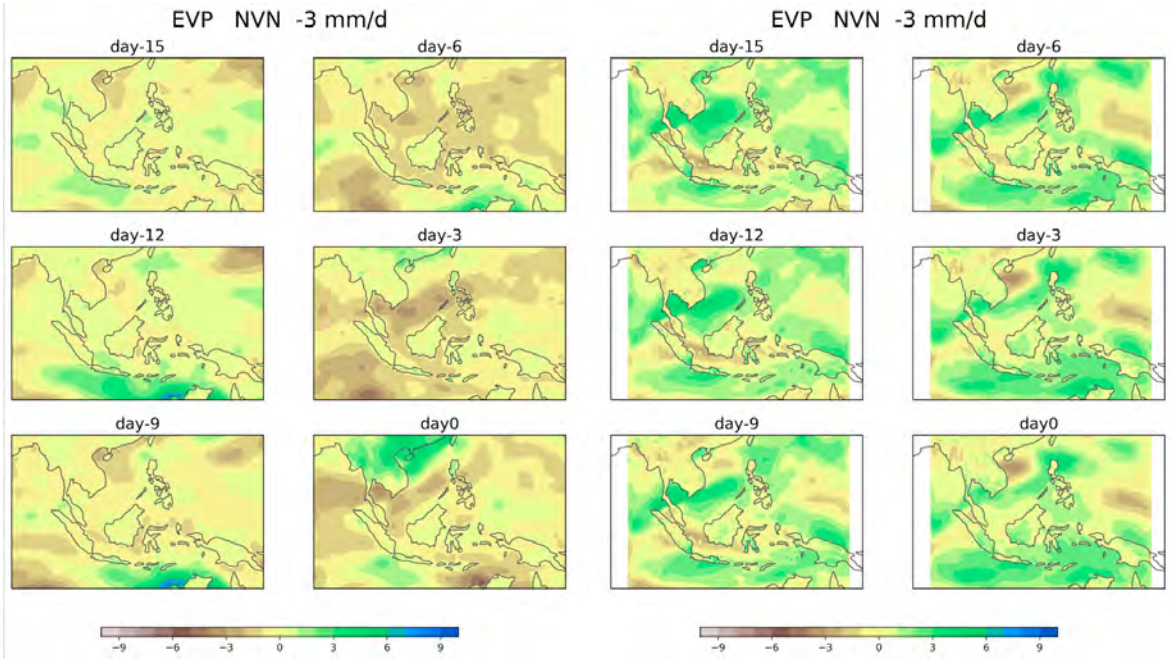

Figure 4.23: as Fig 4.22 but for NVN Dry.

tion over land and ocean in both cases of NVN. The atmosphere shows more evaporation associated with the negative anomaly rainfall over NVN land locally, while it exhibits less

evaporation over southern SCS. The symmetry between wet and dry events of NVN is strong for reanalysis evaporation over land, but not for the large-scale ocean. However, the RegCM composite indicates a difference from the reanalysis composite. The evaporation patterns were not reproduced. The neutral anomaly of evaporation resists over 2 weeks in NVN wet, and for NVN dry, a negative anomaly develops in the south of the Gulf of Tokin, but not for NVN. Especially over the ocean, the evaporation patterns are entirely reversed. The lack of air-sea interaction as well as land processes might be suggested as the difference between RegCM and ERAi, which can be seen as a reasonable explanation for the reversal pattern of evaporation.

4.3.4.2 Central Vietnam - CVN

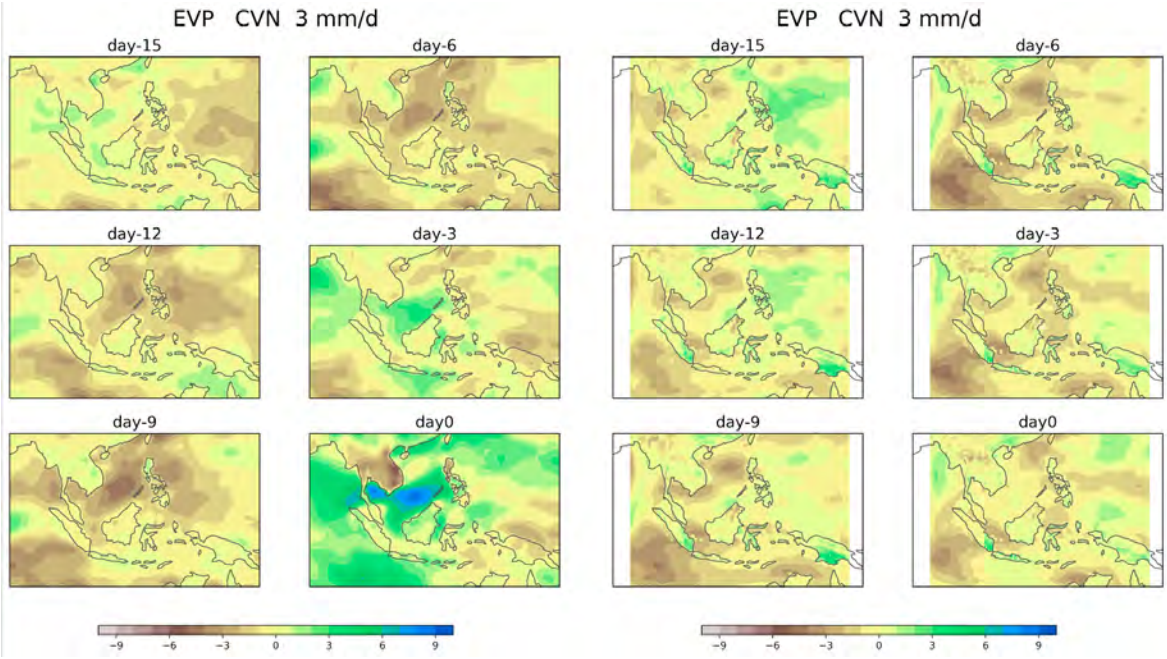

Figure 4.24: Composite of Evaporation anomaly reproduced by ERAI and RegCM4 associated with Large-scale Wet Events exceeding +3mm/day in CVN. The contour interval is 0.1mm/day.

Figure 4.24 and 4.25 show the composite of evaporation anomalies reproduced by ERAi and RegCM4, assembled using the reanalysis index of large-scale wet and dry events in CVN. The ERAi composite shows a much stronger signal compared to the NVN cases. The reversal development of evaporation over land and ocean just close to the CVN region in both cases is seen clearly. The sign change of evaporation anomaly, locally and suddenly, leads to a huge amount of positive/ negative evaporation over the equatorial SCS and negative/positive evaporation anomaly over CVN wet/dry. The RegCM composite shows a slight change in the patterns but does not follow the ERAi composite. Additionally, it can be seen that there is no relation between the RegCM evaporation patterns associated with opposite events on the large-scale over CVN.

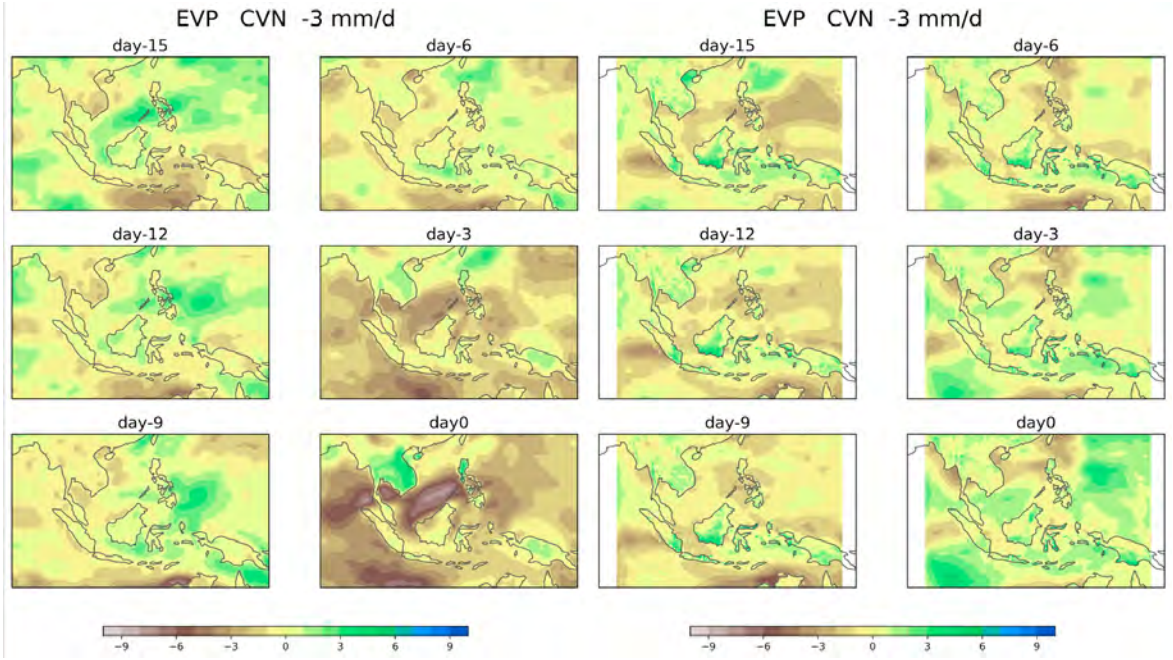

Figure 4.25: as Fig 4.24 but for CVN Dry.

4.3.4.3 South Vietnam - SVN

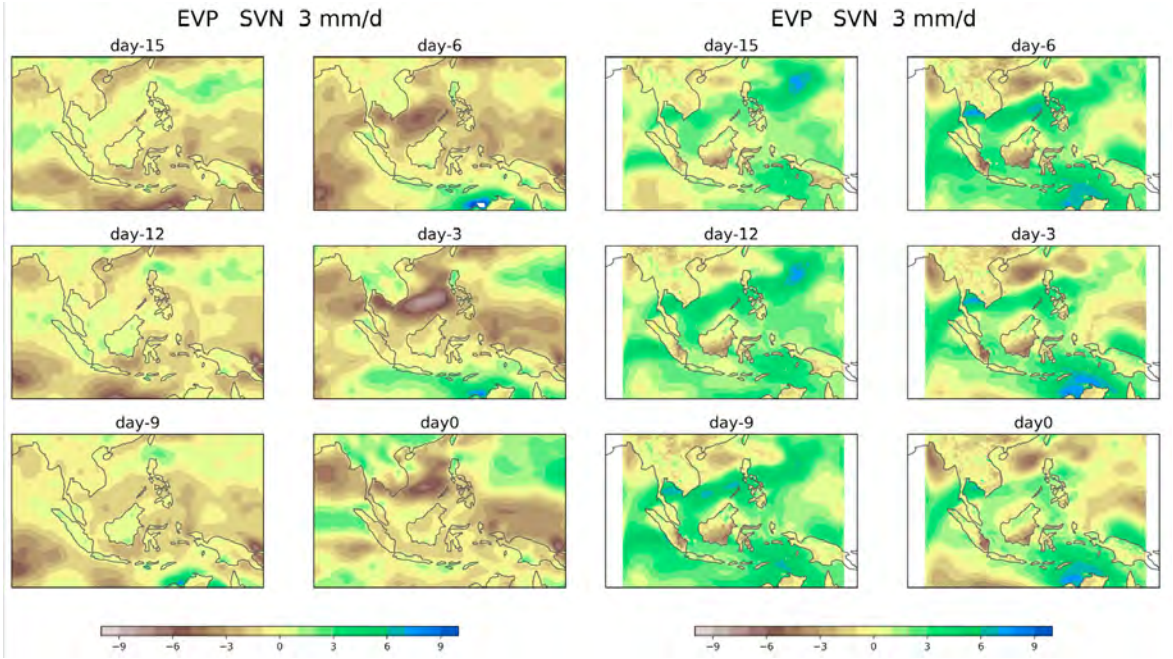

Figure 4.26: Composite of Evaporation anomaly reproduced by ERAI and RegCM4 associated with Large-scale Wet Events exceeding +3mm/day in SVN. The contour interval is 0.1mm/day.

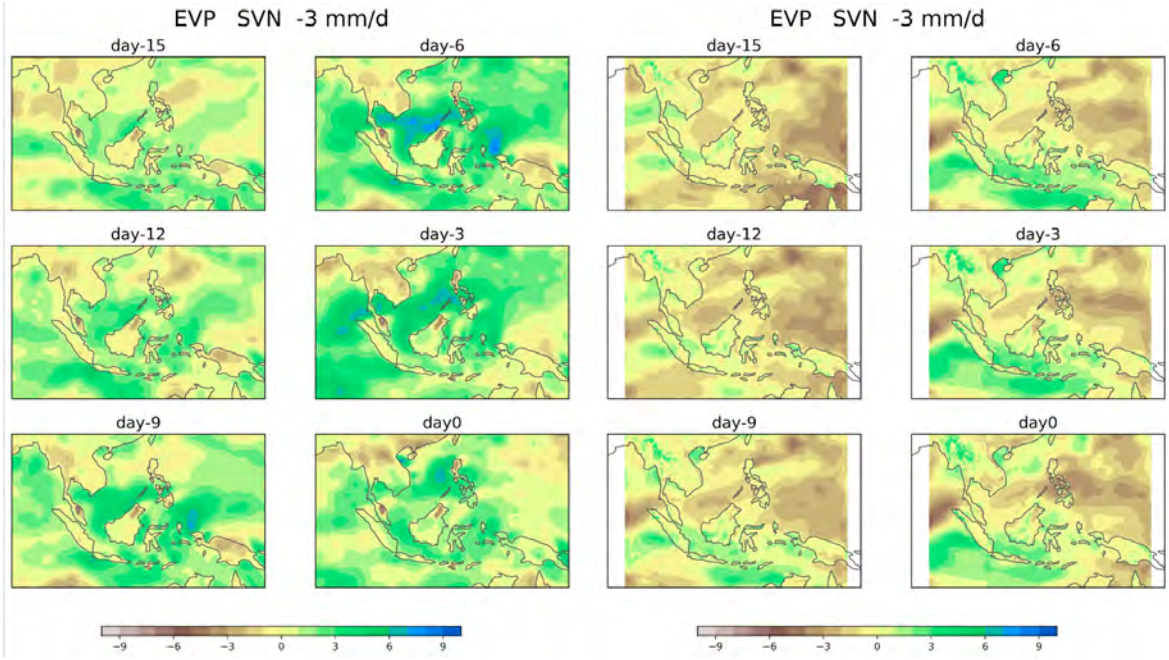

Figure 4.27: as Fig 4.26 but for SVN Dry.

The ERAi and RegCM4 composites of evaporation anomaly assembled using the index of large-scale wet and dry events exceeding ±3mm/day in SVN are shown in Fig 4.26 and 4.27. Similar to the CVN cases, the ERAi composite associated with SVN events shows a strong signal on both sides of the Equator. The negative/ positive evaporation anomalies over the Maritime Continent are a signature associated with SVN wet/ dry events. The development of evaporation anomaly patterns shows that the maximum evaporation (day-6 for SVN wet and day-3 for SVN dry) does not occur at the same time as the day0 of the events. Both cases also show that the evaporation anomaly does not cover SVN. The RegCM composite shows the evaporation patterns with the strongest signal compared to those of RegCM for other cases. These patterns are far from the reanalysis composite on both local and large scales. The evaporation anomaly on a large scale can not be reproduced.

4.3.4.4 Summary and Discussion

This subsection focused on the last term of the moisture budget - evaporation associated with the reanalysis of large-scale rainfall over three subregions in Vietnam generated by RegCM4. A comparison between ERAi and RegCM composite of evaporation has also been made. Generally, the evaporation anomaly patterns reproduced by this RegCM4 configuration show a weaker signal and do not resemble the reanalysis one. The evaporation from both ERAi and RegCM contributes a small part to the moisture budget. The reanalysis data show a contrast of evaporation anomaly between land and sea, and the wet and dry events are quite symmetric across all subregions. But the RegCM data is not organized in that way, although the land-sea contrast appears with a weak signal.

The ERAi composite indicates a strong association between NVN events and local evaporation anomaly, while those of SVN are more associated with the oceanic anomaly over SCS, and CVN events are mixed cases.

The big difference between the ERAi and RegCM composite of evaporation anomalies suggests an inadequate representation of air-sea interaction in the regional model(Juneng et al., 2016).

4.4 Chapter's conclusion

In this chapter, we used the output of a RegCM4 simulation, with the configuration previously defined by the $CORDEX_SEA$ community, to study the impact of large-scale forcing on the circulation in Vietnam, which is embedded in the lateral boundary condition - ERAi reanalysis dataset. We assessed the model's ability to reproduce the rainfall anomaly over three subregions in Vietnam, as well as other moisture budget terms such as the vertically integrated moisture flux convergence (VIMC), the tendency of the moisture column (TIMC), and evaporation.

The output of the 25-km-resolution RegCM4 experiment forced by ERAi as LBCs from 1979 to 2008, is used to assemble a composite based on an index derived from the reanalysis of large-scale rainfall intraseasonal variation over three Vietnam subregions. The RegCM4 composite of rainfall anomaly reproduces well the WET and DRY events over North Vietnam and CVN wet events. In particular, the RegCM composites show that the development of local and the Pacific regions in NVN wet and dry events and CVN-wet are strongly related to the ERAi composite. However, only the large-scale patterns of rainfall in northwestern Pacific/Indonesia are reproduced with no local rainfall anomaly reproduced in agreement with the reanalysis composite of South Vietnam and CVN dry. The signals over the South China Sea are associated with those local rainfall anomalies seen in the ERAi composite that was not generated by the RegCM4 model.

The VIMC generated by the RegCM4 shows relatively good agreement with the rainfall anomaly, except for an exaggeration over the high elevation area. This could be attributed to the convection scheme that leads to the rainfall anomaly over the subregions. The TIMC shows a small part in the moisture budget and is strongly associated with the anomaly of large-scale rainfall. Particularly, the moistening of the atmosphere occurs in association with the positive rainfall anomaly in the reanalysis data.

The evaporation associated with the Vietnam subregion events in the large-scale reanalysis observation shows a significant difference from other terms in the moisture budget. The evaporation anomaly patterns are not reproduced in all cases. The ERAi composite shows the land-sea contrast and the opposition between wet and dry events of evaporation, while the RegCM composite exhibits a weak signal with no relevance.

The link between the large-scale forcing associated with the regional events and the rainfall

anomaly reproduced by the RegCM4 model forced by that forcings has been unraveled by the composite. The extratropical forcing plays an important role in modulating large-scale patterns of rainfall over the whole domain of Southeast Asia in all events. Especially, the NVN wet and dry events show the best rainfall anomaly reproduction. However, for SVN events, the large-scale forcing is not attributed to the local rainfall anomaly. The similar large-scale forcing between SVN and NVN events only explains the large-scale rainfall anomaly patterns. The lack of tropical signals, especially over the South China Sea suggests the model failure in the reproduction of the tropical propagation that is attributed to the local rainfall anomaly over SVN.

The qualitative assessment for the role of extratropical forcings and tropical propagation is seen interestingly in CVN wet and dry events. Both wet and dry events over CVN show symmetrical large-scale forcings as well as symmetrical tropical eastward propagation in Chapter 2 from the reanalysis composite. However, the large-scale forcings play a more important role in stimulating the CVN wet in both large-scale patterns over the whole domain and local events. In CVN dry, the large-scale forcing shows less attribution to the rainfall anomaly here. Particularly, the large-scale rainfall is simulated by RegCM but weak signals in general and no significant anomaly of rainfall over CVN regions.

Conclusion and perspectives

Conclusion & Perspectives in English

The annual cycle of Vietnamese rainfall is strongly conditioned by the Asian monsoon system. However, the intraseasonal variability also has a large amplitude and exhibits considerable complexity, with much variation between the Vietnam subregions. Previous studies have used a variety of approaches to diagnose the timescales, patterns, and associated 3D-circulation of Vietnam subregional rainfall ISV. The link between the rainfall intraseasonal variation and moisture flux divergence has also been exploited. Vietnam rainfall intraseasonal variations are affected by extratropical and tropical factors. However, the results are often sensitive to the choice of regions, timescales and rainfall criteria employed within the extended summer. Furthermore, comparatively little attention has been paid to the full moisture budget. In this study, our first objective was to assess the contribution of moisture budget terms to regional events separately for positive and negative rainfall anomalies. Our second objective was to analyze these opposite regional events, Wet and Dry, to identify large-scale dynamical precursors and their pathways of influence. We have paid particular attention to the nonlinearity or asymmetry of the influence and we have assessed the sensitivity to choices of region, threshold and composited quantity. This has led to a qualitative assessment of the pathways of influence and the relative roles of extratropical and tropical influences.

For the first objective, we have gathered observational composites of opposite signs of anomalous regional rainfall ISV over Vietnam using the vertically integrated moisture flux convergence as a proxy of rainfall. These composites have been used as the basis of a budget study. For the second objective, the same composites were applied to larger-scale precursors with longer lead times. The observational study was complemented by numerical modeling in the form of a set of heating experiments on the stationary wave configuration of DREAM. These experiments were employed to identify the position of an artificial source that gives the most influence in a range of 2 weeks. Further experiments using nudging were then employed to simulate the realistic sources extracted from the observed composite. We then used Rossby a wave tracing R-package with a set of locations, wave numbers and directions from mid to high latitude over the Northern Hemisphere to trace the propagation of potential Rossby waves to the Vietnam target region on different atmospheric states. Finally, the output of downscaling experiments with the regional model RegCM4.3 was examined, forced with the same ERAi data and employing the same composites as in the observed analysis. The regional model was analyzed to find the impact of the large-scale forcing embedded in the lateral boundary conditions.

Observed composite analysis

We first determined that the vertically integrated moisture flux convergence, VIMC could be used as a proxy for rainfall with the supposed benefit of a more direct link between regional precipitation and large-scale dynamics. The high positive correlation coefficient between vertically integrated moisture flux convergence and rainfall anomalies on intraseasonal timescales was confirmed using the ERAi dataset 1979-2016 May-Oct during the summertime over Vietnam subregions. Wet and Dry events over three Vietnam subregions: North Vietnam - NVN, Central Vietnam - CVN and South Vietnam - SVN, were defined by a regional daily VIMC index with a threshold value. Based on the probability frequency distribution of the VIMC index, threshold values of +/-3 mm/day for the daily regional VIMC index were chosen.

The moisture budget associated with regional rainfall events was calculated including four terms: VIMC, Rainfall, Tendency of vertically integrated moisture column - TIMC and Evaporation -EVP. Rainfall is closely connected with VIMC, and these two terms dominate the moisture budget compared to TIMC and EVP. At regional scales, 2-week-lag composites of VIMC and rainfall anomalies in all cases exhibit a reasonable degree of symmetry between Wet and Dry events that have considerable amplitude at different lead times for the different areas. However, this symmetry is not seen at larger scales.

The 2-week-lag composites of large-scale dynamics associated with regional events indicate the precursors, the possible pathways and the asymmetry between the Wet and Dry events. Two extratropical and one tropical pathway of influence emerge from the observed composites:

+) High-latitude pathway: large-scale quasi-stationary equivalent barotropic patterns slowly build and then spread southwards to influence the region.

+) Jet pathway: along the Asian jet, with smaller-scale baroclinic anomalies of alternating sign, showing eastward group propagation to influence.

+) Equatorial pathway: tropical wavelike propagation with an eastward direction.

Both Wet and Dry events in NVN are essentially influenced by the extratropics with precursors originating from Europe following the extratropical high-latitude pathway in NVN Wet, but the jet pathway in NVN Dry events. NVN Wet events are strongly associated with a western Siberian high and a depression over China, consistent with cold surges diagnosed by Abdillah et al. (2018).

The extratropical pathway suggested in SVN Wet and Dry is similar to NVN Dry and Wet with much stronger signals. However, an asymmetrical slow-eastward-propagation is only seen in SVN events, that resemble the MJO (Van Der Linden et al., 2016).

The CVN region is included in this study from the point of view of a transition region. Two regimes are included in our CVN rectangular box attributed to the presence of the Truong Son Mountain range: real-Central Vietnam on the eastern side of the box has a rainfall peak in the winter monsoon season, and Central Highland on the southwestern side has a summer monsoon rainfall peak. A combination of these two signals is necessarily an average from

separate mechanisms.

From the composite, both Wet and Dry events over CVN shows anomalies following the high-latitude pathway in extratropical rotational flow. These anomalies have opposite signs over Western Asia. The tropical influence is symmetrical between Wet and Dry and takes the form of an eastward propagation, that is faster than SVN.

The sensitivity of our conclusions from the observational analysis has been examined by looking at overlapping events: when the anomalies over CVN coincide with an NVN/SVN composite. We have also diagnosed the sensitivity to different hydrological indices that come from different in-situ data.

When anomalies over CVN are included in NVN events, the asymmetry between Wet and Dry events is considerably reduced. For NVN Wet events that spread to CVN, the precursors are different essentially north of the Asian jet, with a Siberian low developing into a three-pole large-scale low-high-low structure. When NVN Dry events spread to CVN, there is a large-scale high-low-high pattern over Asia. For SVN spreading to CVN, both Wet and Dry events are similar to the isolated events but stronger. Thus, the large-scale precursors are quite sensitive to the choice of regional extent for NVN events, but much less so for SVN events.

Two in-situ rainfall datasets, APHRODITE and VnGP were used to make alternative hydrological indices. The resulting composites show a contrasting sensitivity of the large-scale dynamics associated with NVN and SVN events. For NVN composites there are fairly consistent extratropical flows between the three indices and a strong degree of similarity between APHRO and VnGP. However, SVN composites are more sensitive and show less consistency between the three datasets.

The three pathways of influence and remote precursors found from the observed composite are different between regions as well as between wet and dry for a given region. Can we link these precursors to the differences between dry and wet events over the three subregions of Vietnam? Beyond the observational study that was noticed, further research into these pathways is being done using a modelling approach at various scales.

Global model study and Ray tracing

A set of 648 experiments was carried out with heat sources that act as artificial wave sources at different locations, to find the responses on a fixed basic state and thus determine the most effective location to influence the subsequent circulation in the Vietnam subregions. Pure-dynamical model responses to an artificial wave source in a range of 2 weeks are examined. An influence map is produced based on all experiments corresponding to two separate target regions: North Vietnam - NVN and South Vietnam- SVN.

Tropical heat sources have an influence on both NVN and SVN within a limit of 9 days. However, there is no extratropical source found that can influence SVN in a range of 15 days.

Extratropical heat sources over Europe can influence only the NVN circulation after 12 days, then the responses are reinforced in the following 3 days. The identification of the European region as a likely source of NVN influence is in agreement with the observed composite analysis. The influence maps suggest the extratropical wavetrains and Kelvin waves that resemble some of the teleconnections between VN subregions circulation and remote influence sources.

The European precursors associated with NVN events and the pathway of influence are further investigated by applying nudging techniques on summer climatology basic state basic states. Precursors derived from a 15-day composite of NVN wet and dry events have dipole patterns but are not perfectly symmetrical. The model response displays two different pathways of influence that resemble those from the observed composites. NVN wet precursors propagate at high latitudes and then develop southeastwards. NVN dry precursors develop downstream along the Asian jet. After 15 days of running, the model response is quite similar to the observed composites at day 0 in NVN dry, but not for NVN wet.

On stationary wave configuration of summer climatology basic state, the jet pathways look more reproducible than the high latitude pathway with higher amplitude of anomaly and faster pattern set up. The growth of anomalies along the Asian jet exhibits a growth of dynamical mode that develops from baroclinic instability. From the observed composites, the high-latitude pathway is not the same as the model response.

These European precursors associated with NVN events are further investigated by using a set of six monthly-mean basic states from May to October. The results show the model response is very dependent on the basic state jet. Particularly, the NVN wet precursors are more sensitive to the basic state. The high-latitude pathway is reproduced for the August - October states, basic while for the May basic state the jet pathway is produced. The basic state Atlantic and Asian jets play a role in determining the response patterns to NVN wet precursors. For NVN the model responds to Dry precursors along the jet pathway for all basic states but the baroclinic growth of anomalies depends strongly on the state of the Asian jet. Therefore, the pathway from European precursors leading to an influence over Vietnam depends critically on the interaction between the perturbation anomaly and the state of the jet.

The theoretical analysis of Rossby wave ray tracing on the climatological basic state, as well as other basic states associated with regional events, reveals high-latitude pathways that are consistent with the observed composites. High-latitude pathways emanate from the Europe-Eastern Asia region. The wavenumber K=1 takes 2 weeks to arrive in the Vietnam region, while K=2 takes 1 week, and K=3 takes 3-4 days. The positions of Rossby wave sources that influence the Vietnam regions also depend on the basic state on which it propagates, especially wavenumber K=2 in NVN wet and dry states and K=3 for SVN states. A preferred location for Rossby wave propagation to the Vietnam target region is Mongolia. Wavenumber K=1,3 directly propagates to Vietnam after 1-2 days and is not sensitive to the basic state. The K456 with a smaller scale, propagates much faster following the jet pathway from mid-latitudes with only two-three days. This direct source indicates the way anomalies might grow along the jet (jet pathway) and then directly influence Vietnam via Rossby wave propagation.

Downscaling - Regional model study

The output of the 25-km-resolution RegCM4 experiment forced by ERAi from 1979 to 2008, was used to assemble a composite. The reanalysis index from chapter2 was used to investigate how regional model rainfall is affected by the lateral boundary conditions. Anomalies in rainfall and other moisture budget terms: vertically integrated moisture flux convergence (VIMC), the tendency of the moisture column (TIMC) and evaporation, were calculated to test the model's ability to reproduce the moisture budget associated with wet and dry events.

The large-scale patterns over Southeast Asia are well represented, especially over the North Western Pacific and the Maritime Continent. The generally symmetrical rainfall patterns over the whole domain are compatible with the symmetrical large-scale forcings on the northern side of the area. The replication of ISV rainfall across the Vietnam subregion, such as in NVN wet and dry, and CVN wet events, is mostly driven by extratropical forcings determined from ERAi reanalysis.

RegCM4 is less successful in reproducing local rainfall anomalies for South Vietnam's wet and dry events and dry events over CVN. We believe that this is associated with a lack of equatorial signals, particularly over the South China Sea. It appears that the model configuration has trouble simulating tropical propagation within the domain, especially over the South China Sea which is surrounded by land. Another interpretation is that the tropical influence might be attributed to local rainfall anomaly formation in these cases.

The VIMC generated by the RegCM4 shows relatively good agreement with the rainfall anomaly over the oceanic regions but exaggerates over areas of high elevation. The composite of TIMC shows that a moistening/drying atmosphere is associated with wet and dry events respectively. However, the evaporation anomaly patterns are not reproduced in all cases. This raises the question of whether or not the model can maintain the propagation or even shut down the waves transmitted into the domain.

The reproduction of moisture budget terms by RegCM shows a perfect simulation of TIMC for all events, large-scale patterns of rainfall with consistency with VIMC anomaly, but the reversal of Evaporation for all events. The South China Sea region shows a lack of signal reproduced by RegCM in all cases and terms. In agreement with Juneng et al. (2016), that is a specific region with a strong air-sea exchange that plays an important role in simulating tropical wave propagation to impact the rainfall over Central and South Vietnam.

This downscaling study shows that large-scale dynamics including extratropical and tropical influences are attributed to the wet and dry events over Vietnam subregions differently. The extratropical forcings lead to a large-scale simulated rainfall anomaly in all events. The simulations of local rainfall anomalies over NVN events and CVN wet are successfully reproduced, while the local rainfall over SVN and CVN (dry) are not. It might attribute to the model's ability to a simulation of the significance of tropical eastward propagation in SVN and CVN (dry) seen in the reanalysis composite. That is interesting to note that large-scale dynamics show more predominant extratropical forcing in CVN wet than dry events, while these are symmetrical in both extratropical rotational flow and tropical divergent flow.

Perspectives

The investigation of the observed composites in Chapter 2 for rainfall variability on the intraseasonal timescale over Vietnam subregions has been done with careful consideration of the CVN region. We considered CVN as a buffer zone and used it to evaluate the sensitivity of our results to the extent of our subregions. As argued in many studies specifically for CVN rainfall mechanisms on either annual or intraseasonal timescales, CVN exhibits complex behavior. Topography plays a central role in leading two distinct regimes of rainfall over two halves of the CVN box. Therefore, CVN rainfall should be noticed in future studies to be carefully considered.

Chapter 3 shows the various simulations with the stationary wave configuration that explore two extratropical pathways and possible wave sources according to two target regions NVN and SVN. However, in the stationary wave configuration, some processes are not represented, such as transient-mean flow interaction. Transient systems can have an important modifying effect on high-latitude anomalies. Therefore, more modeling could be done for further investigation. For example, we can use the DREAM - GCM configuration that contains the empirical GCM forcings derived from 38 years ERAi dataset. The GCM forcing could be either a constant seasonal forcing or an annual cycle. The examination of the bias led by the observation could be investigated through long GCM runs using the composites of atmospheric states leading to wet or dry conditions over given Vietnam subregions.

The investigation in Chapter 3 is restricted to the dry-dynamical core of the model. But the events under study include processes that could be strongly modulated by moist dynamics, such as tropical waves. Indeed, the tropical eastward propagation found in SVN events is much slower than a pure tropical wave. Moisture could slow down equatorial wave propagation as reported for the convectively coupled equatorial waves studied by Wheeler and Kiladis (1999); Kiladis et al. (2009). So we can do further investigation using the moist mode in DREAM in comparison with those of the dry mode, or even using the moist model for directly predicting the rainfall over the Vietnam region.

Another possibility worth exploring is that there might be an interaction between precursors, rather than one precursor, that can influence a target region. NVN wet precursors show a high latitude pathway of influence from the nudging experiment that is similar to the propagation of anomalies at high latitudes but does not translate to a local model response for NVN wet events. Thus, a combination of precursors could modulate the pathway of influence in nudging experiments. Particularly, the development of European anomalies is strongly associated with the persistence of the Siberian high two weeks before the actual NVN events.

The downscaling study presented in chapter 4 suggests that tropical propagation is poorly simulated by RegCM4. Further investigation could be undertaken such as an examination of the model's ability to simulate tropical wave propagation. For example, the correct simulation of the MJO is considered an important factor in SVN and CVN rainfall (Van Der Linden et al., 2016), and this can be examined using the indexes provided by NOAA to assemble different phase composites. Other tropical waves such as Kelvin or Equatorial Rossby waves could also

be investigated in this way. Implementing the lack of air-sea coupling in the model suggested by Juneng et al. (2016), the atmospheric-ocean coupled model could be promising research. RegCM4 could be coupled with an ocean model to explicitly represent the heat exchange that is normally missed in atmosphere-only models. Another perspective for RegCM4 work is to change the model domain so that it could be specifically designed for an investigation of Vietnam's climate with fine-tuning of parameters to optimize the fidelity of rainfall simulation in the region.

In this thesis, the approach has been to start from observation to modeling that produced many results; and some results that have been difficult to interpret. Much material has been produced and not all of it has been included in this manuscript. Along the way, my appreciation of Vietnamese rainfall regimes, and the associated multi-scale dynamics has evolved, not only in terms of scientific understanding but also in terms of how to communicate findings that are sometimes complex and nuanced.

Three fundamentally different approaches have been adopted in this thesis: observational analysis, a large-scale dynamical study and regional modeling. Although they have been presented in series the work has been carried out very much in parallel. It is remarkable how the three approaches tell a coherent story about distant causes and regional to local effects, from composite precursors to global scale waves and regional hydrology in the intraseasonal timescale.

However, both approaches are depicted to be sensitive to the datasets, the definition of the index, the methodology and the variations within the season. Particularly, if we constrain the data to focus on individual phenomena or sub-seasons, our results will become less generally applicable and lose significance. Subseasonal analysis is problematic because we can lose the distinction between the timescale of the phenomenon and the period of the dataset.

Besides a coherent picture of patterns of influence between data and modeling studies, it is not yet clear how useful predictability can be associated with the global pathways identified in this thesis. To test this question, many more modeling studies can be conceived to put the general findings of this thesis into more specific contexts. Our preliminary work with the regional model RegCM shows that the large-scale environment associated with our precursor generates model rainfall that is consistent with the observations (at least for North Vietnam). This downscaling model also could be combined with a statistical forecast for the boundary conditions. Beyond academic exercises, it can be examined directly the question of whether it can be used in an operational context. The true test of the theory can be deployed to indicate the performance of a statistical model based on our precursors to Vietnam subregions events.

Conclusion & Perspectives en français

Le cycle annuel des précipitations vietnamiennes est fortement conditionné par le système de mousson asiatique. Cependant, la variabilité intrasaisonnière a également une grande amplitude et présente une complexité considérable, avec beaucoup de variations entre les sous-régions du Vietnam. Des études antérieures ont utilisé une variété d'approches pour diagnostiquer les échelles de temps, les modèles et la circulation 3D associée de la VSI des précipitations sous-régionales au Vietnam. Le lien entre la variation intrasaisonnière des précipitations et la divergence des flux d'humidité a également été exploité. Il a été démontré que les variations intrasaisonnières des précipitations au Vietnam sont affectées par des facteurs extratropicaux et tropicaux. Cependant, les résultats sont souvent sensibles au choix des régions, des échelles de temps et des critères de précipitations employés dans le cadre de l'été prolongé. En outre, on a accordé relativement peu d'attention au bilan d'humidité complet. Dans cette étude, notre premier objectif était d'évaluer la contribution des termes du bilan d'humidité aux événements régionaux séparément pour les anomalies de précipitations positives et négatives. Notre deuxième objectif était d'analyser ces événements régionaux opposés, humides et secs, pour identifier les précurseurs dynamiques à grande échelle et leurs voies d'influence. Nous avons accordé une attention particulière à la non-linéarité ou à l'asymétrie de l'influence et nous avons évalué la sensibilité aux choix de la région, du seuil et de la quantité composée. Ceci a conduit à une évaluation qualitative des voies d'influence et des rôles relatifs des influences extratropicales et tropicales.

Pour le premier objectif, nous avons rassemblé des observations composites de signes opposés de précipitations régionales anomales ISV sur le Vietnam en utilisant la convergence du flux d'humidité intégré verticalement comme indicateur des précipitations. Ces composites ont été utilisés comme base d'une étude budgétaire. Pour le second objectif, les mêmes composites ont été appliqués à des précurseurs à plus grande échelle avec des délais plus longs. L'étude observationnelle a été complétée par une modélisation numérique sous la forme d'un ensemble d'expériences de chauffage sur la configuration d'ondes stationnaires de DREAM. Ces expériences ont été employées pour identifier la position d'une source artificielle qui donne le plus d'influence dans un intervalle de 2 semaines. D'autres expériences utilisant le nudging ont ensuite été employées pour simuler les sources réalistes extraites du composite observé. Nous avons ensuite utilisé le R-package de traçage d'ondes de Rossby avec un ensemble d'emplacements, de nombres d'ondes et de directions de latitude moyenne à élevée sur l'hémisphère nord pour tracer la propagation des ondes de Rossby potentielles vers la région cible du Vietnam pour différents états atmosphériques. Enfin, le résultat des expériences de réduction d'échelle avec le modèle régional RegCM4.3 a été examiné, forcé avec les mêmes données ERAi et en utilisant les mêmes composites que dans l'analyse des observations. Le modèle régional a été analysé pour déterminer l'impact du forçage à grande échelle intégré dans les conditions aux limites latérales.

Analyse composite observée

Nous avons d'abord déterminé que la convergence du flux d'humidité verticalement intégré, VIMC, pouvait être utilisée comme un indicateur des précipitations, avec l'avantage supposé d'un lien plus direct entre les précipitations régionales et la dynamique à grande échelle. Le coefficient de corrélation positif élevé entre la convergence du flux d'humidité verticalement intégré et les anomalies de précipitations sur des échelles de temps intrasaisonnières a été confirmé en utilisant l'ensemble de données ERAi 1979-2016 mai-octobre pendant l'été sur les sous-régions du Vietnam. Les événements humides et secs sur trois sous-régions du Vietnam : Nord Vietnam - NVN, Centre Vietnam - CVN et Sud Vietnam - SVN, ont été définis par un indice VIMC quotidien régional avec une valeur seuil. Sur la base de la distribution de fréquence de probabilité de l'indice VIMC, des valeurs seuils de +/-3 mm/jour pour l'indice VIMC régional quotidien ont été choisies.

Le bilan d'humidité associé aux événements pluvieux régionaux a été calculé en incluant quatre termes : VIMC, Pluie, Tendance de la colonne d'humidité verticalement intégrée - TIMC et Evaporation -EVP. Les précipitations sont étroitement liées au VIMC, et ces deux termes dominent le bilan d'humidité par rapport au TIMC et à l'EVP. À l'échelle régionale, les composites à deux semaines de décalage des anomalies de VIMC et de précipitations présentent dans tous les cas un degré raisonnable de symétrie entre les événements humides et secs qui ont une amplitude considérable à différents délais pour les différentes zones. Cependant, cette symétrie n'est pas observée à des échelles plus grandes.

Les composites à deux semaines de décalage de la dynamique à grande échelle associée aux événements régionaux indiquent les précurseurs, les voies possibles et l'asymétrie entre les événements humides et secs. Deux voies d'influence extratropicales et une voie tropicale émergent des composites observés :

+) Voie des hautes latitudes : des configurations barotropes équivalentes quasi-stationnaires à grande échelle se construisent lentement, puis se propagent vers le sud pour influencer la région.

+Trajectoire du jet : le long du jet asiatique, avec des anomalies baroclines de plus petite échelle de signe alternatif, montrant une propagation de groupe vers l'est pour influencer.

+Trajectoire équatoriale : propagation tropicale ondulatoire avec une direction vers l'est.

Les événements humides et secs du NVN sont essentiellement influencés par les extratropiques, les précurseurs provenant d'Europe suivant la trajectoire des hautes latitudes extratropicales dans les événements humides du NVN, mais la trajectoire du jet dans les événements secs du NVN. Les événements NVN Wet sont fortement associés à un anticyclone de Sibérie occidentale et à une dépression sur la Chine, ce qui correspond aux vagues de froid diagnostiquées par Abdillah et al. (2018).

La trajectoire extratropicale suggérée dans le SVN humide et sec est similaire à celle du NVN sec et humide avec des signaux beaucoup plus forts. Cependant, une propagation

asymétrique lente vers l'est n'est observée que dans les événements SVN, qui ressemblent à la MJO (Van Der Linden et al., 2016).

La région CVN est incluse dans cette étude du point de vue d'une région de transition. En fait, deux régimes sont inclus dans notre boîte rectangulaire CVN attribuée à la présence de la chaîne de montagnes Truong son : le Vietnam central réel, du côté est de la boîte, présente un pic de précipitations pendant la saison de la mousson d'hiver, et le Central Highland, du côté sud-ouest, présente un pic de précipitations pendant la mousson d'été. La combinaison de ces deux signaux est nécessairement une moyenne issue de mécanismes distincts.

D'après le composite, les événements humides et secs sur le CVN montrent des anomalies suivant la trajectoire des hautes latitudes dans le flux rotatif extratropical. Ces anomalies ont des signes opposés sur l'Asie occidentale. L'influence tropicale est symétrique entre le Wet et le Dry et prend la forme d'une propagation vers l'est, plus rapide que celle du SVN.

La sensibilité de nos conclusions de l'analyse observationnelle a été examinée en regardant les événements de chevauchement : lorsque les anomalies sur CVN coïncident avec un composite NVN/SVN. Nous avons également diagnostiqué la sensibilité à différents indices hydrologiques qui proviennent de différentes données in-situ.

Lorsque les anomalies sur le CVN sont incluses dans les événements NVN, l'asymétrie entre les événements humides et secs est considérablement réduite. Pour les événements NVN humides qui s'étendent sur le CVN, les précurseurs sont différents, essentiellement au nord du jet asiatique, avec une dépression sibérienne se développant en une structure tripolaire de basse et haute dépression à grande échelle. Lorsque les événements NVN Dry se propagent au CVN, il y a une structure haute-basse-haute à grande échelle sur l'Asie. Pour le SVN se propageant au CVN, les événements humides et secs sont similaires aux événements isolés mais plus forts. Ainsi, les précurseurs à grande échelle sont assez sensibles au choix de l'étendue régionale pour les événements NVN, mais beaucoup moins pour les événements SVN.

Deux ensembles de données pluviométriques in-situ, APHRODITE et VnGP, ont été utilisés pour réaliser des indices hydrologiques alternatifs. Les composites qui en résultent montrent une sensibilité contrastée de la dynamique à grande échelle associée aux événements NVN et SVN. Pour les composites NVN, les flux extratropicaux sont assez cohérents entre les trois indices, et un fort degré de similarité entre APHRO et VnGP. Cependant, les composites SVN sont plus sensibles, et montrent moins de cohérence entre les trois ensembles de données.

Les trois voies d'influence et les précurseurs à distance trouvés à partir du composite observé sont différents entre les régions ainsi qu'entre le sec et l'humide pour une région donnée. Peut-on relier ces précurseurs aux différences entre les événements secs et humides sur les trois sous-régions du Vietnam ? Au-delà de l'étude observationnelle qui a été remarquée, d'autres recherches sur ces voies sont menées en utilisant une approche de modélisation à différentes échelles.

Etude du modèle global et Ray tracing

Un ensemble de 648 expériences a été réalisé avec des sources de chaleur qui agissent comme des sources de vagues artificielles à différents endroits, pour trouver les réponses sur un état de base fixe et ainsi déterminer l'emplacement le plus efficace pour influencer la circulation ultérieure dans les sous-régions du Vietnam. Les réponses du modèle purement dynamique à une source de vague artificielle dans une gamme de 2 semaines sont examinées. Une carte d'influence est produite sur la base de toutes les expériences correspondant à deux régions cibles distinctes : Nord Vietnam - NVN et Sud Vietnam - SVN.

Les sources de chaleur tropicales ont une influence sur le NVN et le SVN dans une limite de 9 jours. Cependant, aucune source extratropicale n'a été trouvée qui puisse influencer le SVN dans une fourchette de 15 jours. Les sources de chaleur extratropicales sur l'Europe peuvent influencer uniquement la circulation NVN après 12 jours, puis les réponses sont renforcées dans les 3 jours suivants. L'identification de la région européenne comme une source probable d'influence du NVN est en accord avec l'analyse composite observée. Les cartes d'influence suggèrent les trains d'ondes extratropicales et les ondes de Kelvin qui ressemblent à certaines des téléconnexions entre la circulation des sous-régions du VN et les sources d'influence éloignées.

Les précurseurs européens associés aux événements NVN et le chemin d'influence sont étudiés plus en détail en appliquant des techniques de nudging sur les états de base de la climatologie estivale. Les précurseurs dérivés d'un composite de 15 jours d'événements NVN humides et secs présentent des schémas dipolaires mais ne sont pas parfaitement symétriques. La réponse du modèle présente deux voies d'influence différentes qui ressemblent à celles des composites observés. Les précurseurs humides de NVN se propagent à des latitudes élevées et se développent ensuite vers le sud-est. Les précurseurs secs NVN se développent en aval le long du jet asiatique. Après 15 jours de fonctionnement, la réponse du modèle est assez similaire aux composites observés au jour 0 pour le NVN sec, mais pas pour le NVN humide.

Sur la configuration stationnaire des ondes de l'état de base de la climatologie estivale, les trajectoires des jets semblent plus reproductibles que celles des hautes latitudes, avec une plus grande amplitude de l'anomalie et une mise en place plus rapide du modèle. La croissance des anomalies le long du jet asiatique montre la croissance d'un mode dynamique qui se développe à partir de l'instabilité barocline. D'après les composites observés, la trajectoire des hautes latitudes ne correspond pas à la réponse du modèle.

Ces précurseurs européens associés aux événements NVN sont étudiés plus en détail en utilisant un ensemble de six états de base à moyenne mensuelle de mai à octobre. Les résultats montrent que la réponse du modèle est très dépendante du jet d'état de base. En particulier, les précurseurs humides des NVN sont plus sensibles à l'état de base. La trajectoire des hautes latitudes est reproduite pour les états de base d'août à octobre, tandis que pour l'état de base de mai, la trajectoire du jet est produite. Les jets atlantiques et asiatiques de l'état de base jouent un rôle dans la détermination des modèles de réponse aux précurseurs humides NVN. Pour le NVN, le modèle répond aux précurseurs secs le long de la trajectoire du jet pour tous

les états de base mais la croissance barocline des anomalies dépend fortement de l'état du jet asiatique. Par conséquent, le chemin des précurseurs européens menant à une influence sur le Vietnam dépend de façon critique de l'interaction entre l'anomalie de la perturbation et l'état du jet.

L'analyse théorique du traçage de rayons d'ondes de Rossby sur l'état de base climatologique, ainsi que d'autres états de base associés à des événements régionaux, révèle des trajectoires à haute latitude qui sont cohérentes avec les composites observés. Les trajectoires à haute latitude émanent de la région Europe-Asie de l'Est. Le nombre d'ondes K=1 prend 2 semaines pour arriver dans la région du Vietnam, tandis que K=2 prend 1 semaine, et K=3 prend 3-4 jours. Les positions des sources d'ondes de Rossby qui influencent les régions du Vietnam dépendent également de l'état de base sur lequel elles se propagent, notamment le nombre d'onde K=2 dans les états humides et secs du NVN et K=3 pour les états du SVN. Un emplacement privilégié pour la propagation des ondes de Rossby vers la région cible du Vietnam est la Mongolie. Le nombre d'onde K=1,3 se propage directement au Vietnam après 1-2 jours, et n'est pas sensible à l'état de base. Cette source directe indique la manière dont les anomalies peuvent se développer le long du jet (trajectoire du jet) et ensuite influencer directement le Vietnam via la propagation des ondes de Rossby.

Downscaling - Etude du modèle régional

La sortie de l'expérience RegCM4 à résolution de 25 km forcée par ERAi de 1979 à 2008, a été utilisée pour assembler un composite. L'indice de réanalyse du chapitre2 a été utilisé pour étudier comment les précipitations du modèle régional sont affectées par les conditions aux limites latérales. Les anomalies des précipitations et d'autres termes du bilan d'humidité : la convergence du flux d'humidité intégré verticalement (VIMC), la tendance de la colonne d'humidité (TIMC) et l'évaporation, ont été calculées pour tester la capacité du modèle à reproduire le bilan d'humidité associé aux événements humides et secs.

Les modèles à grande échelle sur l'Asie du Sud-Est sont bien représentés, en particulier sur le Pacifique Nord-Ouest et le continent maritime. Les modèles de précipitations généralement symétriques sur l'ensemble du domaine sont compatibles avec les forçages symétriques à grande échelle sur le côté nord de la zone. La réplication des précipitations ISV dans la sous-région du Vietnam, comme dans les événements humides et secs de NVN et CVN, est principalement due aux forçages extratropicaux déterminés à partir de la réanalyse ERAi.

Le RegCM4 réussit moins bien à reproduire les anomalies locales de précipitations pour les événements humides et secs du sud du Vietnam et les événements secs sur la CVN. Nous croyons que cela est associé à un manque de signaux équatoriaux, particulièrement au-dessus de la mer de Chine. Il semble que la configuration du modèle ait du mal à simuler la propagation tropicale dans le domaine, en particulier sur la mer de Chine qui est entourée de terres. Une autre interprétation est que l'influence tropicale pourrait être attribuée à la formation d'anomalies pluviométriques locales dans ces cas.

Le VIMC généré par le RegCM4 montre un accord relativement bon avec l'anomalie de

pluie sur les régions océaniques mais exagère sur les zones de haute altitude. Le composite du TIMC montre qu'une atmosphère humide/sèche est associée à des événements humides et secs respectivement. Cependant, les modèles d'anomalie d'évaporation ne sont pas reproduits dans tous les cas. Cela soulève la question de savoir si le modèle peut ou non maintenir la propagation ou même arrêter les ondes transmises dans le domaine.

La reproduction des termes du bilan d'humidité par le RegCM montre une simulation coherent du TIMC pour tous les événements, des modèles de précipitations à grande échelle avec une cohérence avec l'anomalie VIMC, mais l'inversion de l'évaporation pour tous les événements. La région de la mer de Chine montre une absence de signal reproduit par RegCM dans tous les cas et termes. En accord avec Juneng et al. (2016), c'est une région spécifique avec un fort échange air-mer qui joue un rôle important dans la simulation de la propagation des ondes tropicales pour avoir un impact sur les précipitations sur le centre et le sud du Vietnam.

Cette étude de descent d'échelle montre que la dynamique à grande échelle, y compris les influences extratropicales et tropicales, est attribuée différemment aux événements humides et secs sur les sous-régions du Vietnam. Les forçages extratropicaux conduisent à une anomalie de précipitations simulée à grande échelle dans tous les événements. Les simulations des anomalies de précipitations locales sur les événements NVN et CVN humide sont reproduites avec succès, alors que les précipitations locales sur SVN et CVN (sec) ne le sont pas. Cela pourrait être attribué à la capacité du modèle à une simulation de l'importance de la propagation tropicale vers l'est sur SVN et CVN (sec) vue dans le composite de réanalyse. Il est intéressant de noter que la dynamique à grande échelle montre un forçage extratropical plus prédominant dans les événements humides que secs du CVN, alors que ceux-ci sont symétriques à la fois dans le flux rotatif extratropical et le flux divergent tropical.

Perspectives

L'étude des composites observés dans le chapitre 2 pour la variabilité des précipitations sur l'échelle de temps intrasaisonnière dans les sous-régions du Vietnam a été réalisée en tenant compte de la région CVN. Nous avons considéré la CVN comme une zone tampon et l'avons utilisée pour évaluer la sensibilité de nos résultats à l'étendue de nos sous-régions. Comme le montrent de nombreuses études portant spécifiquement sur les mécanismes pluviométriques de la CVN sur des échelles de temps annuelles ou intrasaisonnières, la CVN présente un comportement complexe. La topographie joue un rôle central dans la conduite de deux régimes distincts de précipitations sur les deux moitiés de la boîte CVN. Par conséquent, les précipitations de la CVN devraient être remarquées dans les études futures pour être soigneusement examinées.

Le chapitre 3 montre les différentes simulations avec la configuration d'onde stationnaire qui explorent deux trajectoires extratropicales et les sources d'onde possibles selon deux régions cibles NVN et SVN. Cependant, dans la configuration d'ondes stationnaires, certains processus ne sont pas représentés, comme l'interaction entre le flux transitoire et le flux moyen.

Les systèmes transitoires peuvent avoir un effet modificateur important sur les anomalies à haute latitude. Par conséquent, une modélisation plus poussée pourrait être effectuée pour une étude plus approfondie. Par exemple, nous pouvons utiliser la configuration DREAM - GCM qui contient les forçages empiriques GCM dérivés de l'ensemble des données ERAi sur 38 ans. Le forçage du GCM peut être soit un forçage saisonnier constant, soit un cycle annuel. L'examen du biais induit par l'observation pourrait se faire par le biais de longs integrations de GCM utilisant les composites d'états atmosphériques conduisant à des conditions humides ou sèches sur des sous-régions données du Vietnam.

L'étude du chapitre 3 est limitée au cœur dynamique sec du modèle. Mais les événements étudiés comprennent des processus qui pourraient être fortement modulés par la dynamique humide, comme les ondes tropicales. En effet, la propagation tropicale vers l'est observée dans les événements SVN est beaucoup plus lente qu'une onde tropicale pure. L'humidité pourrait ralentir la propagation des ondes équatoriales comme cela a été rapporté pour les ondes équatoriales couplées par convection étudiées par Wheeler and Kiladis (1999); Kiladis et al. (2009). Nous pouvons donc effectuer des recherches plus approfondies en utilisant le mode humide dans DREAM en comparaison avec le mode sec, ou même en utilisant le modèle humide pour prédire directement les précipitations sur la région du Vietnam.

Une autre possibilité qui mérite d'être explorée est qu'il pourrait y avoir une interaction entre les précurseurs, plutôt qu'un seul précurseur, qui peut influencer une région cible. Les précurseurs humides du NVN montrent une voie d'influence à haute latitude dans l'expérience de nudging qui est similaire à la propagation des anomalies à haute latitude, mais qui ne se traduit pas par une réponse locale du modèle pour les événements humides du NVN. Ainsi, une combinaison de précurseurs pourrait moduler la voie d'influence dans les expériences de nudging. En particulier, le développement des anomalies européennes est fortement associé à la persistance de l'anticyclone sibérien deux semaines avant les événements NVN réels.

L'étude de réduction d'échelle présentée au chapitre 4 suggère que la propagation tropicale est mal simulée par RegCM4. D'autres études pourraient être entreprises, notamment un examen de la capacité du modèle à simuler la propagation des ondes tropicales. Par exemple, la simulation correcte de la MJO est considérée comme un facteur important dans les précipitations SVN et CVN (Van Der Linden et al., 2016), et cela peut être examiné en utilisant les indices fournis par la NOAA pour assembler différents composites de phase. D'autres ondes tropicales telles que les ondes de Kelvin ou les ondes de Rossby équatoriales pourraient également être étudiées de cette manière. Compte tenu de l'absence de couplage air-mer dans le modèle suggéré par Juneng et al. (2016), le modèle couplé atmosphère-océan pourrait faire l'objet d'une recherche prometteuse. Le modèle RegCM4 pourrait être couplé à un modèle océanique afin de représenter explicitement les échanges de chaleur qui ne sont normalement pas pris en compte dans les modèles atmosphériques. Une autre perspective pour les travaux sur le RegCM4 est de modifier le domaine du modèle afin qu'il puisse être spécifiquement conçu pour une étude du climat du Viêt Nam avec un réglage fin des paramètres pour optimiser la fidélité de la simulation des précipitations dans la région.

Dans cette thèse, l'approche a consisté à partir de l'observation pour aboutir à une modélisation qui a produit de nombreux résultats ; et certains résultats ont été difficiles à interpréter.

Beaucoup de matériel a été produit et tout n'a pas été inclus dans ce manuscrit. En cours de route, mon appréciation des régimes pluviométriques vietnamiens et des dynamiques multi-échelles associées a évolué, non seulement en termes de compréhension scientifique, mais aussi en termes de communication de résultats parfois complexes et nuancés.

Trois approches fondamentalement différentes ont été adoptées dans cette thèse : une analyse observationnelle, une étude dynamique à grande échelle et une modélisation régionale. Bien qu'ils aient été présentés en série, les travaux ont été menés en parallèle. Il est remarquable de constater que les trois approches racontent une histoire cohérente sur les causes lointaines et les effets régionaux et locaux, depuis les précurseurs composites jusqu'aux vagues à l'échelle mondiale et à l'hydrologie régionale à l'échelle intrasaisonnière.

Cependant, les deux approches sont décrites comme étant sensibles aux ensembles de données, à la définition de l'indice, à la méthodologie et aux variations au sein de la saison. En particulier, si nous limitons les données pour nous concentrer sur des phénomènes individuels ou des sous-saisons, nos résultats deviendront moins généralement applicables et perdront de leur importance. L'analyse sous-saisonnière est problématique car nous pouvons perdre la distinction entre l'échelle de temps du phénomène et la période de l'ensemble de données.

Outre une image cohérente des modèles d'influence entre les données et les études de modélisation, il n'est pas encore clair dans quelle mesure une prévisibilité utile peut être associée aux voies globales identifiées dans cette thèse. Pour répondre à cette question, de nombreuses autres études de modélisation peuvent être conçues pour placer les résultats généraux de cette thèse dans des contextes plus spécifiques. Notre travail préliminaire avec le modèle régional RegCM montre que l'environnement à grande échelle associé à notre précurseur génère des précipitations modélisées qui sont cohérentes avec les observations (au moins pour le nord du Vietnam). Ce modèle de descente d'échelle pourrait également être combiné avec une prévision statistique des conditions aux limites. Au-delà des exercices académiques, il est possible d'examiner directement la question de savoir s'il peut être utilisé dans un contexte opérationnel. Le véritable test de la théorie peut être déployé pour indiquer la performance d'un modèle statistique basé sur nos précurseurs des événements des sous-régions du Vietnam.

Appendix A

Moisture budget

Our inferences about anomalous rainfall events start with a consideration of the regional moisture budget. Conservation of water in the atmosphere which can be expressed in sigma coordinates as shown by Banacos and Schultz (2005) - Eq. 4.2. The source, expressed as evaporation minus precipitation, balances the tendency of the moisture column (TMC) and the VIMC over a given area. Temporal variations in VIMC may present a reasonable proxy to investigate directly the link between the hydrological cycle and the associated large scale circulation as in Sohn et al. (2004). For example, the VIMC shows a high positive correlation with the daily rainfall over Thailand (Chansaengkrachang et al., 2018).

$$\frac{1}{g}\int \frac{dq}{dt}d\sigma + \frac{1}{g}\int \bigtriangledown(q.V)d\sigma = E - P \tag{4.2}$$

$$TMC - VIMC = E - P \tag{4.3}$$

with

$$TMC = \frac{1}{g}\int \frac{dq}{dt}d\sigma \;\; and \;\; VIMC = -\frac{1}{g}\int \bigtriangledown(q.V)d\sigma \tag{4.4}$$

Fig. 4.28 shows the growth of the four terms in the moisture budget for each regional composite from day-9 to day-0. The dominant terms in all cases are the growing anomalies of VIMC and PPT. Although the two are well correlated in time before day-3, there is some discrepancy between them, likely arising from different discretisation on horizontal grids and integration in sigma coordinates in the presence of topography.

Growth rates of VIMC appear symmetrical between Wet and Dry events for all regions, while the PPT rate departs from symmetry for NVN and CVN. The growth rate of VIMC is highest prior to CVN Wet, but the growth rate of precipitation is highest over NVN Wet. For Dry events, both VIMC and PPT generally have a higher growth rate over NVN than others. The growth of spatial patterns of VIMC and PPT will be presented in the next section.

Prior to Wet events, there is a moistening of the atmosphere as the TMC increases, and a reduction in EVP. The reverse is seen for Dry events. These two terms remain small but not negligible compared to PPT and VIMC, and even compared to the budget residual at the time of an event. Again we see asymmetrical growth for these terms prior to Wet and Dry events over one region, as well as differences between regions.

For Wet events, the TMC develops slightly differently between the regions. It generally increases over SVN and CVN from day-9 to day-0, while it peaks at day-3 prior to NVN

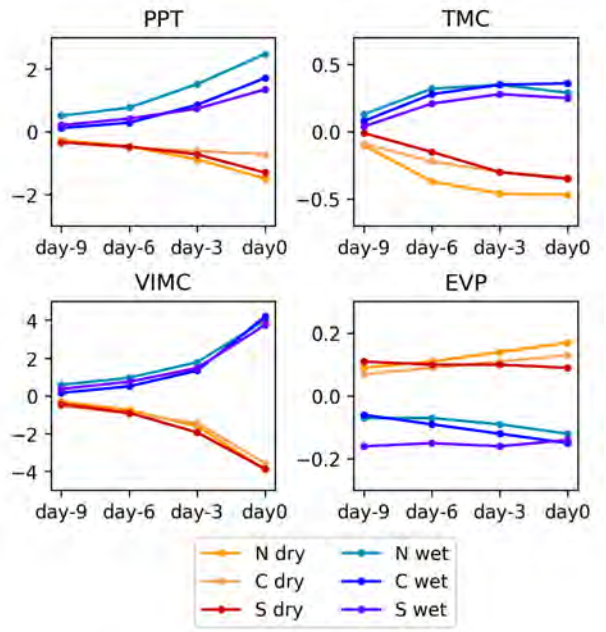

Figure 4.28: Moisture budget components: Precipitation (PPT), Vertically Integrated Moisture Flux Convergence (VIMC), Tendency of Moisture Column (TMC) and Evaporation (EVP) of Wet and Dry events averaged over NVN, CVN and SVN at lagged day -9, -6, -3 and 0.

Wet. The growth rate of TMC is highest in CVN Wet, followed by SVN and NVN Wet. SVN Wet follows with a drier atmosphere prior to day-9 where TMC is nearly zero. For Dry events, TMC generally decreases over all regions from day-9 to day-0. In NVN it decreases sharply from day-9 with the highest rate, but in CVN it develops more gradually. In SVN, as for the Wet events, there is again a zero-starting point on day-9. Although the TMC contributes a minor part (approximately 10%) of the moisture budget, it may still be an important contributor to asymmetries in rainfall patterns between Wet and Dry events as the drying or moistening of the atmosphere are not the same between Wet and Dry events in all regions.

EVP anomalies are negative for Wet events and positive for Dry events over all regions and are mostly symmetrical. The EVP develops gradually in NVN and CVN Wet and Dry events. For SVN, there are higher levels of anomalous EVP at day-15 compared to the others in both Wet and Dry events (not shown). These remain negative/positive prior to Wet/Dry events throughout the two weeks, especially remaining stable from day-9 to day-0.

ENSO effects

The composite of rainfall and VIMC anomalies associated with the Wet and Dry events in NVN and SVN including/excluding the ENSO months based on MEI bimonthly index are

presented in Fig 4.29-4.32. There is a small effect of ENSO on the composite of rainfall in both NVN and SVN events. The less spatial extension of the wet area is shown in the Wet composite by including ENSO, while the less dry area is found in Dry composites. The ENSO show more impact in NVN wet and SVN dry composite. Particularly the anomaly over Western Pacific disappear with the presence of ENSO which could be attributed to the distinction between NVN and other regions. Thus, ENSO should be removed to investigate purely dynamical influences on rainfall ISV over the Vietnam subregion.

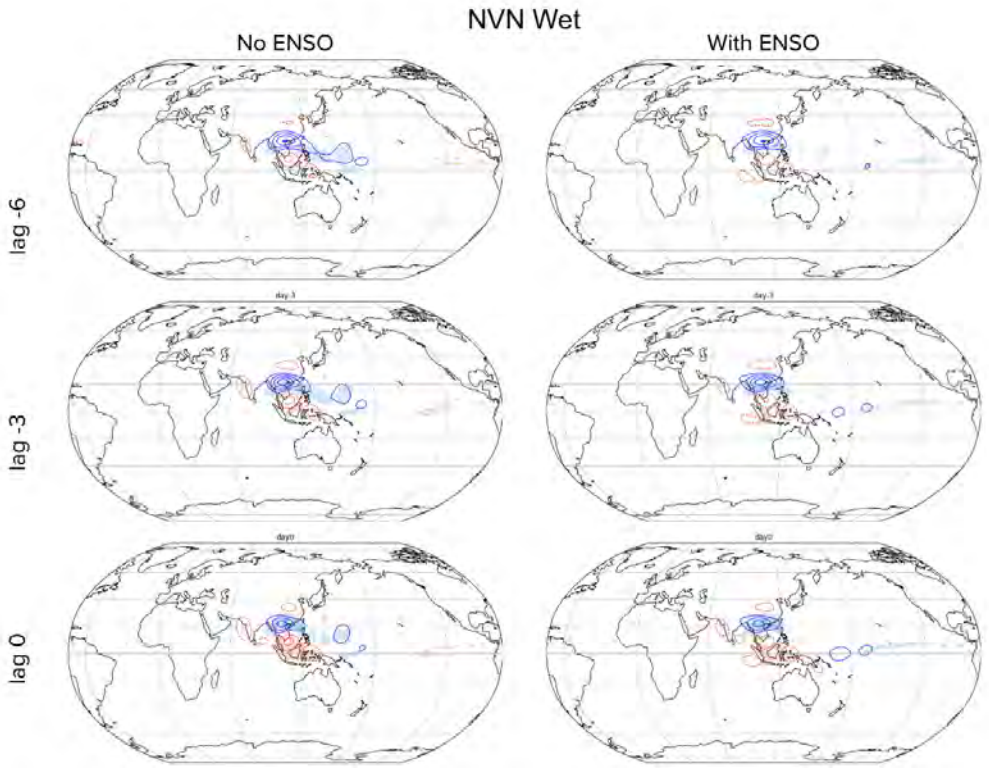

Figure 4.29: Composite of rainfall and VIMC anomaly associated with NVN Wet events. Left is excluded ENSO events by excluding the bimonthly MEI index in the data. Right is composite retaining ENSO. As shown in Fig 6 in submitted paper 2.2.3.

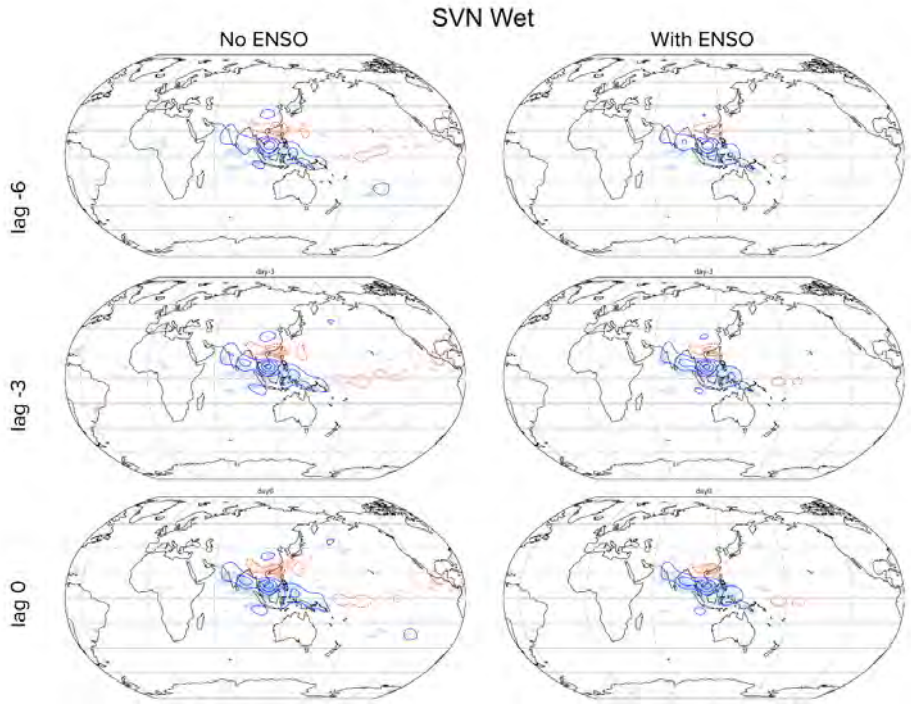

Figure 4.30: As Fig 4.29 but for SVN Wet.

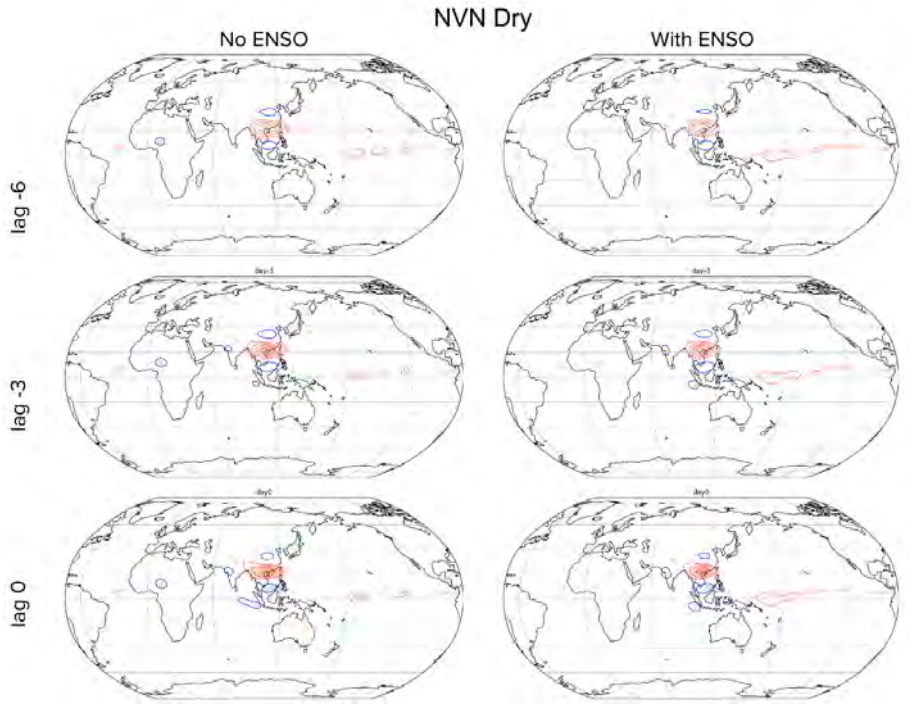

Figure 4.31: As Fig 4.29 but for NVN Dry.

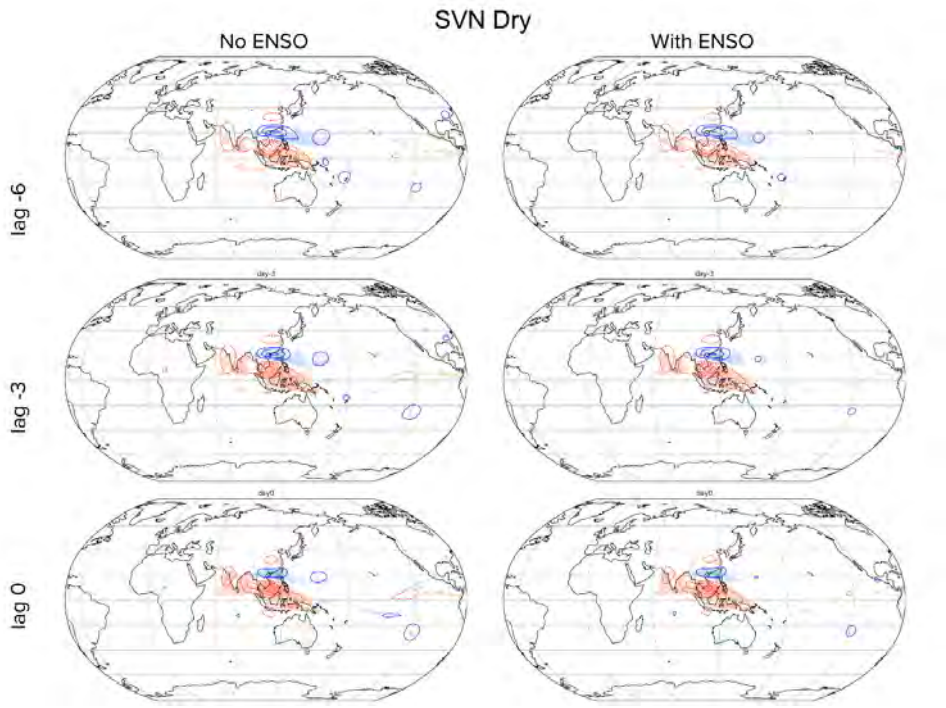

Figure 4.32: As Fig 4.29 but for SVN Dry.

Appendix B

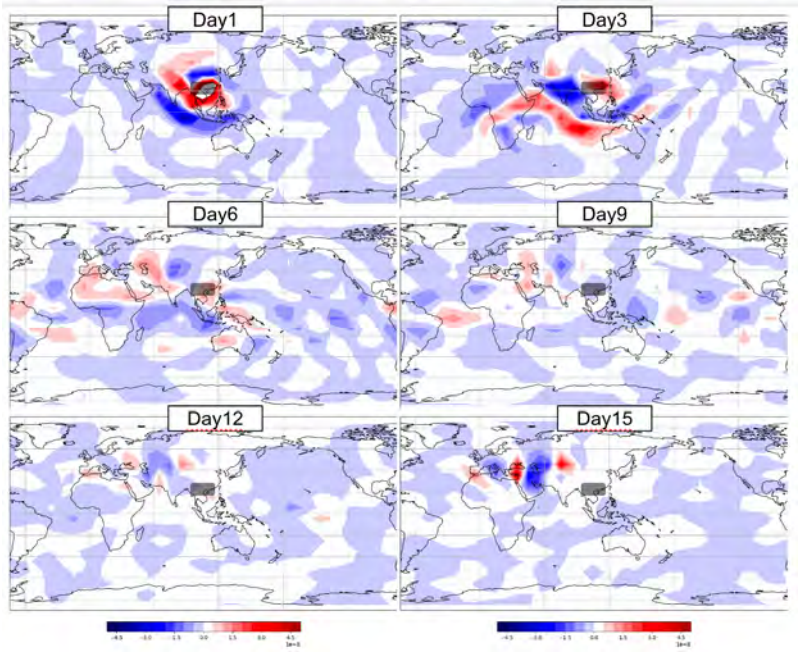

Figure 4.33: The influence function map on divergence at 250mb over NVN. As in Fig 3.9.

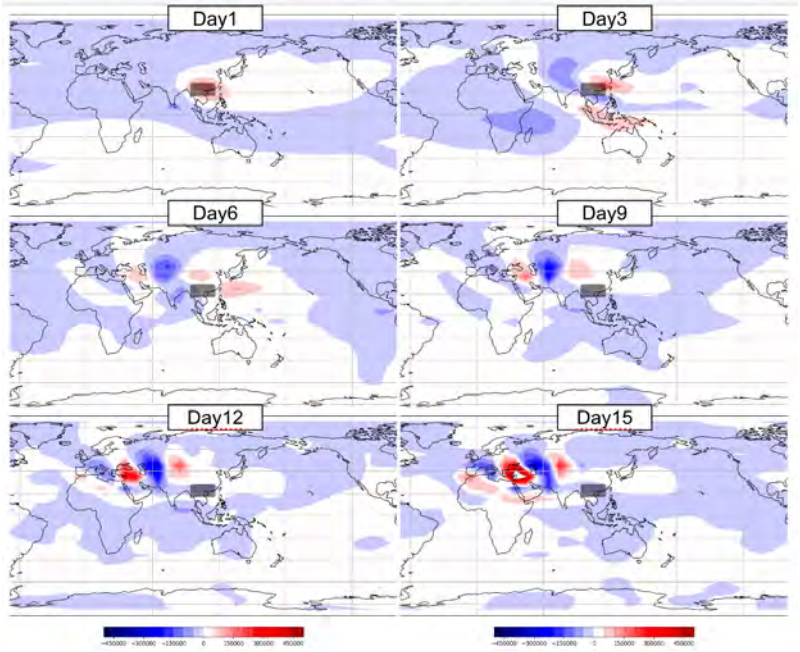

Figure 4.34: The influence function map on streamfunction at 250mb over NVN. As in Fig 3.9.

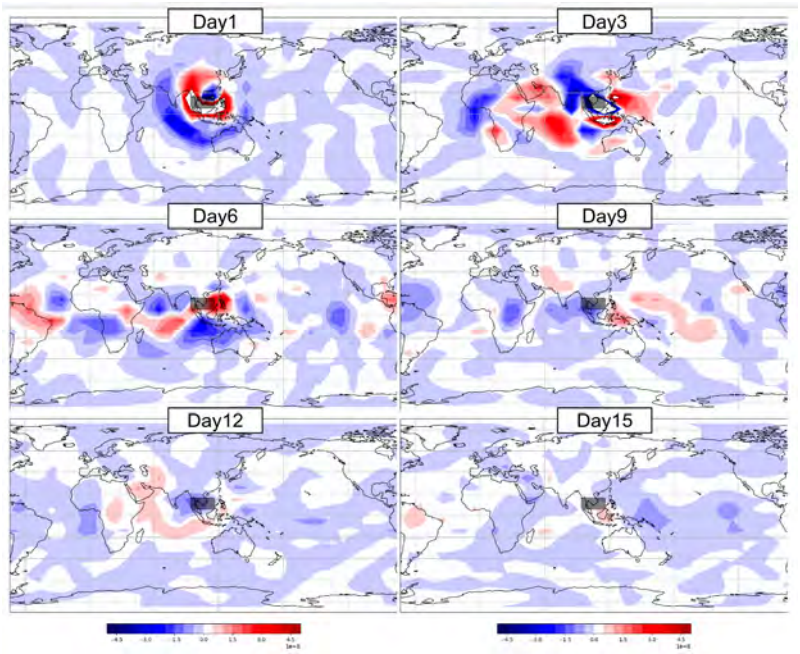

Figure 4.35: The influence function map on divergence at 250mb over SVN. As in Fig 3.9.

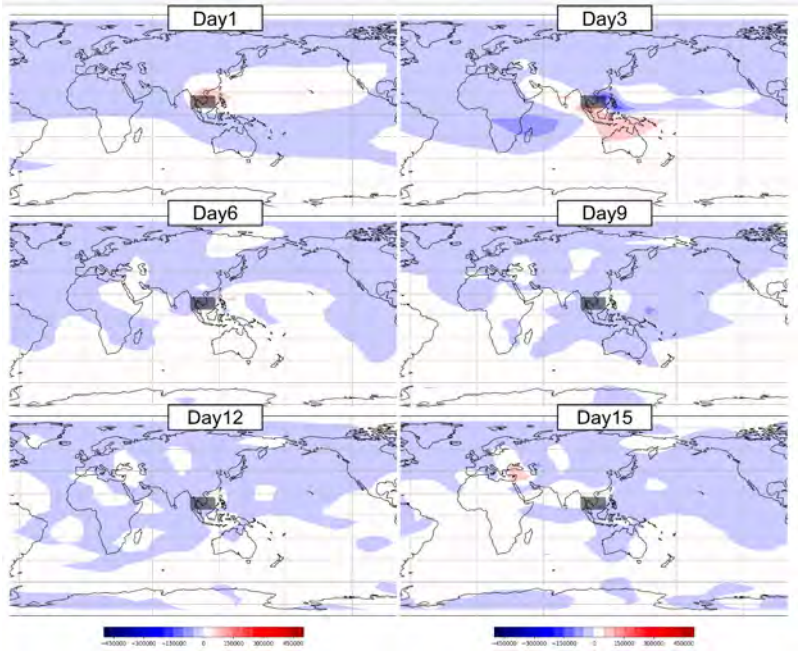

Figure 4.36: The influence function map on streamfunction at 250mb over SVN. As in Fig 3.9.

Appendix C

Summerize calculation in Hoskins and Ambrizzi 1993 for Rossby wave tracing:

On a basic state, the zonal wind brings the expression of dispersion relation for barotropic Rossby wave perturbation to a westerly flow $\bar{U}$:

(1):

$$\omega = \bar{U}k - \frac{\beta_* k}{K^2} \tag{4.5}$$

(2) Where:

$$\beta_* = \beta - \frac{\partial^2 \bar{U}}{\partial y^2} \tag{4.6}$$

β_* is the meridional gradient of absolute vorticity and$K = (k^2 + l^2)^{0.5}$ is the total wave number. The vector group velocity is:

(3)

$$c_g = (u_g, v_g) = (\frac{\partial \omega}{\partial k}, \frac{\partial \omega}{\partial l}) = (c, 0) + (\frac{2\beta_*}{K^2}) cos\alpha \hat{K} \tag{4.7}$$

where $c = \omega/k$ is the eastward phase speed, $\hat{K}$ is the unit vector normal to the wave crests and troughs with a positive eastward component and α is the angle this vector makes with the eastward direction.

For Stationary Rossby waves $\omega = 0$ and $c = 0$ (4)

$$K = K_s = (\frac{\beta_*}{\bar{U}})^{0.5} \tag{4.8}$$

K_s is possible if the flow is westerly $\bar{U}$ is positive, and β_* is positive. From (3) and (4), we have:

(5)

$$\mathbf{c_g} = c_g \hat{K} \tag{4.9}$$

where $c_g = 2\bar{U} cos\alpha$.

Considering in a 2D field, the basic flow varies slowly in latitude compared with the scale of the waves, thus the wavenumber in x-axis - k - is constants but in the y-axis, the wavenumber

- l - varies but followed the local dispersion relation:

$$k = const$$
$$k^2 + l^2 = K_s^2$$

The α is: $tan\alpha = \frac{l}{k}$

The k and l changes:

$$\frac{d_g k}{dt} = 0$$
$$\frac{d_g l}{dt} = \frac{K_s}{l}$$
$$\frac{d_g K_s}{dt} = \frac{K_s}{l} v_g \frac{dK_s}{dy}$$

From (5) we have $v_g/l = c_g/K_s$, so

$$\frac{d_g l}{dt} = c_g \frac{dK_s}{dy} \tag{4.10}$$

Then the bending of the ray is as followed:

$$\frac{d_g tan\alpha}{dt} = (1/k) c_g \frac{dK_s l}{dy} \tag{4.11}$$

or

$$\frac{d_g \alpha}{dt} = \frac{k}{K_s^2} c_g \frac{dK_s l}{dy} \tag{4.12}$$

In Mecator coordinate, the calculation is presented in Karoly 1981 as below:

$$x = a\lambda$$
$$y = aln(1 + sin\theta)/cos\theta$$

where λ is longitude, θ latitude and a radius of the Earth. Then the Laplacian is:

$$\nabla^2 = \frac{1}{cos^2\theta} \left(\frac{\partial^2}{\partial x^2} + \frac{\partial^2}{\partial y^2} \right) = \frac{\nabla_M^2}{cos^2\theta} \tag{4.13}$$

And the velocity in the Mercator projection is $V_M = (u_M, v_M) = v/cos\theta$ The equation for

the horizontal streamfuntion ψ takes the form:

$$\left(\frac{\partial}{\partial t} + u_M \frac{\partial}{\partial x} + v_M \frac{\partial}{\partial y}\right)\left(\frac{\nabla_M^2 \psi}{cos^2\theta}\right) + \frac{2\Omega cos^2\theta}{a}\left(\frac{1}{cos^2\theta}\frac{\partial \psi}{\partial x}\right) = F \tag{4.14}$$

Where Ω is the Earth's rotation rate and F is the forcing of the mean flow.

This equation is linearized about a time-mean basic state, with streamfunction $\bar{\psi}(x, y)$, which is a function of longitude as well as latitude. The equation for the perturbation streamfunction can then be written as:

$$\left(\frac{\partial}{\partial t} + \bar{u}_M \frac{\partial}{\partial x} + \bar{v}_M \frac{\partial}{\partial y}\right) \nabla_M^2 \psi' + \bar{q}_y \psi'_x + \bar{q}_x \psi'_y = 0 \tag{4.15}$$

Where $\bar{q} = \nabla_M^2 \bar{\psi}/cos^2\theta + 2\Omega sin\theta$is the absolute vorticity on the sphere and $\bar{q}_y = \beta_M$. Thus, the dispersion relation obtained is:

$$\omega = \bar{u}_M k + \bar{v}_M l + (\bar{q}_x l - \bar{q}_y k)/K^2 \tag{4.16}$$

Then the group velocity is then:

$$u_g = \bar{u}_M + [(k^2 - l^2)\bar{q}_y - 2kl\bar{q}_x]/K^4$$
$$v_g = \bar{v}_M + [(k^2 - l^2)\bar{q}_x + 2kl\bar{q}_y]/K^4$$

Bibliography

Abdillah, M.R., Kanno, Y., Iwasaki, T., 2018. Tropical–extratropical interactions associated with east asian cold air outbreaks. part ii: Intraseasonal variation. Journal of Climate 31, 473–490.

Abdillah, M.R., Kanno, Y., Iwasaki, T., Matsumoto, J., 2021. Cold surge pathways in east asia and their tropical impacts. Journal of Climate 34, 157–170.

Anthes, R.A., 1977. A cumulus parameterization scheme utilizing a one-dimensional cloud model. Monthly Weather Review 105, 270–286. URL: https://doi.org/10.1175/1520-0493(1977)105<0270:acpsua>2.0.co;2, doi:10.1175/1520-0493(1977)105<0270:acpsua>2.0.co;2.

Banacos, P.C., Schultz, D.M., 2005. The use of moisture flux convergence in forecasting convective initiation: Historical and operational perspectives. Weather and Forecasting 20, 351–366.

BENNETT, J.R., YOUNG, J.A., 1971. THE INFLUENCE OF LATITUDINAL WIND SHEAR UPON LARGE-SCALE WAVE PROPAGATION INTO THE TROPICS. Monthly Weather Review 99, 202–214. URL: https://doi.org/10.1175/1520-0493(1971)099<0202:tiolws>2.3.co;2, doi:10.1175/1520-0493(1971)099<0202:tiolws>2.3.co;2.

Briegleb, B.P., 1992. Delta-eddington approximation for solar radiation in the NCAR community climate model. Journal of Geophysical Research 97, 7603. URL: https://doi.org/10.1029/92jd00291, doi:10.1029/92jd00291.

Chansaengkrachang, K., Luadsong, A., Aschariyaphotha, N., et al., 2018. Vertically integrated moisture flux convergence over southeast asia and its relation to rainfall over thailand. Pertanika J Sci & Technol 26, 235–246.

Charney, J.G., 1969. A further note on large-scale motions in the tropics. Journal of the Atmospheric Sciences 26, 182–185. URL: https://doi.org/10.1175/1520-0469(1969)026<0182:afnols>2.0.co;2, doi:10.1175/1520-0469(1969)026<0182:afnols>2.0.co;2.

Chen, T.C., Yen, M.C., Tsay, J.D., Thanh, N.T.T., Alpert, J., 2012. Synoptic development of the hanoi heavy rainfall event of 30–31 october 2008: Multiple-scale processes. Monthly Weather Review 140, 1219 – 1240. doi:10.1175/MWR-D-11-00111.1.

Cheng, J., Bambrick, H., Yakob, L., Devine, G., Frentiu, F.D., Toan, D.T.T., Thai, P.Q., Xu, Z., Hu, W., 2020. Heatwaves and dengue outbreaks in hanoi, vietnam: New evidence on early warning. PLOS Neglected Tropical Diseases 14, e0007997. URL: https://doi.org/10.1371/journal.pntd.0007997, doi:10.1371/journal.pntd.0007997.

Chow, K.C., Chan, J.C.L., Pal, J.S., Giorgi, F., 2006. Convection suppression criteria applied to the mit cumulus parameterization scheme for simulating the asian summer monsoon. Geophysical Research Letters 33. URL: https://agupubs.onlinelibrary.wiley.com/doi/abs/10.1029/2006GL028026, doi:https://doi.org/10.1029/2006GL028026, arXiv:https://agupubs.onlinelibrary.wiley.com/doi/pdf/10.1029/2006GL028026.

Coelho, C.A.S., Cardoso, D.H.F., Firpo, M.A.F., 2015. Precipitation diagnostics of an exceptionally dry event in são paulo, brazil. Theoretical and Applied Climatology 125, 769–784. URL: https://doi.org/10.1007/s00704-015-1540-9, doi:10.1007/s00704-015-1540-9.

Cruz, F.T., Narisma, G.T., Dado, J.B., Singhruck, P., Tangang, F., Linarka, U.A., Wati, T., Juneng, L., Phan-Van, T., Ngo-Duc, T., Santisirisomboon, J., Gunawan, D., Aldrian, E., 2017. Sensitivity of temperature to physical parameterization schemes of RegCM4 over the CORDEX-southeast asia region. International Journal of Climatology 37, 5139–5153. URL: https://doi.org/10.1002/joc.5151, doi:10.1002/joc.5151.

Davies, H.C., Turner, R.E., 1977. Updating prediction models by dynamical relaxation: an examination of the technique. Quarterly Journal of the Royal Meteorological Society 103, 225–245. URL: https://doi.org/10.1002/qj.49710343602, doi:10.1002/qj.49710343602.

Dee, D.P., Uppala, S.M., Simmons, A.J., Berrisford, P., Poli, P., Kobayashi, S., Andrae, U., Balmaseda, M.A., Balsamo, G., Bauer, P., Bechtold, P., Beljaars, A.C.M., van de Berg, L., Bidlot, J., Bormann, N., Delsol, C., Dragani, R., Fuentes, M., Geer, A.J., Haimberger, L., Healy, S.B., Hersbach, H., Hólm, E.V., Isaksen, L., Kållberg, P., Köhler, M., Matricardi, M., McNally, A.P., Monge-Sanz, B.M., Morcrette, J.J., Park, B.K., Peubey, C., de Rosnay, P., Tavolato, C., Thépaut, J.N., Vitart, F., 2011. The era-interim reanalysis: configuration and performance of the data assimilation system. Quarterly Journal of the Royal Meteorological Society 137, 553–597. doi:https://doi.org/10.1002/qj.828.

Dickinson, M., Molinari, J., 2002. Mixed rossby–gravity waves and western pacific tropical cyclogenesis. part i: Synoptic evolution. Journal of the Atmospheric Sciences 59, 2183–2196. URL: https://doi.org/10.1175/1520-0469(2002)059<2183:mrgwaw>2.0.co;2, doi:10.1175/1520-0469(2002)059<2183:mrgwaw>2.0.co;2.

Dickinson, R., Errico, R., Giorgi, F., Bates, G., 1989. A regional climate model for the western united states. Climatic Change 15. URL: https://doi.org/10.1007/bf00240465, doi:10.1007/bf00240465.

Dickinson, R.E., Henderson-Sellers, A., Kennedy, P.J., . Biosphere-atmosphere transfer scheme (bats) version le as coupled to the ncar community climate model. technical note. [ncar (national center for atmospheric research)] URL: https://www.osti.gov/biblio/5733868.

Eden, J.M., Widmann, M., Maraun, D., Vrac, M., 2014. Comparison of gcm- and rcm-simulated precipitation following stochastic postprocessing. Journal of Geophysical Research: Atmospheres 119, 11,040–11,053. URL: https://agupubs.onlinelibrary.wiley.

com/doi/abs/10.1002/2014JD021732, doi:https://doi.org/10.1002/2014JD021732, arXiv:https://agupubs.onlinelibrary.wiley.com/doi/pdf/10.1002/2014JD021732.

Elvidge, A.D., Renfrew, I.A., 2016. The causes of foehn warming in the lee of mountains. Bulletin of the American Meteorological Society 97, 455 – 466. URL: https://journals.ametsoc.org/view/journals/bams/97/3/bams-d-14-00194.1.xml, doi:10.1175/BAMS-D-14-00194.1.

Emanuel, K.A., 1991. A scheme for representing cumulus convection in large-scale models. Journal of the Atmospheric Sciences 48, 2313–2329. URL: https://doi.org/10.1175/1520-0469(1991)048<2313:asfrcc>2.0.co;2, doi:10.1175/1520-0469(1991)048<2313:asfrcc>2.0.co;2.

Emanuel, K.A., Živković-Rothman, M., 1999. Development and evaluation of a convection scheme for use in climate models. Journal of the Atmospheric Sciences 56, 1766–1782. URL: https://doi.org/10.1175/1520-0469(1999)056<1766:daeoac>2.0.co;2, doi:10.1175/1520-0469(1999)056<1766:daeoac>2.0.co;2.

FAO, 2016. El-niÑo event in viet nam - agriculture, food security and livelihood needs assessment in response to drought and salt water intrusion .

Ferrett, S., Yang, G.Y., Woolnough, S.J., Methven, J., Hodges, K., Holloway, C.E., 2019. Linking extreme precipitation in southeast asia to equatorial waves. Quarterly Journal of the Royal Meteorological Society 146, 665–684. URL: https://doi.org/10.1002/qj.3699, doi:10.1002/qj.3699.

Fink, A., Speth, P., 1997. Some potential forcing mechanisms of the year-to-year variability of the tropical convection and its intraseasonal (25–70-day) variability. International Journal of Climatology 17, 1513–1534. doi:https://doi.org/10.1002/(SICI)1097-0088(19971130)17:14<1513::AID-JOC210>3.0.CO;2-U.

Giorgi, F., 2019. Thirty years of regional climate modeling: Where are we and where are we going next? Journal of Geophysical Research: Atmospheres URL: https://doi.org/10.1029/2018jd030094, doi:10.1029/2018jd030094.

Giorgi, F., Bates, G.T., 1989. The climatological skill of a regional model over complex terrain. Monthly Weather Review 117, 2325–2347. URL: https://doi.org/10.1175/1520-0493(1989)117<2325:tcsoar>2.0.co;2, doi:10.1175/1520-0493(1989)117<2325:tcsoar>2.0.co;2.

Giorgi, F., Bi, X., Pal, J., 2004. Mean, interannual variability and trends in a regional climate change experiment over europe. II: climate change scenarios (2071?2100). Climate Dynamics 23, 839–858. URL: https://doi.org/10.1007/s00382-004-0467-0, doi:10.1007/s00382-004-0467-0.

Giorgi, F., Coppola, E., Solmon, F., Mariotti, L., Sylla, M., Bi, X., Elguindi, N., Diro, G., Nair, V., Giuliani, G., Turuncoglu, U., Cozzini, S., Güttler, I., O'Brien, T., Tawfik, A., Shalaby, A., Zakey, A., Steiner, A., Stordal, F., Sloan, L., Brankovic, C., 2012. RegCM4:

model description and preliminary tests over multiple CORDEX domains. Climate Research 52, 7–29. URL: https://doi.org/10.3354/cr01018, doi:10.3354/cr01018.

Giorgi, F., Marinucci, M.R., Bates, G.T., 1993. Development of a second-generation regional climate model (RegCM2). part i: Boundary-layer and radiative transfer processes. Monthly Weather Review 121, 2794–2813. URL: https://doi.org/10.1175/1520-0493(1993)121<2794:doasgr>2.0.co;2, doi:10.1175/1520-0493(1993)121<2794:doasgr>2.0.co;2.

GIZENERGY.ORG.VN, . Nganh dien o viet nam - http://gizenergy.org.vn/vn/knowledge-resources/power-sector-vietnam .

Grell, G., Dudhia, J., Stauffer, D., 1994. A description of the fifth-generation Penn State/NCAR Mesoscale Model (MM5). Technical Report. URL: http://opensky.ucar.edu/islandora/object/technotes:170, doi:10.5065/D60Z716B.

Grell, G.A., 1993. Prognostic evaluation of assumptions used by cumulus parameterizations. Monthly Weather Review 121, 764–787. URL: https://doi.org/10.1175/1520-0493(1993)121<0764:peoaub>2.0.co;2, doi:10.1175/1520-0493(1993)121<0764:peoaub>2.0.co;2.

GSO.GOV.VN, . Thong cao bao chi tinh hinh lao dong viec lam quy iv 2021 va chi so phat trien con nguoi viet nam 2016-2020 - https://www.gso.gov.vn/du-lieu-va-so-lieu-thong-ke/2022/01/thong-cao-bao-chi-tinh-hinh-lao-dong-viec-lam-quy-iv-nam-2021-va-chi-so-phat-trien-con-nguoi-viet-nam-2016-2020/ .

Hall, N., Leroux, S., 2022. DREAM User Manual: Dynamical Research Empirical Atmospheric Model. URL: https://dream-gcm.github.io/about-the-model/.

Hall, N.M.J., 2000. A simple GCM based on dry dynamics and constant forcing. Journal of the Atmospheric Sciences 57, 1557–1572. URL: https://doi.org/10.1175/1520-0469(2000)057<1557:asgbod>2.0.co;2, doi:10.1175/1520-0469(2000)057<1557:asgbod>2.0.co;2.

Hall, N.M.J., Derome, J., 2000. Transience, nonlinearity, and eddy feedback in the remote response to el niño. Journal of the Atmospheric Sciences 57, 3992–4007. URL: https://doi.org/10.1175/1520-0469(2001)058<3992:tnaefi>2.0.co;2, doi:10.1175/1520-0469(2001)058<3992:tnaefi>2.0.co;2.

Hall, N.M.J., Le, H.H., Leroux, S., 2020. The extratropical response to a developing MJO: forecast and climate simulations with the DREAM model. Climate Dynamics 55, 813–829. URL: https://doi.org/10.1007/s00382-020-05299-y, doi:10.1007/s00382-020-05299-y.

Hall, N.M.J., Thibaut, S., Marchesiello, P., 2016. Impact of the observed extratropics on climatological simulations of the MJO in a tropical channel model. Climate Dynamics 48, 2541–2555. URL: https://doi.org/10.1007/s00382-016-3221-5, doi:10.1007/s00382-016-3221-5.

Herrmann, M., Ngo-Duc, T., Trinh-Tuan, L., 2020. Impact of climate change on sea surface wind in southeast asia, from climatological average to extreme events: results from a dynamical downscaling. Climate Dynamics 54, 2101–2134. URL: https://doi.org/10.1007/s00382-019-05103-6, doi:10.1007/s00382-019-05103-6.

Holloway, C.E., Neelin, J.D., 2009. Moisture vertical structure, column water vapor, and tropical deep convection. Journal of the Atmospheric Sciences 66, 1665 – 1683. URL: https://journals.ametsoc.org/view/journals/atsc/66/6/2008jas2806.1.xml, doi:10.1175/2008JAS2806.1.

Holtslag, A.A.M., Bruijn, E.I.F.D., Pan, H.L., 1990. A high resolution air mass transformation model for short-range weather forecasting. Monthly Weather Review 118, 1561–1575. URL: https://doi.org/10.1175/1520-0493(1990)118<1561:ahramt>2.0.co;2, doi:10.1175/1520-0493(1990)118<1561:ahramt>2.0.co;2.

Hoskins, B.J., Ambrizzi, T., 1993. Rossby wave propagation on a realistic longitudinally varying flow. Journal of the Atmospheric Sciences 50, 1661–1671. URL: https://doi.org/10.1175/1520-0469(1993)050<1661:rwpoar>2.0.co;2, doi:10.1175/1520-0469(1993)050<1661:rwpoar>2.0.co;2.

Hoskins, B.J., Karoly, D.J., 1981. The steady linear response of a spherical atmosphere to thermal and orographic forcing. Journal of the Atmospheric Sciences 38, 1179–1196. URL: https://doi.org/10.1175/1520-0469(1981)038<1179:tslroa>2.0.co;2, doi:10.1175/1520-0469(1981)038<1179:tslroa>2.0.co;2.

Hoskins, B.J., Simmons, A.J., 1975. A multi-layer spectral model and the semi-implicit method. Quarterly Journal of the Royal Meteorological Society 101, 637–655. URL: https://doi.org/10.1002/qj.49710142918, doi:10.1002/qj.49710142918.

Hoskins, B.J., Yang, G.Y., 2000. The equatorial response to higher-latitude forcing. Journal of the Atmospheric Sciences 57, 1197–1213. URL: https://doi.org/10.1175/1520-0469(2000)057<1197:terthl>2.0.co;2, doi:10.1175/1520-0469(2000)057<1197:terthl>2.0.co;2.

Inatsu, M., Kimoto, M., 2009. A scale interaction study on east asian cyclogenesis using a general circulation model coupled with an interactively nested regional model. Monthly Weather Review 137, 2851–2868. URL: https://doi.org/10.1175/2009mwr2825.1, doi:10.1175/2009mwr2825.1.

Jin, F., Hoskins, B.J., 1995. The direct response to tropical heating in a baroclinic atmosphere. Journal of the Atmospheric Sciences 52, 307–319. URL: https://doi.org/10.1175/1520-0469(1995)052<0307:tdrtth>2.0.co;2, doi:10.1175/1520-0469(1995)052<0307:tdrtth>2.0.co;2.

Juneng, L., Tangang, F., Chung, J., Ngai, S., Tay, T., Narisma, G., Cruz, F., Phan-Van, T., Ngo-Duc, T., Santisirisomboon, J., Singhruck, P., Gunawan, D., Aldrian, E., 2016. Sensitivity of southeast asia rainfall simulations to cumulus and air-sea flux parameterizations in RegCM4. Climate Research 69, 59–77. URL: https://doi.org/10.3354/cr01386, doi:10.3354/cr01386.

Karoly, D.J., 1983. Rossby wave propagation in a barotropic atmosphere. Dynamics of Atmospheres and Oceans 7, 111–125. URL: https://doi.org/10.1016/0377-0265(83)90013-1, doi:10.1016/0377-0265(83)90013-1.

Kessler, W.S., McPhaden, M.J., Weickmann, K.M., 1995. Forcing of intraseasonal kelvin waves in the equatorial pacific. Journal of Geophysical Research 100, 10613. URL: https://doi.org/10.1029/95jc00382, doi:10.1029/95jc00382.

Kiehl, J.T., Hack, J.J., Bonan, G.B., Boville, B.A., Williamson, D.L., Rasch, P.J., 1998. The national center for atmospheric research community climate model: Ccm3, journal = Journal of Climate 11, 1131–1149. URL: https://doi.org/10.1175/1520-0442(1998)011<1131:tncfar>2.0.co;2, doi:10.1175/1520-0442(1998)011<1131:tncfar>2.0.co;2.

Kiladis, G.N., Wheeler, M.C., Haertel, P.T., Straub, K.H., Roundy, P.E., 2009. Convectively coupled equatorial waves. Reviews of Geophysics 47. URL: https://agupubs.onlinelibrary.wiley.com/doi/abs/10.1029/2008RG000266, doi:https://doi.org/10.1029/2008RG000266.

Köppen, W., 2011. The thermal zones of the earth according to the duration of hot, moderate and cold periods and to the impact of heat on the organic world - die wärmezonen der erde, nach der dauer der heissen, gemässigten und kalten zeit und nach der wirkung der wärme auf die organische welt betrachtet 1884. Meteorologische Zeitschrift 20, 351–360. URL: http://dx.doi.org/10.1127/0941-2948/2011/105, doi:10.1127/0941-2948/2011/105.

Kucharski, F., Kang, I.S., Straus, D., King, M.P., 2010. Teleconnections in the atmosphere and oceans. Bulletin of the American Meteorological Society 91, 381–383. URL: https://doi.org/10.1175/2009bams2834.1, doi:10.1175/2009bams2834.1.

Laing, A., Evans, J.L., 2011. Introduction to Tropical Meteorology 2nd Edition: A Comprehensive Online Print Textbook Version 2.0. The COMET Program.

Laprise, R., de Elía, R., Caya, D., Biner, S., Lucas-Picher, P., Diaconescu, E., Leduc, M., Alexandru, A., and, L.S., 2008. Challenging some tenets of regional climate modelling. Meteorology and Atmospheric Physics 100, 3–22. URL: https://doi.org/10.1007/s00703-008-0292-9, doi:10.1007/s00703-008-0292-9.

Lau, K.M., Kim, K.M., Yang, S., 2000. Dynamical and boundary forcing characteristics of regional components of the asian summer monsoon. Journal of Climate 13, 2461 – 2482. URL: https://journals.ametsoc.org/view/journals/clim/13/14/1520-0442_2000_013_2461_dabfco_2.0.co_2.xml, doi:10.1175/1520-0442(2000)013<2461:DABFCO>2.0.CO;2.

Lau, W.K.M., Waliser, D.E., 2011. Intraseasonal Variability in the Atmosphere-Ocean Climate System. 2 ed., Springer Berlin, Heidelberg.

Li, B., Clarke, A.J., 1994. An examination of some enso mechanisms using interannual sea level at the eastern and western equatorial boundaries and the zonally averaged equatorial

wind. Journal of Physical Oceanography 24, 681 – 690. URL: https://journals.ametsoc.org/view/journals/phoc/24/3/1520-0485_1994_024_0681_aeosem_2_0_co_2.xml, doi:10.1175/1520-0485(1994)024<0681:AEOSEM>2.0.CO;2.

Li, X., Gollan, G., Greatbatch, R.J., Lu, R., 2018. Intraseasonal variation of the east asian summer monsoon associated with the madden–julian oscillation. Atmospheric Science Letters 19, e794. URL: https://rmets.onlinelibrary.wiley.com/doi/abs/10.1002/asl.794, doi:https://doi.org/10.1002/asl.794, arXiv:https://rmets.onlinelibrary.wiley.com/doi/pdf/10.1002/asl.794.

Liebmann, B., Hendon, H.H., Glick, J.D., 1994. The relationship between tropical cyclones of the western pacific and indian oceans and the madden-julian oscillation. Journal of the Meteorological Society of Japan. Ser. II 72, 401–412. doi:10.2151/jmsj1965.72.3_401.

Lin, H., Brunet, G., 2018. Extratropical response to the MJO: Nonlinearity and sensitivity to the initial state. Journal of the Atmospheric Sciences 75, 219–234. URL: https://doi.org/10.1175/jas-d-17-0189.1, doi:10.1175/jas-d-17-0189.1.

van der Linden, R., Fink, A.H., Phan-Van, T., Trinh-Tuan, L., 2016. Synoptic-dynamic analysis of early dry-season rainfall events in the vietnamese central highlands. Monthly Weather Review 144, 1509 – 1527. doi:10.1175/MWR-D-15-0265.1.

Lorenz, P., Jacob, D., 2005. Influence of regional scale information on the global circulation: A two-way nesting climate simulation. Geophysical Research Letters 32, n/a–n/a. URL: https://doi.org/10.1029/2005gl023351, doi:10.1029/2005gl023351.

Luca, A.D., de Elía, R., Laprise, R., 2011. Potential for added value in precipitation simulated by high-resolution nested regional climate models and observations. Climate Dynamics 38, 1229–1247. URL: https://doi.org/10.1007/s00382-011-1068-3, doi:10.1007/s00382-011-1068-3.

Madden, R.A., Julian, P.R., 1972. Description of global-scale circulation cells in the tropics with a 40–50 day period. Journal of Atmospheric Sciences 29, 1109 – 1123. doi:10.1175/1520-0469(1972)029<1109:DOGSCC>2.0.CO;2.

Mapes, B., Tulich, S., Lin, J., Zuidema, P., 2006. The mesoscale convection life cycle: Building block or prototype for large-scale tropical waves? Dynamics of Atmospheres and Oceans 42, 3–29. URL: https://www.sciencedirect.com/science/article/pii/S0377026506000340, doi:https://doi.org/10.1016/j.dynatmoce.2006.03.003. atmospheric Convection and Wave Interactions (title for cover spine) Atmospheric Convection and Wave Interactions: Convective Life Cycles and Scale Interactions in Tropical Waves (title for Special Issue title page).

Marbaix, P., Gallée, H., Brasseur, O., van Ypersele, J.P., 2003. Lateral boundary conditions in regional climate models: A detailed study of the relaxation procedure. Monthly Weather Review 131, 461–479. URL: https://doi.org/10.1175/1520-0493(2003)131<0461:lbcirc>2.0.co;2, doi:10.1175/1520-0493(2003)131<0461:lbcirc>2.0.co;2.

Matsuno, T., 1966. Quasi-geostrophic motions in the equatorial area. Journal of the Meteorological Society of Japan. Ser. II 44, 25–43. URL: https://doi.org/10.2151/jmsj1965.44.1_25, doi:$10.2151/jmsj1965.44.1_25$.

Ngo-Duc, T., Tangang, F.T., Santisirisomboon, J., Cruz, F., Trinh-Tuan, L., Nguyen-Xuan, T., Phan-Van, T., Juneng, L., Narisma, G., Singhruck, P., Gunawan, D., Aldrian, E., 2016. Performance evaluation of RegCM4 in simulating extreme rainfall and temperature indices over the CORDEX-southeast asia region. International Journal of Climatology 37, 1634–1647. URL: https://doi.org/10.1002/joc.4803, doi:10.1002/joc.4803.

Nguyen, D.Q., Renwick, J., McGregor, J., 2014. Variations of surface temperature and rainfall in vietnam from 1971 to 2010. International Journal of Climatology 34, 249–264.

Nguyen, P.L., Bador, M., Alexander, L.V., Lane, T.P., Ngo-Duc, T., 2022. More intense daily precipitation in CORDEX-SEA regional climate models than their forcing global climate models over southeast asia. International Journal of Climatology 42, 6537–6561. URL: https://doi.org/10.1002/joc.7619, doi:10.1002/joc.7619.

Nguyen-Le, D., Matsumoto, J., Ngo-Duc, T., 2014. Climatological onset date of summer monsoon in vietnam. International Journal of Climatology 34, 3237–3250. doi:https://doi.org/10.1002/joc.3908.

Pal, J.S., Giorgi, F., Bi, X., Elguindi, N., Solmon, F., Gao, X., Rauscher, S.A., Francisco, R., Zakey, A., Winter, J., Ashfaq, M., Syed, F.S., Bell, J.L., Diffenbaugh, N.S., Karmacharya, J., Konaré, A., Martinez, D., da Rocha, R.P., Sloan, L.C., Steiner, A.L., 2007. Regional climate modeling for the developing world: The ictp regcm3 and regcnet. Bulletin of the American Meteorological Society 88, 1395 – 1410. URL: https://journals.ametsoc.org/view/journals/bams/88/9/bams-88-9-1395.xml, doi:10.1175/BAMS-88-9-1395.

Pal, J.S., Small, E.E., Eltahir, E.A.B., 2000. Simulation of regional-scale water and energy budgets: Representation of subgrid cloud and precipitation processes within RegCM. Journal of Geophysical Research: Atmospheres 105, 29579–29594. URL: https://doi.org/10.1029/2000jd900415, doi:10.1029/2000jd900415.

Rehbein, A., Ambrizzi, T., Ibarra-Espinosa, S., Dutra, L.M.M., 2020. raytracing: An R package for identification and tracking the atmospheric Rossby waves. URL: https://github.com/salvatirehbein/raytracing.

Roca, R., Alexander, L.V., Potter, G., Bador, M., Jucá, R., Contractor, S., Bosilovich, M.G., Cloché, S., 2019. Frogs: a daily 1x1 gridded precipitation database of rain gauge, satellite and reanalysis products. Earth System Science Data 11, 1017–1035. doi:10.5194/essd-11-1017-2019.

Roundy, P.E., 2008. Analysis of convectively coupled kelvin waves in the indian ocean mjo. Journal of the Atmospheric Sciences 65, 1342 – 1359. URL: https://journals.ametsoc.org/view/journals/atsc/65/4/2007jas2345.1.xml, doi:10.1175/2007JAS2345.1.

Simmons, A.J., Burridge, D.M., 1981. An energy and angular-momentum conserving vertical finite-difference scheme and hybrid vertical coordinates. Monthly Weather Review 109,

758–766. URL: https://doi.org/10.1175/1520-0493(1981)109<0758:aeaamc>2.0.co;2, doi:10.1175/1520-0493(1981)109<0758:aeaamc>2.0.co;2.

Smith, E.T., Sheridan, S.C., 2020. Where do cold air outbreaks occur, and how have they changed over time? Geophysical Research Letters 47. URL: https://doi.org/10.1029/2020gl086983, doi:10.1029/2020gl086983.

Sohn, B.J., Smith, E.A., Robertson, F.R., Park, S.C., 2004. Derived over-ocean water vapor transports from satellite-retrieved e-p datasets. Journal of Climate 17, 1352 – 1365. doi:10.1175/1520-0442(2004)017<1352:DOWVTF>2.0.CO;2.

Stan, C., Straus, D.M., Frederiksen, J.S., Lin, H., Maloney, E.D., Schumacher, C., 2017. Review of tropical-extratropical teleconnections on intraseasonal time scales. Reviews of Geophysics 55, 902–937. URL: https://doi.org/10.1002/2016rg000538, doi:10.1002/2016rg000538.

Takasuka, D., Satoh, M., 2020. Dynamical roles of mixed rossby–gravity waves in driving convective initiation and propagation of the madden–julian oscillation: General views. Journal of the Atmospheric Sciences 77, 4211–4231. URL: https://doi.org/10.1175/jas-d-20-0050.1, doi:10.1175/jas-d-20-0050.1.

Takaya, K., Nakamura, H., 2005. Mechanisms of intraseasonal amplification of the cold siberian high. Journal of the Atmospheric Sciences 62, 4423–4440. URL: https://doi.org/10.1175/jas3629.1, doi:10.1175/jas3629.1.

Tangang, F., Chung, J.X., Juneng, L., Supari, Salimun, E., Ngai, S.T., Jamaluddin, A.F., Mohd, M.S.F., Cruz, F., Narisma, G., Santisirisomboon, J., Ngo-Duc, T., Tan, P.V., Singhruck, P., Gunawan, D., Aldrian, E., Sopaheluwakan, A., Grigory, N., Remedio, A.R.C., Sein, D.V., Hein-Griggs, D., McGregor, J.L., Yang, H., Sasaki, H., Kumar, P., 2020. Projected future changes in rainfall in southeast asia based on CORDEX–SEA multi-model simulations. Climate Dynamics 55, 1247–1267. URL: https://doi.org/10.1007/s00382-020-05322-2, doi:10.1007/s00382-020-05322-2.

Tangang, F.T., Juneng, L., Salimun, E., Vinayachandran, P.N., Seng, Y.K., Reason, C.J.C., Behera, S.K., Yasunari, T., 2008. On the roles of the northeast cold surge, the borneo vortex, the madden-julian oscillation, and the indian ocean dipole during the extreme 2006/2007 flood in southern peninsular malaysia. Geophysical Research Letters 35. doi:https://doi.org/10.1029/2008GL033429.

Taylor, K.E., Stouffer, R.J., Meehl, G.A., 2012. An overview of CMIP5 and the experiment design. Bulletin of the American Meteorological Society 93, 485–498. URL: https://doi.org/10.1175/bams-d-11-00094.1, doi:10.1175/bams-d-11-00094.1.

Tibay, J., Cruz, F., Tangang, F., Juneng, L., Ngo-Duc, T., Phan-Van, T., Santisirisomboon, J., Singhruck, P., Gunawan, D., Aldrian, E., Narisma, G.T., 2021. Climatological characterization of tropical cyclones detected in the regional climate simulations over the CORDEX-SEA domain. International Journal of Climatology 41, 4236–4252. URL: https://doi.org/10.1002/joc.7070, doi:10.1002/joc.7070.

Tran, M.C., 2005. Khi tuong va Khi hau dai cuong - Vietnamese. Nxb ĐHQGHN.

Truong, N.M., Tuan, B.M., 2018. Large-scale patterns and possible mechanisms of 10–20-day intra-seasonal oscillation of the observed rainfall in vietnam. International Journal of Climatology 38, 3801–3821.

Truong, N.M., Tuan, B.M., 2019. Structures and mechanisms of 20–60-day intraseasonal oscillation of the observed rainfall in vietnam. Journal of Climate 32, 5191–5212.

Tuan, B.M., 2019. Extratropical forcing of submonthly variations of rainfall in vietnam. Journal of Climate 32, 2329–2348.

USGS.GOV, . The atmosphere and the water cycle - https://www.usgs.gov/special-topics/water-science-school/science/atmosphere-and-water-cycle .

Van Der Linden, R., Fink, A.H., Pinto, J.G., Phan-Van, T., Kiladis, G.N., 2016. Modulation of daily rainfall in southern vietnam by the madden–julian oscillation and convectively coupled equatorial waves. Journal of Climate 29, 5801–5820.

Vu-Thanh, H., Ngo-Duc, T., Phan-Van, T., 2013. Evolution of meteorological drought characteristics in vietnam during the 1961–2007 period. Theoretical and Applied Climatology 118, 367–375. URL: https://doi.org/10.1007/s00704-013-1073-z, doi:10.1007/s00704-013-1073-z.

Wang, B., LinHo, 2002. Rainy season of the asian–pacific summer monsoon. Journal of Climate 15, 386 – 398. URL: https://journals.ametsoc.org/view/journals/clim/15/4/1520-0442_2002_015_0386_rsotap_2.0.co_2.xml, doi:10.1175/1520-0442(2002)015<0386:RSOTAP>2.0.CO;2.

Wang, B., Xiang, B., Lee, J.Y., 2013. Subtropical high predictability establishes a promising way for monsoon and tropical storm predictions. Proceedings of the National Academy of Sciences 110, 2718–2722. URL: https://www.pnas.org/doi/abs/10.1073/pnas.1214626110, doi:10.1073/pnas.1214626110, arXiv:https://www.pnas.org/doi/pdf/10.1073/pnas.1214626110.

Wang, B., Xu, X., 1997. Northern hemisphere summer monsoon singularities and climatological intraseasonal oscillation. Journal of Climate 10, 1071 – 1085. URL: https://journals.ametsoc.org/view/journals/clim/10/5/1520-0442_1997_010_1071_nhsmsa_2.0.co_2.xml, doi:10.1175/1520-0442(1997)010<1071:NHSMSA>2.0.CO;2.

WEBSTER, P.J., 1973. Remote forcing of the time-independent tropical atmosphere. Monthly Weather Review 101, 58–68. URL: https://doi.org/10.1175/1520-0493(1973)101<0058:rfottt>2.3.co;2, doi:10.1175/1520-0493(1973)101<0058:rfottt>2.3.co;2.

Webster, P.J., Holton, J.R., 1982. Cross-equatorial response to middle-latitude forcing in a zonally varying basic state. Journal of the Atmospheric Sciences 39, 722–733. URL: https://doi.org/10.1175/1520-0469(1982)039<0722:certml>2.0.co;2, doi:10.1175/1520-0469(1982)039<0722:certml>2.0.co;2.

Wheeler, M., Kiladis, G.N., 1999. Convectively coupled equatorial waves: Analysis of clouds and temperature in the wavenumber–frequency domain. Journal of the Atmospheric Sciences 56, 374 – 399. URL: https://journals.ametsoc.org/view/journals/atsc/56/3/1520-0469_1999_056_0374_ccewao_2.0.co_2.xml, doi:10.1175/1520-0469(1999)056<0374:CCEWAO>2.0.CO;2.

Wheeler, M., Kiladis, G.N., Webster, P.J., 2000. Large-scale dynamical fields associated with convectively coupled equatorial waves. Journal of the Atmospheric Sciences 57, 613 – 640. URL: https://journals.ametsoc.org/view/journals/atsc/57/5/1520-0469_2000_057_0613_lsdfaw_2.0.co_2.xml, doi:10.1175/1520-0469(2000)057<0613:LSDFAW>2.0.CO;2.

worldbank.org, a. The-world-bank-group and the-asian-development-banky profile: Vietnam (2021), the world bank group and the asian development bank .

worldbank.org, b. Trends and Variability of Rainfall over Vietnam.

Wu, P., Fukutomi, Y., Matsumoto, J., 2012. The impact of intraseasonal oscillations in the tropical atmosphere on the formation of extreme central vietnam precipitation. SOLA 8, 57–60.

Yang, G.Y., Hoskins, B.J., 1996. Propagation of rossby waves of nonzero frequency. Journal of the Atmospheric Sciences 53, 2365–2378. URL: https://doi.org/10.1175/1520-0469(1996)053<2365:porwon>2.0.co;2, doi:10.1175/1520-0469(1996)053<2365:porwon>2.0.co;2.

Yatagai, A., Kamiguchi, K., Arakawa, O., Hamada, A., Yasutomi, N., Kitoh, A., 2012. Aphrodite: Constructing a long-term daily gridded precipitation dataset for asia based on a dense network of rain gauges. Bulletin of the American Meteorological Society 93, 1401 – 1415. URL: https://journals.ametsoc.org/view/journals/bams/93/9/bams-d-11-00122.1.xml, doi:10.1175/BAMS-D-11-00122.1.

Yokoi, S., Matsumoto, J., 2008. Collaborative effects of cold surge and tropical depression–type disturbance on heavy rainfall in central vietnam. Monthly Weather Review 136, 3275–3287.

Yokoi, S., Satomura, T., 2005. An observational study of intraseasonal variations over southeast asia during the 1998 rainy season. Monthly weather review 133, 2091–2104.

Yokoi, S., Satomura, T., Matsumoto, J., 2007. Climatological characteristics of the intraseasonal variation of precipitation over the indochina peninsula. Journal of Climate 20, 5301–5315.

Zeng, X., Beljaars, A., 2005. A prognostic scheme of sea surface skin temperature for modeling and data assimilation. Geophysical Research Letters 32, n/a–n/a. URL: https://doi.org/10.1029/2005gl023030, doi:10.1029/2005gl023030.

Zeng, X., Zhao, M., Dickinson, R.E., 1998. Intercomparison of bulk aerodynamic algorithms for the computation of sea surface fluxes using TOGA COARE and TAO data. Journal

of Climate 11, 2628–2644. URL: https://doi.org/10.1175/1520-0442(1998)011<2628:iobaaf>2.0.co;2, doi:10.1175/1520-0442(1998)011<2628:iobaaf>2.0.co;2.

Zhang, C., 2005. Madden-julian oscillation. Reviews of Geophysics 43. URL: https://doi.org/10.1029/2004rg000158, doi:10.1029/2004rg000158.